NORTHWESTERN UNIVERSITY

DNA-Functionalized Interfaces Studied by Second Harmonic Generation

A DISSERTATION

SUBMITTED TO THE GRADUATE SCHOOL
IN PARTIAL FULFILLMENT OF THE REQUIREMENTS

for the degree

DOCTOR OF PHILOSOPHY

Field of Chemistry

By

Faith Christianna Boman

EVANSTON, ILLINOIS

December 2008

ABSTRACT

DNA-Functionalized Interfaces Studied by Second Harmonic Generation

Faith C. Boman

The nonlinear optical technique, second harmonic generation (SHG), is applied here for the first time to probe single and double strand DNA (ssDNA and dsDNA) chemically attached to fused quartz/water interfaces. DNA interfaces are often a critical functional component of biodetection, thus, the development of molecular biosensors requires a thorough investigation of the physical and chemical properties of interfacial DNA. This work advances our understanding of DNA on a molecular level, as well as predicts and quantifies macromolecular interactions, improving and optimizing biodiagnostic capabilities, and understanding life processes.

Specifically, we use the SHG $\vec{\chi}^{(3)}$ technique to study the thermodynamic parameters of ssDNA bound to an insulator surface by probing the interfacial potentials set up by the phosphate charges along the nucleotide backbone. Using the Gouy-Chapman-Stern model, we calculate surface charge densities between 9×10^{-3} C/m^2 to 3×10^{-2} C/m^2 for T_{15}-T_{35} oligonucleotides, which correspond to DNA densities of approximately 5×10^{11} strands/cm^2. We also calculate the interfacial potentials and interfacial free energy densities of the charged DNA interfaces. We then take advantage of the π-π^* transitions of the oligonucleotide bases to probe the electronic structure of ssDNA and dsDNA with resonantly enhanced SHG. We find the SH signal of the DNA is maximum at 260 nm, the same as that of DNA in the bulk.

We demonstrate that a strong nonlinear optical linear dichroism response is obtained when surface-bound DNA hybridizes with solution phase complementary strands, and, therefore, we use polarization-resolved SHG-LD to differentiate between the chiral properties of ssDNA and dsDNA. We track the chiral duplex formation of surface-bound DNA oligonucleotides *in situ* and in real time, and determine that hybridization occurs within 2 hours, which we confirm with fluorescence measurements. We also use vibrational sum frequency generation (SFG) to track changes in the ordering of the DNA duplex, as well as changes in local and supramolecular chirality when oligonucleotide strands hybridize. Therefore, we sense the four significant intrinsic characteristics of native DNA, namely electronic resonance, charge, vibrational transitions, and chirality.

_____

Professor Franz M. Geiger

Research Advisor

ACKNOWLEDGEMENTS

Obviously, I must thank my research advisor first and foremost. Franz, you have been instrumental in helping shape my research and, in general, my overall outlook on science. You can rest assured that I will always use the terms spectra and spectrum appropriately, and I will never forget watching you jump around in your balloon-filled office during your tenure celebration. My committee members, Profs. Van Duyne, Barron, and O'Halloran, have also been a great resource to me as a grad student. Thanks for the input on my experiments. It drove me to develop a comprehensive understanding of the science behind my research project.

The Geiger group members have been my friends these past 5 years in addition to being great co-workers. To the original Geigerinos- Amanda, Andrea, Catherine, Chris, and Michael- thanks so much for setting a good example. Each of you had such a unique set of talents that there was a noticeable void in the group after you graduated. When I had problems getting my experiments to work properly or needed a paper proofread, you always were there to help. You have no idea how much I appreciate that. You all are such great scientists, and I love picking your brains. To those who joined the group after me- Grace, Kim, Juli, Patrick, Avi, Jessica, Jen, Ehow, and Joe- you kept me going and pushed me to be a better scientist. Thanks for putting up with all the endless questions I've had while writing my thesis; you were invaluable to me. To my summer mentees- Laurel, Boyee, Allison, Anne, and Sussan- even though I was supposed to be teaching you about chemistry, I think I might have learned more in the process. You made the summers interesting, and your boundless enthusiasm kept me motivated.

The Northwestern Chemistry Department staff has been very helpful during my time here. In particular, Ann Wheatley, thanks for taking so much time to help me with paycheck, tax,

tuition, and reimbursement issues. Also, I have really enjoyed working with the NSEC office staff. Deb and Kathy, you guys have done a wonderful job with the center and you always put a smile on my face at all the poster sessions and annual meetings.

I've had a lot of friends at Northwestern, but Ami, Paige, and Haley really stand out. Ami, I've known you since my first week here, and we've had a lot of fun together. You've always been there for me. The Chicago Cultural Club was a great way to conclude our last year as students. Haley, you were an enormous help to me in my career planning. Paige, you're not only my friend, but also a fellow Obama devotee, volleyball teammate, and roommate all rolled into one. It's fantastic to know people that don't restrict their conversations merely to science.

Last, but certainly not least, I would like to thank my family. My parents taught me from a very young age that I could accomplish anything that I set my mind to. They worked hard so that I would be able to have the opportunity to succeed. Plus, I had a never-ending supply of books; just try to find a picture of me on vacation where I'm not reading. Mom, you might have once thought that I got a Ph.D. just to top you educationally, but you were really my inspiration to strive to be an intelligent woman. I can always depend on you to think I'm the smartest person in the world, even though I'm pretty sure that's not the case. Dad, I love how you looked up all the words in the magazine article about my research just to understand what it is I actually do at school. It means a lot to me that you care enough to delve into chemistry. Evelyn, you have been an excellent example to me of how to be a strong woman. Your pep talks encouraged me to stick up for myself and demand more out of life. Josh, you were a great younger brother. Even though we sometimes seemed polar opposites in our school interests, you helped me realized that there are a lot of interesting things to learn about to life other than science and math.

To my parents

TABLE OF CONTENTS

LIST OF FIGURES

LIST OF TABLES

CHAPTER 1

Introduction to DNA Biodetection

Portions of this chapter are reproduced in part
with permission from the American Chemical Society:

Boman, F.C.; Musorrafiti, M.J.; Gibbs, J.M.; Stepp B.R.; Salazar, A.M.; Nguyen, S.T.; Geiger, F.M. "DNA Single Strands Tethered to Fused Quartz/Water Interfaces Studied by Second Harmonic Generation." *Journal of the American Chemical Society*, **2005**, *127*, 15368-15369.

Stokes, G.Y.; Gibbs-Davis, J.M.; Boman, F.C.; Stepp, B.R.; Condie, A.G.; Nguyen, S.T.; Geiger, F.M. "Making 'Sense' of DNA." *Journal of the American Chemical Society*, **2007**, *129*, 7492-7493.

Boman, F.C.; Gibbs-Davis, J.M.; Heckman, L.M.; Stepp, B.R.; Nguyen, S.T.; Geiger, F.M. "DNA at Aqueous/Solid Interfaces- Chirality-Based Detection via Second Harmonic Generation Activity." *Journal of the American Chemical Society*, **2008**, *in press.*

1.1 Importance of Interfaces

Molecules at interfaces behave differently than in bulk media.[1-7] The asymmetry, density, and confined geometry of an interface can change reaction timescales and alter a molecule's chemical properties, such as its thermodynamics,[8-12] kinetics,[13-18] and spectral signatures.[19-25] Because of these unique properties, there has been considerable interest focused on characterizing interfacial boundaries, as well as the molecular interactions that occur there. There are six different kinds of interfaces: liquid/liquid, solid/solid, gas/solid, gas/liquid, and liquid/solid.[1-6] Liquid/liquid interfaces are important in oil-water emulsions,[26,27] membrane transport,[28-30] and liposomes.[31,32] Solid/solid interfaces can involve lubrication,[33,34] adhesion,[35,36] and microelectronics thin films,[37,38] and catalytic converters[39] and heterogeneous catalysis[40] involve the air/solid interface; and acid rain,[41,42] marine aerosols,[43,44] and soap films[45,46] involve the air/liquid interface. One of the most common interfaces is the liquid/solid interface, which plays a key role in surfactant coatings,[47] medical implants,[48-50] metallic nanoparticles,[51-53] clay microparticle colloids,[54] oil recovery,[55,56] bridge support corrosion,[57,58] water treatment,[59,60] and liquid crystal displays.[61] Solid/liquid interfaces are very important in the mobility of heavy metal pollutants[62-69] and agricultural antibiotics,[70,71] acid-base processes,[72-75] microbial biofilms,[76] ligand-receptors,[77] and DNA biosensor surface processes.[78-83] Here, the interaction of molecules in solution with metal oxides involves many significant chemical reactions and processes such as solvation, precipitation, and adsorption.[2,8,84-89]

1.2 Biosensors and Medical Diagnostics

Biointerfaces have rapidly developed into one of the most studied systems in chemistry,

biology, engineering, and medicine.[48,49,83,90-99] The applications of biointerfaces include, but are not limited to, pathogen detection, engineered microenvironments, regenerative medicine, medical implants, neural interfaces, targeted drug delivery, membranes, nanotubes, peptides, carbohydrates, and DNA. Biointerfaces are often a critical functional component of biodetection. Biosensor devices utilize biological reactions to detect target molecues.[100-109] They consist of a biological recognition element and a physical transducer to transmit a signal. Some benefits of a biosensor are its miniaturization, short response time, ease of use, and elimination of prior sample separation steps. However, there remain problems with instability, sample matrix electrochemical interference, and biofouling.[104,110] Lab-on-a-chip systems are able to integrate multiple processes, such as sample preparation and DNA array detection, into one device.[110-115]

The first biosensor was used to monitor blood glucose levels, and now glucose biosensing technology has progressed to handheld devices and implanted sensors.[116,117] Human blood serum can also be screened for cholesterol,[118] as well as creatinine which helps in the diagnoses of renal and muscular malfunctions.[119] Fluorescent immunoassays for microbial warfare agents rely on antibodies binding to antigens,[120] and there is an infectious disease test for the mRNA sequence of the anthrax toxin.[121-123] Biosensors can detect the influenza viral strain,[124] HIV in saliva,[125] and Alzheimer's disease antibodies.[126-128] Human neural stem cell growth and differentiation can be monitored with biosensors.[129] Conformational changes, such as engineered proteins that undergo ligand-induced folding[130] and DNA aptamers that selectively detect unlabeled proteins are also biological processes that can be characterized using biosensors.[131-133] A genetic test is available for the BRCA 1 and 2 genes, which have been linked to hereditary breast and ovarian cancers,[134-136] and pregnant women can be screened for biomarkers of Down's syndrome[137] and preterm

birth.[138] The Human Genome Project has sequenced and identified the genes of an individual human genome.[139-143] Scientists are even going so far as to develop robust, molecular-recognition sensor arrays for use on a mission to Mars to find evidence of life by detecting hereditary molecules like DNA chiral amino acids.[144,145] Therefore, due to the vast array of biodiagnostic systems, we need to characterize biointerfaces thoroughly.

1.3 Immobilization of DNA Oligonucleotides at an Interface

The DNA double helix is emblematic for the basis of all life processes[146-149] and has received significant attention in many areas of science.[150-156] DNA can exhibit unique molecular recognition properties, many of which are now being exploited in materials synthesis and biodetection schemes that are based on the hybridization, i.e. duplex formation of oligonucleotides with complementary nucleic acid targets.[150,153,155,157-160] There is much interest in surface-bound (sb) DNA hybridization and melting processes, however numerous critical details relating to the mechanisms are not yet known.[105] Fundamental studies are necessary to understand the physical processes that govern DNA interactions on a molecular level. Such mechanistic insight into biomolecular systems will help predict their responses to various conditions, such as salt, pH, temperature, surface material, DNA density, linker attachment, free energy densities, interfacial potentials, and structural properties, guiding current engineering work on biosensor applications.[110] Therefore, the development of molecular biosensors specific to the detection and characterization of DNA requires a thorough investigation of these conditions for the optimization of chip-based strategies for biodiagnostic applications.

1.4 Common Biointerface Characterization Techniques

Hybridization biosensors involve the immobilization of single strand DNA on a transducer surface and the detection of duplex formation.[110] While DNA hybridization in aqueous media is well understood,[148] our molecular-level understanding of DNA duplex formation at interfaces is not as in depth. Despite this interest in sb-DNA, it has been a challenge to differentiate between signals that originate from bulk molecules and interfacial molecules. Common interfacial characterization techniques used in this endeavor (vide infra) can be classified under three categories: optical, electrochemical, and gravimetric methods, where binding events result in changes to the refractive index, charge, and mass, respectively.[109,110]

Studies of interfacial DNA have successfully employed fluorescence microscopy,[161-166] Förster resonance energy transfer (FRET),[167-170] colorimetry,[171-176] interferrometry,[177-179] electrochemistry,[180-182] and nanoparticle[153,183-185] and radioactive labeling.[186] While intense research has focused on characterizing interfacial DNA for biodiagnostic purposes, these studies require the synthesis of labeled oligonucleotides or other analytes to afford detection. Tagging DNA has many experimental advantages and can afford important molecular-level information.[162,183,186-188] The measurable reported is a response based directly on the label and not the DNA itself. There is a possibility that the label can sterically interfere with the system if it is quite large and if the sb-DNA is packed densely. Also, labeling methods further can complicate the biodetection process and add extra time and cost to the preparation of the analytes.

Molecularly specific and label-free probes for the direct detection of DNA-based structures at interfaces[78,189-194] are highly desirable, both from a fundamental science perspective, as well as in the context of the demanding engineering aspects associated with high-throughput

screening, biochip function, and disease detection. Label-free techniques such as surface plasmon resonance (SPR) spectroscopy,[157,189,190,195,196] localized surface plasmon resonance (LSPR) spectroscopy,[197-199] impedance spectroscopy,[200-202] quartz crystal microgravimetry (QCM),[203-207] atomic force microscopy (AFM),[191,205,208-211] x-ray photoelectron spectroscopy (XPS),[212-214] Fourier transform infrared (FTIR) spectroscopy,[78,215-217] second harmonic generation (SHG) spectroscopy,[192,194] and sum frequency generation (SFG)[193,218-220] spectroscopy are used to characterize sb-DNA without modification. These techniques are advantageous for biodetection because they eliminate the synthetic steps necessary for radioactive tags, fluorescent markers, nanoparticle probes, and electrochemical labels, as well as the possible chemical differences such a bulky group would cause in reactions.

1.5 Project Goals and Overview

Here, we have taken the first steps toward label-free DNA characterization by applying nonlinear optical methods to study DNA strands chemically attached to fused quartz/water interfaces (Figure 1.1a-d). Second harmonic generation (SHG) spectroscopy is an interface-specific technique that can access a large number of quantitative parameters on a wide variety of system conditions.[7,19,221-223] While SHG does not replace other interface-specific detection techniques, it is advantageous because of the vast range of experimental analysis that it can explore with one detection system. We note that we are the first group in the world to study DNA using nonlinear optics, and several other international groups have followed suit.[218-220]

We have used SHG to study single and double strand DNA on an insulator surface, and have determined thermodynamic state properties, such as the surface charge density, the

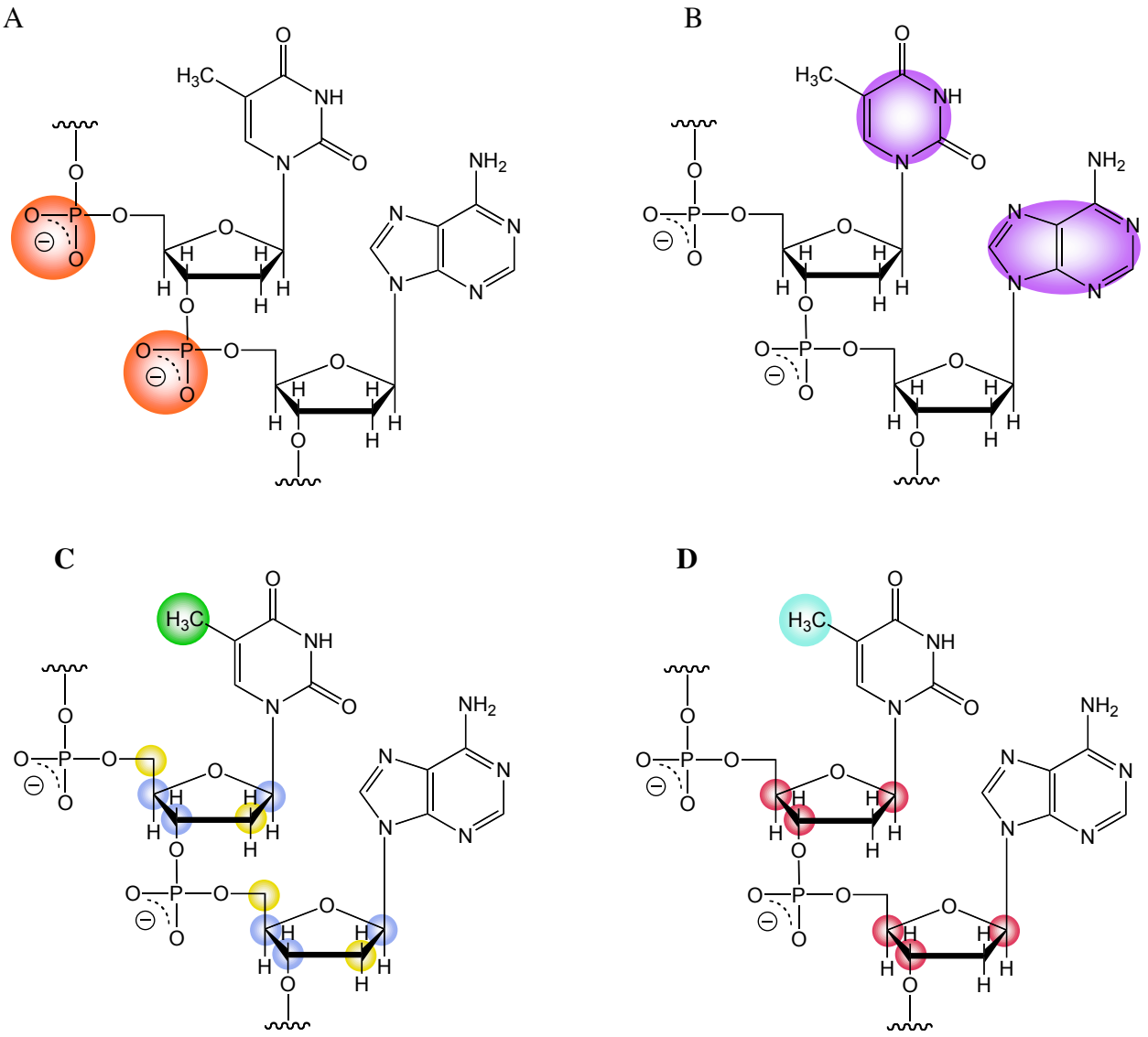

Figure 1.1. Overview of Experimental Focus for DNA Oligonucleotides
A) The $\vec{\chi}^{(3)}$ technique uses the negative charges on the phosphate backbone as intrinsic labels and is applied to calculate surface change density and assess the thermodynamics of the sb-DNA strands. **B**) Resonance-enhanced SHG probes the π–π^* electronic transitions of the DNA bases. SFG looks at **C**) the CH stretching region and **D**) the stereogenic centers of the DNA strands.

interfacial potential, and the change in interfacial free energy density, and have probed the electronic resonance of the DNA bases and the chiral response from duplex formation. We also have used sum frequency generation (SFG) spectroscopy to probe the vibrational resonance of the DNA and fluorescence confocal microscopy to image the DNA surfaces. This work has important implications for predicting and controlling macromolecular interactions, improving biodiagnostics, and understanding life processes.

Our experiments were carried out on fused quartz hemispherical lenses functionalized with a succinimide-terminated silane that was then reacted with a 3'-amine-terminated thymine DNA strand. The single strand DNA surfaces were hybridized by exposure to the complementary DNA strand in solution. The functionalized surface was placed under Millipore water maintained at pH 7 using HCl and NaOH, and the ionic strength was adjusted using NaCl. Using a tunable optical parametric amplifier pumped by a 120-fsec, 1-kHz, regeneratively amplified Ti:sapphire laser system,[224] SHG signals from the functionalized aqueous/solid interface were obtained on and off DNA electronic resonance near total internal reflection at room temperature.

Chapter 2 discusses the theoretical framework behind SHG and describes our laser system and experimental conditions. Chapter 3 outlines the preparation steps required for surface functionalization. Chapter 4 introduces the $\vec{\chi}^{(3)}$ technique for off-resonant charge density screening and describes the calculations for surface charge density, DNA surface coverage, interfacial potential, and interfacial free energy density of single strand DNA interfaces. Chapter 5 focuses on the electronic resonance-enhancement of the sb-DNA strands. Chapter 6 examines the chiral properties of duplex DNA, quantifies hybridization time scales, and incorporates fluorescence confocal microscopy control studies. Chapter 7 concludes with an outlook on the

future of interfacial DNA characterization and biodetection. Appendix 1 describes the synthesis of our NHS linker and DNA strands, Appendix 2 shows our method of verifying SH signal, Appendix 3 details the theoretical framework of waveplates and polarizers, and Appendix 4 includes additional fluorescence control studies. Appendix 5 highlights the SFG vibrational spectra of single and double strand DNA. It focuses on the modes of local stereogenic centers and supramolecular chirality, as it relates to the order of assembly of the DNA strands.

CHAPTER 2

Nonlinear Optical Applications for Biointerfaces

Portions of this chapter are reproduced in part
with permission from the American Chemical Society:

Boman, F.C.; Musorrafiti, M.J.; Gibbs, J.M.; Stepp B.R.; Salazar, A.M.; Nguyen, S.T.; Geiger, F.M. "DNA Single Strands Tethered to Fused Quartz/Water Interfaces Studied by Second Harmonic Generation." *Journal of the American Chemical Society*, **2005**, *127*, 15368-15369.

Stokes, G.Y.; Gibbs-Davis, J.M.; Boman, F.C.; Stepp, B.R.; Condie, A.G.; Nguyen, S.T.; Geiger, F.M. "Making 'Sense' of DNA." *Journal of the American Chemical Society*, **2007**, *129*, 7492-7493.

Boman, F.C.; Gibbs-Davis, J.M.; Heckman, L.M.; Stepp, B.R.; Nguyen, S.T.; Geiger, F.M. "DNA at Aqueous/Solid Interfaces- Chirality-Based Detection via Second Harmonic Generation Activity." *Journal of the American Chemical Society*, **2008**, *in press.*

2.1 Introduction

Nonlinear optics (NLO) is a rapidly growing field that describes the nonlinear behavior of light as it interacts with matter.[1,2] NLO includes many forms of optical phenomena, with two of the most common being second harmonic generation (SHG)[1,3-9] and sum frequency generation (SFG).[1,6,10-14] SHG will be the focus of this work, and SFG will be discussed in Appendix 5. SHG is a powerful and versatile tool that can be used to characterize buried, as well as exposed interfaces. Furthermore, it is a coherent, non-destructive technique that can probe interfaces *in situ* and in real time. SHG is sensitive enough to detect submonolayer surface densities and is molecularly specific because it is enhanced by molecular electronic transitions.[7-9] In SHG, the measured signal is the result of the NLO response of a noncentrosymmetric medium in the presence of a strong, applied electric field oscillating at particular frequency.[1,2,15] This response consists of frequency doubling of the probe light field at an interface (Figure 2.1a-b). SHG is electric dipole forbidden in bulk liquids, gases, and centrosymmetric solids, but because inversion symmetry is broken at the boundaries between interfaces, SHG is interface-specific, eliminating the difficulties in differentiating between bulk and interfacial optical responses.[4,6-8,12,16-18] The significant roles that interfaces play have already been discussed in Chapter 1.

2.2 Nonlinear Optics

2.2.1 Second Harmonic Generation Theory

An electric field, $\vec{E}_\omega$, propagating in time t, at frequency ω, can be described by:[1,2,7]

$$\vec{E}_\omega = Ee^{-i\omega t} \tag{2.1}$$

where E is the magnitude of the oscillating electric field. Electrons in a dielectric material under

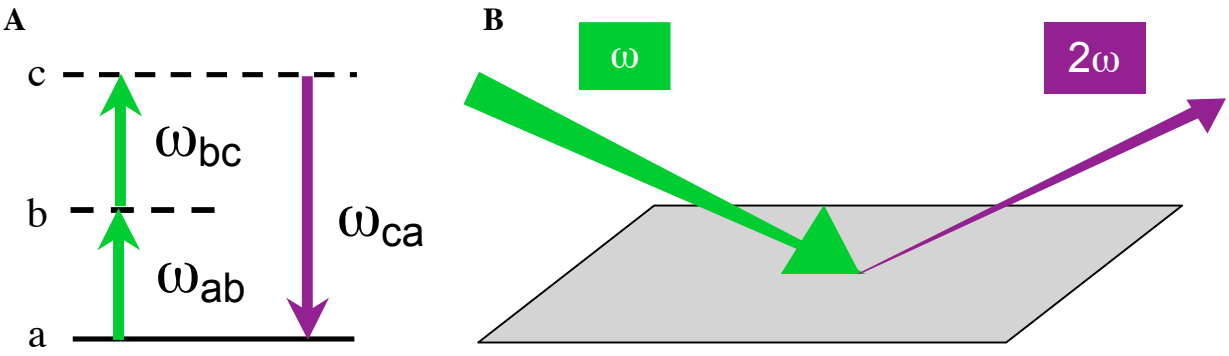

Figure 2.1. Schematic of Second Harmonic Generation
A) Energy level diagram of SHG. The frequency of the SH light field, ω_{ca}, is equal to twice the frequency of the fundamental light field, $\omega_{ab}=\omega_{bc}$. **B**) A schematic representation of the fundamental light field, ω, as it probes the interface and produces the SH light field, 2ω.

the influence of this field can be described by a polarization, $\vec{P}$. In conventional optics, $\vec{P}$ is linearly proportional to the incident electric field,

$$\vec{P} = \vec{\vec{\chi}}^{(1)}\vec{E} \tag{2.2}$$

where $\vec{\vec{\chi}}^{(1)}$ is the linear susceptibility tensor. In nonlinear optics, the polarization, $\vec{P}$, can be expressed as a power series.[1,2,19]

$$\vec{P} = \vec{P}^{(1)} + \vec{P}^{(2)} + \vec{P}^{(3)} + ... \tag{2.3}$$

where $\vec{P}^{(2)}$ and $\vec{P}^{(3)}$ are the second- and third-order nonlinear polarizations. The even-order terms, such as $\vec{P}^{(2)}$, are non-zero in noncentrosymmetric media. The odd-order terms, such as $\vec{P}^{(1)}$ and $\vec{P}^{(3)}$, are non-zero in centrosymmetric and noncentrosymmetric media, and $\vec{P}^{(3)}$ is discussed further in Chapter 4. The same considerations apply to the higher order polarizations terms.

For second-order NLO processes, the square root of the measured SH signal, I_{SHG}, is equal to the magnitude of the electric field of the second harmonic beam, $E_{2\omega}$, at frequency 2ω.[1,2]

$$\sqrt{I_{SHG}} = E_{2\omega} \tag{2.4}$$

$\vec{E}_{2\omega}$ is directly proportional to the second-order nonlinear polarization, $\vec{P}^{(2)}_{2\omega}$, which is equal to the product of the second-order susceptibility tensor, $\vec{\vec{\chi}}^{(2)}$, and the fundamental electric fields, $\vec{E}_{\omega}$, as shown in Equation 2.5.[1,2]

$$\vec{E}_{2\omega} \propto \vec{P}^{(2)}_{2\omega} = \vec{\vec{\chi}}^{(2)}\vec{E}_{\omega}\vec{E}_{\omega} \tag{2.5}$$

The $\vec{\vec{\chi}}^{(2)}$ tensor is an intrinsic property of the interface and contains structural information that can be probed by polarization-resolved experiments (see Chapter 6). It is composed of both a non-resonant, $\vec{\vec{\chi}}^{(2)}_{NR}$, and resonant, $\vec{\vec{\chi}}^{(2)}_{Rv}$, term.[1,2]

$$\vec{\vec{\chi}}^{(2)} = \vec{\vec{\chi}}^{(2)}_{NR} + \sum_{\nu=1}^{n} \vec{\vec{\chi}}^{(2)}_{R\nu} e^{i\gamma_\nu} \tag{2.6}$$

The resonant term in Equation 2.6 includes contributions from resonant states, ν, and relative phases, γ_ν, and is equal to the number of resonant, adsorbed molecules, N_{ads}, times the second-order molecular polarizability tensor, $\vec{\vec{\alpha}}^{(2)}$, averaged over all molecular orientations.[1,2]

$$\vec{\vec{\chi}}^{(2)}_{R\nu} = N_{ads} \left\langle \vec{\vec{\alpha}}^{(2)} \right\rangle \tag{2.7}$$

Equation 2.7, therefore, connects the molecular scale with our macroscopic system scale.

Under conditions when the fundamental beam probes a surface-bound molecule at a frequency ω, such that either ω or 2ω matches a molecular electronic transition frequency, $\vec{\vec{\alpha}}^{(2)}$ is resonantly enhanced. The expression for this enhancement is given by:[1,2,20]

$$\vec{\vec{\alpha}}^{(2)} = -\frac{4\pi^2 e^3}{h^2} \sum_{b,c} \frac{\vec{\mu}_{ab} \cdot \vec{\mu}_{bc} \cdot \vec{\mu}_{ca}}{(\omega_{ab} - \omega + i\Gamma_{ab})(\omega_{ca} - 2\omega + i\Gamma_{ca})} \tag{2.8}$$

where $\vec{\mu}_{ab}$, $\vec{\mu}_{bc}$, and $\vec{\mu}_{ca}$ are the transition dipole moments, a, b, and c represent the ground, intermediate, and final states, respectively ($\omega_{ca} = \omega_{ab} + \omega_{ba}$, Figure 2.1a), Γ_{ab} and Γ_{ca} are the damping coefficients of the electronic transition, e is the elementary charge on an electron, and h is Planck's constant. When an electronic resonance is matched by either ω or 2ω, the real part of the denominator approaches zero, $\vec{\vec{\alpha}}^{(2)}$ is enhanced and both $\vec{\vec{\chi}}^{(2)}_{R\nu}$ and I_{SHG} increase, assuming $\vec{\vec{\chi}}^{(2)}_{R\nu}$ and $\vec{\vec{\chi}}^{(2)}_{NR}$ constructively interfere. Resonant SHG will be discussed further in Chapter 5.

2.2.2 Applications of SHG

SHG was first demonstrated in 1961,[3] and over the past three decades, has been widely developed as a method to study interfaces. Many reviews have been published on the topic.[4,6-8,16-18,21,22] Due to its interface-specificity, SHG is an excellent tool for monitoring the adsorption of

pollutants,[23-29] biopolymers,[30-33] and antibiotics[34-36] to an interface. SHG has been used to probe the kinetics,[37-39] dynamics,[6,16,40-46] molecular transport,[47-49] and orientation[50-58] of molecules at interfaces. Interfacial potentials and surface charge densities have been quantified with the SHG $\vec{\vec{\chi}}^{(3)}$ technique.[19,49,59-66] SHG surface analogues of LD, ORD, and CD have also been applied to study chiral molecules,[5,22,67-75] and SHG microscopy[76] has been used to image Langmuir films[77,78] and biological interfaces.[79-82] We have used SHG to study DNA-functionalized interfaces by characterizing surface charge density, interfacial potential and free energy density, DNA density, hybridization time, duplex chirality, and DNA base electronic resonance-enhancement.[83-85]

2.3 Experimental Description

2.3.1 Laser and Detection System

Detailed descriptions of the experimental aspects of SHG are available elsewhere,[1,8,86] and a schematic of our laser and detection system[23,38] is shown in Figure 2.2. SHG studies were carried out on a Ti:sapphire regenerative amplifier system (120 fs, 1 kHz, 1 W, 800 nm, Hurricane, Spectra-Physics),[87] pumped by a solid-state Nd:YLF laser (1 kHz, 527 nm, Evolution, Positive Light, Inc.),[88] equipped with laser diodes (ARR26C020W080502A11B200, Cutting Edge Optronics), and seeded with a mode-locked Ti:sapphire laser (80 MHz, 800 nm, Mai Tai, Spectra-Physics).[89] This laser system pumps an ultrafast optical parametric amplifier (OPA-800C, Spectra-Physics),[90] that produces visible femtosecond pulses, tunable over a broad wavelength region (480-800 nm). The timing between the mode-locked seed source and the amplifier is controlled with a synchronization and delay generator (SDG II, Positive Light, Inc).

The fundamental beam is directed through a series of filters and optics before reflecting

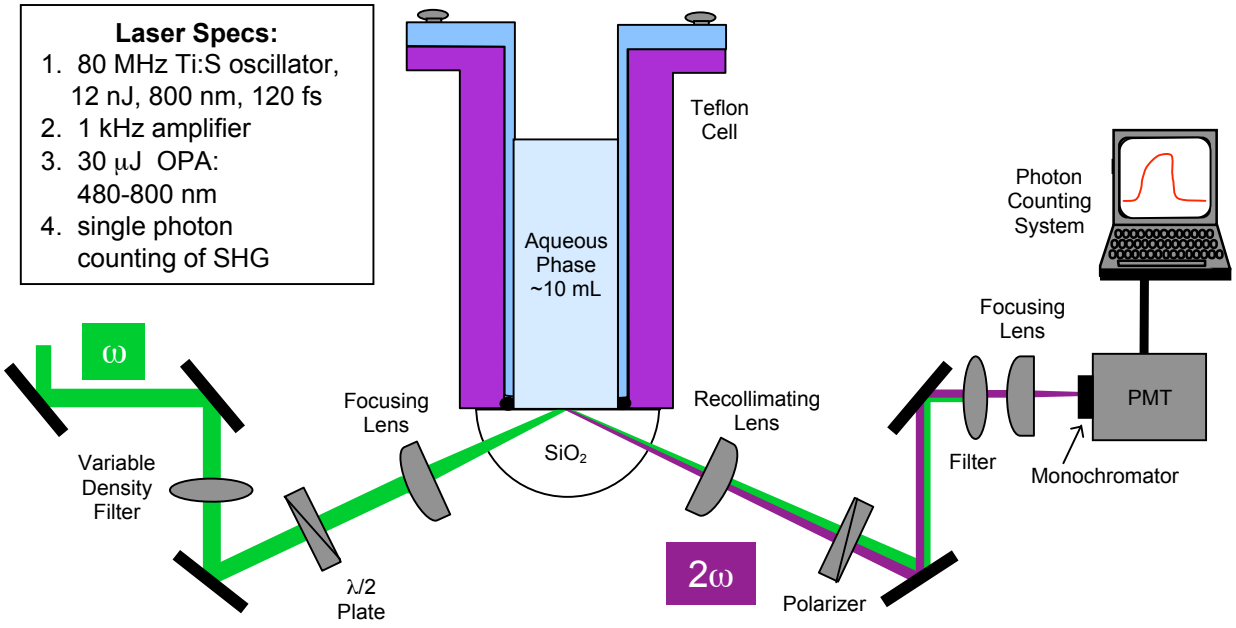

Figure 2.2. Diagram of Laser and Detection System
The beam paths of the fundamental (green) and SH (purple) laser beams are traced. The key optical components in the setup are labeled, and laser specifications are included in the inset.

off the interface, where the SH beam is generated. All optomechanics are from Thorlabs and Newport Corporation. All mirrors are laser quality Al-MgF_2 (D310200, Esco Products). A detailed description of the beam paths of the fundamental and SH beams between the OPA and the detector is included in Section 2.3.3. The reflected SH beam is focused into a monochromator with 300-μm entrance and exit slit widths (200-800 nm range, 6-0102, Optometrics USA, Inc.). The SH signal is collected with a photomultiplier tube (PMT) with a 5 × 8 mm^2 photocathode (R585, Hamamatsu Corporation), amplified with a 350-MHz preamplifier (SR445A, Stanford Research Systems) and recorded with a gated photon counter (SR400, Stanford Research Systems). Typical signal intensities are on the order of 0-200 counts per second.

2.3.2 OPA Configuration

The OPA produces a visible beam that is tunable over a broad visible wavelength range: 480-800 nm.[90] The 800-nm beam from the Hurricane passes through a beam splitter, where 10% is redirected through a sapphire plate to produce white light. The remaining 90% again passes through a beam splitter, where another 10% is split off into a pre-amplifier beam. The white light and pre-amplifier beams overlap and pass through a nonlinear gain medium- a β-barium Borate (BBO) crystal (0453-6020, Spectra-Physics)- and form signal (ω_s= 1.0-1.6 μm) and idler (ω_i= 1.6-3.0 μm) beams. These beams are reflected back through the BBO crystal and overlap with the original 800-nm pump beam. The pump, signal, and idler beams, $\omega_p, \omega_s, \omega_i$, respectively, then pass collinearly through another BBO crystal to produce the light used in the SHG experiments ($\omega_p = \omega_s + \omega_i$). Two different OPA configurations were used to produce different wavelength ranges: second harmonic (SH) and sum-frequency mixing (SFM). The SH option doubles the frequency of the signal beam ($\omega_{SH} = 2\omega_s$) to produce a wavelength range of 570-800

nm (BBO Type I, 0451-5062, Spectra-Physics), which then passes through a polarizer before exiting the OPA. This option was used for the off-resonance SHG experiments (see Chapter 4). The SFM option mixes the signal beam with the residual pump beam ($\omega_{SFM}= \omega_p+\omega_s$) to produce a wavelength range of 480-533 nm (BBO Type II, 0451-8301, Spectra-Physics), which is reflected off three dichroic mirrors to select for the SFM beam. This option was used for the on-resonance SHG experiments (see Chapters 5 and 6). The output wavelength is selected for by changing the delay stages and by angle tuning the BBO crystals.

2.3.3 Layout of Optical Line

The 800-nm light field emerging from the Hurricane was measured using a power meter (407A, Spectra-Physics) and ranged from 0.7 to 1.0 W. The tunable visible light field emerging from the OPA was measured using an energy meter (EPM1000-0110L99, Molectron) and varied up to 5 μJ for the SH option and up to 30 μJ for the SF mixing option. Under typical experimental conditions, the input power was reduced to approximately 0.5 μJ with a 465-nm long-pass filter (Edmund Optics, Inc.) and a circular neutral variable density filter (NT53-212, Edmund Optics, Inc.) to prevent thermal damage (see Appendix A2.1). Due to its high power, the intensity of the green fundamental beam was also reduced with a BG-38 Schott band filter (NT46-434, Edmund Optics, Inc.) and glass microscope slides (1-mm thick, 22-310-397, Thermo Fisher Scientific). Its polarization was changed with an achromatic half waveplate (400-700 nm, uncoated, MWPAA2-12, Karl Lambrecht Corporation) before being directed onto the surface.

The beam was focused with a 25-mm diameter, 100-mm focal length lens (01 LAO 523, Melles-Griot) that was controlled by a 1-D microtranslational stage, producing an approximately 30-μm diameter laser spot-size. The beam was incident on the surface at an angle 60° from the

surface normal, which is near total internal reflection (TIR) for our fused quartz/water system, where the critical angle is 66°. The reflected fundamental and SH beams were recollimated with a 25-mm diameter, 100-mm focal length lens (01 LUP 031, Melles-Griot), and their polarization was selected with a Glan Taylor polarizer (E grade calcite, BB MgF_2 anti-reflective coating, MGTYE20, Karl Lambrecht Corporation). The reflected fundamental beam was rejected using a UV-transmitting/Vis-absorbing filter (9863, Kopp Glass, Inc.), isolating the SH beam before being directed into the monochromator and PMT (see Section 2.3.1).

2.4 Sample Configuration and Experimental Conditions

Functionalized fused quartz hemispheres (1" diameter, QU-HS-25, UV-grade SiO_2, ISP Optics) were clamped with a Viton O-ring to a 10-mL volume, custom-built Teflon (virgin electrical grade Teflon 174® PTFE, McMaster-Carr) sample cell (Figure 2.3) on a 3-D microtranslational stage (Figure 2.4). The surfaces were kept under Millipore water maintained at pH 7 using HCl and NaOH, and the ionic strength was adjusted using NaCl. The use of a buffer was avoided because it could give rise to a significant $\vec{\vec{\chi}}^{(3)}$ response in the mM concentration regime where much of our data is collected. Previous SHG experiments in our lab had been performed under flow conditions,[23,38] but due to the limited volume of DNA solution available, our SHG experiments were conducted under static conditions. New aqueous phases were prepared and mixed by pipetting solutions in and out of the sample cell. SH signals from the functionalized aqueous/solid interfaces were obtained at 300-350 nm and 245-270 nm, which are off and on two-photon electronic resonance, respectively with the DNA. All experiments were carried out at room temperature.

2.5 Summary

In conclusion, second harmonic generation spectroscopy is a very useful technique that can be used to characterize DNA-functionalized fused quartz/water interfaces *in situ* and in real time. The SH signal originates solely from the noncentrosymmetric interface and not the bulk. Our Ti:sapphire tunable laser system allows us to probe the surface-bound DNA on and off electronic resonance, select the input energy, and control the input and output polarization states of the electric fields. We can also vary the aqueous phase salt concentration and pH, as well as exposure of the surface bound DNA to complementary strand DNA in the Teflon sample cell.

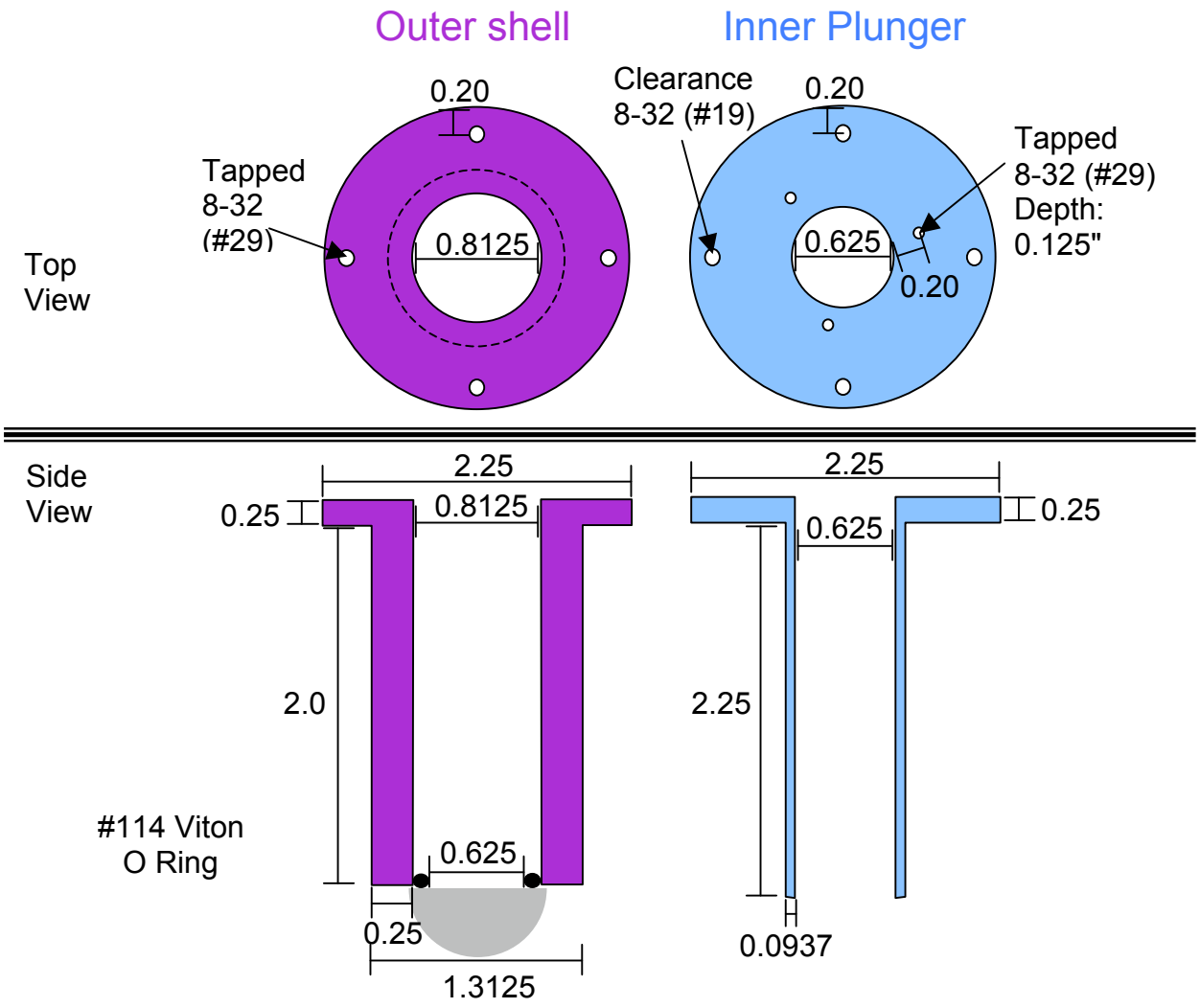

Figure 2.3. Schematic Diagram of Teflon Sample Cell
The specifications of the inner plunger (purple) and outer shell (blue) of the custom-built Teflon sample cell are shown in a top-down and side-on view, including placement of the fused quartz hemisphere and Viton O-ring. Measurements are given in inches.

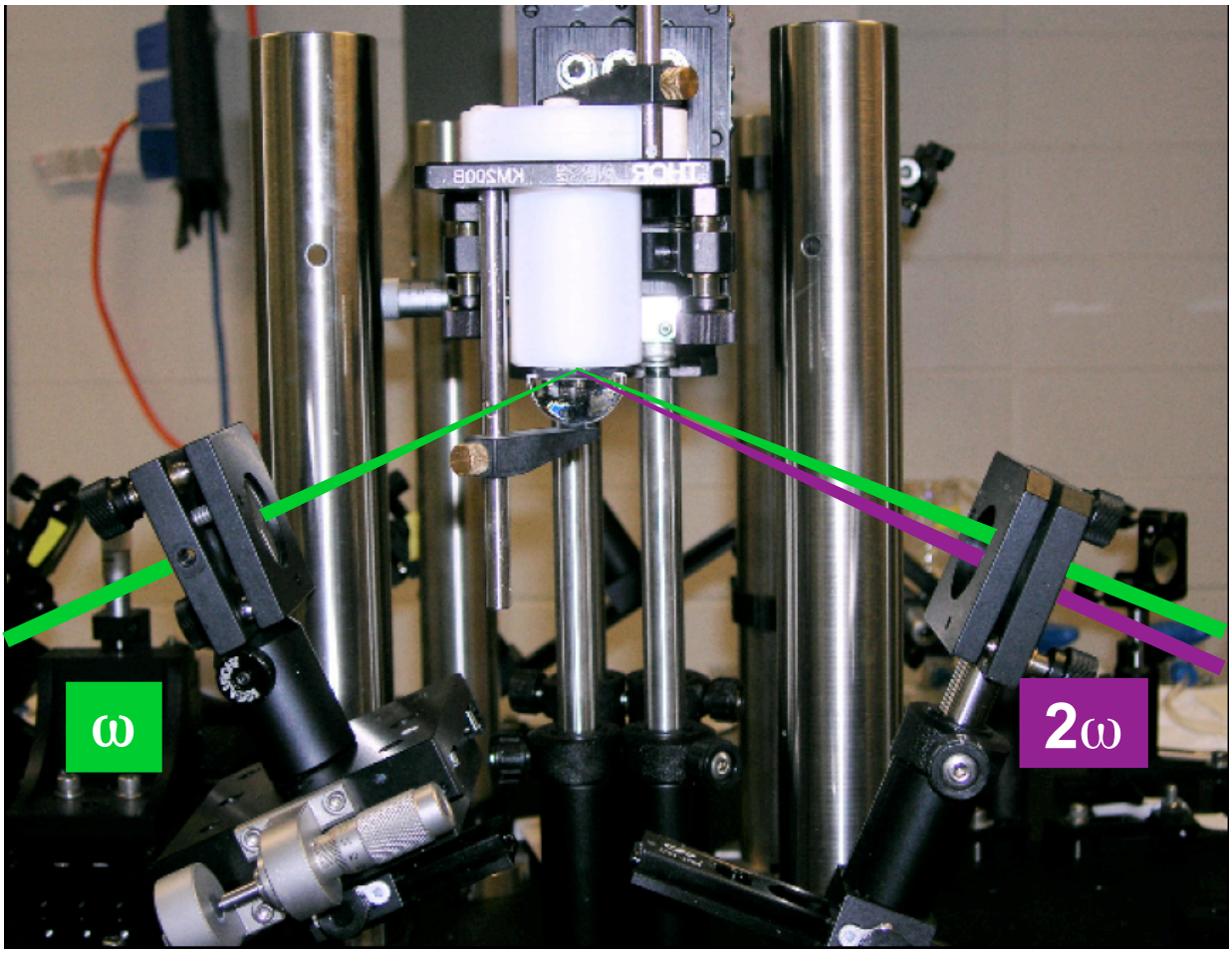

Figure 2.4. Photograph of SHG Experimental Setup
A side-on photograph of a portion of the SHG experimental setup is shown. The fundamental beam (green), ω, passes through a focusing lens, reflects off the fused quartz/aqueous interface, where a SH beam (purple), 2ω, is generated. Both beams then pass through a recollimating lens.

CHAPTER 3

Preparation of DNA-Functionalized Interfaces

Portions of this chapter are reproduced in part
with permission from the American Chemical Society:

Boman, F.C.; Musorrafiti, M.J.; Gibbs, J.M.; Stepp B.R.; Salazar, A.M.; Nguyen, S.T.; Geiger, F.M. "DNA Single Strands Tethered to Fused Quartz/Water Interfaces Studied by Second Harmonic Generation." *Journal of the American Chemical Society*, **2005**, *127*, 15368-15369.

Stokes, G.Y.; Gibbs-Davis, J.M.; Boman, F.C.; Stepp, B.R.; Condie, A.G.; Nguyen, S.T.; Geiger, F.M. "Making 'Sense' of DNA." *Journal of the American Chemical Society*, **2007**, *129*, 7492-7493.

Boman, F.C.; Gibbs-Davis, J.M.; Heckman, L.M.; Stepp, B.R.; Nguyen, S.T.; Geiger, F.M. "DNA at Aqueous/Solid Interfaces- Chirality-Based Detection via Second Harmonic Generation Activity." *Journal of the American Chemical Society*, **2008**, *in press.*

3.1 Introduction

Functionalized fused quartz hemispheres were chosen as a model biosensor surface because they have been widely used for the attachment of self assembled monolayers and polymers for detection purposes.[1-3] Fused quartz forms stable, covalent bonds with molecules via a trichlorosilane linker.[2-11] It is an inexpensive, optically transparent insulator that is compatible with silicon technology.[2] The signal originates from the surface-bound molecules and not from an externally applied field, such as with a gold surface.[12-14] Mimicking the biosensor surfaces in this manner simplifies the characterization of surface-bound oligonucleotides and allows for a better understanding of how those systems function on a molecular level.[1,15]

A versatile attachment strategy was developed in order to custom-design our functionalized surfaces. The approach taken allows us to vary the length and sequence of our DNA, as well as the way in which it is linked to the surface. We chose a trichlorosilane terminated with an *N*-hydroxysuccinimide (NHS) ester as the linker molecule. NHS is an activated ester, making it a good leaving group.[16,17] This flexible linker forms strong bonds with the surface, forming a monolayer, and also readily reacts with amine-terminated DNA strands.[18-20] We chose short oligonucleotide strands (between 15 and 40 bases) composed entirely of thymine and adenine. Except when noted, the thymine strands were used as the surface-bound strand, and the adenine strands were used as the complementary sequence.

The first reaction in the DNA attachment procedure involves reacting a trichlorosilane linker terminated with an NHS ester with the hydroxy groups of the fused quartz surfaces, forming covalent bonds (step 1, Figure 3.1),[2,4,7-9] and annealing in an oven to promote crosslinking.[2,14,21,22] Afterwards, a 10-μM solution of single strand DNA (ssDNA) dissolved in a

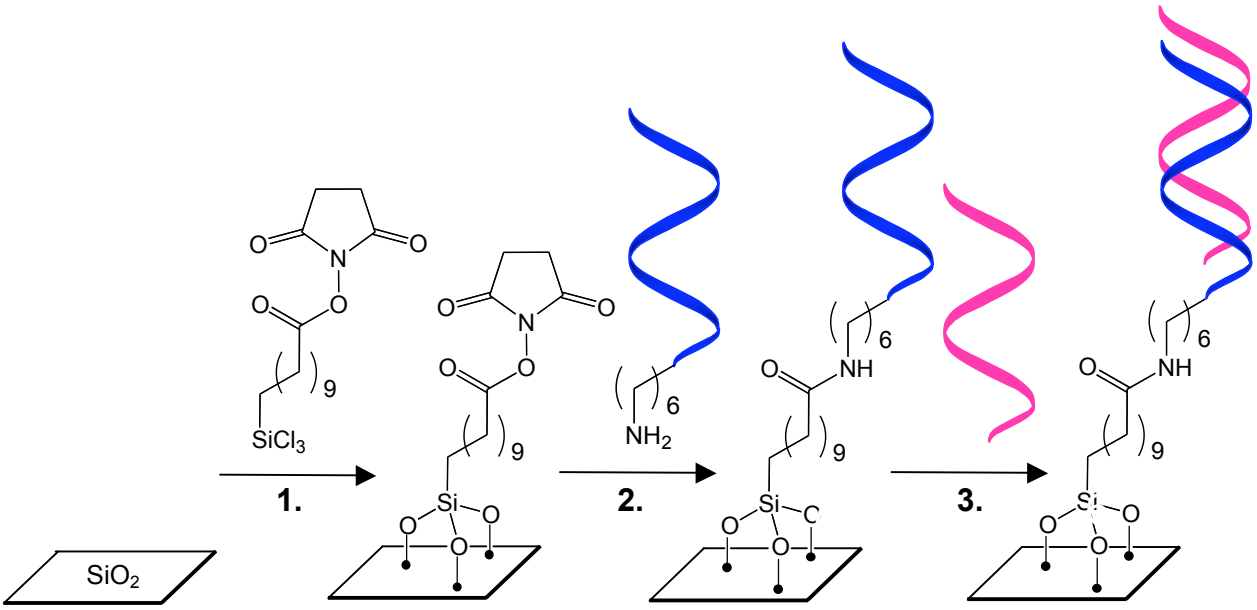

Figure 3.1. NHS Linker and DNA Attachment via Amide Bond Formation
Step **1**) Reaction of N-hydroxysuccinimide (NHS) ester-terminated siloxane with hydroxyl groups of fused quartz. Step **2**) 3'-Amine-terminated DNA strand coupled to NHS linker forming an amide bond. Step **3**) Complementary strand hybridized to surface-bound DNA.

sodium tetraborate buffer was reacted to form an amide bond between the NHS ester of the linker and the amine of the ssDNA (step 2, Figure 3.1).[1] Finally, the functionalized surfaces were rinsed with water and then covered with a 10-μM solution of complementary strand dissolved in 0.25 M NaCl solution to hybridize the DNA strands (step 3, Figure 3.1). The synthesis of the NHS linker and DNA oligonucleotides is described in Appendix 1.

3.2 Substrate Preparation

3.2.1 Lens Cleaning

All SHG laser measurements were performed on functionalized fused quartz hemispheres (1" diameter, QU-HS-25, UV-grade SiO_2, ISP Optics). All SFG, contact angle goniometry, and fluorescence confocal microscopy measurements were performed on functionalized glass microscope slides (Fisher Scientific) cut into 2 cm × 1 cm sizes (see Appendices 3 and 4). All experiments required clean, hydroxy-terminated fused quartz surfaces for proper reaction with the linker and DNA molecules. Therefore, the fused quartz hemisphere surfaces were cleaned prior to surface functionalization by 1) exposure to Nochromix[1,8] solution (VWR), 2) rinsing with methanol and copious rinsing with DI water, 3) washing in methanol for 15 minutes in an ultrasonic bath (Aquasonic model 75T, 90W), 4) rinsing with methanol, 5) drying in an oven (Fisher) at 100°C for 1 hour, and 6) radiation by air in a plasma cleaner/sterilizer chamber[1,8] (Harrick PDC 32G) at high power for 30 seconds. The hemispheres were then allowed to sit at room temperature to equilibrate with ambient conditions. All glass slides were cleaned using steps 3-6, and new lenses were not exposed to the Nochromix solution. Since this cleaning procedure removes all covalently bound molecules and regenerates new hydroxyl groups on the

surface, the hemispheres were reused numerous times over a period of 6 months up to 1 year. Fresh samples were prepared for each experiment.

3.2.2 Surface Modification with NHS Ester Linker

All dry solvents were dried using the Dow-Grubbs solvent system[23] under argon and saturated with argon prior to use. All compounds were purchased from Aldrich and used as received. Ultrapure water (18.2 MΩ·cm resistivity) was obtained from a Millipore Milli-Q Biocel system. All pH values were measured with an Orion 3 Star pH meter (13-642-250, Thermo Fisher Scientific). The surface modification of the fused quartz hemispheres was performed in a custom-built Teflon cell that allowed only the flat surface of the hemisphere to come into contact with the reaction mixture. The glass slides were reacted on their unfrosted side in a glass Petri dish.

Two methods for the attachment of the linker molecule were used. In the first method, the linker compound, 11-(trichlorosilyl)-undecanoic acid NHS-ester, was reacted with the fused quartz substrate under ambient conditions. Dry toluene (10 mL) was placed in a 20-mL scintillation vial with a solvent-resistant cap, and to it Millipore water (10 μL) was added.[2,7] The toluene mixture was then sonicated for 1 minute until it was turbid. The linker compound (6 mg, 0.014 mmol) was weighed into another vial at which point the toluene/water mixture was added followed by sonication for 5 minutes. The cleaned, equilibrated slides and fused quartz hemispheres were then covered with the solution of the trichlorosilane (1.4 mM) and allowed to react for 4 hours. The trichlorosilyl mixture was transferred by pipette from the surface, and each slide was individually rinsed with toluene (5 × 1 mL), sonicated in toluene for 5 minutes, and allowed to anneal in a 100 °C oven for 1 hour. This surface functionalization procedure was

discontinued because the linker was observed to polymerize in solution and form a precipitate.

In the second method, the linker attachment reaction was performed in a Nexus controlled N_2 atmosphere system glove box (VAC). The inert atmosphere of the glove box prevents the trichlorosilane of the linker from self-polymerizing in the presence of water[24] and is, therefore, the preferred method. The linker compound (10 mg, 0.023 mmol) was weighed into a scintillation vial with a solvent-resistant cap and dissolved in 1 mL of dry toluene. The cleaned, equilibrated fused quartz hemispheres and slides were then covered with the trichlorosilyl solution (2.3 mM) and allowed to react for 1 hour. In later experiments, substrates were functionalized with an NHS linker concentration an order of magnitude lower (0.23 mM). The trichlorosilyl solution was transferred by pipette from the surface, and each lens and slide were individually rinsed with toluene (5 × 1 mL), removed from the glove box, washed in toluene for 5 minutes in an ultrasonic bath, rinsed in methanol and then water, and allowed to anneal in a 100 °C oven for 1 hour. The NHS linker-modified surfaces were then functionalized further or used immediately in the SHG measurements.

3.2.3 Single Strand DNA Immobilization

3'-Amine-terminated ssDNA (3'-H_2N-C_7H_{13}(OH)-T_n-5', where n = 15, 20, 25, 30, 35, or 40) was covalently linked to the surface-bound hydrocarbon chain via an amide bond. A C_7 spacer between the amine end and the phosphate-sugar backbone alleviated the steric hindrance between the DNA bases and the NHS ester. In sodium tetraborate buffer (4.77 g/1L, 0.0237 M, pH 9.0), ssDNA (1 mL, 10 μM) was pipetted onto the linker-modified quartz surface and allowed to react for 6 hours. Following the reaction period, the surface was rinsed with Millipore water (4 × 2 mL) and dried in air. Lens samples measured prior to hybridization (i.e. the ssDNA-

modified surface) were covered until they were analyzed by SHG. Glass slides were dried with a stream of nitrogen and placed in an evacuated dessicator.

3.2.4 Double Strand DNA Hybridization

Double strand DNA (dsDNA) surfaces were generated from the hybridization of the ssDNA surfaces with their complementary sequence. Hybridization involves forming hydrogen bonds between each pair of complementary bases so that the two strands can associate together to form a duplex in equilibrium.[25-27] A freshly prepared ssDNA-modified surface was immediately coupled to its complementary strand (10 μM, 3'-A_n-5', where n = 15, 20, 25, 30, 35, or 40) in a 0.25 M NaCl solution at pH 7 for 4 hours. Later experiments involved hybridization times of 2 hours (see Chapter 6.3.3 and 6.4.2).

3.3 Contact Angle Goniometry Measurements

3.3.1 Hydrophobic Linker Transition

Contact angle measurements were used to determine the extent of the NHS linker reaction with the fused quartz substrates. This technique assesses whether or not the surface has been covered with nonpolar molecules by observing the increase in the angle between the water and the surface as the surface changes from hydrophilic to hydrophobic (Figure 3.2a).[28-32] Clean fused quartz and glass are polar, while the NHS ester head group is nonpolar. Water contact angles were performed with a FTÅ125 Goniometer (First Ten Ångstroms). The average contact angle measured for a clean, unreacted glass slide without NHS linker was 3.9(6)°, and the average contact angle for the functionalized NHS slides (10 mg/mL) was 68(4)° (Figure 3.2b). Therefore, contact angles are a good measure of the extent of the hydrophobic NHS reaction.

A

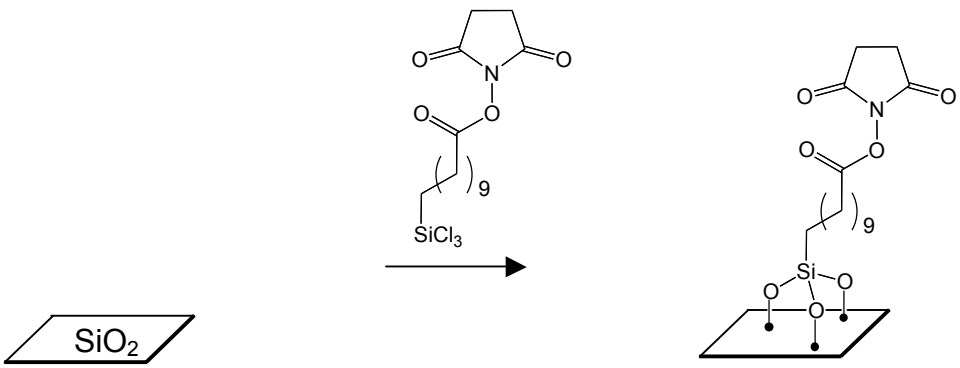

B

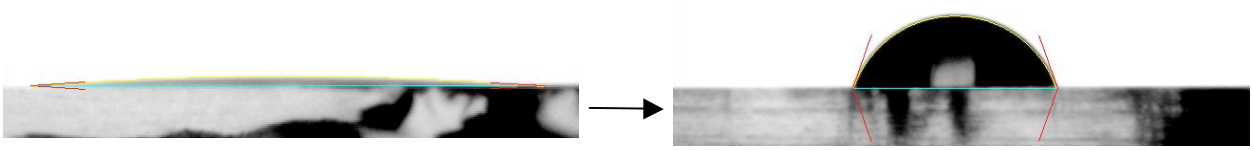

Figure 3.2. Contact Angles of Glass and NHS-Functionalized Surfaces
A) Reaction of the trichlorosilane with the fused quartz surface. **B**) Contact angle images taken of a water droplet with the same sessile volume (~2 μL) showing a clean glass microscope slide before (4.09°) and after (70.8°) functionalization.

3.3.2 Linker Concentration

Synthesis of the NHS linker compound is a time-consuming process, involving multiple synthesis steps (see Appendix 1). In order to conserve NHS linker reagent and time, contact angle measurements were performed to determine the minimal concentration of linker needed for full surface coverage of the glass slides. Samples at each concentration were made in duplicate. Contact angles were measured for 4 different concentrations of NHS linker in toluene: 1.0, 2.5, 5.0, and 10.0 mg/mL. Previous experimental methods used 10 mg/mL.

The average contact angle for glass slides reacted with a 10-mg/mL NHS linker concentration had a mean value of 68(4)°. The contact angles did not significantly decrease as the linker concentration was reduced by up to an order of magnitude (Figure 3.3). The average contact angle for glass slides reacted with a 1-mg/mL NHS linker concentration had a similar mean value of 76(3)°. This result shows that the hydrocarbon linker concentration could be decreased to 1 mg/mL while still maintaining a full surface coverage. Once discovered, subsequent surfaces were functionalized with this smaller linker concentration.

3.3.3 Variations on Substrate Preparation

Additional contact angle measurements were conducted in order to optimize the NHS surface preparation. NHS slides were first prepared at a linker concentration of 2.5-mg/mL, and after the 1-hour reaction, the solution was immediately pipetted onto a new set of slides for a second reaction. It was shown that the contact angles did not differ within error between the first and second use of the same solution of NHS linker on a surface (Table 3.1a). For the first use of 2.5 mg/ml of NHS linker in toluene, a contact angle was measured to be 70(4)°, and for the second use on different samples, the average contact angle was 69(4)°. Therefore, it is possible to

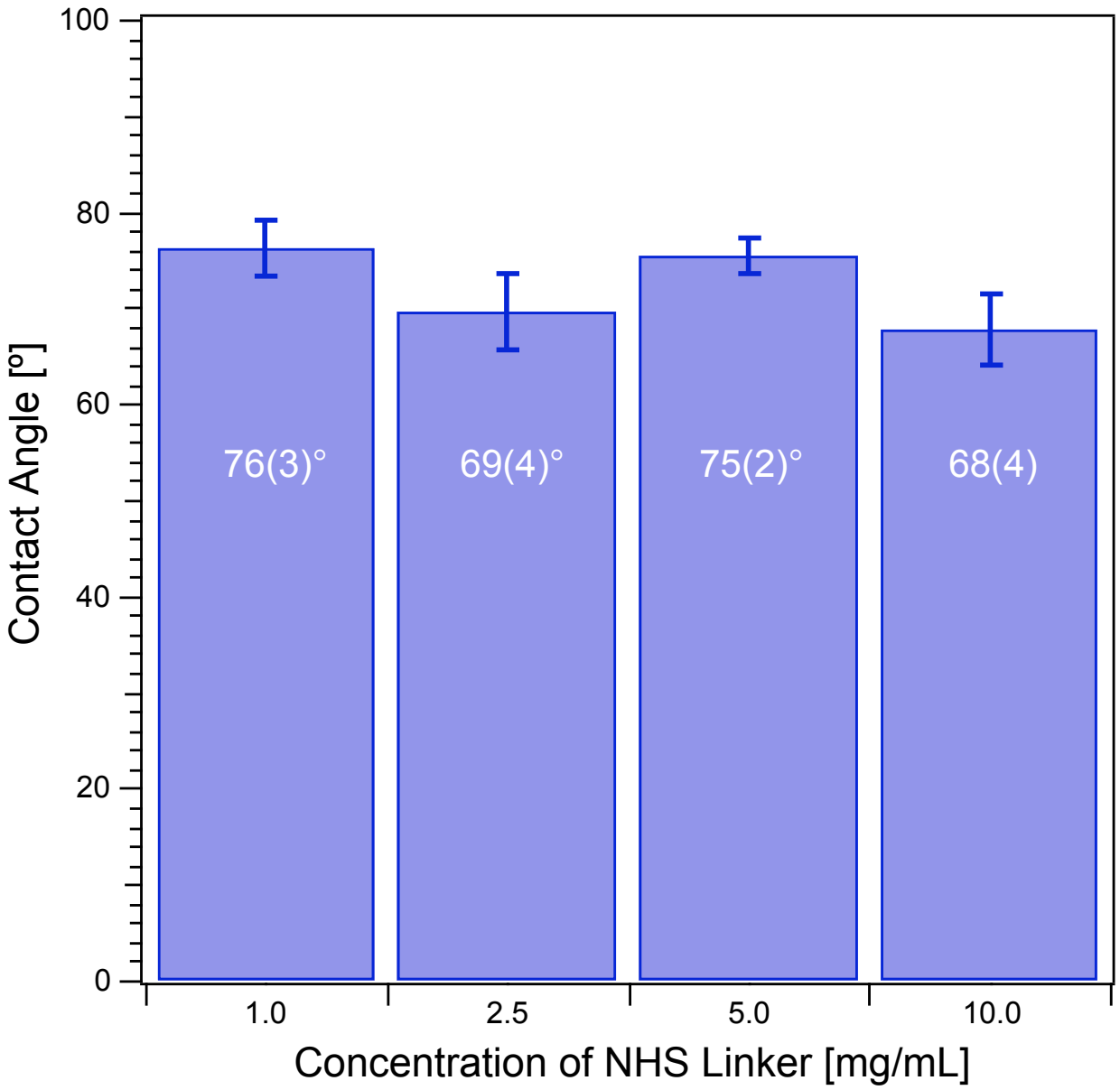

Figure 3.3. Contact Angle as a Function of NHS Linker Concentration
Contact angles were measured on surfaces functionalized with various concentrations of the NHS linker. 7-10 Measurements were collected on at least 4 samples per surface. The average angles for 1.0, 2.5, 5.0, and 10.0 mg/mL are 76(3)°, 69(4)°, 75(2)°, and 68(4)°, respectively.

A

NHS [mg/mL]	θ - 1st use	θ - 2nd use
2.5	70(4)°	69(4)°
5.0	67(4)°	69(4)°

B

NHS [mg/mL]	Sonication?	θ
1.0	N	81(5)°
5.0	N	81(7)°
1.0	Y	76(3)°
5.0	Y	75(2)°

Table 3.1. Surface Preparation Characterized by Contact Angle Goniometry
A) Contact angles, θ, show no significant change when NHS reaction solution is reused a 2nd time to functionalize slides. **B**) Sonicating slides after functionalization removes hydrophobic particles and reduces the standard deviation in the measurements.

reuse the NHS linker solution for sequential reactions in the glove box without significant changes in the NHS surface coverage.

Contact angles were also used to determine an appropriate rinsing procedure following the NHS linker reaction with the glass slides and fused quartz hemispheres. Previously, samples were only rinsed in toluene after removal from the glove box and then annealed in the oven (vide supra). Small, polymerized linker clusters were visible while rinsing. To determine how these clusters effected sample preparation, average contact angles were measured for both sonicated and non-sonicated solutions of 1- and 5-mg/mL NHS (Table 3.1b). The standard deviations of the non-sonicated samples were larger than those of the sonicated samples, which indicates that sonication produces a more uniform distribution of NHS. Not all the clusters were removed by toluene rinsing; thus, the sonication step is necessary for an even NHS sample coverage. The sonication effects were also studied by fluorescence confocal microscopy (see Appendix 4.2.2).

3.4 Summary

In conclusion, we have developed a versatile functionalization strategy for the preparation of our DNA interfaces, which serve as mimics of biosensor surfaces. The NHS linker covalently tethers the DNA oligonucleotides to the fused quartz hemispheres via a hydrocarbon chain and an amide bond. We are able to choose the length and sequence of the DNA strands, as well as any 5’ or 3’-modifications. The preparation conditions have been well characterized, and the cleaning process and reaction steps are optimized for achieving an evenly distributed DNA surface coverage. A standardized surface preparation procedure is essential for SHG and SFG experiments, which provide insight into how DNA-functionalized interfaces behave.

CHAPTER 4

SHG $\chi^{(3)}$ Technique for Off-Resonant Charge Screening

Portions of this chapter are reproduced in part
with permission from the American Chemical Society:

Boman, F.C.; Musorrafiti, M.J.; Gibbs, J.M.; Stepp B.R.; Salazar, A.M.; Nguyen, S.T.; Geiger, F.M. "DNA Single Strands Tethered to Fused Quartz/Water Interfaces Studied by Second Harmonic Generation." *Journal of the American Chemical Society*, **2005**, *127*, 15368-15369.

Stokes, G.Y.; Gibbs-Davis, J.M.; Boman, F.C.; Stepp, B.R.; Condie, A.G.; Nguyen, S.T.; Geiger, F.M. "Making 'Sense' of DNA." *Journal of the American Chemical Society*, **2007**, *129*, 7492-7493.

Boman, F.C.; Gibbs-Davis, J.M.; Heckman, L.M.; Stepp, B.R.; Nguyen, S.T.; Geiger, F.M. "DNA at Aqueous/Solid Interfaces- Chirality-Based Detection via Second Harmonic Generation Activity." *Journal of the American Chemical Society*, **2008**, *in press*.

4.1 Introduction

Second harmonic generation (SHG)[1-9] was used as an optical voltmeter to obtain, without the use of labels, the full thermodynamic state information for surface-bound (sb) DNA as a function of the ionic strength in the surrounding aqueous solution. This method, pioneered by Eisenthal and co-workers[10-13] and Shen and co-workers[14] who called it the "$\vec{\vec{\chi}}^{(3)}$technique", is applied here to track the interfacial potential set up by the phosphate charges along the backbone of the oligonucleotides. The phosphate groups act as intrinsic labels, eliminating the need for any DNA modification. In the $\vec{\vec{\chi}}^{(3)}$technique, the nonlinear optical response, the SH E-field, is expressed as proportional to the interfacial electrostatic potential (vide infra).[10,14] From the interfacial potential, we calculated the surface charge density, and then, since the number of charges per DNA strand is known, we determined the DNA surface coverage.[15-17] In order to determine the aforementioned thermodynamic parameters, as well as the interfacial free energy density, SHG $\vec{\vec{\chi}}^{(3)}$ charge screening experiments were carried out by measuring the SH signal generated by single-strand DNA (ssDNA) covalently attached to the fused quartz/water interface in the presence of increasing bulk NaCl concentration maintained at pH 7.

4.1.1 Electrostatic Field Established at Interface

The $\vec{\vec{\chi}}^{(3)}$ technique[10-14] is interface-specific due to the localization of charges at the interface and can be used to directly measure the interfacial potential, Φ_o,[7,10-12,18] with high sensitivity.[19-23] In this method, the square root of the measured SHG intensity, which yields the SH E-field, is expressed via a second-order response (Chapters 2 and 5) to which one adds a third-order term, stemming from an electrostatic field interacting with the third order nonlinear susceptibility tensor, $\vec{\vec{\chi}}^{(3)}$.[24-26] The third-order process involves the interaction of three electric

fields at the interface. When a high number density of charges exists at an interface under low charge screening conditions, a large electrostatic field, $\vec{\Phi}$, is produced which extends far into the bulk solution. On a molecular level, the interfacial potential polarizes and aligns the water molecules within the diffuse electric double layer (EDL), presumed to be present at a charged aqueous/solid interface.[27-29]

The third-order susceptibility, $\vec{P}_{2\omega}^{(3)}$, is equal to the product of $\vec{\vec{\chi}}^{(3)}$, the two applied electric probe fields, $\vec{E}_{\omega}$, oscillating at a frequency ω, and the electrostatic field, $\vec{\Phi}$, which can be integrated from the interface, at z=0, to the bulk, at z=∞. This yields Equation 4.1, where the potential is Φ_o at the interface and decays to 0 far into the bulk.[2,8,11,28]

$$\vec{P}_{2\omega}^{(3)} = \vec{\vec{\chi}}^{(3)}\vec{E}_{\omega}\vec{E}_{\omega}\vec{\Phi} = \vec{\vec{\chi}}^{(3)}\vec{E}_{\omega}\vec{E}_{\omega}\int_0^{\infty}\vec{\Phi}(z)dz = \vec{\vec{\chi}}^{(3)}\vec{E}_{\omega}\vec{E}_{\omega}\Phi_o \tag{4.1}$$

For a charged interface, the expression for $\vec{P}_{2\omega}^{(3)}$ can be inserted into Equation 2.3, and, therefore, the SH E-field, $\vec{E}_{2\omega}$, can be described as a sum of second- and third-order terms.[11,12,24-26,30-36]

$$\vec{E}_{2\omega} \propto \vec{P}_{2\omega} = \vec{\vec{\chi}}^{(2)}\vec{E}_{\omega}\vec{E}_{\omega} + \vec{\vec{\chi}}^{(3)}\vec{E}_{\omega}\vec{E}_{\omega}\Phi_o \tag{4.2}$$

The incident electric field, $\vec{E}_{\omega}$, is held constant throughout the experiments, and $\vec{\vec{\chi}}^{(2)}$ and $\vec{\vec{\chi}}^{(3)}$ are constants related to the intrinsic properties of the interface and the energy of the incident laser.

There are two explanations for the origin of the $\vec{\vec{\chi}}^{(3)}$ process: an electronic and orientational contribution to $\vec{\vec{\chi}}^{(3)}$ [11,28,37,38] and a self-heterodyning of $\vec{\vec{\chi}}^{(2)}$ and $\vec{\vec{\chi}}^{(3)}$. In the first case, there is a purely electronic third-order nonlinear polarizability, $\vec{\vec{\alpha}}^{(3)}$, from the probed water molecules. Also, the polarization and net orientation of the water molecules breaks the inversion symmetry of the bulk solution and contributes to the SH signal, where normally they are randomly oriented and do not contribute to $\vec{\vec{\chi}}^{(2)}$. The sum of these two contributions is expressed

in the third-order polarization, $\vec{P}_{2\omega}^{(3)}$. The relative magnitude of $\vec{\vec{\chi}}^{(3)}$ with respect to $\vec{\vec{\chi}}^{(2)}$ can be estimated for the water molecules. Typically, $\vec{\vec{\chi}}^{(3)}$ is around 5-7 orders of magnitude smaller than $\vec{\vec{\chi}}^{(2)}$.[8] The number of water molecules at the surface that contributes to $\vec{\vec{\chi}}^{(2)}$ is 1-2 orders of magnitude smaller than the number in the volume probed by the laser that contributes to $\vec{\vec{\chi}}^{(3)}$ (30-μm diameter spot size, 30 Å^3 per water molecule, 0.5-10-nm Debye length, [NaCl]= 0.001-0.5 M). Therefore, the net water molecule contribution to $\vec{\vec{\chi}}^{(3)}$ is approximately 3-6 orders of magnitude smaller than the contribution to $\vec{\vec{\chi}}^{(2)}$.

In the second case, the small magnitude of $\vec{\vec{\chi}}^{(3)}$ can be probed in an optical self-heterodyned fashion,[39-47] where the third-order term acts as a local oscillator and drives the second-order response with remarkable sensitivity. The SH signal, I_{SHG}, is equal to the square modulus of the polarization at the frequency 2ω. Because this is composed of a $\vec{\vec{\chi}}^{(2)}$ and $\vec{\vec{\chi}}^{(3)}$ term, the polarization includes a cross term proportional to $\vec{\vec{\chi}}^{(2)}\vec{\vec{\chi}}^{(3)}$. While the $\left|\vec{\vec{\chi}}^{(3)}\right|^2$ term is negligible and the $\left|\vec{\vec{\chi}}^{(2)}\right|^2$ term dominates, the cross term still contributes to the SH signal.

$$I_{SHG} = \left|\vec{P}_{2\omega}\right|^2 = \left|\vec{\vec{\chi}}^{(2)}\vec{E}_{\omega}\vec{E}_{\omega} + \vec{\vec{\chi}}^{(3)}\vec{E}_{\omega}\vec{E}_{\omega}\Phi_o\right|^2 \tag{4.3}$$

By detecting at a frequency away from an electronic resonance of the sb-DNA, the non-resonant SH signal can be isolated from $\vec{\vec{\chi}}_{Rv}^{(2)}$, according to Equation 4.2. If the experiments are carried out at constant pH and varied salt concentrations, the measured SH E-field response yields the surface charge density[10,14,19-23] via various EDL models.[27,48,49] For a ssDNA-functionalized surface at a high salt concentration, a large number of counterions are present to stabilize and screen the negative charges along the phosphate backbone (Figure 4.1a-b). Thus, Φ_o

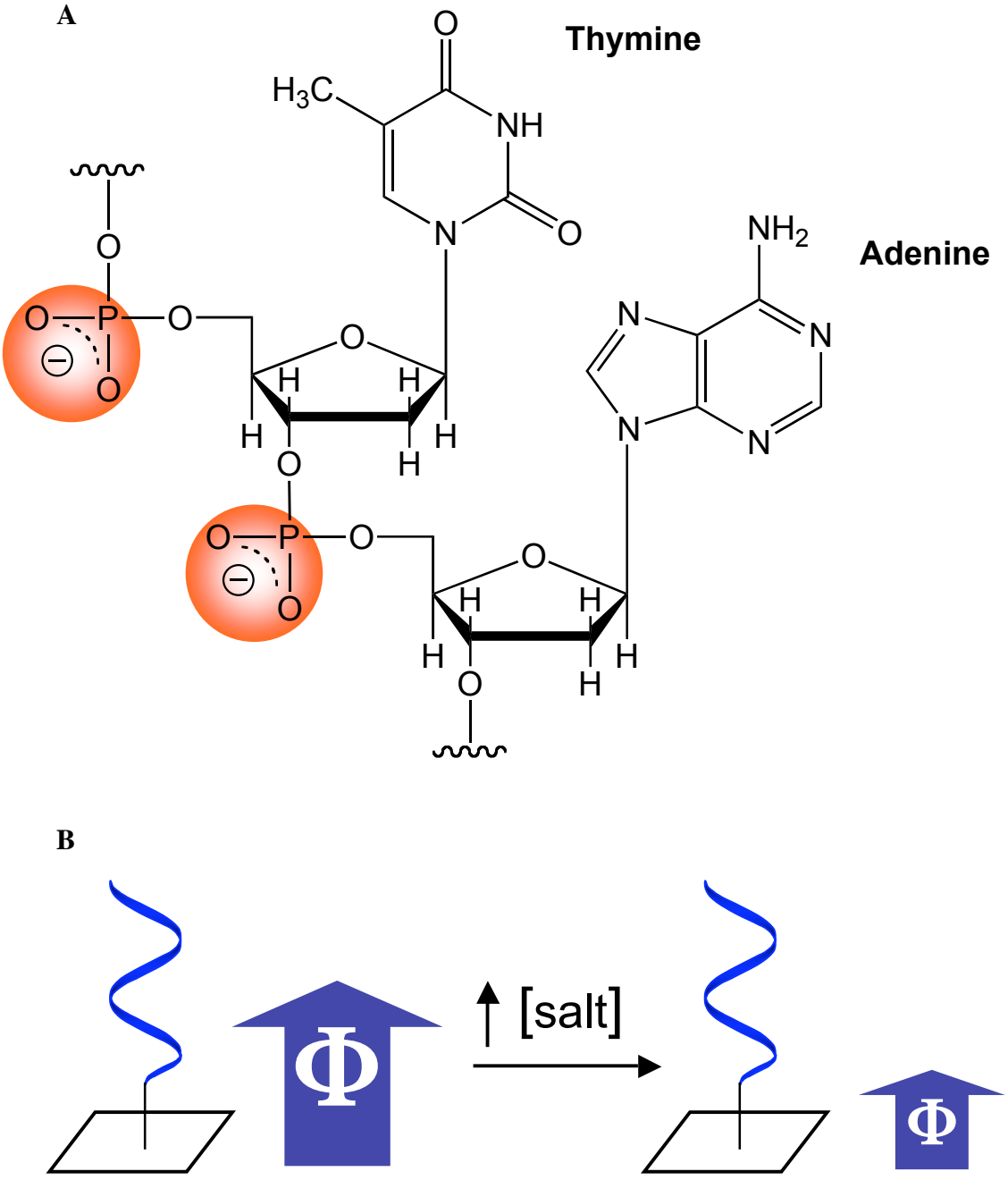

Figure 4.1. Charge Screening of the DNA Phosphate Backbone
A) Negative charges on the phosphate groups along DNA backbone act as intrinsic labels in the nonlinear optical measurements. Thymine and adenine bases are shown. **B**) Negatively charged DNA strands setup a large interfacial potential. As the concentration of counterions is increased, the charges are screened out, lowering the interfacial potential.

is small and, according to Equation 4.2, results in a smaller $\ddot{\chi}^{(3)}$ contribution to the SH E-field. In contrast, at low salt concentrations, fewer counterions are present in the solution to screen the negative charges, leading to a higher total Φ_o and SH E-field. A near-neutral surface, such as the uncharged NHS linker, would not be expected to exhibit a large charge screening effect.

4.1.2 Gouy-Chapman Model of Interfacial Potential

One of the most commonly accepted EDL models for describing a potential at a planar charged interface is the Gouy-Chapman (GC) model,[14,49-53] otherwise known as the Diffuse Layer model.[54-56] The GC model assumes the potential is established by a uniform sheet of charge submersed in a z:z symmetric electrolyte solution. In the context of our work on DNA, the charges are distributed along the DNA strands on the surface. Although the GC model is limited in scope, it is useful as a springboard for more complex models.[57-59] The GC theory has been used to describe the EDL for metal oxide/water interfaces,[53-56,60] where the interfacial potential as a function of electrolyte solution is an exact solution to the Poisson-Boltzman equation:[27,61,62]

$$\Phi_o = \frac{2k_BT}{ze}\sinh^{-1}\left(\sigma_o\left(\frac{\pi}{2\varepsilon k_BTc}\right)^{1/2}\right) \tag{4.4}$$

where σ_o is the surface charge density, k_B is the Boltzman constant, T is the temperature, z is the valence of the salt, e is the elementary charge on an electron, ε is the dielectric constant of water, and c is the electrolyte concentration.

It is assumed that ε is constant within the region measured and does not deviate significantly from its bulk value of 78 at 25 °C. A sensitivity analysis of ε was performed for Φ_o and the results are shown in Figure 4.2. The dielectric constant is a few percent lower in salt solutions. This dependence on salt concentration and ion identity is given by:[48,63]

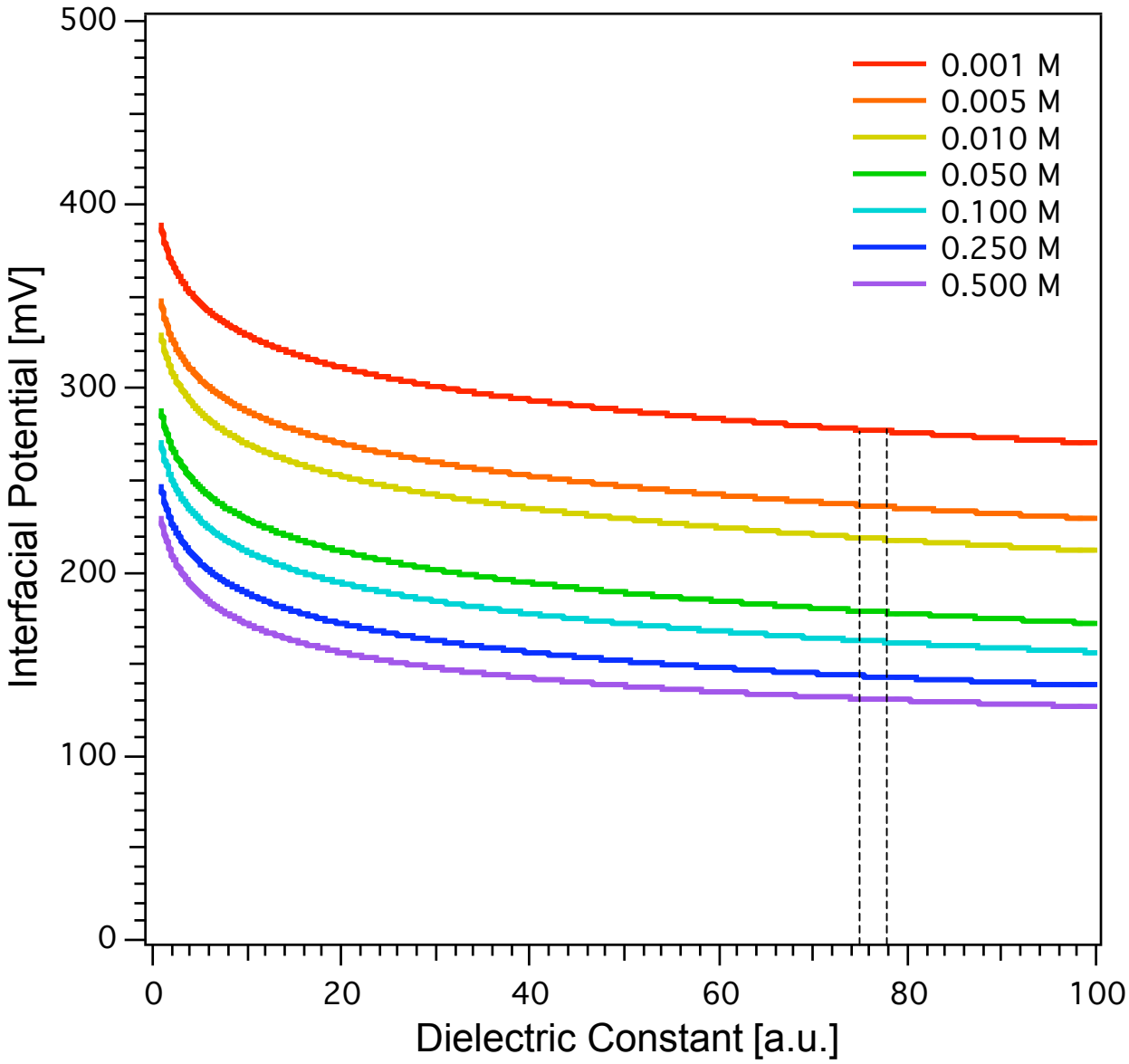

Figure 4.2. Sensitivity Analysis of Dielectric Constant for Interfacial Potential
The interfacial potential, Φ_o, is shown as a function of the dielectric constant of water, ε, for NaCl concentrations ranging from 0.001 M to 0.500 M. The interfacial potential was calculated with the surface charge density, σ_o, for T_{25} DNA. The dashed lines indicate the range that ε varies, 75.25-79.99, for the NaCl concentrations used in our experiments. The GCS model assumes that ε does not significantly deviate from its bulk value of 78 at 25 °C.

$$\varepsilon_{ss} = \varepsilon_{sw} + \delta c \tag{4.5}$$

where ε_{ss} is the static dielectric of the salt solution, ε_{sw} is the static dielectric of water, and δ is the dielectric decrement. For NaCl solutions, δ is –5.5, and ε_{ss} ranges from 77.99 for 0.001 M to 75.25 for 0.5 M. According to Figure 4.2, the magnitude of Φ_o increases only 0.33% and 0.44% for these concentrations; therefore, treating ε as its bulk value is a valid approximation.

When pH is held constant, σ_o does not change, making c, the electrolyte concentration, the only independent variable since $\vec{\vec{\chi}}^{(2)}$, $\vec{\vec{\chi}}^{(3)}$, $\vec{E}_\omega$ and are constant values for a particular system. Therefore, Equation 4.2 can be simplified into a practical equation for the $\vec{\vec{\chi}}^{(3)}$ technique:

$$\sqrt{I_{SHG}} = E_{SHG} \propto A + B\Phi_o \tag{4.6}$$

Equation 4.6 demonstrates that a change in I_{SHG} directly results from a change in Φ_o.

4.2 Thermodynamic Analysis of Charged Interfaces

4.2.1 Surface Charge Density

In order to quantify the number density of the sb-DNA strands, we screened the interfacial charges along the DNA backbone by adding increasing amounts of NaCl to the aqueous solution above the surface while recording the SHG signal intensity. The T_{15} ssDNA and NHS linker-functionalized fused quartz/water interfaces were prepared as described in Chapter 3 and buried under an aqueous solution that ranged from 1.0 mM to 1.0 M NaCl at pH 7. Using the $\vec{\vec{\chi}}^{(3)}$ technique, the interfacial potential originating from the tethered ssDNA was modeled as a function of NaCl concentration (Figure 4.3). The surface was probed with 0.7 μJ of 640-nm p-polarized fundamental light, and the p-polarized SH signal was collected at 320 nm using single

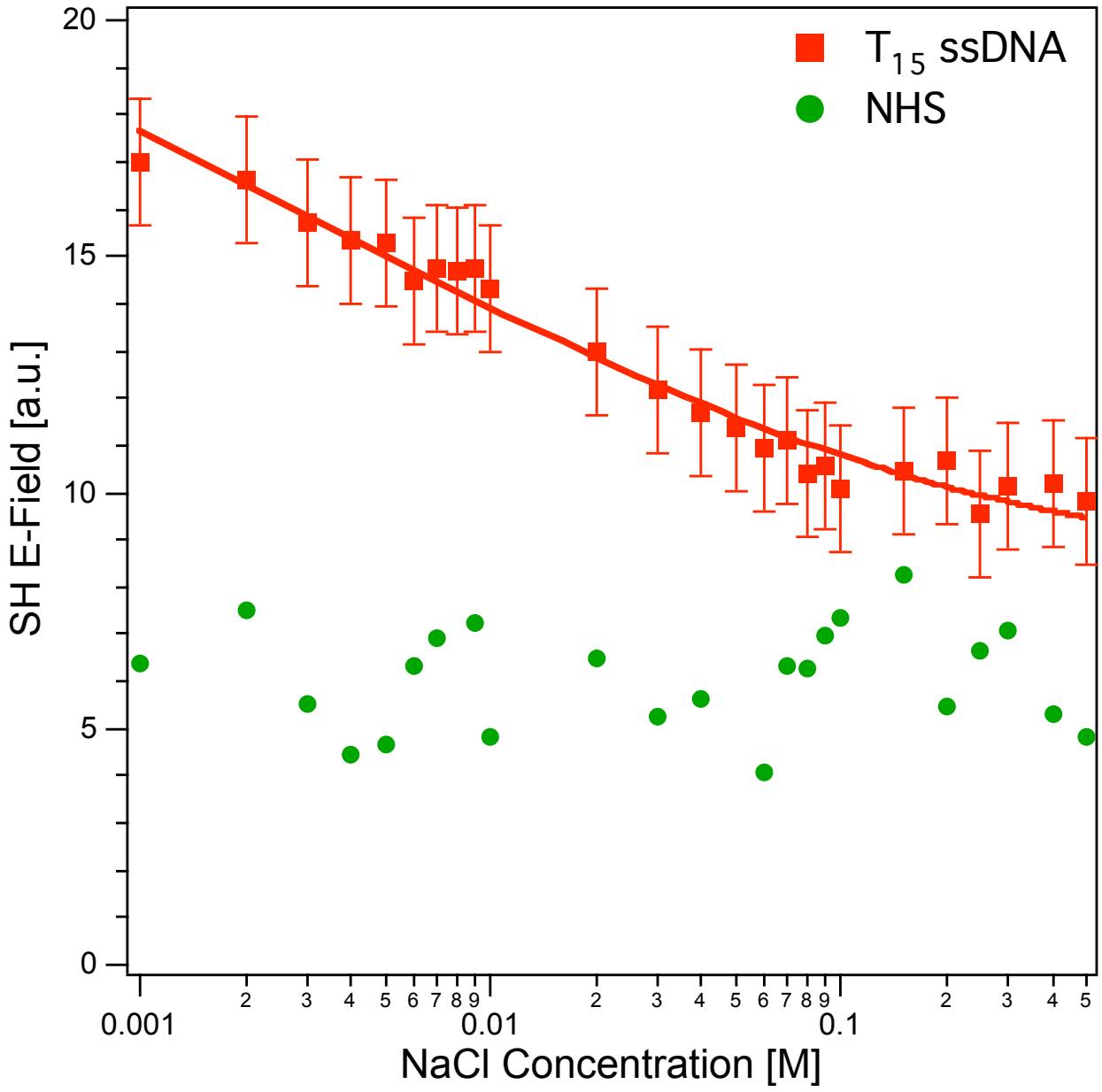

Figure 4.3. SH E-Field vs. Salt Concentration for T_{15} and NHS Linker
The SH E-field (p-in/p-out) is shown vs. salt concentration on a log scale at pH 7 for the T_{15} ssDNA (red squares) and the NHS linker (green circles) anchored to a fused quartz/water interface. The interfacial potential is calculated using the GC model (red line).

photon counting techniques. In order to verify that the contribution for $\vec{\chi}^{(2)}$ is not in resonance with the applied E-field, we collected SH spectra of the NHS linker- and the ssDNA-functionalized interfaces (see Chapter 5). Neither the NHS linker of the ssDNA exhibit an electronic resonance in the UV-Vis wavelength region examined here, therefore, there is no interference from a resonant contribution to the SH signal.

Figure 4.3 shows that the measured SH E-field of the NHS-functionalized interface remains relatively constant and does not show appreciable salt screening, as was expected from a neutral interface. In contrast, the T_{15} ssDNA-functionalized interface exhibits screening of the interfacial potential, setup by the negative charges along the DNA phosphate backbone, with increased NaCl concentration. The GC model was applied according to the procedure outlined by Eisenthal and coworkers[10,18,28] in order to quantify the interfacial surface potential, and the fit to Equation 4.6 for the T_{15} ssDNA is also shown in Figure 4.3. The surface charge density, σ_o, was calculated as $9(2) \times 10^{-3}$ C/m^2 for the single-stranded oligonucleotide.[21]

4.2.2 DNA Surface Coverage

If the $\vec{\chi}^{(3)}$ experiment samples all negative charges along the backbone equally, the calculated surface charge density of $9(2) \times 10^{-3}$ C/m^2 would correspond to a surface coverage, Γ, around $5(1) \times 10^{11}$ strands/cm^2 or 0.8 pmol/cm^2. This is in agreement with the experimental range between 1×10^{11} and 3×10^{13} strands/cm^2 for DNA surface density values on gold and silica obtained from other surface techniques, such as x-ray photoelectron spectroscopy (XPS), Fourier-transform IR (FTIR) spectroscopy, atomic force microscopy (AFM), surface plasmon resonance (SPR) spectroscopy, electrochemistry, and fluorescence.[64-72]

4.3 Variation of DNA Oligonucleotide Strand Lengths

We again applied SHG as an optical voltmeter to determine the interfacial potential of oligonucleotides of varying lengths. The DNA strand densities were calculated under the assumption that the SH signal uniformly samples each oligonucleotide base, and charge contribution was resolved by varying the length of the tethered DNA strands. The average surface charge resulting from an individual base can be inferred from the linear relationship between the number of charges per strand and the surface charge density. Therefore, charge screening experiments were performed on fused quartz/water interfaces functionalized with oligonucleotides containing 15, 25, 30 and 35 thymine nucleotides. Each charge screening experiment was carried out in triplicate, and the data were normalized to the SHG intensity at the highest salt concentration.

4.3.1 Limitations in the Gouy-Chapman Model

We again fit the GC model to our data as in Section 4.2.1, but the fits were not able to differentiate between the different surface change densities for each strand length. Therefore, because of the large error in the fit, we concluded that a more rigorous model was necessary for our system. We fit the Gouy-Chapman-Stern (GCS) model[49,52-56,73-77] to the data because of its versatility in describing the surface behavior of a variety of analytes over a wide range of ionic strengths (Figure 4.4). In contrast to the GC model, which only uses the diffuse layer to describe the interfacial potential,[53,56,75,78] the GCS model takes into account the capacitor-like layer formed by the screening metal ions and the charged phosphates.

Another important consideration with respect to the GCS model is that the interfacial potential remains approximately linearly dependent on surface charge density even at high

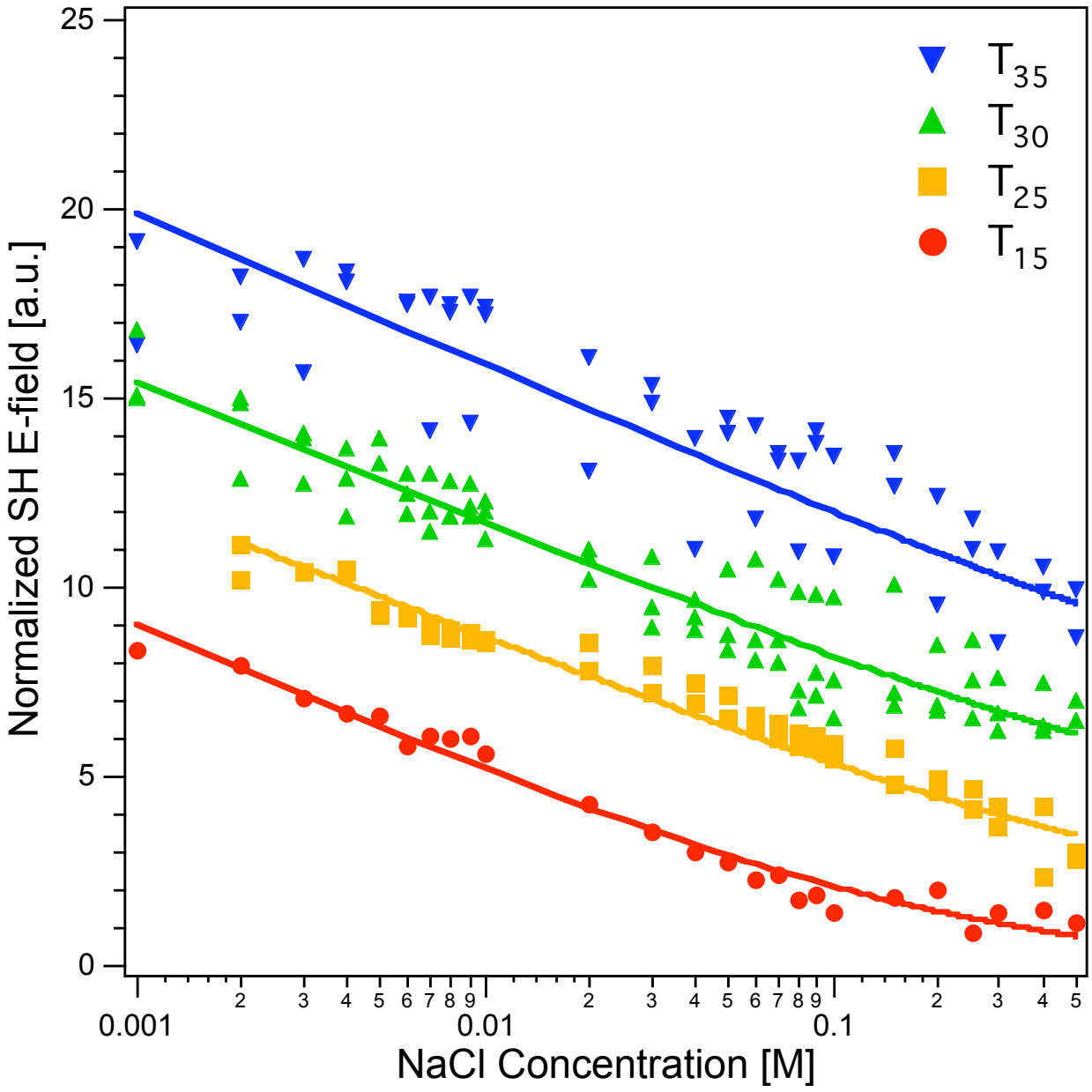

Figure 4.4. SH E-Field vs. Salt Concentration for a Range of DNA Strand Lengths
The SH E-field (p-in/p-out) is shown vs. salt concentration on a log scale at pH 7 for the T_{15} (red circles), T_{25} (orange squares), T_{30} (green triangles), and T_{35} (blue triangles) ssDNA oligonucleotides anchored to a fused quartz/water interface. The data for each DNA length are offset on the y-axis for clarity. The interfacial potentials are calculated using the GCS model (solid lines).

surface charge densities. The GC model fails at high surface charge densities and interfacial potentials exceeding ~100 mV,[23,38] which occurs because the sensitivity of the potential on the surface charge density becomes highly nonlinear, and consequently, the SHG sensitivity becomes highly nonlinear (Figure 4.5).[79] Therefore, we conclude that the GCS model is better suited for analyzing ssDNA charge screening data.

4.3.2 Gouy-Chapman-Stern Model of Interfacial Potential

The GCS model describes the screening counterions at the Stern Layer (Figure 4.6a).[73,77]The surface contains the surface charge density, σ_o, and interfacial potential, Φ_o. The diffuse plane divides the Stern and the diffuse layers and contains the surface charge density, σ_d, and potential Φ_d. The constant capacitance approach is used to describe the inner Stern layer, and the GC model is used to describe the outer diffuse layer (Figure 4.6b). In our system, the Stern layer contains the negatively charged DNA strands. These strands are not point charges evenly distributed along the surface but instead extend into the aqueous solution with a charge gradient. We treat this layer of DNA as having a constant capacitance, C, where the interfacial potential decreases linearly over a short distance and then decays exponentially as in a normal GC model.

The equations for C and Φ_o according to the GCS model are shown below:[49,52-56,73-77,80]

$$C = \frac{\sigma_o}{\Phi_o - \Phi_d} \tag{4.7}$$

$$\Phi_o = \frac{\sigma_o}{C} + \Phi_d \tag{4.8}$$

$$\Phi_o = \frac{\sigma_o}{C} + \frac{2k_BT}{ze}\sinh^{-1}\left(\sigma_d\left(\frac{\pi}{2\varepsilon k_BTc}\right)^{1/2}\right) \tag{4.9}$$

where σ_o is the surface charge density defined in Section 4.3.1, and C is the constant capacitance

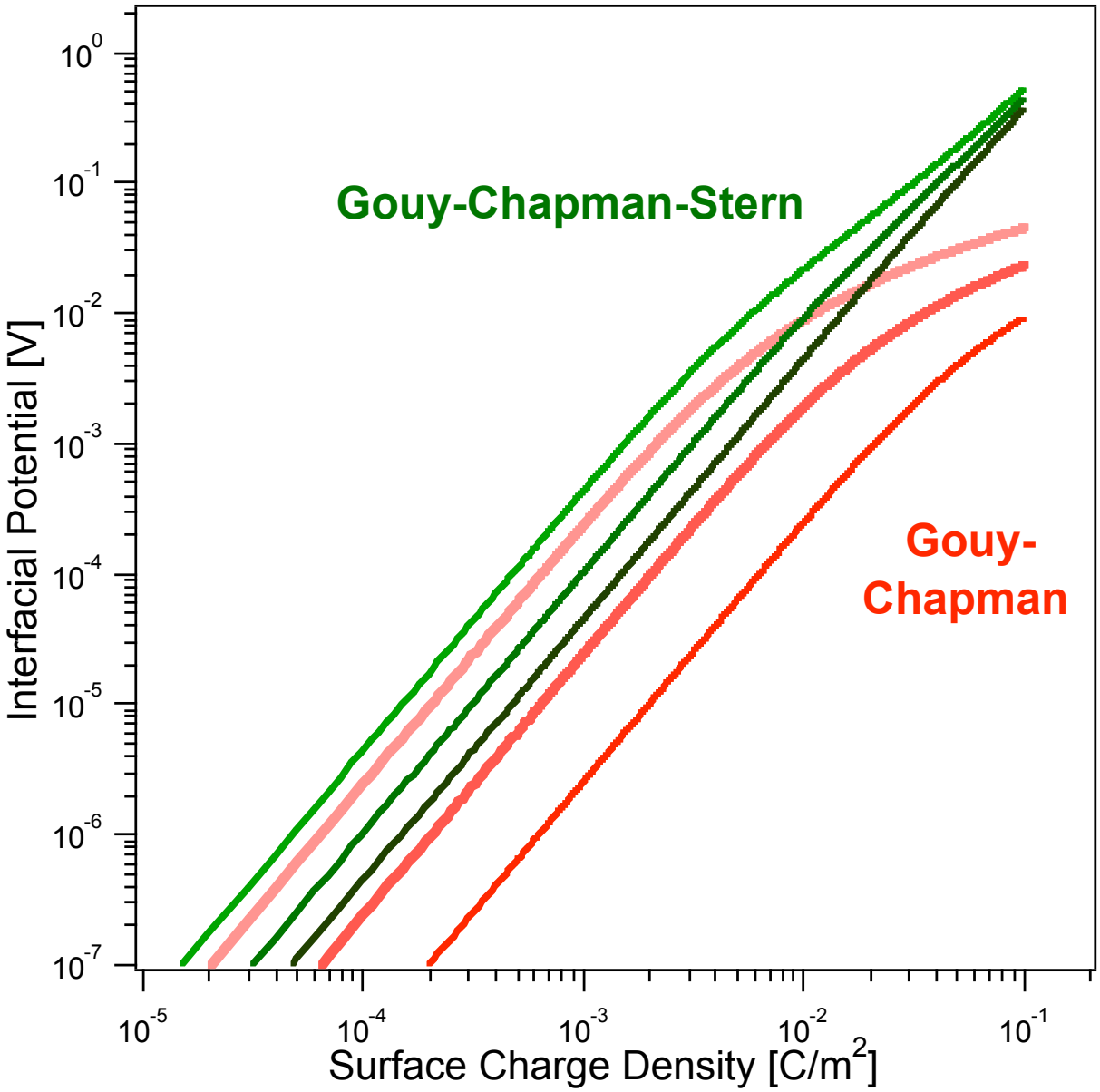

Figure 4.5. Comparison of Interfacial Potential Models
Plots of the GC and GCS models for interfacial potential vs. surface charge density are shown. The GC model is depicted by light to dark red traces, representing NaCl concentration of 0.01, 0.10, and 1.00 M. The GCS model is depicted by light to dark green traces, also representing NaCl concentrations of 0.01, 0.10, and 1.00 M. The GCS model is more sensitive at higher σ_o because the GC model becomes nonlinear at potentials greater than 100 mV.

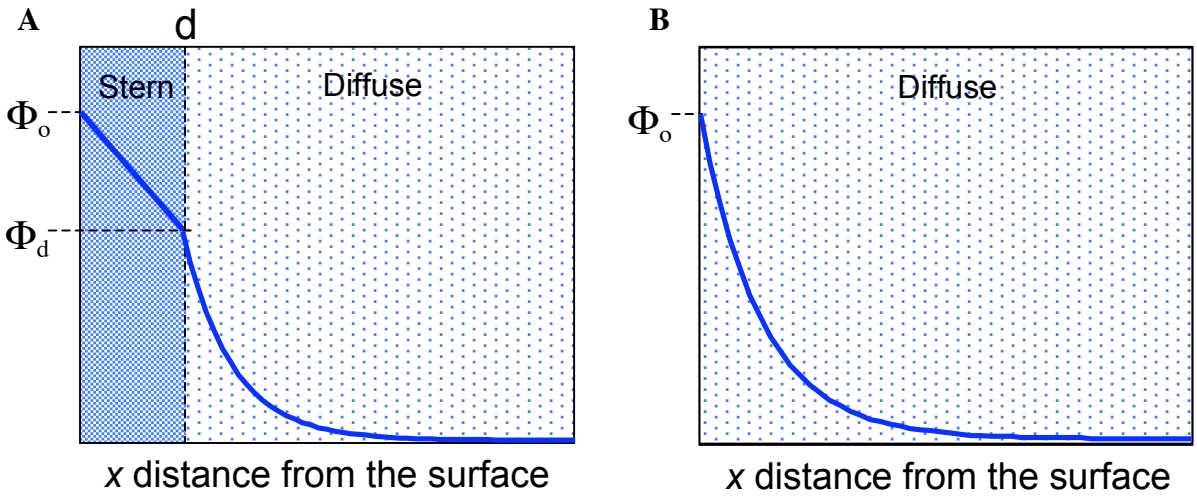

Figure 4.6. Models of Interfacial Potential for the Electric Double Layer
A) Gouy-Chapman-Stern model
B) Gouy-Chapman model

of the Stern layer. We treat C as 0.2 F/m^2, which is commonly used in the GCS model to describe mineral oxide interfaces because it is in reasonable agreement with theoretical potentials in the diffuse place and experimentally observed ξ potentials from electrokinetic studies.[53,56,75] The surface change density σ_d is a theoretical value, and because the EDL is considered electroneutral, $\sigma_o + \sigma_d = 0$.[48,73] The countercharge from the Na^+ ions is diffuse and not specifically adsorbed to the sb-DNA. Therefore, $\sigma_d = -\sigma_o$, and Equation 4.9 can be simplified by substituting σ_o into the arcsinh term.

4.3.3 Surface Charge Density and DNA Surface Coverage

The surface charge densities that were obtained from the GCS model increase linearly with the number of nucleotides (Table 4.1), when fit to the data as shown in Figure 4.7. The slope of a linear least squares fit results in 1.0(1) charges per added nucleotide, which is consistent with the notion that each nucleotide carries a charge of -1 on each phosphate group.[16] Taking the surface charge density and dividing it by the elementary charge on an electron, 1.602 x 10^{-19} C,[62] and the nucleotide length yields an average DNA oligonucleotide strand density of 5 x 10^{11} strands/cm^2 or 0.8 pmol/cm^2 for the various strand lengths investigated here (Table 4.1, Figure 4.7 inset). Given the fact that we are studying the aqueous/solid interface with a focused laser beam illuminating a 30-μm diameter spot, we conclude that we are detecting the SHG response from ~6 attomoles of DNA at the interface. This remarkable sensitivity is due to the self-heterodyning nature of the experiment, in which the second-order response can be viewed as the local oscillator while the third-order terms can be considered the signal.[37] We note that the experiments presented here probe the native systems, i.e. they are label free.

Assuming a uniform distribution of DNA, a strand density of 5 × 10^{11} strands/cm^2

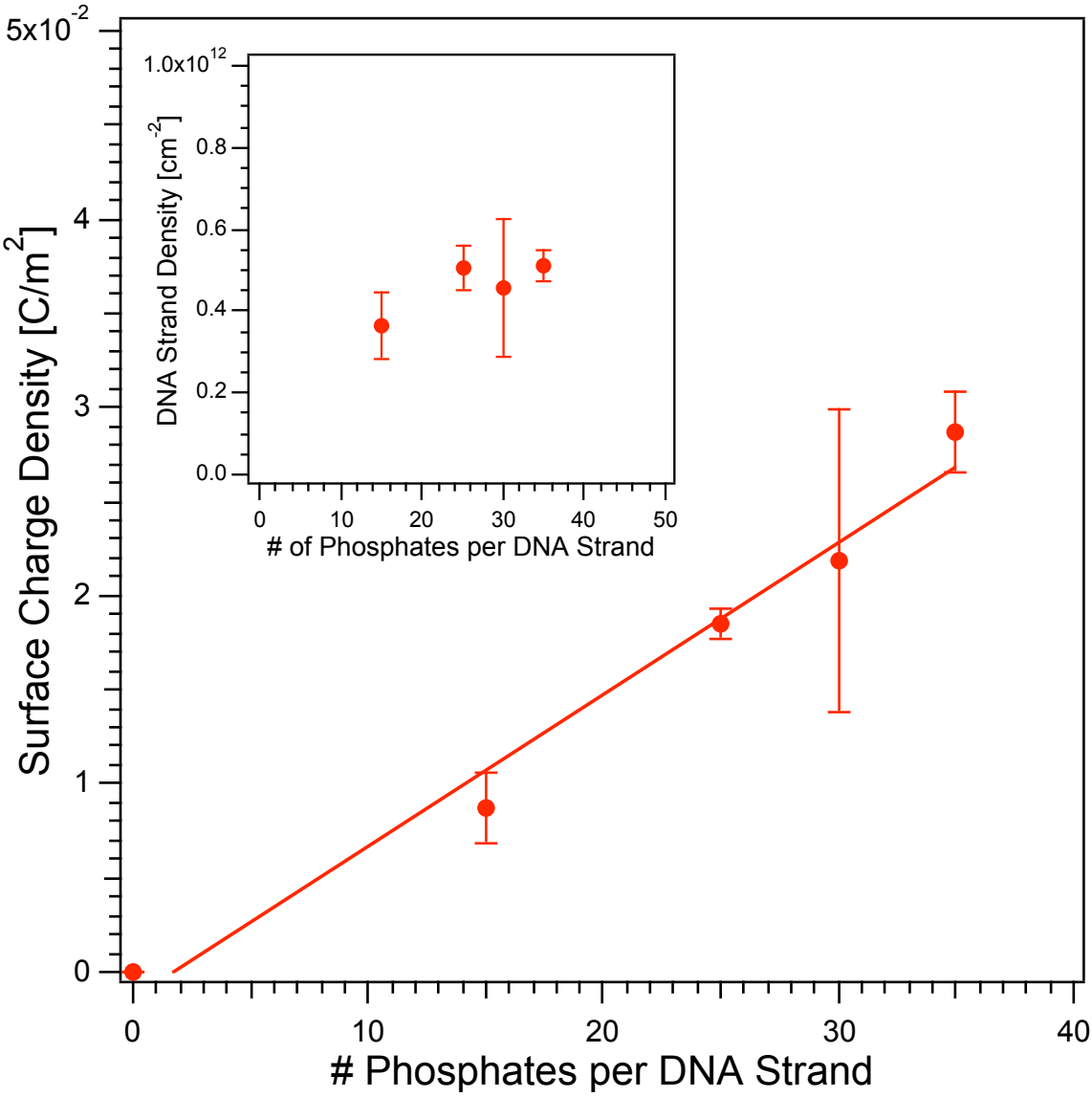

Figure 4.7. Surface Charge Density and DNA Strand Density
Surface charge density (calculated from the GCS model) as a function of the number of charged phosphates per DNA strand. The slope of a linear least squares fit results in 1.0(1) charges per each nucleotide. Inset: The average DNA strand density as a function of DNA nucleotides is 5×10^{11} per cm^2.

# Oligonucleotides	σ_o (C/m^2)	Γ (strands/cm^2)
15	$9(2) \times 10^{-3}$	$3.9(1) \times 10^{11}$
25	$1.9(1) \times 10^{-2}$	$4.8(2) \times 10^{11}$
30	$2.2(1) \times 10^{-2}$	$5(2) \times 10^{11}$
35	$2.9(2) \times 10^{-2}$	$5.3(4) \times 10^{11}$

Table 4.1. Surface Charge Densities and DNA Strand Densities
The surface charge densities, σ_o, for the T_{15}, T_{25}, T_{30}, and T_{35} ssDNA interfaces were calculated according to the GCS model for interfacial potential. The average DNA strand density, Γ, for each ssDNA interface was calculated based on the σ_o and number of negatively charged phosphates per strand.

corresponds to 200 nm^2 surface area per DNA strand. A T_{25}:A_{25} DNA duplex is 8.5 nm long with a 2.0 nm diameter.[16] A schematic representation of a DNA duplex, drawn to scale, is shown with a side and top-down view in Figure 4.8 to give an approximate picture of the space occupied by a DNA strand on the surface. This strand density allows for a possible 100% hybridization efficiency because there is sufficient room for the ssDNA to move on the surface and access the incoming complementary strands and because the strands are not so close as to repel.[81-86]

4.3.4 Interfacial Potential and Interfacial Free Energy Density

To further analyze the data, we have plotted the interfacial potential for the different DNA strand lengths as a function of NaCl concentration from the calculated surface charge densities (Figure 4.9). Between 0.001 M and 0.5 M NaCl, Φ_o decreases from 190(20) to 60(13) mV in absolute value for the T_{15} surface and from 350(15) to 200(14) mV for the T_{35} surface. These ranges are in agreement with theoretical predictions by Pettitt and co-workers.[87]

The change in interfacial free energy density, $\Delta\gamma$, is the product of σ and the change in Φ_o (with respect to a neutral surface), according to the Lippmann equation:[27]

$$\Delta\gamma = -\sigma_o \cdot \Delta\Phi_o \tag{4.10}$$

Equation 4.10 includes the reorganization energy from solvent contributions, such that $\Delta\gamma$ can be treated as a free energy term, ΔG. The inset of Figure 4.9 shows $|\Delta\gamma|$ as a function of NaCl concentration. For the T_{15} and T_{35} surfaces, $|\Delta\gamma|$ decreases from 0.16(5) to 0.05(3) $\mu J/cm^2$ and from 1.0(1) to 0.56(8) $\mu J/cm^2$, respectively, over the same range of NaCl. The free energy describes the energetics that drive molecules from solution to the interface.[27,62,73,88] A small free energy drives more negatively charged molecules to a negatively charged interface than a large free energy would;[27,62,73,88] therefore, this plot shows that the DNA-functionalized interfaces are

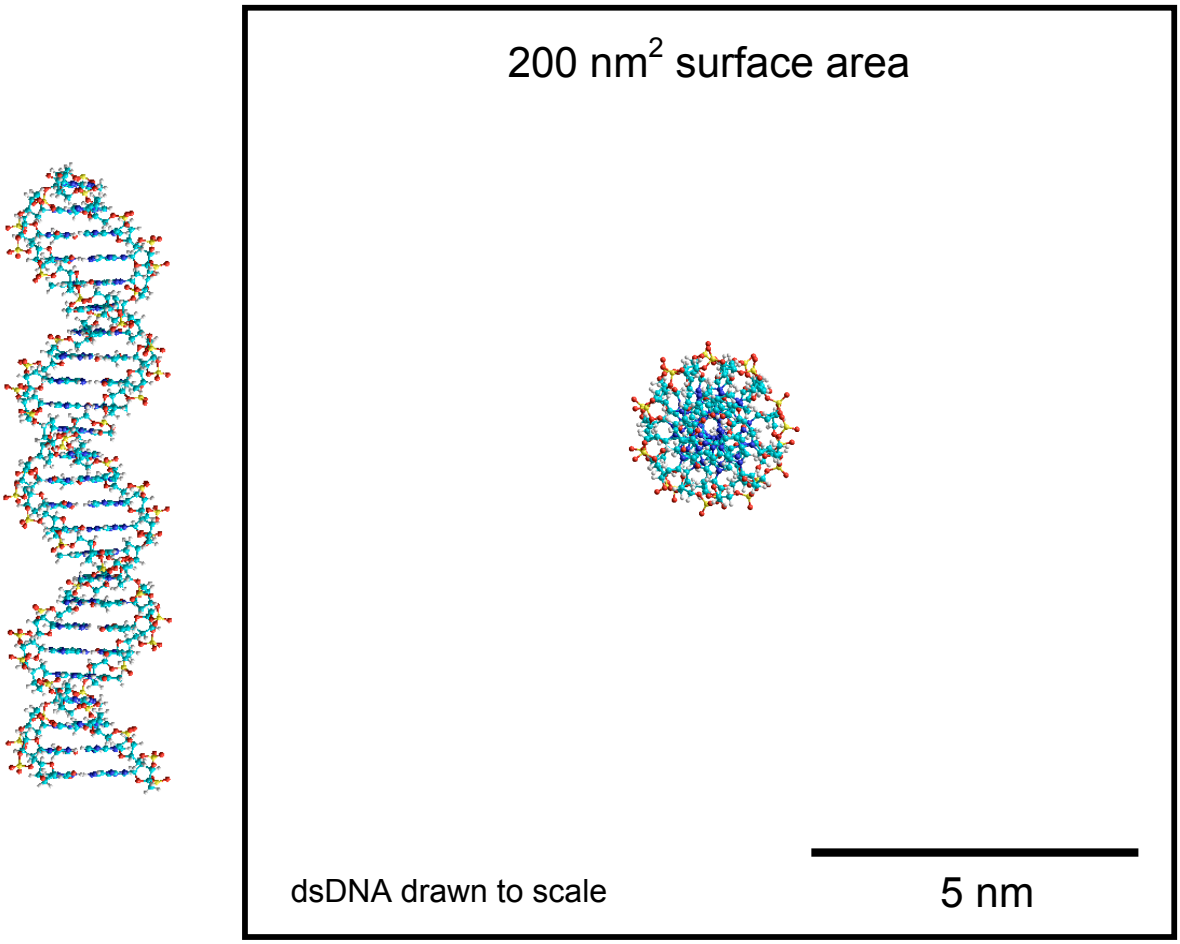

Figure 4.8. Schematic of Approximate Surface Area Per DNA Duplex
Assuming a uniform distribution of DNA, a strand density of 5×10^{11} strands/cm^2 corresponds to 200 nm^2 surface area per DNA strand. The T_{25}:A_{25} DNA duplex is 8.5 nm in length and 2.0 nm in diameter. A DNA duplex (drawn to scale) is shown with a side and top-down view in order to give an approximate picture of the space it occupies on the surface.

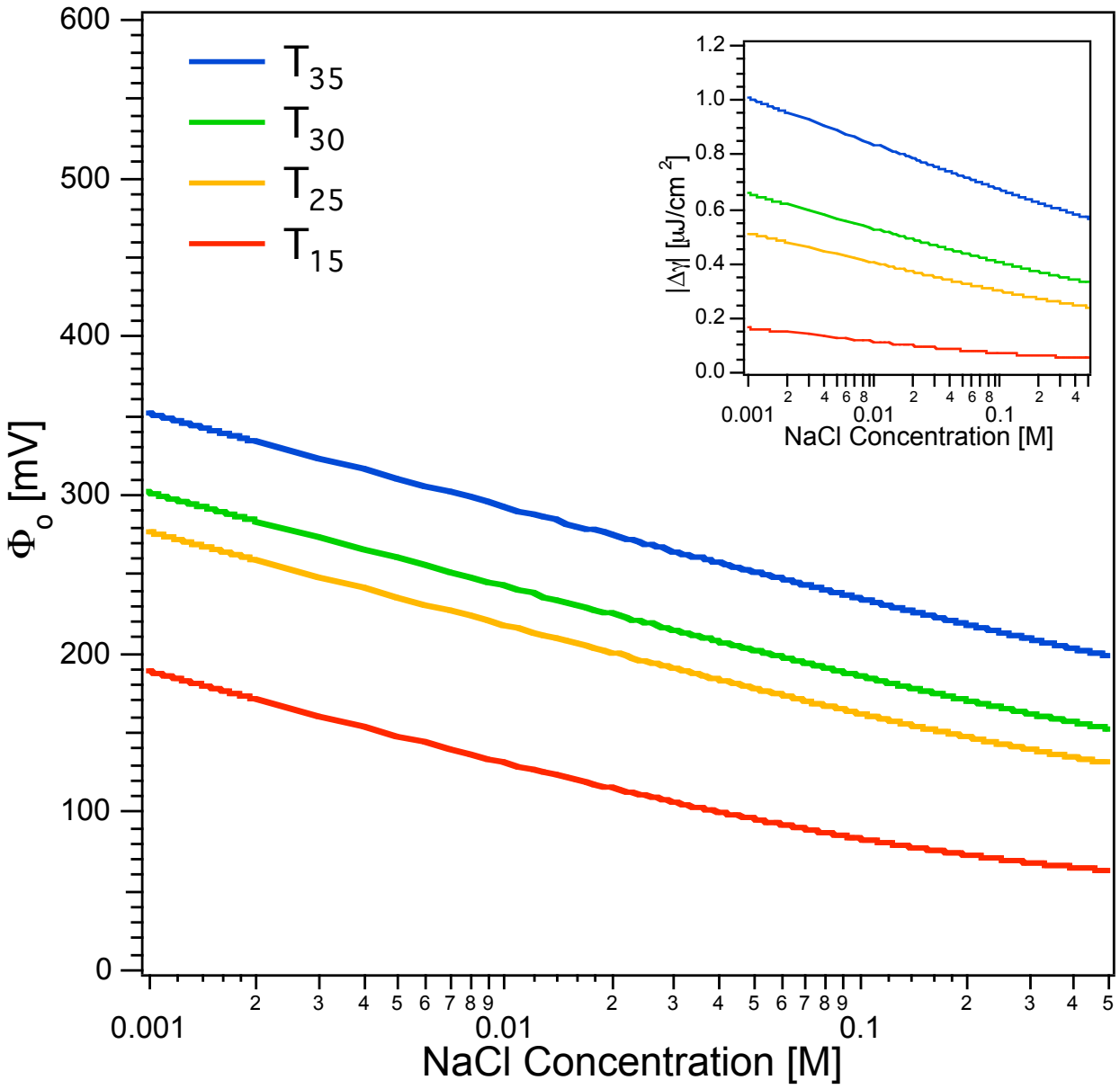

Figure 4.9. Interfacial Potentials and Interfacial Free Energy Densities
Interfacial potentials are shown for the T_{15} (red), T_{25} (orange), T_{30} (green), and T_{35} (blue) DNA single strands as a function of salt concentration on a log scale as calculated from the GCS model. **Inset**: Absolute value of interfacial free energy densities as a function of salt concentration on a log scale are shown for the same DNA single strands as calculated from the Lippmann equation. The slopes increase as the DNA lengths decrease.

more likely to hybridize at high salt concentrations where the negative charges are screened.

4.4 Summary

In conclusion, we have shown that the surface charge density, interfacial potential, and the change in the interfacial free energy density for ssDNA covalently attached to fused quartz/water interfaces can be determined via nonlinear optical measurements, namely the $\vec{\vec{\chi}}^{(3)}$ technique. We have quantified the absolute number densities of DNA oligonucleotides, and these experiments yield DNA surface densities of 4-6 × 10^{11} strands per cm^2, which correspond to ~6 attomoles of DNA in the spot of the laser beam. These results were made possible by a fit of theGouy-Chapman-Stern model that includes a constant capacitance term. Our approach circumvents experimental challenges associated with preparing labeled oligonucleotides and does not require surfaces with high dielectric constants. The results from our measurement can aid in improving the design of new biomaterials and highly sensitive sensors for biodiagnostics. The thermodynamic state information obtained from our $\vec{\vec{\chi}}^{(3)}$ experiments has important implications for predicting and controlling macromolecular DNA behavior and can be used to test and advance theoretical frameworks for understanding biomolecular interactions.

CHAPTER 5

SHG Electronic Resonance Enhancement

Portions of this chapter are reproduced in part
with permission from the American Chemical Society:

Boman, F.C.; Musorrafiti, M.J.; Gibbs, J.M.; Stepp B.R.; Salazar, A.M.; Nguyen, S.T.; Geiger, F.M. “DNA Single Strands Tethered to Fused Quartz/Water Interfaces Studied by Second Harmonic Generation.” *Journal of the American Chemical Society*, **2005**, *127*, 15368-15369.

Boman, F.C.; Gibbs-Davis, J.M.; Heckman, L.M.; Stepp, B.R.; Nguyen, S.T.; Geiger, F.M. “DNA at Aqueous/Solid Interfaces- Chirality-Based Detection via Second Harmonic Generation Activity." *Journal of the American Chemical Society*, **2008**, *in press*.

5.1 Introduction

We have used resonantly enhanced second harmonic generation (SHG)[1-8] as a label-free method to probe, for the first time, electronic transitions of DNA oligonucleotide bases[9-12] by tuning the incident laser to a wavelength at the two-photon electronic resonance of the π-π* transitions that are intrinsic to the bases.[13-16] Resonant SHG experiments were carried out by measuring the SH signal generated by single and double strand DNA (ssDNA and dsDNA) covalently linked to the fused quartz/water interface under 0.25 M NaCl at pH 7. The SH spectra were then compared to the UV-Vis spectra of the DNA in bulk solution. Here, we demonstrate that a strong nonlinear optical response is observed from the DNA-functionalized interfaces due to the resonant enhancement of the second order polarizability tensor.[17,18] The highly sensitive nature of resonant SHG allows for the label-free, sub-monolayer detection of surface-bound (sb) DNA at buried aqueous/solid interfaces *in situ* and in real time.[6-8]

5.2 Electronic Resonance of Bulk DNA

5.2.1 Molecular Structure of DNA

The molecular structure of DNA, originally published by Watson and Crick in 1953 using x-ray diffraction images from Franklin,[19] is composed of two hydrogen-bonded polynucleotide strands aligned in a right-handed, double helix that run anti-parallel to each other (Figure 5.1).[9-12,20] The ribose sugar-phosphate backbone is on the outside of the helix, the purine (adenine and guanine) and pyrimidine (thymine and cytosine) bases are connected to the backbone but face inward towards each other, and the base pair plane is oriented perpendicular to the axis of the double helix. Bases pairs are formed from hydrogen bonds between one purine and one

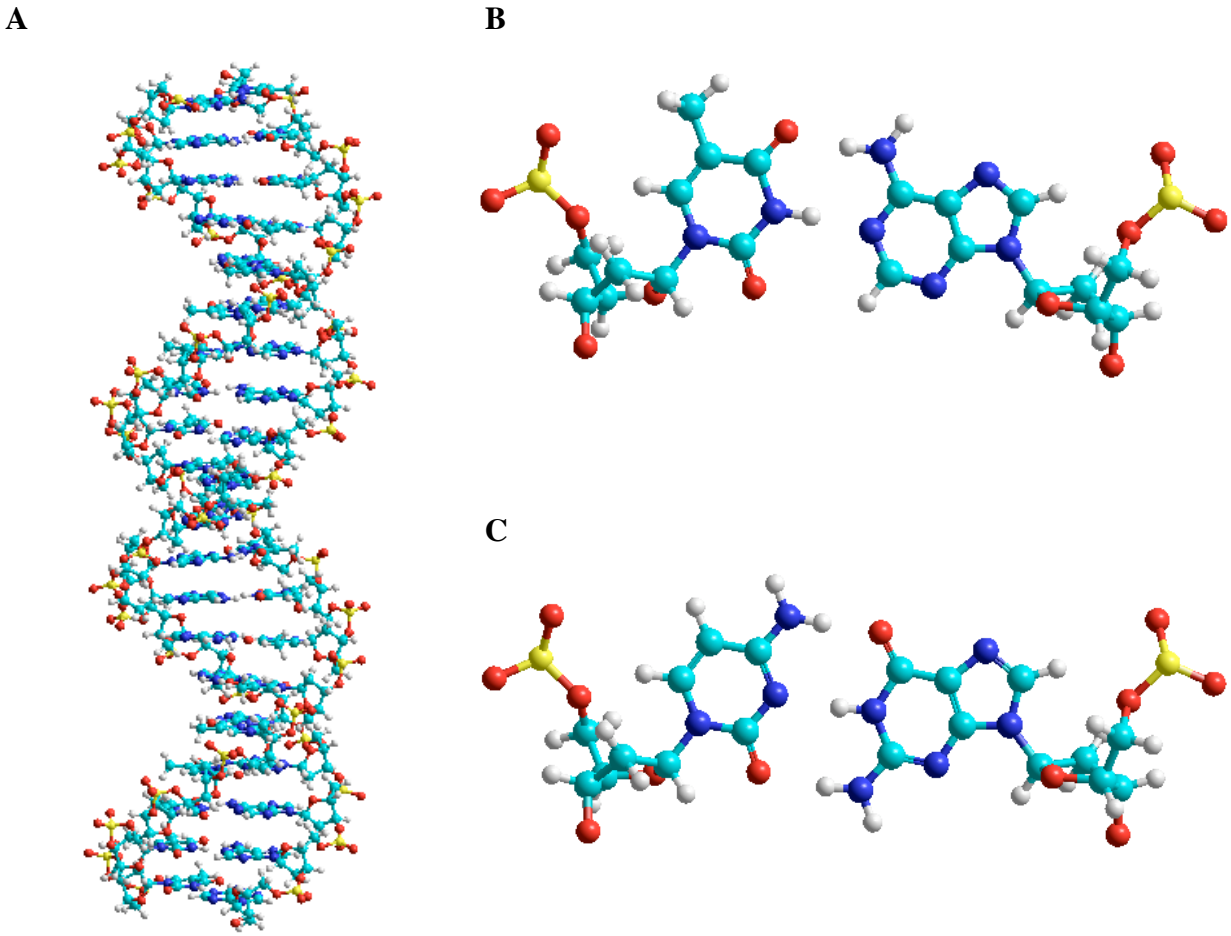

Figure 5.1. Molecular Structure of DNA
A) Side view of a two full turns of a DNA double helix consisting of 20 base pairs. Top-down view of an **B**) adenine-thymine (A:T) base pair and a C) guanine-cytosine (G:C) base pair.

pyrimidine. They are unique in that adenine always pairs with thymine (A:T) and guanine always pairs with cytosine (G:C). The A:T and G:C base pairs establish 2 and 3 hydrogen bonds, respectively, and the G:C bond is stronger.[9-12] The energetics of the double helix depend on the number of A:T and G:C pairs, as well as the specific base sequence; the number of hydrogen bonds and base stacking contribute to the overall energy involved.[20-24] The thermodynamic parameters have been approximated by a nearest-neighbor calculation, where the average ΔG°_{37} = –8.0 kJ·mol^{-1}, the average ΔH°_{37} = –41 kJ·mol^{-1}, and the average ΔS°_{37} = –104 J·mol^{-1}K^{-1}.[20]

Parameters such as temperature, denaturants, pH, and ionic strength affect the stability of the DNA strands.[9-12] Each base has a negative charge on the phosphate group at pH 7, and the strands repel each other unless they are screened by counterions. High temperature, extreme pH, and low ionic strength favor the ssDNA form, and under these conditions the formation of dsDNA is energetically unfavorable. The transition from an ordered double helix to a disordered structure is called melting, and the reverse process where complementary strands hydrogen bond and base stack to form a helix is called hybridization.[9-12]

5.2.2 UV-Vis Absorption Spectra of Bulk DNA

The four DNA chromophore bases, shown in Figure 5.2, absorb at a particular frequency, ν, as a function of concentration, c, according to Beer's Law:[25-27]

$$A = \varepsilon(\nu)cl \qquad (5.1)$$

where ε is the extinction coefficient, given in L·mol^{-1}·cm^{-1} and l is the path length in cm. UV-Vis spectroscopy typically probes molecules whose electronic resonance transitions lie in the 200-800 nm wavelength region. The absorbance of a molecule varies for each type of allowed electronic transition between energy levels (Figure 5.3).[25-28] According to Equation 5.1, the UV-Vis absorbance of a sample is proportional to its extinction coefficient, which depends highly on

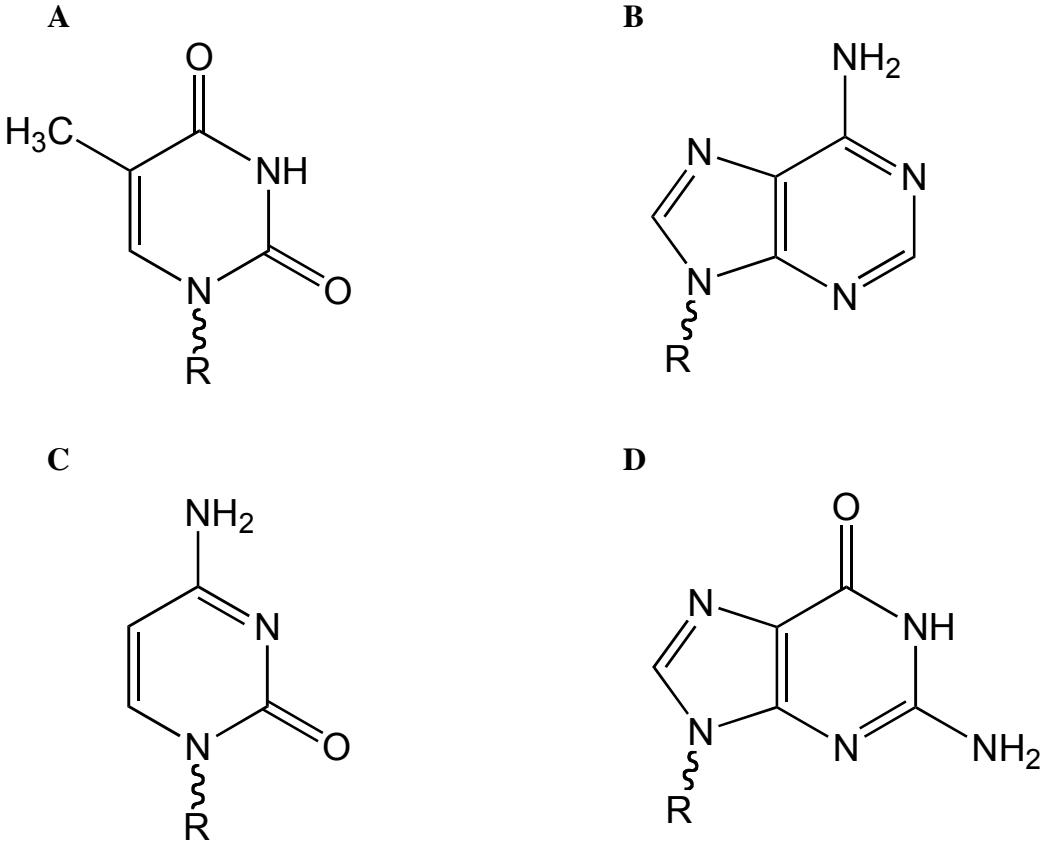

Figure 5.2. Chemical Structure of DNA Bases
The molecular structure of the four DNA bases **A**) adenine, **B**) thymine, **C**) cytosine, and **D**) guanine are shown. DNA bases are chromophores and absorb in the UV-Vis region.

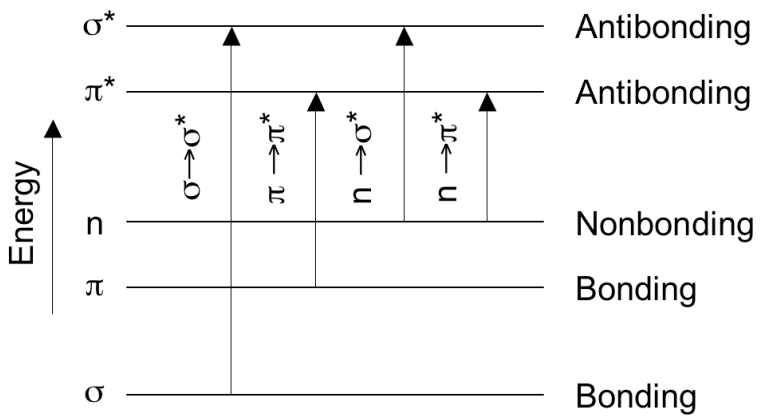

Figure 5.3. Electronic Molecular Energy Levels
Adapted figure of the electronic molecular energy levels involved in UV-Vis absorption spectroscopy.[26] The electronic transitions include: $\sigma \rightarrow \sigma^*$, $\pi \rightarrow \pi^*$, $n \rightarrow \sigma^*$, and $n \rightarrow \pi^*$. The σ orbital represents a symmetric overlap of orbitals with respect to the bond axis, the π orbital represents a parallel overlap of orbital lobes, the n orbital represents a non-bonding orbital like a lone pair, and the * denotes an anti-bonding orbital.[25-28]

the transition probability and cross-section of the molecule. For n→π* transitions, ε is on the order of 10^1-10^2, but for π→π* transitions, ε is on the order of 10^3 to 10^5.[25-28]

DNA has an absorption maximum, λ_{max}, at 260 nm in bulk solution.[11,14,29-32] Even though the four bases are unique, their absorption bands overlap enough to make this approximation valid. The extinction coefficients for an individual nucleotide are on the order of 10^4 (T= 8700, A= 15400, C=, 7400, and G= 11500 $M^{-1}cm^{-1}$), and for short oligonucleotides, the extinction coefficients from the bases sum together and are on the order of 10^5 (T_{25}= 203100, A_{25}= 242400, C_{25}= 180200, and G_{25}= 253900 $M^{-1}cm^{-1}$).[33] The absorbance contains contributions primarily from a π→π* transition but also an n→π*.[11,14,29-32] The π→π* transition is quite strong and is polarized parallel to the plane of the base. This transition originates from the delocalized π electrons in the aromatic bases. Non-bonding electron pairs from the O and N atoms participate in the n→π* transition which is polarized perpendicular to the plane of the base. There are weaker transitions near 200 nm, but because of the interference with the absorbance of water, these peaks are not observed in an aqueous environment.[34] The UV-Vis spectra of T_{15} ssDNA, T_{15}:A_{15} dsDNA, and the NHS linker are shown in Figure 5.4. The ssDNA and dsDNA absorption peaks have a λ_{max} at 256(8) nm and 259(7) nm, respectively, while the NHS linker does not absorb at this wavelength.

When ssDNA bases are oriented randomly, their corresponding dipoles additively contribute to a spectrum. Alternatively, the dipoles of base pairs of a duplex are ordered in a helical array along the axis and are directed inward. Due to this arrangement, the dipoles partially cancel and cause a spectral effect called hypochromism, in which the extinction coefficient of the duplex is less than the sum of the extinction coefficients of the two complementary strands.[34,35] (Figure 5.5) Figure 5.4 illustrates hypochromism, where the absorbance of the dsDNA is less than that of ssDNA. High temperature and low ionic strength cause the strands to melt and the extinction coefficient and absorption to increase, but λ_{max} does

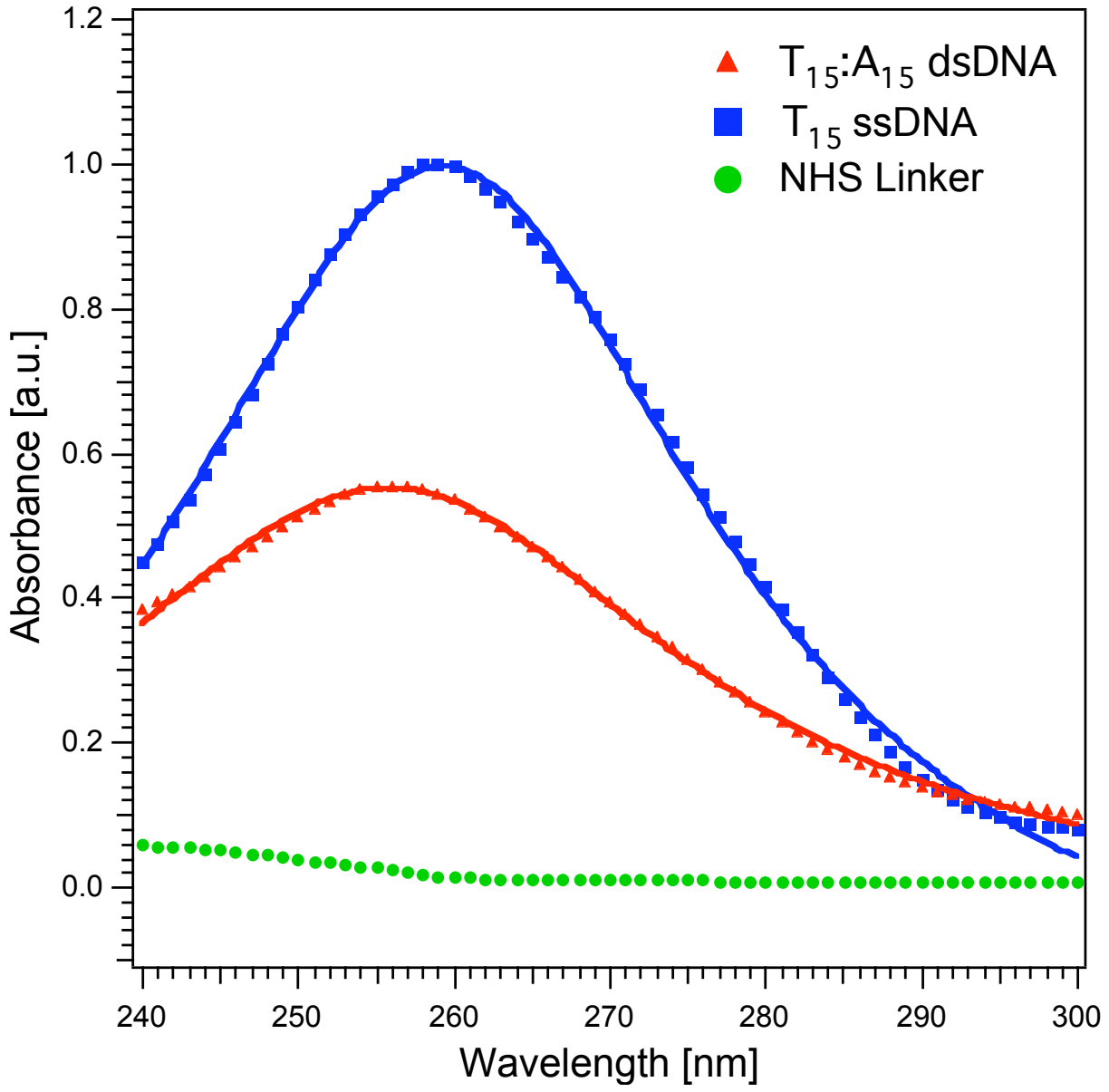

Figure 5.4. UV-Vis Absorption Spectra of Bulk DNA and NHS Linker
The UV-Vis spectra of the NHS linker (green circles) in toluene, and the T_{15} ssDNA (blue squares) and T_{15}:A_{15} dsDNA (red triangles) in 0.25 M NaCl. A Lorentzian function was fit to the data (solid lines). The ssDNA has a λ_{max} at 259(7) nm, and the dsDNA has a λ_{max} at 256(8) nm. All spectra have been normalized.

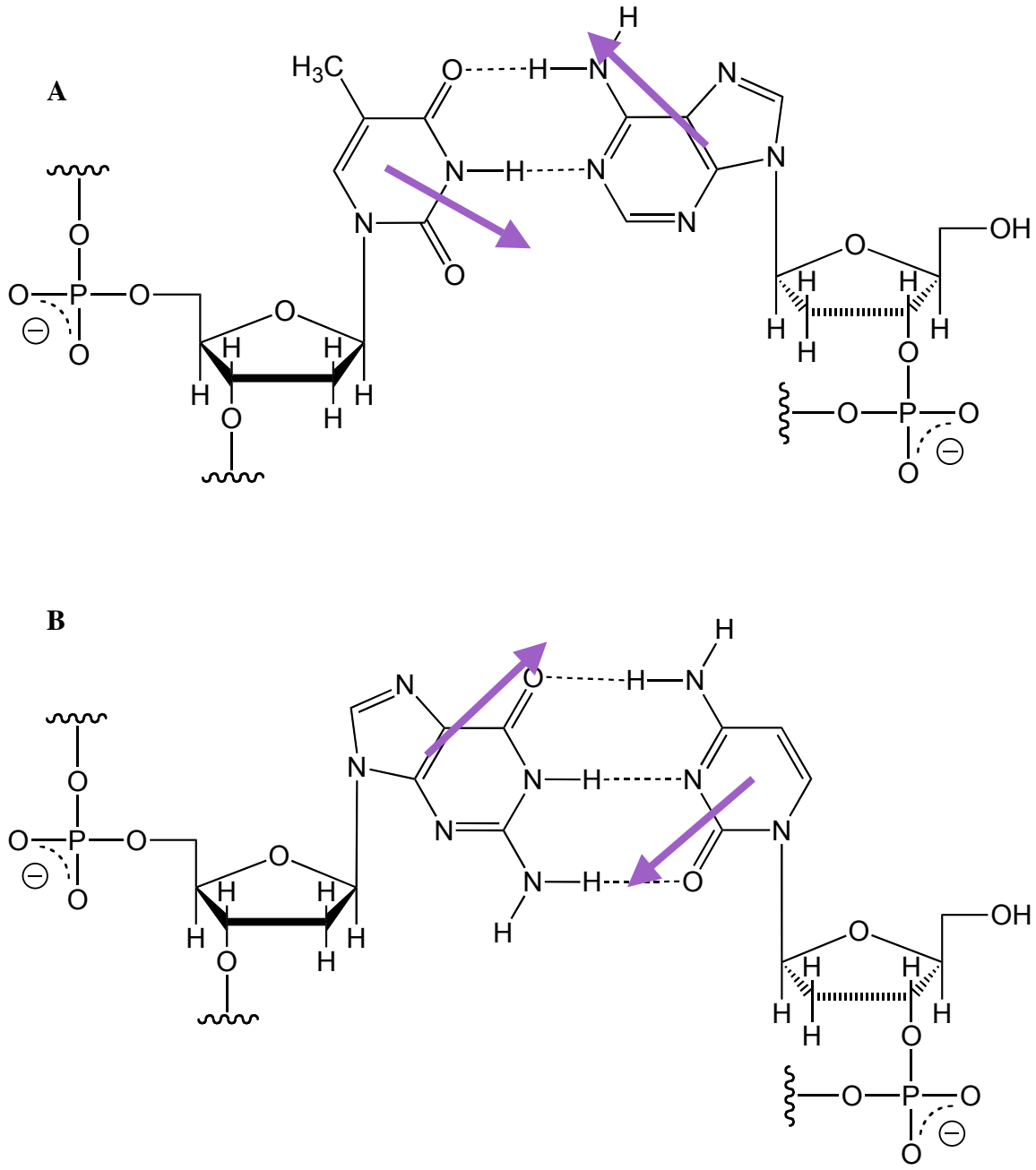

Figure 5.5. Dipole Vectors in Watson-Crick Base Pairs
The theoretical dipole vectors of individual DNA chromophores have been calculated by Roos and co-workers.[14,30,31] The vectors are shown superimposed on the **A**) adenine-thymine (A:T) and **B**) guanine-cytosine (G:C) Watson-Crick base pairs.

not change more than a few nanometers. The spectral change in absorption when the DNA strands undergo melting and hybridization allows for the study of secondary structure in DNA,[35] such as in a thermal denaturation experiment which calculates the temperature at which dsDNA melts by measuring changes in the absorbance at 260 nm.[36]

5.3 Second Harmonic Electronic Resonance of Surface-Bound DNA

5.3.1 Second Harmonic Spectra of NHS Linker and DNA

Resonantly enhanced SHG theory has already been described in Chapter 2.2.1. The square root of our SH signal, I_{SHG}, increases as $\ddot{\alpha}^{(2)}$ is resonantly enhanced. To determine the wavelengths at which maximal two-photon resonance occurs in our system, we measured the SHG spectra of the NHS linker-, T_{25} ssDNA-, and T_{25}:A_{25} dsDNA-functionalized fused quartz/water interfaces. The samples were prepared as described in Chapter 3. All spectra were recorded *in situ* at the aqueous/solid interface, at pH 7, and in the presence of 0.25 M NaCl. The energy of the fundamental probe light field was maintained at 0.5 μJ, which is well below the damage threshold (see Appendix A2.1). The functionalized interfaces were probed at a fundamental of 490-550 nm and the corresponding SH signal was collected at 245-275 nm. The SHG spectra of the ssDNA and the NHS linker were also taken at 300-350 nm to ensure this range was off DNA electronic resonance. This wavelength range was also used to probe ssDNA-functionalized interfaces with the $\ddot{\chi}^{(3)}$ technique in Chapter 4.

The p-in/p-out resonant SHG spectra[37-39] are shown in Figure 5.6. A Lorentzian fit[37,39] to the spectra shows that the electronic resonance occurs at 259(1) nm with a 6(1) nm full width-half maximum (FWHM) for the T_{25} single strand and at 260(1) nm with a 6(1) nm FWHM for

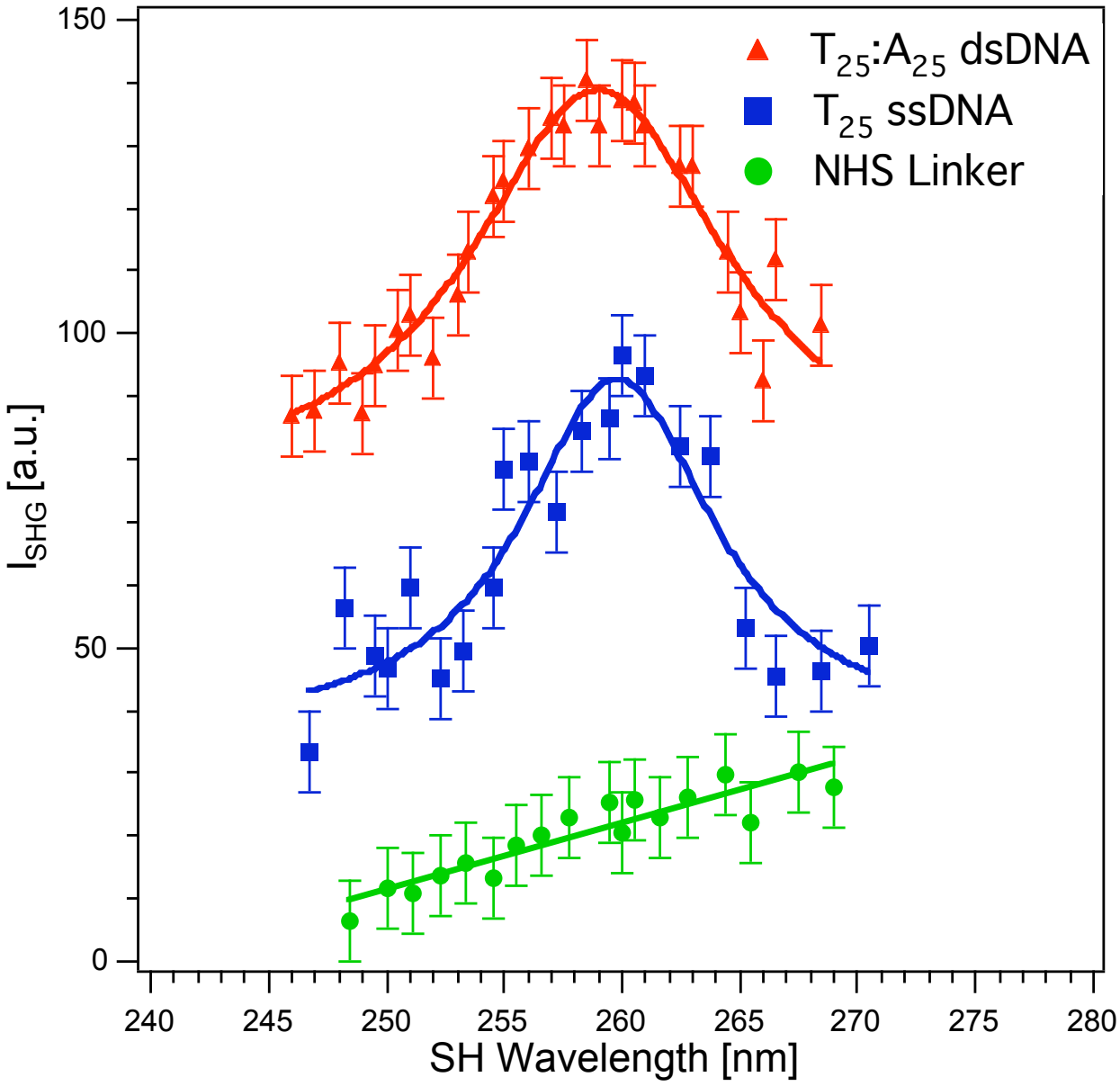

Figure 5.6. Resonant SHG Spectra of DNA-Functionalized Interfaces
The resonant SHG spectra of the T_{25} ssDNA (blue squares) and T_{25}:A_{25} dsDNA (red triangles) in 0.25 M NaCl are shown. The non-resonant NHS linker (green circles) in 0.25 M NaCl is also included. A Lorentzian function was fit to the DNA data (solid lines). The ssDNA has a λ_{max} at 260(1) nm, and the dsDNA has a λ_{max} at 259(1) nm. Spectra were measured in triplicate, normalized to each other, boxcar averaged over 2 points, and offset.

the sb-T_{25}:A_{25} duplex. These results are consistent with the strong $\pi \rightarrow \pi^*$ transitions of thymine and adenine bases that are present in the single strand and the duplex.[40,41] There is no red or blue shift of the λ_{max} in the UV-Vis absorbance spectra shown in Figure 5.4, but the bandwidths of the DNA spectral peaks are much narrower on the surface than in bulk. The p-in/p-out non-resonant SHG spectra are shown in Figure 5.7. A linear function was fit to the spectra, verifying that no spectral features are present when probed with wavelengths off two-photon electronic resonance.

5.3.2 Filter Transmission Spectrum

The resonant SHG spectra in Figure 5.6 show a slight gradient in the non-resonant background, which is especially noticeable in the NHS linker spectrum. This is not observed in the non-resonant SHG spectra (Figure 5.7). We determined that the difference between the backgrounds in the spectra was due to the filter positioned in front of the monochromator. The transmission spectrum of the filter is shown in Figure 5.8. This filter absorbs the visible light between 420-670 nm, removing the visible fundamental beam, and transmits UV light between 230-420 nm, allowing the SH beam to pass through (see Chapter 2.3.3). A magnified view of the transmission spectrum in wavelength region of the resonant SHG experiments (240-280 nm) is shown in the inset of Figure 5.8. The decrease in filter transmission in this wavelength range clearly explains the wavelength-dependent gradient in the SH signal between 245-270 nm. The common problem with filters that transmit in the UV[42] should be kept in mind when collecting spectra in this range, although it does not prevent measuring the resonant SH spectra of DNA.

5.3.3 Hybridization Time Trace

We then tracked the SH signal of the T_{25} ssDNA interface at 260 nm *in situ*, for 6 hours, as it was exposed to a 10-μM A_{25} solution in 0.25 M NaCl at pH 7. This is akin to a temperature

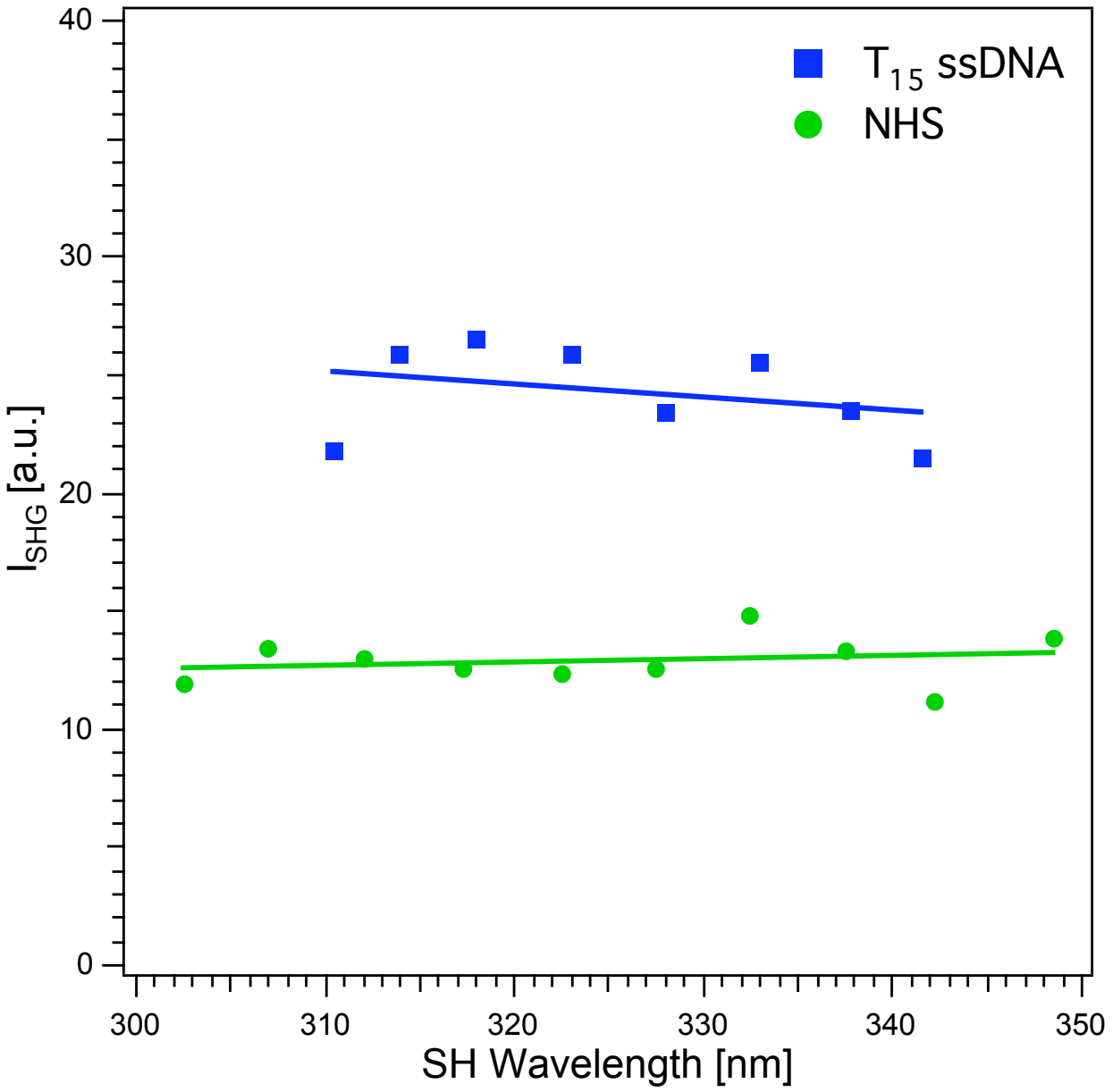

Figure 5.7. Non-Resonant SHG Spectra of Functionalized Interfaces
The non-resonant SHG spectra of the T_{15} ssDNA (blue squares) and NHS linker (green circles) in 0.25 M NaCl are shown. A linear function was fit to the data (solid lines). The ssDNA and NHS do not contain any spectral features. Spectra represent duplicate measurements of the functionalized interfaces.

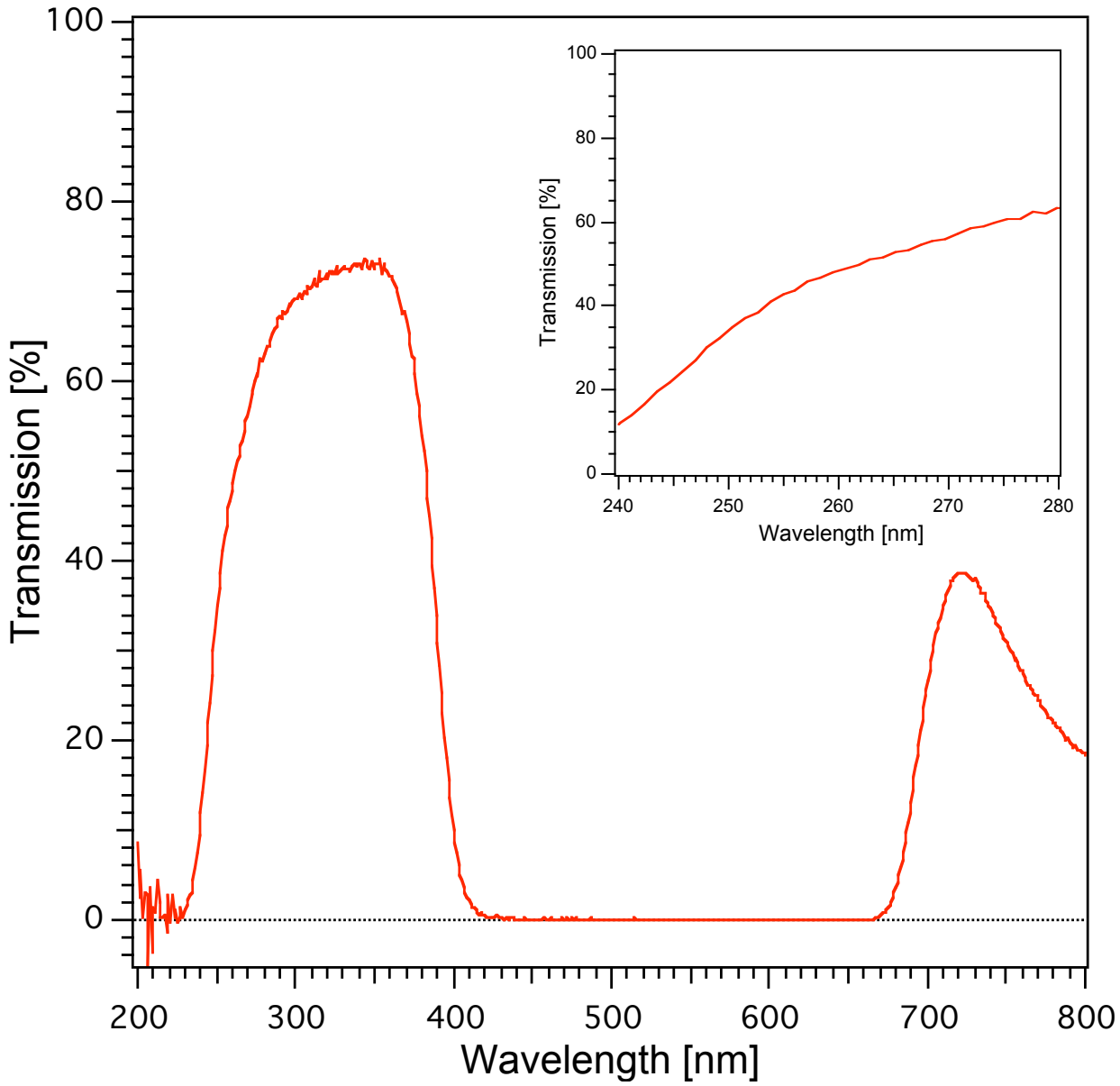

Figure 5.8. Thin Schott Filter Transmission Spectrum
Transmission spectrum of the thin Schott glass filter used to remove the visible fundamental beam and allow the SH beam to pass. The filter absorbs in the visible region and transmits in the UV region. **Inset**: Magnified view of the transmission spectrum in wavelength region of resonant SHG experiments (240-280 nm).

melting curve experiment. We did not see a decrease in the SH signal as the two strands hybridize with one another due to the hypochromic effect observed in bulk solution. This is because the complementary strand is in the aqueous phase when not hybridized to the sb-DNA, and, therefore, only one strand contributes to the SH signal. Upon hybridization, the SH signal is generated from both strands but is reduced from the dipole cancellation. We believe that the hypochromic effect could only be seen in a system is which both complementary strands are at the interface regardless of their hybridization state, for example a DNA hairpin sequence.

The absolute SH signal intensities of the ssDNA and dsDNA that we observe vary slightly from experiment to experiment. Neither of the functionalized interfaces consistently had a larger SH signal intensity than the other, irrespective of wavelength. Due to the variance in SH signal intensities of the ssDNA- and dsDNA-functionalized interfaces, it was not feasible to measure the kinetics and time scale of the hybridization and melting processes at the p-in/p-out polarization combination. Therefore, another experimental method was used to track changes in secondary structure and is discussed in Chapter 6.

5.4 Summary

In conclusion, we have applied resonantly enhanced second harmonic generation spectroscopy to probe the electronic resonance of the π-π^* transitions of single and double strand DNA covalently attached to fused quartz/water interfaces without the use of labels. These are the first electronic resonant SHG measurements of surface-bound DNA. We have found that the SH spectra of the DNA-functionalized interfaces display the same λ_{max} at 260 nm that is found in UV-Vis spectroscopy of bulk DNA solutions and that our NHS linker does not interfere with the

spectra. Therefore, label-free nonlinear optical measurements can be used to characterize sub-monolayer concentrations of DNA strands *in situ* at a buried interface, and these measurements can be used to assist the chemists, engineers, biologists, and doctors that are involved in the design and optimization of new biodiagnostic materials.

CHAPTER 6

SHG Linear Dichroism of Chiral Interfaces

Portions of this chapter are reproduced in part
with permission from the American Chemical Society:

Boman, F.C.; Gibbs-Davis, J.M.; Heckman, L.M.; Stepp, B.R.; Nguyen, S.T.; Geiger, F.M. "DNA at Aqueous/Solid Interfaces- Chirality-Based Detection via Second Harmonic Generation Activity." *Journal of the American Chemical Society*, **2008**, *in press*.

6.1 Introduction

We have applied second harmonic generation (SHG)[1-8] as a label-free method to obtain the full thermodynamic state information for surface-bound (sb) DNA at the fused quartz/water interface[9,10] (Chapter 4) and to probe the electronic resonance modes of the DNA bases[10] (Chapter 5). Here, we tune the incident laser wavelength to be in two-photon resonance with the electronic π-π^* transitions that are intrinsic to the bases.[11-14] We then take advantage of chiral SHG activity[15,16] to distinguish between single and double strand DNA (ssDNA and dsDNA) covalently bound to fused quartz/water interfaces. We demonstrate that a strong nonlinear optical linear dichroic response is obtained without the use of labels when adenine and thymine bases undergo Watson-Crick base pairing to form a double helix.[17-20] Together with this high sensitivity, the molecular-specific nature afforded by nonlinear optics allows for the tracking of sb-DNA as it undergoes hybridization with its complementary strands *in situ* and in real time.[6-8]

6.2 Chiral Spectroscopy Techniques

While experiments using tagged DNA can yield important molecular-level information for DNA in interfacial environments,[21-25] label-free probes have the advantage of detecting DNA at surfaces and interfaces directly and with molecular specificity.[9,10,26-30] From a fundamental science perspective and in the context of addressing the demanding engineering aspects associated with biomedical sensing, probing DNA at interfaces with direct methods that report on the native system is highly desirable.

Chiral spectroscopy techniques play an important part in this pursuit. Chirality refers to the handedness of an object, and chiral molecules are non-superimposable on their mirror images

(Figure 6.1).[18,31] Proteins and DNA oligonucleotides are chiral molecules, therefore, biological systems are widely characterized with chiral techniques,[32-36] particularly linear dichroism (LD), also referred to as optical rotatory dispersion (ORD), and circular dichroism (CD).[31,37-39] These techniques require the polarization of the fundamental light to be controlled with a waveplate or selected with a linear polarizer (see Appendix 3 for a mathematical analysis of polarized light, waveplates, and polarizers). Linear-polarized light is a plane electromagnetic wave, and circular-polarized light is an electromagnetic wave traced out by a vector circling about its axis of propagation.[40] A schematic of linear, plane-polarized light is shown in Figure 6.2.[41,42]

6.2.1 Linear Chiral Spectroscopies

The optical activity of a chiral molecule depends on the refractive index, η, which is the ratio of the speed of light in a vacuum, c, with the speed of light in a medium, ν.[43]

$$\eta = \frac{c}{\nu} \tag{6.1}$$

The complex refractive index has a real component, η, which is important in reflection and refraction, and an imaginary component, k, the absorption index, which is important in optical absorption and is related to the molar extinction coefficient, ε.[40]

$$\vec{\eta} = \eta + ik \tag{6.2}$$

For a transparent material, $k = 0$ and $\vec{\eta} = \eta$. Optical activity occurs when η and ε change for different polarizations of light. For example, when L_{cp} and R_{cp} pass through a chiral sample one absorbs more strongly than the other, and after they exit the sample they are out of phase. The phase difference is reflected in the difference in refractive index, $\Delta\vec{\eta}$.[40]

$$\Delta\vec{\eta} = (\eta_L - \eta_R) + i(k_L - k_R) \tag{6.3}$$

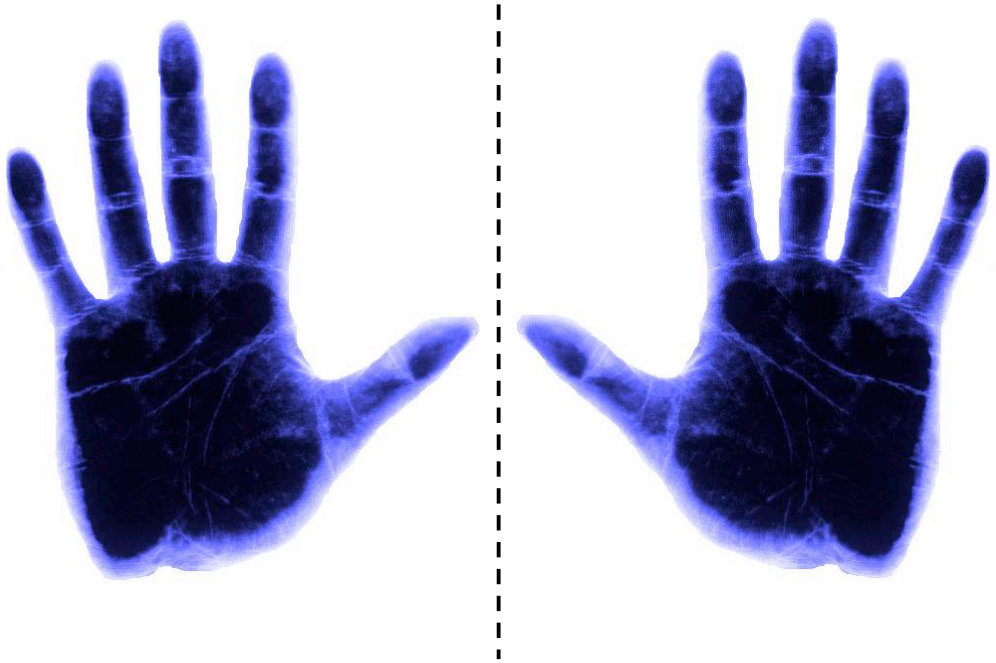

Figure 6.1. Non-Superimposable Chiral Hands
The author's right hand and its mirror image are shown. Left and right hands are non-superimposable on each other, and are, therefore, chiral objects.

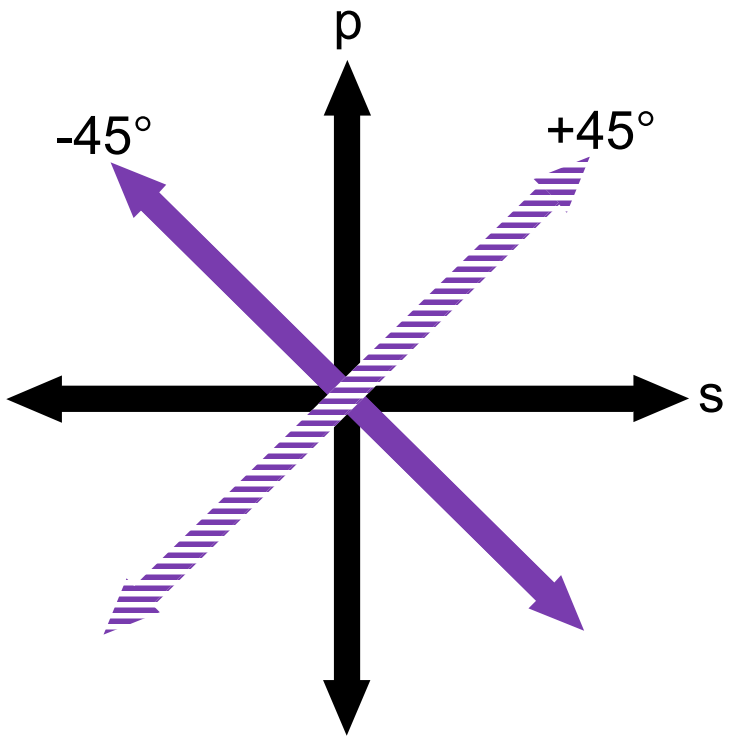

Figure 6.2. Chiral Description of Plane-Polarized Light
A half waveplate selects for p, s, -45°, and +45°-polarized fundamental light. p-Polarized light is aligned parallel with respect to the plane of incidence of the fundamental beam, and s-polarized light is aligned perpendicular with respect to the plane of incidence. The -45° and +45° polarizations are mirror images of each other (e.g. left and right hands), and they selectively probe chirality in the system studied at angles of 45° with respect to the plane of incidence.

The optical activity of the refractive index originates from the rotational strength, R_{ab}, of a molecule. R_{ab} is the scalar product of the sum over states of imaginary components of the electronic and magnetic transition moments, $\vec{\mu}_{ab}$ and $\vec{m}_{ba}$, respectively.[40,44-46]

$$\Delta\vec{\eta} \propto R_{ab} = \sum_{b} \mathrm{Im}(\vec{\mu}_{ab} \cdot \vec{m}_{ba}) \tag{6.5}$$

For a chromophore to be optically active, it must have parallel components of $\vec{\mu}$ and $\vec{m}$.

LD and CD spectroscopies depend on the optical activity of a chiral molecule. The linear birefringence of a molecule, LD, depends on the change in refractive index.

$$LD \propto \eta_L - \eta_R \tag{6.6}$$

The experiment measures the difference between the absorbance of linear polarized (lp) light parallel to the applied electric field, $A_{\parallel}$, and perpendicular to the applied electric field, $A_{\perp}$.[31,40-42]

$$LD = A_{\parallel} - A_{\perp} \tag{6.7}$$

The circular birefringence, CD, depends on a change in absorptive index.

$$CD \propto k_L - k_R \tag{6.8}$$

CD experiments detect differences in absorbance of left circular polarized (cp) light, L_{cp}, and right circular polarized light, R_{cp}, $A_{L,}$ and A_R, respectively:[31,40-42]

$$CD = A_L - A_R \propto \varepsilon_L - \varepsilon_R \tag{6.9}$$

which is often given as the difference in ε to normalize for concentration. While LD and CD are important techniques for accessing the chiral properties of DNA in bulk solution,[32-34,36] their signal intensities are quite weak when compared to isotropic absorbance intensities (~0.1%).

6.2.2 Nonlinear Chiral Spectroscopies

Second-order nonlinear optical techniques have a remarkable ability to probe chirality in molecules. Second harmonic generation circular dichroism (SHG-CD) is a technique pioneered

by Hicks and co-workers[44,45,47,48] and Persoons and co-workers[15,16] that probes chiral molecules, at an interface with a signal enhancement of 10^3 over traditional CD. Second harmonic generation optical rotatory dispersion (SHG-ORD)[49,50] has also been used to probe nonlinear chiroptical responses in chiral molecules. Here, second harmonic generation linear dichroism (SHG-LD)[51-54] experiments have been conducted to characterize the DNA duplex chirality and further elucidate the macromolecular chiral change upon hybridization.

The intensity of SH light, I_{SHG}, is given by the general form:[51,55]

$$I_{SHG} = \left| f\vec{E}^{p}_{\omega}\vec{E}^{p}_{\omega} + g\vec{E}^{p}_{\omega}\vec{E}^{s}_{\omega} + h\vec{E}^{s}_{\omega}\vec{E}^{s}_{\omega} \right|^2 \tag{6.10}$$

where $\vec{E}^{p}_{\omega}$ and $\vec{E}^{s}_{\omega}$ are the p- and s-polarized components of the applied electric fields, respectively, and the complex parameters *f*, *g*, and *h* are linear combinations of components of the nonlinear susceptibility tensor, $\vec{\chi}^{(2)}$, which describes the macroscopic system (see Equations 2.4 and 2.5). The complex parameters can be broken up into their p- and s-polarization components where f_p, g_p, and h_s are non-vanishing for achiral interfaces and f_s, g_s, and h_p are non-vanishing for chiral interfaces.[15,16,48] While this description works well on a phenomenological-level for analyzing data, molecular-level interpretations are possible with approaches by Shen and co-workers[56] and Simpson and co-workers.[54,57] The reader is referred to these descriptions until consensus on this subject has been reached.

After substituting $\vec{E}^{p}_{\omega} = \pm i\vec{E}^{s}_{\omega}$, for cp light, and $\vec{E}^{p}_{\omega} = \pm\vec{E}^{s}_{\omega}$, for lp light (see Appendix A3.2), into Equation 6.10, the intensities of SHG-CD and SHG-LD, $I_{SHG\text{-}CD}$ and $I_{SHG\text{-}LD}$ are:[51,55]

$$I_{SHG-CD} = \left| -f + g \pm ih \right|^2 I^2_{\omega} \tag{6.11}$$

$$I_{SHG-LD} = \left| f + g \pm h \right|^2 I^2_{\omega} \tag{6.12}$$

where the upper and lower signs correspond to right- and left-hand polarizations in Equation 6.11 and +45° and -45° linear polarizations in Equation 6.12. Therefore, the general formulas for SHG-CD and SHG-LD are as follows:[51,55]

$$\Delta I_{SHG-CD} = I_{2\omega}^{Lcp} - I_{2\omega}^{Rcp} = 4\,\mathrm{Im}\left[(f-g)h^*\right]I_{\omega}^2 \tag{6.13}$$

$$\Delta I_{SHG-LD} = I_{2\omega}^{-45^\circ} - I_{2\omega}^{+45^\circ} = -4\,\mathrm{Re}\left[(f+g)h^*\right]I_{\omega}^2 \tag{6.14}$$

where ΔI_{SHG-CD} is the difference between the intensities of L_{cp} and R_{cp}, $I_{2\omega}^{Lcp}$ and $I_{2\omega}^{Rcp}$, at the SH frequency, 2ω, and ΔI_{SHG-CD} is the difference between the intensities of -45°- and +45°-plane polarized light, $I_{2\omega}^{-45^\circ}$ and $I_{2\omega}^{+45^\circ}$. SHG-CD probes the imaginary components of the complex parameters, whereas SHG-LD probes the real components, making the two techniques complementary but not identical to each other.

There have been three explanations proposed for the microscopic and macroscopic origins of this effect:[58,59] 1) interactions between magnetic dipoles and interference between magnetic and electric dipoles,[15,44,51,60] 2) intrinsic chirality from the electric-dipole approximation,[48,61] and 3) macromolecular orientation effects.[53,58]

The first description for the source of chiroptical effects is based on the helical motion of electrons, similar to the origin of linear chiral spectroscopies discussed in the previous section. Under the electric/magnetic dipole model, two photons from the electronic transition moment, $\vec{\mu}$, interact with a photon from the magnetic transition moment, $\vec{m}$. When the photon associated with $\vec{m}$ is at frequency ω, the nonlinear polarization, $\vec{P}_{2\omega}$, is given as:[15,16,62-64]

$$\vec{P}_{2\omega} = \vec{\vec{\chi}}^{eee}\vec{E}_{\omega}\vec{E}_{\omega} + \vec{\vec{\chi}}^{eem}\vec{E}_{\omega}\vec{B}_{\omega} \tag{6.15}$$

where $\vec{E}_{\omega}$ and $\vec{B}_{\omega}$ are the incident electric and magnetic fields. The usual electric dipole

susceptibility, $\vec{\vec{\chi}}^{eee}$, depends on $\vec{\mu}_{ab} \cdot \vec{\mu}_{bc} \cdot \vec{\mu}_{ca}$, and is referred to as $\vec{\vec{\chi}}^{(2)}$ elsewhere. The first-order electric-magnetic dipole susceptibility, $\vec{\vec{\chi}}^{eem}$, depends on $\vec{\mu}_{ab} \cdot \vec{\mu}_{bc} \cdot \vec{m}_{ca}$. When the photon associated with $\vec{m}$ is at frequency 2ω, the nonlinear magnetization, $\vec{M}_{2\omega}$, is given as:[15,16,62-64]

$$\vec{M}_{2\omega} = \vec{\vec{\chi}}^{mee} \vec{E}_{\omega} \vec{E}_{\omega} \tag{6.16}$$

where $\vec{\vec{\chi}}^{mee}$ is the electric-magnetic dipole susceptibility, which depends on $\vec{m}_{ab} \cdot \vec{\mu}_{bc} \cdot \vec{\mu}_{ca}$. The three nonlinear susceptibilities, $\vec{\vec{\chi}}^{eee}$, $\vec{\vec{\chi}}^{eem}$, and $\vec{\vec{\chi}}^{mee}$, all have their own chiral complex parameters, f_s, g_s, and h_p, which contribute to Equations 6.13 and 6.14.

It has been suggested that this effect has only minor contributions in oriented systems because measured values for $\vec{m}$ are several orders of magnitude smaller than $\vec{\mu}$. The magnetic component in Equation 6.15 is self-heterodyned because the SH signal is dependent on the square modulus of $\vec{P}_{2\omega}$, but it is still several orders of magnitude smaller than the pure electric component, making it difficult to establish this as the reason for such high nonlinear chiral signal intensities.[52,59] It is generally thought that the enhancement in the nonlinear signal over the linear signal is due to the orientation of the molecules at the interface. The other explanations for the molecular origin of chiroptical effects describe the contribution to chiral elements of $\vec{\vec{\chi}}^{(2)}$.

The second explanation describes coupled oscillators under the electric-dipole approximation. For identical, interacting chromophores, the chiral tensor elements of the macroscopic hyperpolarizability tensor, $\vec{\beta}^{(2)}$, additively contribute to $\vec{\vec{\chi}}^{(2)}$ (see Equation 2.7).[2,65] Under two-photon absorption (TPA) resonant conditions, $\vec{\beta}^{(2)}$ can be described by its 27 matrix elements, β_{ijk}, summed over excited states:[52,58,66]

$$\beta_{ijk} = \sum_{n} \frac{-\mu_{0n}^{i}\left(\alpha_{n0}^{jk}\right)_{TPA}}{4\hbar\left(\omega_{n} - \omega_{2\omega} - i\Gamma_{n}\right)} \tag{6.17}$$

where μ_{0n}^{i} is the electric transition dipole elements between the ground state, 0, and an excited state, n, α_{n0}^{jk} is the tensor element for TPA between 0 and n where, ω_n and $\omega_{2\omega}$ are the frequencies of the excited state and SH light field, respectively, $\hbar$ is Planck's constant divided by 2π, and Γ_n is the damping coefficient of the TPA transition.

For identical, non-interacting chromophores, the 27 matrix elements of $\vec{\chi}^{(2)}$, χ_{IJK}, can be expressed as N_{ads} multiplied by the sum of the β_{ijk}, acted on by R, the coordinate transform matrix that relates the molecular coordinates, i, j, k, to the lab coordinates, x, y, and z:[52,58,66]

$$\chi_{IJK} = N_{ads} \sum_{i,j,k=x,y,z} \left\langle R_{ii} R_{jj} R_{kk} \right\rangle \beta_{ijk} \tag{6.18}$$

The chiral χ_{IJK} tensor elements are nonzero and sum together to contribute to $\vec{\chi}^{(2)}$.[58]

The third explanation for chiroptical effects describes achiral chromophores that have a macromolecular chiral orientation.[59] The DNA double helix, which has D_∞ symmetry, is an example of this system. When Equation 6.18 is explicitly evaluated for achiral chromophores in a chiral array, there are four nonzero matrix elements: χ_{ZZZ}, χ_{ZXX}, $\chi_{XZZ} = \chi_{XZX}$, and $\chi_{XYZ} = \chi_{XZY} = -\chi_{YXZ} = -\chi_{YZX}$.[58] Even though the chromophores are not chiral themselves, their chiral orientation allows their chiroptical properties to be probed with SHG. Therefore, chiral SHG techniques are expected to play a key role in probing the chiral hybridization transition that DNA undergoes between its ssDNA form and its dsDNA form.

6.3 SHG-LD Measurements of Functionalized Interfaces

6.3.1 CHARMM Molecular Modeling

DNA duplexes are oriented as right-handed, anti-parallel helices[17-20]. A 3-D molecular model of ssDNA and dsDNA on a fused quartz surface, calculated by Dr. Stefano Tonzani, is shown in Figure 6.3a-b. CHARMM[67,68] is a common force field for studying the structure of biomolecules. This simulation used CHARMM 27[69] (Chemistry at HARvard Macromolecular Mechanics) to calculate the structure of the nucleic acids with Na^+ cations.[70,71] This molecular model of DNA shows that for small lengths of oligonucleotides, the ssDNA strand is randomly oriented but the dsDNA is a rigid, ordered duplex with macromolecular chirality.

A DNA duplex would be expected to exhibit a different nonlinear chiroptical response than ssDNA, which does not form a double helix under our experimental conditions. Therefore, SHG-CD and SHG-LD have the ability to probe the secondary structure of DNA-functionalized interfaces. Given the previous studies on resonantly enhanced chiral SHG studies,[45,48,49,53,58,72] the difference in the NLO chiral response of sb-DNA should be particularly pronounced when the experiment is conducted on electronic resonance. This would, in principle, allow us to tracking hybridization with a nonlinear analogue of LD directly at an interface.

6.3.2 Linear Dichroic Ratios

Following our previous work (see Chapters 3 and 5), we chemically attached T_{25} ssDNA to the flat side of fused quartz hemispheres, resulting in surface charge densities measured using the $\ddot{\chi}^{(3)}$ method that are consistent with surface coverages around 5×10^{11} strands/cm^2. To form the sb-duplex with the complementary A_{25} sequence, the T_{25}-functionalized substrate was placed

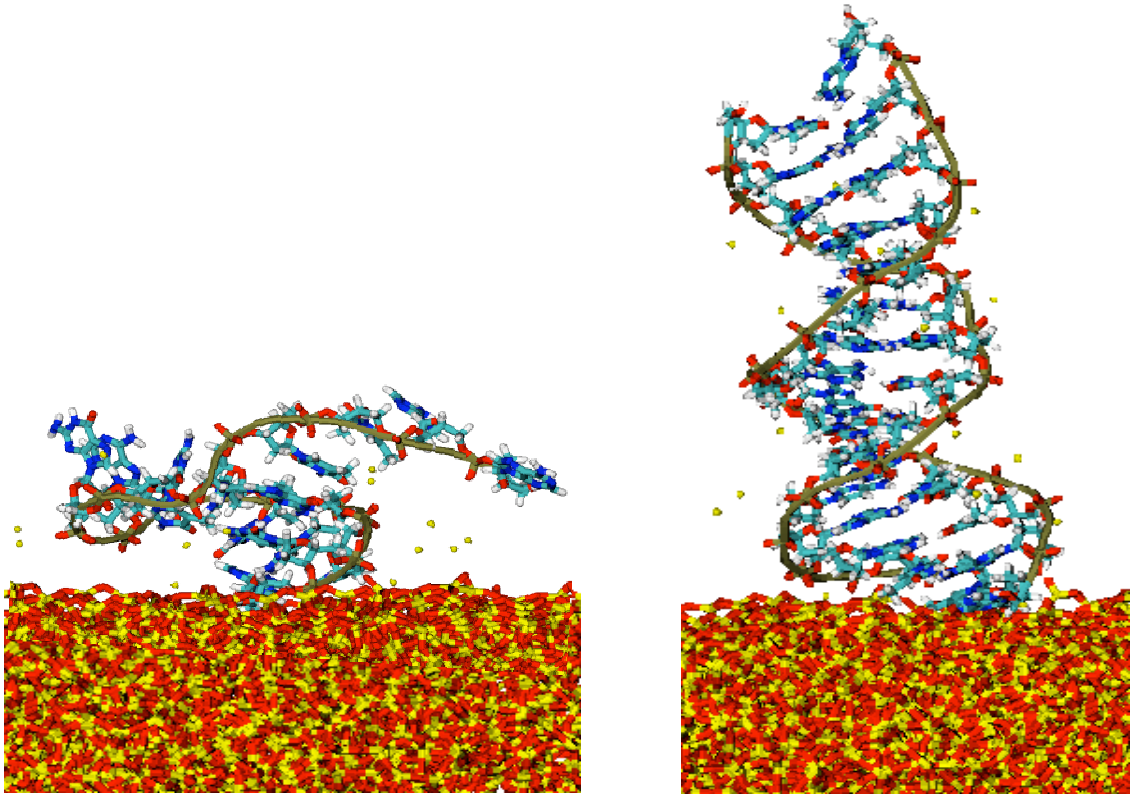

Figure 6.3. CHARMM Molecular Model of ss and dsDNA on Fused Quartz
CHARMM 27 calculation of nucleic acids with Na^+ ions on fused quartz. The simulation was run for 2-3 nanoseconds, the water potential was described with TIP3P[73] for a concentration of 0.1 atm, and the force field parameters for the fused quartz surface have already been calculated.[74]

in a 10-μM solution of A_{25} in pH 7 containing an electrolyte concentration of 0.25 M NaCl.

After identifying the sb-DNA strands via resonantly enhanced SHG, we determined the p-polarized SHG linear dichroic (SHG-LD) ratios for the T_{25} ssDNA and the sb-T_{25}:A_{25} dsDNA. Specifically, we probed the interface with light fields plane-polarized ±45° with respect to the field of incidence using an achromatic half waveplate (400-700 nm, uncoated, MWPAA2-12, Karl Lambrecht Corporation) and recorded the p-polarized SHG intensity selected by a Glan Taylor polarizer (E grade calcite, BB MgF_2 anti-reflective coating, MGTYE20, Karl Lambrecht Corporation).[53] This signal detection scheme is akin to heterodyne detection of the weak SHG E-field obtained with the chirality-selective p-in/s-out polarization combination while using the strong E-field generated with the p-in/p-out polarization combination, which probes achiral signal contributions as the local oscillator.[30] When divided by their average, the difference in the two SHG intensities yields the SHG-LD ratio, which we express as a percentage:[45,51,54]

$$\mathrm{SHG-LD_{ratio}} = \frac{\Delta I_{\mathrm{SHG-LD}}}{I_{\mathrm{ave}}} = \frac{\left(I_{2\omega}^{-45^\circ} - I_{2\omega}^{+45^\circ}\right)}{\frac{1}{2}\left(I_{2\omega}^{-45^\circ} + I_{2\omega}^{+45^\circ}\right)} \tag{6.19}$$

Functionalized fused quartz/water interfaces were probed with ±-45°-linearly polarized light, and the p-polarized SH signal was collected. Figure 6.4 shows the average SH signal intensities for the NHS linker, T_{25} ssDNA, and T_{25}:A_{25} dsDNA samples at 260 nm. The ssDNA interface showed a slight difference between the -45°-in/p-out and +45°-in/p-out settings, but the dsDNA difference was more noteworthy. The non-resonance average SH signals were also collected at 250 nm (Figure 6.5), but did not display significant differences in the ±45°-in/p-out signals. Interestingly, when the incident wavelength is tuned either away from or onto two-photon resonance, the average ±45°-in/p-out polarization combination yields as many SHG

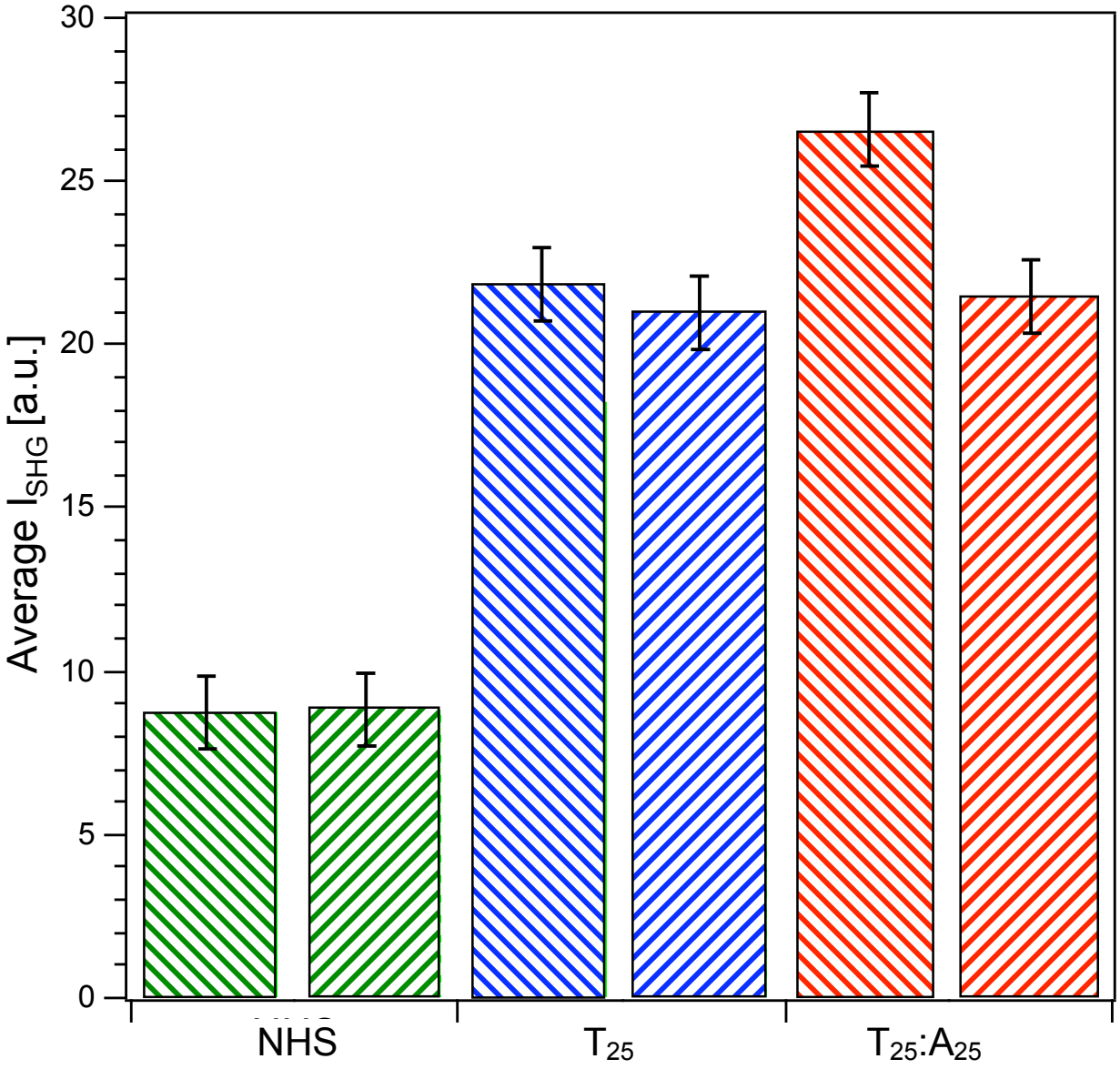

Figure 6.4. Absolute SH Signal for ±45°-in/p-out On-Resonance
The average absolute SH signal for plane-polarized ±45°-in/p-out light collected on electronic resonance for DNA (260 nm). The downward diagonal stripe bars represent -45°-in/p-out, and the upward diagonal stripe bars represent +45°-in/p-out. The NHS linker, T_{25} ssDNA, and T_{25}:A_{25} dsDNA surfaces were measured for N= 4, N= 9, and N= 4 surfaces, respectively.

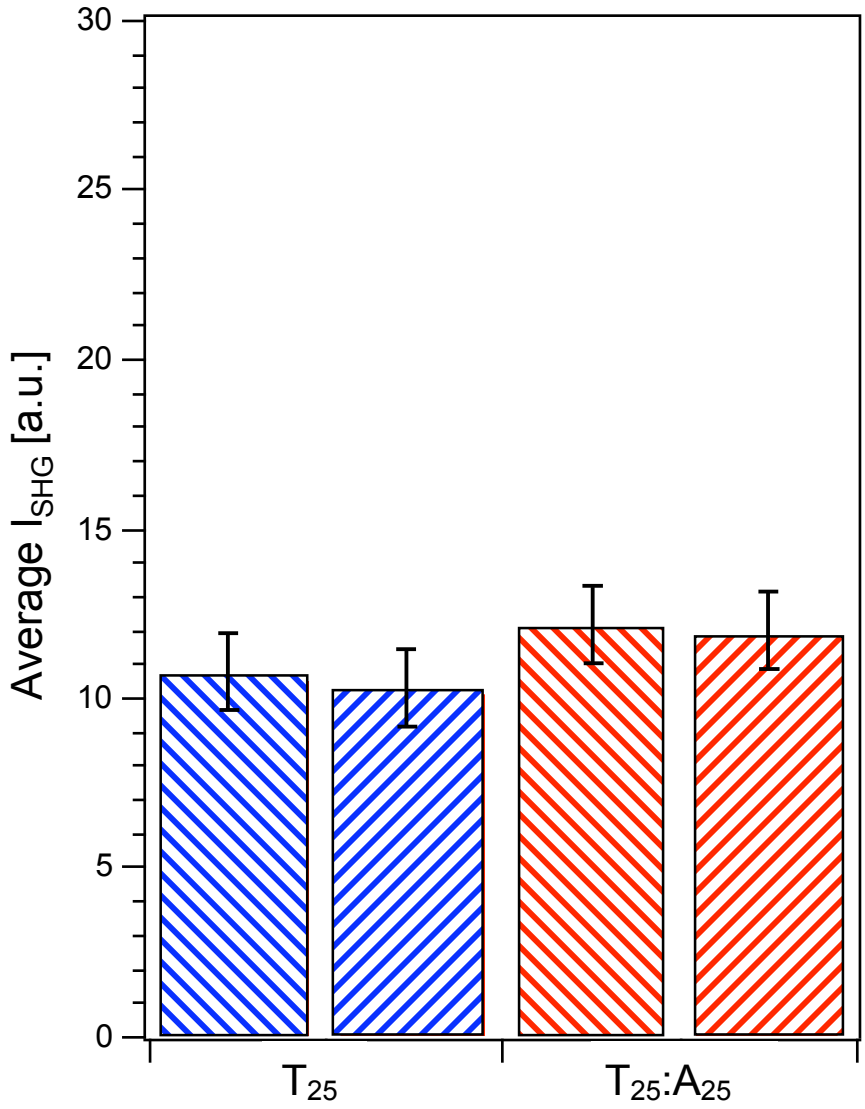

Figure 6.5. Absolute SH Signal for ±45°-in/p-out Off-Resonance
The average absolute SH signal for plane-polarized ±45°-in/p-out light collected off electronic resonance for DNA (250 nm). The downward diagonal stripe bars represent -45°-in/p-out, and the upward diagonal stripe bars represent +45°-in/p-out. The T_{25} ssDNA and T_{25}:A_{25} dsDNA surfaces were averaged for N= 9 and N= 11 measurements, respectively.

counts, within error, for the T_{25}:A_{25} dsDNA as for the T_{25} ssDNA. The substantial increase in the SHG-LD response when going from the T_{25} ssDNA to the sb-T_{25}:A_{25} dsDNA is, thus, mainly due to the signal difference between the ±45°-in/p-out polarization combination and not an overall signal intensity change in the p-in/p-out polarization.

The SHG-LD ratios of these interfaces were calculated according Equation 6.19 for resonant (Figure 6.6) and non-resonance (Figure 6.7) wavelengths. The achiral NHS linker has a negligible SHG-LD ratio (-2.0% ± 5.8%), which is expected. When the incident wavelength is in two-photon resonance with the electronic π-π* transitions of the bases, the T_{25} ssDNA exhibits only a slight SHG-LD response that falls within the uncertainly of the measurement (1.1% ± 3.3%). In contrast, the sb-T_{25}:A_{25} dsDNA exhibits a strong SHG-LD response (19% ± 5.8%). When the incident wavelength is tuned away from two-photon resonance, both interfaces show a weak SHG-LD response (4.0% ± 1.9% for the ssDNA and 3.2% ± 1.5% for the dsDNA).

6.3.3 Hybridization Time Trace

Our previous SHG experiments have relied on an *in situ* DNA hybridization time of 2-6 hours, creating a large time constraint in the lab. Since the laser output stability and alignment decreases after a few hours, unnecessarily long hybridization times were undesirable. Thus, we set out to determine the shortest possible reaction times needed for the complementary strand to completely bind to the sb-DNA. We tracked the SHG-LD response of DNA oligonucleotides on and off electronic resonance, as a function of time during hybridization (Figure 6.8). The T_{25} ssDNA interface was measured for over 2 hours with 0.25 M NaCl at pH 7, after which it was exposed to the complementary strand A_{25} in the same salt solution.

The results indicate that the hybridization process causes an increase in the SHG-LD

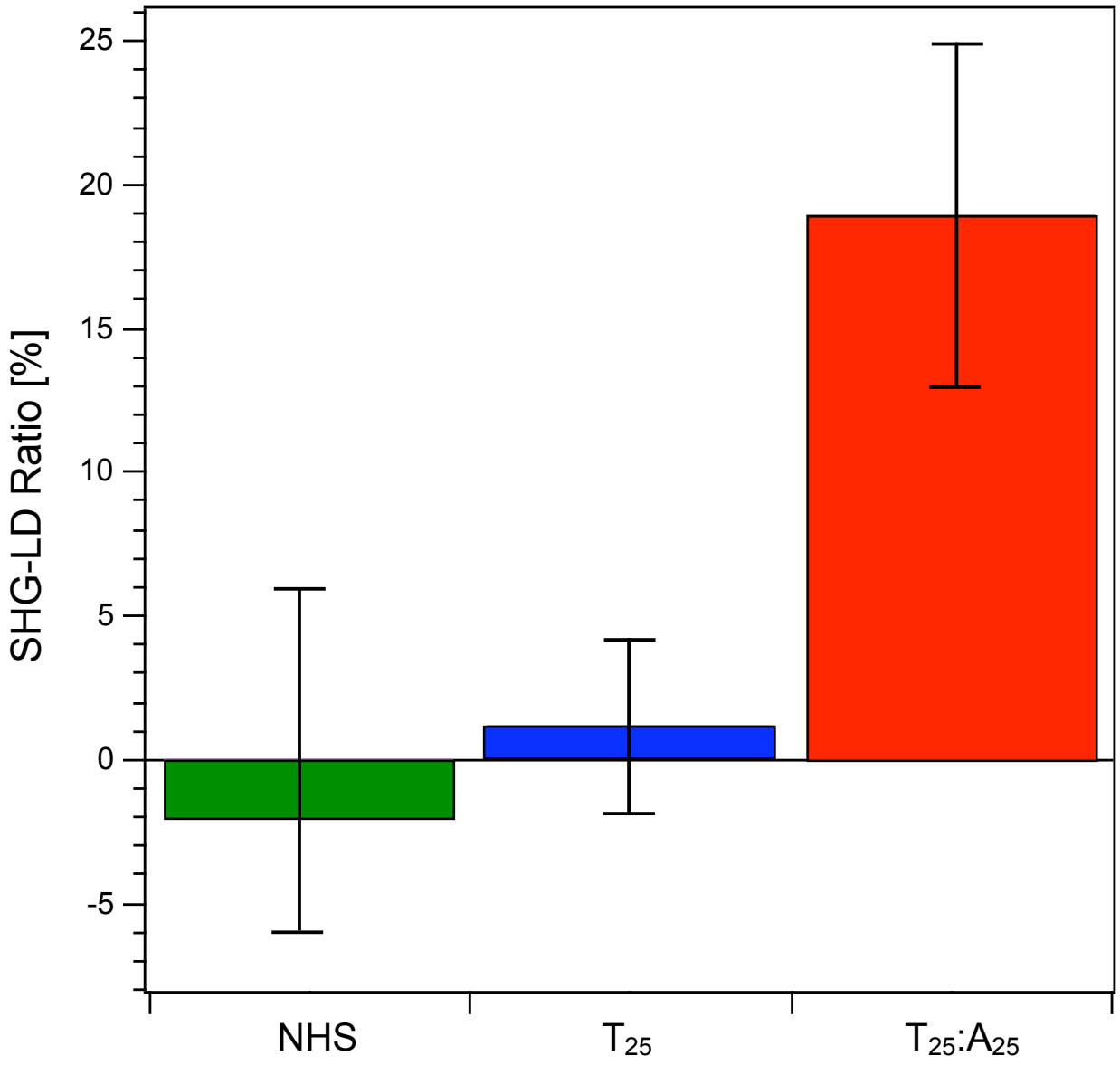

Figure 6.6. Resonant SHG-LD Ratios for Functionalized Interfaces
The SHG-LD ratios were calculated from the difference and average of the SH signals at ±45°-in/p-out according to Equation 6.19 on electronic resonance for DNA (260 nm). The error bars are the standard deviations of the average SHG-LD.

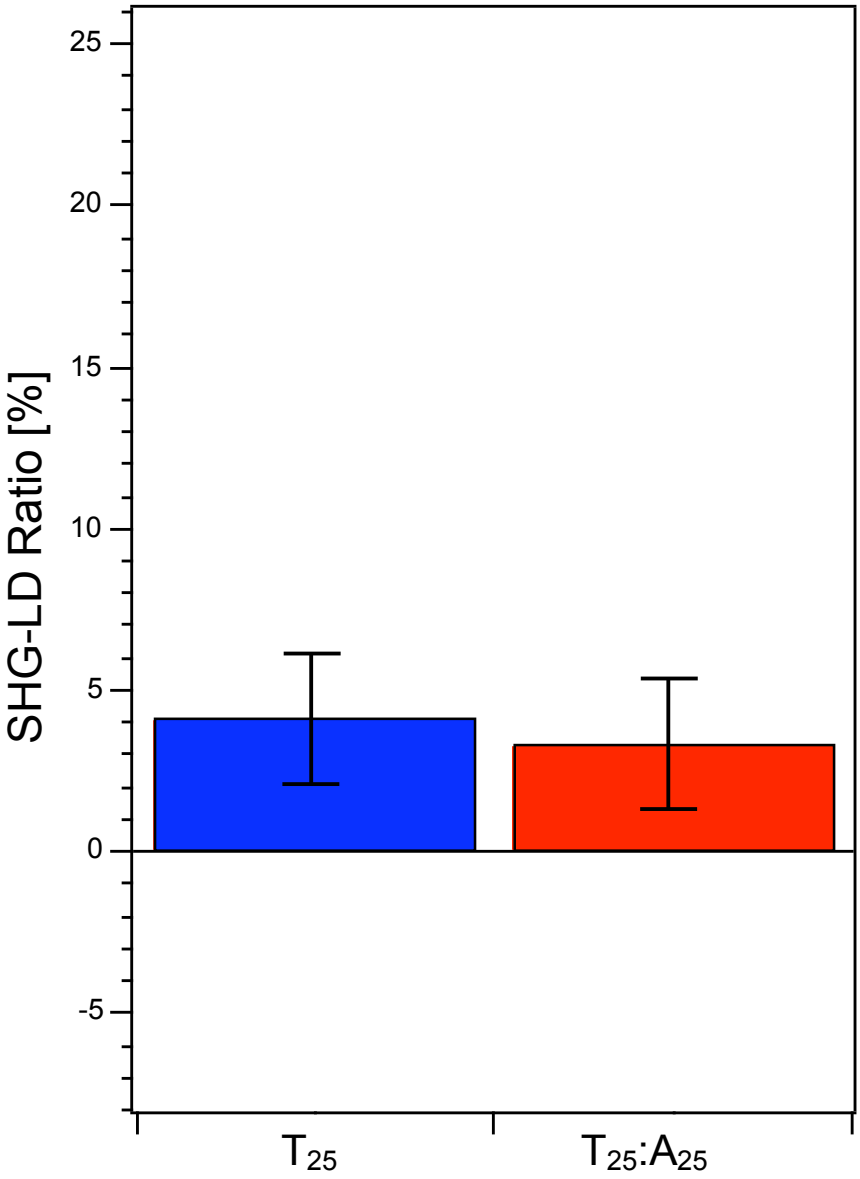

Figure 6.7. Non-Resonant SHG-LD Ratios for Functionalized Interfaces
The SHG-LD ratios were calculated from the difference and average of the SH signals at ±45°-in/p-out according to Equation 6.19 of electronic resonance for DNA (250 nm). The error bars are the standard deviations of the average SHG-LD.

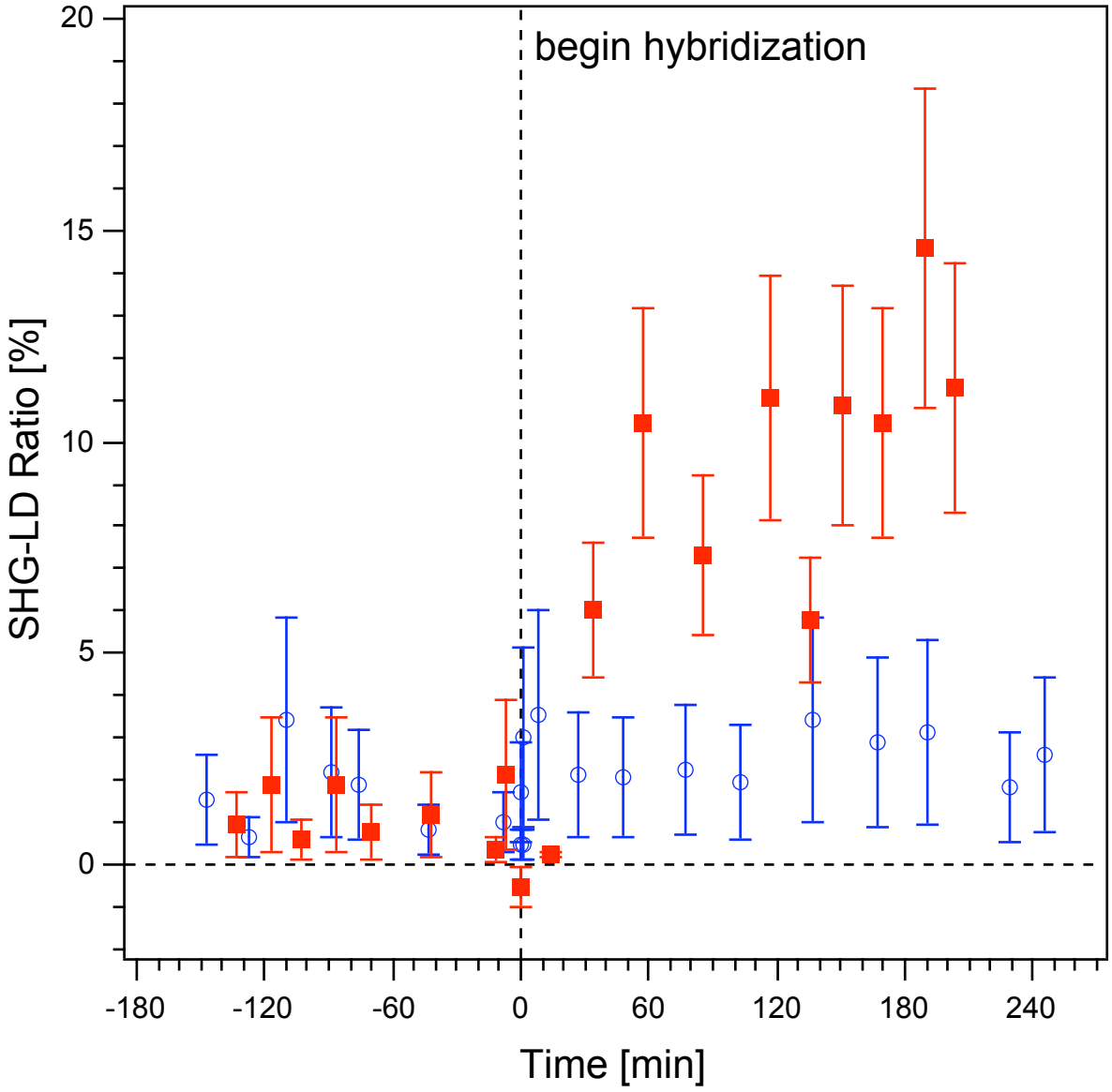

Figure 6.8. DNA Hybridization Time Determined by SHG-LD Ratios
The T_{25} ssDNA interface was measured for ~2 hours with 0.25 M NaCl at pH 7 and then ~4 hours with the complementary A_{25} strand in the same salt solution at 10 μM for wavelengths both on (260 nm, red squares) and off (250 nm, blue empty circles) DNA electronic resonance. SHG-LD ratios were calculated from the average ±45°-in/p-out SH signals according to Equation 6.19.

ratio, consistent with the data shown in Figure 6.6. As expected, the SHG LD ratio does not change beyond what is observed for ssDNA when the laser is tuned off of electronic resonance. Pre-hybridization times show that the increase in SHG-LD ratio remains constant within error. After the introduction of the complementary strand, the SHG-LD ratio gradually increases up to 2 hours and does not significantly change at later times. Therefore, we conclude that hybridization is complete after 2 hours. This finding greatly reduces the time spent waiting for hybridization to finish in SHG experiments. We emphasize that the experiments were carried out without changing the optical alignment, sample cell location, or laser spot position. We note that it would be challenging to observe these chiral responses with other label-free detection methods.

6.4 Fluorescence of Functionalized Surfaces

In addition to SHG-LD, fluorescence confocal microscopy[75-80] was used as a complementary technique to determine the hybridization time of sb-DNA, as well as to image the NHS linker-, tagged and non-tagged T_{25} ssDNA-, and tagged T_{25}:A_{25} dsDNA-functionalized surfaces. Fluorescence measurements carried out for similar time ranges show a comparable result to the SHG-LD measurements, however these experiments require an off-line approach utilizing many samples whose hybridization process was stopped at a given time. More detailed control studies regarding specific binding and sample preparation are described in Appendix 4.

6.4.1 Tagged ssDNA and dsDNA Surfaces

A wide variety of fluorescent tags are used for this type of detection.[25,81] Fluorescein is a commonly exploited dye,[82-84] and its small size makes it an optimal tag for this investigation (Figure 6.9). An LSM 510 Meta Laser Scanning Microscope (Zeiss) with a 20x objective and 55-

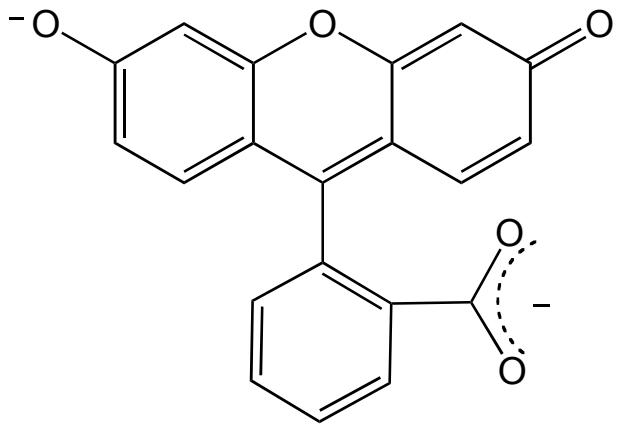

Figure 6.9. Chemical Structure of Fluorescein
Fluorescein was chemically attached to the DNA strands as a fluorescent tag due to its intense green fluorescence emission.

nm xy resolution was used to image the surfaces. The dye was excited with a 488-nm Argon laser, and the fluorescence was collected with a green bandpass emission filter (500-530 nm). Untagged NHS linker slides were reacted with 5'-flourescein tagged T_{25} ssDNA, and untagged T_{25} ssDNA slides were hybridized with 3'-fluorescein tagged complementary A_{25} DNA to form tagged T_{25}:A_{25} dsDNA slides as shown in Figure 6.10a-b (see Chapter 3). In order to avoid photobleaching, the fluorescein-tagged samples were covered in aluminum foil throughout the entire sample preparation, minimizing light exposure.

Each tagged DNA strand appears as a bright spot in the captured image, and the mean brightness of the fluorescent image is directly proportional to the amount of hybridized, sb-DNA. Therefore, the ssDNA slides were imaged in order to observe a general surface coverage, and the dsDNA slides were imaged in order to observe the extent of hybridization (Figure 6.11a-d). The mean brightness of each 100 × 100 μm^2 imaged section of the functionalized surface was calculated with ImageJ 1.40g software (National Institutes of Health).

6.4.2 Variation of Hybridization Times

To compare the extent of hybridization due to a variation in hybridization reaction times, 10 different ssDNA slides were exposed to the solution of tagged complementary DNA for time lengths ranging from 5 minutes to 4 hours, rinsed with 0.25M NaCl, and imaged (Figure 6.12). After a period of 30 minutes, the brightness of the images was observed, indicating a significant amount of DNA hybridized at the surface. The brightness continued to increase for hybridization times up to 2 hours, at which point the intensity did not significantly increase. Therefore, we have succeeded in characterizing the time of DNA hybridization for our system- 2 hours. These results also complement the hybridization time range measured in the SHG-LD experiment

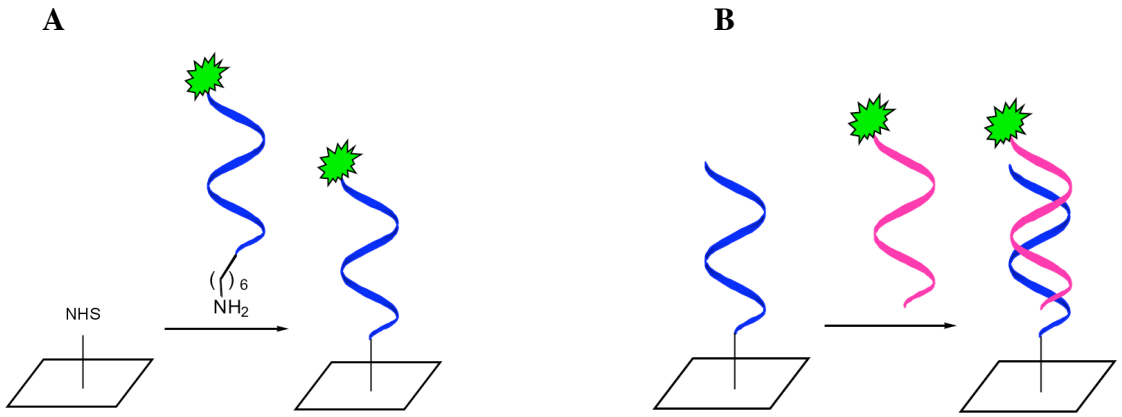

Figure 6.10. Preparation of Fluorescently Tagged ssDNA and dsDNA Surfaces
A) Schematic of 5'-fluorescein-tagged 3'-amine-terminated T_{25} ssDNA reacted with the NHS linker, forming an amide bond. **B**) Schematic of 3'-fluorescein-tagged A_{25} DNA hybridized with the sb-T_{25} ssDNA, forming a duplex.

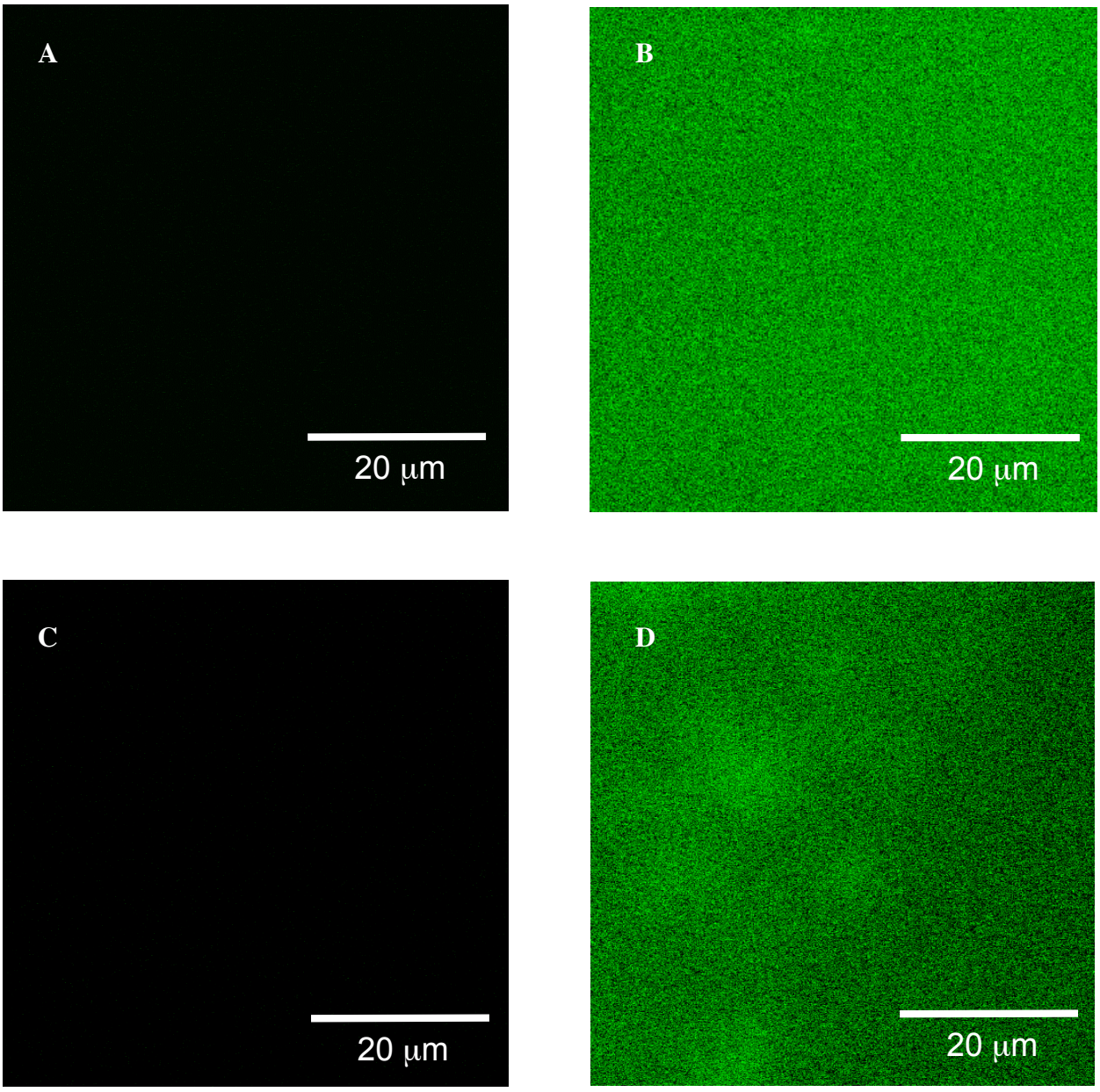

Figure 6.11. Fluorescently Imaged Functionalized-Surfaces
A) Untagged NHS linker slide. **B**) 5'-Fluorescein-tagged T_{25} ssDNA slide. **C**) Untagged T_{25} ssDNA slide. **D**) 3'-Fluorescein-tagged T_{25}:A_{25} dsDNA slide.

(Section 6.3.2) and are shown overlapped in Figure 6.12.

6.5 Summary

In conclusion, we have demonstrated that a strong NLO linear dichroic response is obtained when adenine and thymine bases undergo Watson-Crick base pairing to form a double helix. These are the first electronic measurements of chirality from sb-DNA. Given the high sensitivity and the label-free, molecularly specific nature afforded by nonlinear optical studies of DNA at aqueous/solid interfaces, real-time investigations of interfacial DNA hybridization and melting are now possible on the native system. The results obtained from these experiments should lead to improved biodiagnostic applications and new biologically relevant materials.

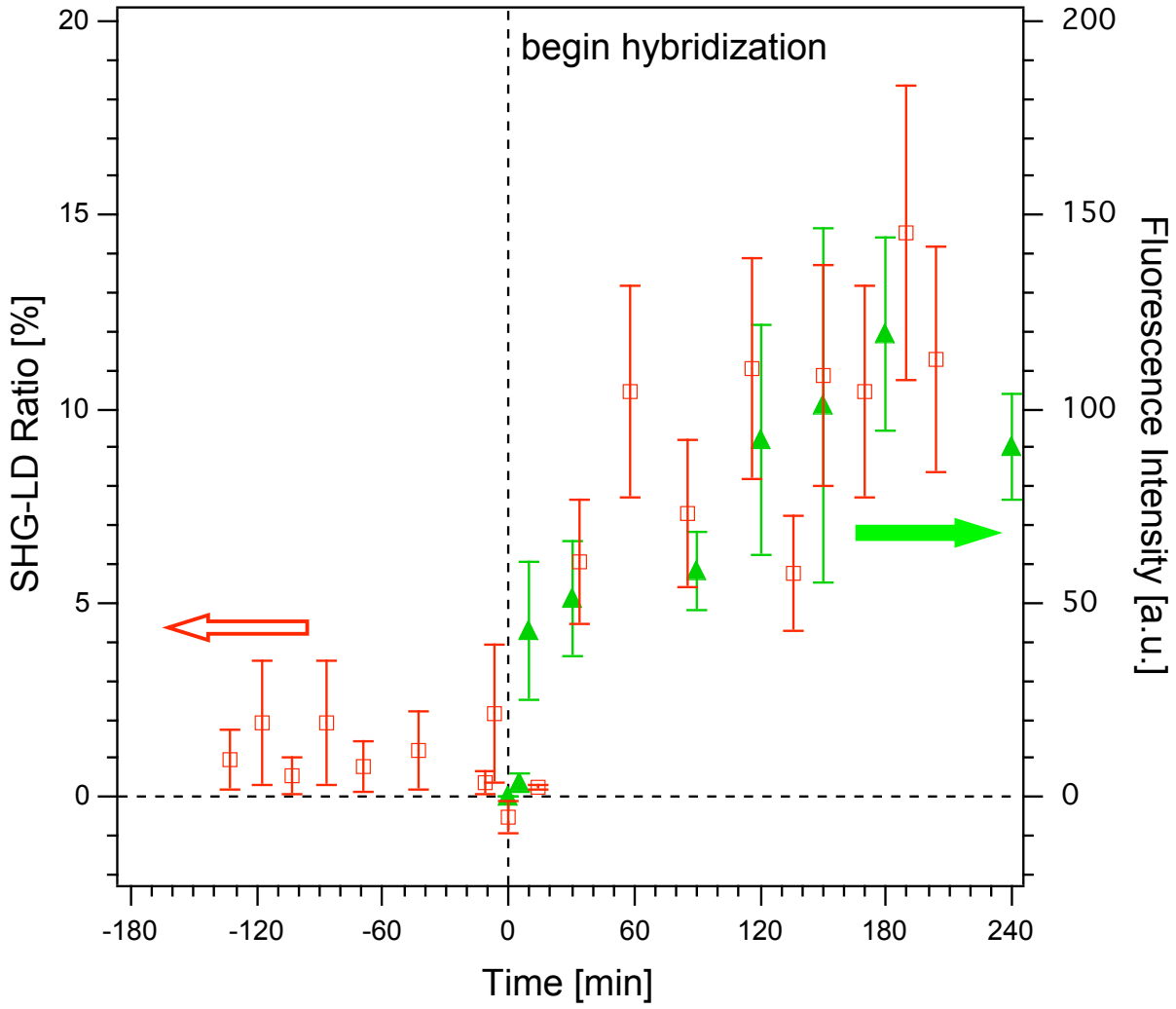

Figure 6.12. DNA Hybridization Time Determined by Fluorescence
Fluorescence confocal microscopy was used to image 10 different T_{25} ssDNA slides exposed to the solution of tagged complementary A_{25} DNA for time lengths ranging from 5 minutes to 4 hours and then rinsed with 0.25 M NaCl. The fluorescence data are shown overlapped with the SHG-LD ratios from Figure 6.7 and correlate to the same 2-hour hybridization time range.

CHAPTER 7

Outlook

Routine DNA detection, analysis, and sequencing have greatly benefited from extrinsic optical, electrochemical, or radiological labels, but labeled molecular-level studies of DNA are ultimately limited by their indirect nature and so is the information derived from them. As a result, our molecular-level understanding of DNA-target interactions is now just beginning to be understood. Clearly, fundamental advances in understanding the interaction of DNA with targets at a biosensor interface will continue to pave the way for developing faster, more sensitive, and increasingly more accurate methods of detecting disease markers and viruses.

We have made great progress in our novel application of nonlinear optics towards the study of DNA-functionalized interfaces, yet there remain many areas that have yet to be explored. Here, we outline a plan that our research could take in the future in order to continue this endeavor. These experiments build on our recent pioneering studies that apply, for the first time, second- and third-order nonlinear optical laser spectroscopies to DNA-functionalized fused quartz/water interfaces,[1-3] and include expansions of the resonantly enhanced SHG and $\vec{\chi}^{(3)}$ technique studies, as well as the introduction of liquid/solid SFG and heterodyne SHG imaging.

It is worthwhile to further investigate applications of resonantly enhanced SHG for DNA-functionalized interfaces. In Chapter 5, we probed, for the first time, the electronic modes of the DNA bases[3] by tuning the incident laser to a wavelength at the two-photon electronic resonance of the π-π^* transitions that are intrinsic to the bases.[4-7] In Chapter 6, we used second harmonic generation linear dichroism (SHG-LD)[8-11] to distinguish between single and double strand DNA (ssDNA and dsDNA)[3] by demonstrating that a strong nonlinear dichroic response is obtained when two complementary DNA strands form a double helix.[12-15] We will continue this work and apply SHG-LD to measure hybridization time for different lengths and sequences of DNA.

Hairpin DNA structures present an interesting system,[16-25] since their hybridization is not diffusion-limited and would be expected to exhibit shorter reaction time scales and possibly faster kinetics. Our group is currently using polarization-resolved SHG to study the binding of heavy metal pollutants, such as Pb^{2+} and Sr^{2+}, to DNA aptamers, forming chiral G-quadruplex structures important in biogeochemical systems.[26-33]

An additional future area of interest involves using the SHG $\vec{\chi}^{(3)}$ technique[34-38] to improve our modeling of interfacial potential and surface charge density. In Chapter 4, we used the Gouy-Chapman-Stern model[39-49] to obtain the full thermodynamic state information for surface-bound DNA as a function of the ionic strength in the surrounding aqueous solution.[1-3] We calculated surface charge densities and DNA strand densities of ssDNA between 15 and 35 bases long. We will investigate DNA with longer strand lengths and determine if there is a limit on the linear relationship between surface charge density and DNA strand length.

Another important extension of the work discussed here is using SFG to probe DNA at the liquid/solid interface. We discuss how SHG can be used to study DNA at the air/solid interface in Appendix 5,[2] but to monitor hybridization kinetics, the surface-bound DNA must be exposed to the aqueous phase *in situ*. This SFG system has already been built in our lab and polarization-resolved SFG is currently being used to detect changes in DNA chirality upon hybridization. We will use this setup to also look at the kinetics and time scales of the 3'-amine-terminated ssDNA reacting with the NHS linker to form an amide bond (see Chapter 3). The hybridization kinetics will be explored as the DNA strand length and sequence is changed. We will investigate how the hybridization and melting processes occur at a surface, i.e. whether it is a gradual, multi-step process or a sudden, two-state process.[50-52]

Perhaps the most valuable of all future work is heterodyne SHG $\ddot{\chi}^{(3)}$ imaging[53-61] of interfacial potentials, surface charge densities, and energies. Our results will be correlated with topological and chemical scanning probes such as atomic force microscopy (AFM), x-ray mapping, ellipsometry, secondary ion mass spectrometry (SIMS), and optical microscopy. We will interface an entry-level commercial fluorescence-grade microscope with our lasers and a CCD camera and image the scattered SHG either from the rear face of a prism or in reflection mode. We will be able to image 100 × 100 μm^2 areas, which we can prepare with nm- and μm-sized patterns using microcontact printing and dip-pen nanolithography.[62]

Using optical heterodyne detection, which is a powerful method for improving the sensitivity of coherent spectroscopies,[63-70] including that of SFG,[71] we will expand the sensitivity limit of our SHG $\ddot{\chi}^{(3)}$ imaging experiments. We will mix the signal E-field with an externally added local oscillator E-field at the SHG frequency. The intensity arises from the square modulus of the sum of the local and the signal E-fields at the detector, which is given by the cross term if the phases are matched.[72-74] The heterodyned images yield interfacial maps of electronic DNA resonances, charge density and potential, vibrational transitions, and chirality and are well suited for tracking the spatial and temporal evolution of nonlinear optical signals from the DNA. We will examine whether target recognition by the surface-bound oligonucleotides causes the surface charge density to evolve at or near "hot spots" as an oscillatory pattern, as a wave front, or at randomly distributed sites, a few possibilities for which literature precedents regarding surface reactions exist.[57,75-78] For patterned systems, we will study the cooperative behavior exhibited by the surfaces by changing the size and spacing of the chemical patterns to match that of, for instance, bulk vs. surface diffusion lengths and times.

REFERENCES

CHAPTER 1

1. Adamson, A. W. *Physical Chemistry of Surfaces*. 5th ed.; John Wiley & Sons, Inc.: New York, 1990; p 777.

2. Morel, F. M. M.; Hering, J. G. *Principles and Applications of Aquatic Chemistry*. John Wiley & Sons, Inc.: New York, 1993; p 588.

3. Somorjai, G. A. *Introduction to Surface Chemistry and Catalysis*. John Wiley & Sons, Inc.: New York, 1994; p 667.

4. Stumm, W.; Morgan, J. J. *Aquatic Chemistry: Chemical Equilibria and Rates in Natural Waters*. 3rd ed.; John Wiley & Sons, Inc.: New York, 1996; p 1022.

5. Langmuir, D. *Aqueous Environmental Geochemistry*. Prentice Hall: Upper Saddle River, NJ, 1997; p 600.

6. Gentle, I. *Interfacial Science: An Introduction.* Oxford University Press: New York, 2005; p 247.

7. Eisenthal, K. B. Equilibrium and Dynamic Processes at Interfaces by Second Harmonic and Sum Frequency Generation. *Annual Review of Physical Chemistry* **1992,** *43*, 627-661.

8. Brown, G. E.; Henrich, V. E.; Casey, W. H.; Clark, D. L.; Eggleston, C.; Felmy, A.; Goodman, D. W.; Gratzel, M.; Maciel, G.; McCarthy, M. I.; Nealson, K. H.; Sverjensky, D. A.; Toney, M. F.; Zachara, J. M. Metal Oxide Surfaces and Their Interactions with Aqueous Solutions and Microbial Organisms. *Chemical Reviews* **1999,** *99*, 77-174.

9. Linford, R. G. The Derivation of Thermodynamic Equations for Solid Surfaces. *Chemical Reviews* **1978,** *78*, 81-95.

10. Watterson, J. H.; Piunno, P. A. E.; Wust, C. C.; Krull, U. J. Effects of Oligonucleotide Immobilization Density on Selectivity of Quantitative Transduction of Hybridization of Immobilized DNA. *Langmuir* **2000,** *16*, 4984-4992.

11. Somorjai, G. A. The Evolution of Surface Chemistry. A Personal View of Building the Future on Past and Present Accomplishments. *Journal of Physical Chemistry B* **2002,** *106*, 9201-9213.

12. Heimel, G.; Romaner, L.; Zojer, E.; Bredas, J.-L. The Interface Energetics of Self-Assembled Monolayers on Metals. *Accounts of Chemical Research* **2008,** *41*, 721-729.

13. Voges, A. B.; Stokes, G. Y.; Gibbs-Davis, J. M.; Lettan, R. B.; Bertin, P. A.; Pike, R. C.; Nguyen, S. T.; Scheidt, K. A.; Geiger, F. M. Insights into Heterogeneous Atmospheric Oxidation Chemistry: Development of a Tailor-Made Synthetic Model for Studying Tropospheric Surface Chemistry. *Journal of Physical Chemistry C* **2007,** *111*, 1567-1578.

14. Atkinson, R.; Arey, J. Atmospheric Degradation of Volatile Organic Compounds. *Chemical Reviews* **2003,** *103*, 4605-4638.

15. Martin, S. T. Phase Transitions of Aqueous Atmospheric Particles. *Chemical Reviews* **2000,** *100*, 3403-3454.

16. Ravishankara, A. R. Heterogeneous and Multiphase Chemistry in the Troposphere. *Science* **1997,** *276*, 1058-1065.

17. Kang, H. C.; Weinberg, W. H. Modeling the Kinetics of Heterogeneous Catalysis. *Chemical Reviews* **1995,** *95*, 667-676.

18. Hattori, H. Heterogeneous Basic Catalysis. *Chemical Reviews* **1995,** *95*, 537-558.

19. Corn, R. M.; Higgins, D. A. Optical Second Harmonic Generation as a Probe of Surface Chemistry. *Chemical Reviews* **1994,** *94*, 107-125.

20. Gates, S. M. Surface Chemistry in the Chemical Vapor Deposition of Electronic Materials. *Chemical Reviews* **1996,** *96*, 1519-1532.

21. Richmond, G. L. Molecular Bonding and Interactions at Aqueous Surfaces as Probed by Vibrational Sum Frequency Spectroscopy. *Chemical Reviews* **2002,** *102*, 2693-2724.

22. Weckhuysen, B. M.; Wachs, I. E.; Schoonheydt, R. A. Surface Chemistry and Spectroscopy of Chromium in Inorganic Oxides. *Chemical Reviews* **1996,** *96*, 3327-3350.

23. Ghosh, S. K.; Pal, T. Interparticle Coupling Effect on the Surface Plasmon Resonance of Gold Nanoparticles: From Theory to Applications. *Chemical Reviews* **2007,** *107*, 4797-4862.

24. Zhao, J.; Li, B.; Onda, K.; Feng, M.; Petek, H. Solvated Electrons on Metal Oxide Surfaces. *Chemical Reviews* **2006,** *106*, 4402-4427.

25. Willets, K. A.; Van Duyne, R. P. Localized Surface Plasmon Resonance Spectroscopy and Sensing. *Annual Review of Physical Chemistry* **2007,** *58*, 267-297.

26. Wang, Z.; Fingas, M. Separation and Characterization of Petroleum Hydrocarbons and Surfactant in Orimulsion Dispersion Samples. *Environmental Science & Technology* **1996,** *30*, 3351-3361.

27. Chen, C.-C.; Lee, W.-J. Using Oily Wastewater Emulsified Fuel in Boiler: Energy Saving and Reduction of Air Pollutant Emissions. *Environmental Science & Technology* **2008,** *42*, 270-275.

28. Alper, J. Breaching the Membrane. *Science* **2002,** *296*, 838-839.

29. Schmidt, A. A. Membrane Transport: The Making of a Vesicle. *Nature* **2002,** *419*, 347-349.

30. Gouaux, E.; MacKinnon, R. Principles of Selective Ion Transport in Channels and Pumps. *Science* **2005,** *310*, 1461-1465.

31. Discher, D. E.; Eisenberg, A. Polymer Vesicles. *Science* **2002,** *297*, 967-973.

32. Allen, T. M.; Cullis, P. R. Drug Delivery Systems: Entering the Mainstream. *Science* **2004,** *303*, 1818-1822.

33. Grant, L. M.; Tiberg, F. Normal and Lateral Forces between Lipid Covered Solids in Solution: Correlation with Layer Packing and Structure. *Biophysical Journal* **2002,** *82*, 1373-1385.

34. Briscoe, W. H.; Titmuss, S.; Tiberg, F.; Thomas, R. K.; McGillivray, D. J.; Klein, J. Boundary Lubrication Under Water. *Nature* **2006,** *444*, 191-194.

35. Crosby, A. J.; Hageman, M.; Duncan, A. Controlling Polymer Adhesion with "Pancakes". *Langmuir* **2005,** *21*, 11738-11743.

36. Lee, J.; Fearing, R. S. Contact Self-Cleaning of Synthetic Gecko Adhesive from Polymer Microfibers. *Langmuir* **2008,** *24*, 10587-10591.

37. Younes, O.; Zhu, L.; Rosenberg, Y.; Shacham-Diamand, Y.; Gileadi, E. Electroplating of Amorphous Thin Films of Tungsten/Nickel Alloys. *Langmuir* **2001,** *17*, 8270-8275.

38. Hua, F.; Shi, J.; Lvov, Y.; Cui, T. Patterning of Layer-by-Layer Self-Assembled Multiple Types of Nanoparticle Thin Films by Lithographic Technique. *Nano Letters* **2002,** *2*, 1219-1222.

39. Kean, A. J.; Harley, R. A.; Littlejohn, D.; Kendall, G. R. On-Road Measurement of Ammonia and Other Motor Vehicle Exhaust Emissions. *Environmental Science & Technology* **2000,** *34*, 3535-3539.

40. Heitbaum, M.; Glorius, F.; Escher, I. Asymmetric Heterogeneous Catalysis. *Angewandte Chemie International Edition* **2006,** *45*, 4732-4762.

41. Calvert, J. G.; Lazrus, A.; Kok, G. L.; Heikes, B. G.; Walega, J. G.; Lind, J.; Cantrill, C. A. Chemical Mechanisms of Acid Generation in the Troposphere. *Nature* **1985,** *317*, 27-35.

42. Smol, J. P. *Pollution of Lakes and Rivers : A Paleoenvironmental Perspective* 2nd ed.; Blackwell Publishing: Malden, MA, 2008; p 383.

43. Abbatt, J. P. D.; Waschewsky, G. C. G. Heterogeneous Interactions of HOBr, HNO_3, O_3, and NO_2 with Deliquescent NaCl Aerosols at Room Temperature. *Journal of Physical Chemistry A* **1998,** *102*, 3719-3725.

44. Sorooshian, A.; Lu, M. L.; Brechtel, F. J.; Jonsson, H.; Feingold, G.; Flagan, R. C.; Seinfeld, J. H. On the Source of Organic Acid Aerosol Layers above Clouds. *Environmental Science & Technology* **2007,** *41*, 4647-4654.

45. Pilpel, N. Soap Films in Flotation, Dispersion, and Lubrication. *Chemical Reviews* **1966,** *66*, 29-46.

46. Stavans, J.; Glazier, J. A. Soap Froth Revisited: Dynamic Scaling in the Two-Dimensional Froth. *Physical Review Letters* **1989,** *62*, 1318-1321.

47. Miranda, P. B.; Pflumio, V.; Saijo, H.; Shen, Y. R. Conformation of Surfactant Monolayers at Solid/Liquid Interfaces. *Chemical Physics Letters* **1997,** *264*, 387-392.

48. Park, J. B.; Lakes, R. S. *Biomaterials: An Introduction.* 2nd ed.; Plenum Press: New York, 1992; p 394.

49. *Handbook of Biomaterials Evaluation : Scientific, Technical, and Clinical Testing of Implant Materials*. Taylor & Francis: Philadelphia, PA, 1999; p 915.

50. Chen, Z.; Shen, Y. R.; Somorjai, G. A. Studies of Polymer Surfaces by Sum Frequency Generation Vibrational Spectroscopy. *Annual Review of Physical Chemistry* **2002,** *53*, 437-465.

51. Freeman, R. G.; Hommer, M. B.; Grabar, K. C.; Jackson, M. A.; Natan, M. J. Ag-Clad Au Nanoparticles: Novel Aggregation, Optical, and Surface-Enhanced Raman Scattering Properties. *Journal of Physical Chemistry* **1996,** *100*, 718-724.

52. Link, S.; El-Sayed, M. A. Spectral Properties and Relaxation Dynamics of Surface Plasmon Electronic Oscillations in Gold and Silver Nanodots and Nanorods. *Journal of Physical Chemistry B* **1999,** *103*, 8410-8426.

53. McConnell, W. P.; Novak, J. P.; Brousseau, L. C.; Fuierer, R. R.; Tenent, R. C.; Feldheim, D. L. Electronic and Optical Properties of Chemically Modified Metal Nanoparticles and Molecularly Bridged Nanoparticle Arrays. *Journal of Physical Chemistry B* **2000,** *104*, 8925-8930.

54. Yan, E. C. Y.; Liu, Y.; Eisenthal, K. B. In Situ Studies of Molecular Transfer between Microparticles by Second-Harmonic Generation. *Journal of Physical Chemistry B* **2001,** *105*, 8531-8537.

55. Jayanti, S.; Britton, L. N.; Dwarakanath, V.; Pope, G. A. Laboratory Evaluation of Custom-Designed Surfactants To Remediate NAPL Source Zones. *Environmental Science & Technology* **2002,** *36*, 5491-5497.

56. Quinn, J.; Geiger, C.; Clausen, C.; Brooks, K.; Coon, C.; O'Hara, S.; Krug, T.; Major, D.; Yoon, W. S.; Gavaskar, A.; Holdsworth, T. Field Demonstration of DNAPL Dehalogenation Using Emulsified Zero-Valent Iron. *Environmental Science & Technology* **2005,** *39*, 1309-1318.

57. Vladimir, N. Prestressed Bridges and Marine Environment. *Journal of Structural Engineering* **1990,** *116*, 3191-3205.

58. Eiji, I.; Masatsugu, N.; Etsuko, K.; Hideki, N.; Takuya, T. Environment and Condition for Corrosion of Weathering Steel Bridge in Niigata. *Journal of Structual Engineering A* **2005,** *51A*, 1119-1128.

59. Isaac, R. A.; Gil, L.; Cooperman, A. N.; Hulme, K.; Eddy, B.; Ruiz, M.; Jacobson, K.; Larson, C.; Pancorbo, O. C. Corrosion in Drinking Water Distribution Systems: A Major Contributor of Copper and Lead to Wastewaters and Effluents. *Environmental Science & Technology* **1997,** *31*, 3198-3203.

60. Melitas, N.; Conklin, M.; Farrell, J. Electrochemical Study of Arsenate and Water Reduction on Iron Media Used for Arsenic Removal from Potable Water. *Environmental Science & Technology* **2002,** *36*, 3188-3193.

61. Boamfa, M. I.; Kim, M. W.; Maan, J. C.; Rasing, T. Observation of Surface and Bulk Phase Transitions in Nematic Liquid Crystals. *Nature* **2003,** *421*, 149-152.

62. Brannvall, M. L.; Bindler, R.; Renberg, I.; Emteryd, O.; Bartnicki, J.; Billstrom, K. The Medieval Metal Industry Was the Cradle of Modern Large-Scale Atmospheric Lead

Pollution in Northern Europe. *Environmental Science & Technology* **1999,** *33*, 4391-4395.

63. Barbier, F.; Duc, G.; Petit-Ramel, M. Adsorption of Lead and Cadmium Ions from Aqueous Solution to the Montmorillonite/Water Interface. *Colloids and Surfaces A: Physicochemical and Engineering Aspects* **2000,** *166*, 153-159.

64. Mifflin, A. L.; Gerth, K. A.; Weiss, B. M.; Geiger, F. M. Surface Studies of Chromate Binding to Fused Quartz/Water Interfaces. *Journal of Physical Chemistry A* **2003,** *107*, 6212-6217.

65. Minamisawa, M.; Minamisawa, H.; Yoshida, S.; Takai, N. Adsorption Behavior of Heavy Metals on Biomaterials. *Journal of Agricultural and Food Chemistry* **2004,** *52*, 5606-5611.

66. Perez, G.; Lopez-Mesas, M.; Valiente, M. Assessment of Heavy Metals Remobilization by Fractionation: Comparison of Leaching Tests Applied to Roadside Sediments. *Environmental Science & Technology* **2008,** *42*, 2309-2315.

67. Hayes, P. L.; Malin, J. N.; Konek, C. T.; Geiger, F. M. Interaction of Nitrate, Barium, Strontium and Cadmium Ions with Fused Quartz/Water Interfaces Studied by Second Harmonic Generation. *Journal of Physical Chemistry A* **2008,** *112*, 660-668.

68. Konek, C. T.; Musorrafiti, M. J.; Voges, A. B.; Bertin, P. A.; Nguyen, S. T.; Geiger, F. M. Tracking the Interaction of Transition Metal Ions with Environmental Interfaces Using Second Harmonic Generation. In *Adsorption of Metals by Geomedia II*, Barnett, M.; Kent, D., Eds. Elsevier: New York, 2008; Vol. 7, pp 95-124.

69. Malin, J. N.; Hayes, P. L.; Geiger, F. M. Interactions of Ca, Zn, and Cd Ions at Buried Solid/Water Interfaces Studied by Second Harmonic Generation. *Journal of Physical Chemistry C* **2008**.

70. Kulshrestha, P.; Giese, R. F.; Aga, D. S. Investigating the Molecular Interactions of Oxytetracycline in Clay and Organic Matter: Insights on Factors Affecting Its Mobility in Soil. *Environmental Science & Technology* **2004,** *38*, 4097-4105.

71. Hayes, P. L.; Gibbs-Davis, J. M.; Musorrafiti, M. J.; Mifflin, A. L.; Scheidt, K. A.; Geiger, F. M. Environmental Biogeochemistry Studied by Second-Harmonic Generation: A Look at the Agricultural Antibiotic Oxytetracycline. *Journal of Physical Chemistry C* **2007,** *111*, 8796-8804.

72. Pearson, R. G. Hard and Soft Acids and Bases. *Journal of the American Chemical Society* **1963,** *85*, 3533-3539.

73. Bordwell, F. G. Equilibrium Acidities in Dimethyl Sulfoxide Solution. *Accounts of Chemical Research* **1988,** *21*, 456-463.

74. Hynes, J. T. Physical Chemistry: The Protean Proton in Water. *Nature* **1999,** *397*, 565-567.

75. Gibbs-Davis, J. M.; Kruk, J. J.; Konek, C. T.; Sheidt, K. A.; Geiger, F. M. Jammed Acid-Base Chemistry at Interfaces. *Journal of the American Chemical Society* **2008,** *130*, 15444-15447.

76. Huang, L.-N.; De Wever, H.; Diels, L. Diverse and Distinct Bacterial Communities Induced Biofilm Fouling in Membrane Bioreactors Operated under Different Conditions. *Environmental Science & Technology* **2008,** *42*, 8360–8366.

77. Bongrand, P. Ligand-Receptor Interactions. *Reports on Progress in Physics* **1999,** *62*, 921-968.

78. Boncheva, M.; Scheibler, L.; Lincoln, P.; Vogel, H.; Aakerman, B. Design of Oligonucleotide Arrays at Interfaces. *Langmuir* **1999,** *15*, 4317-4320.

79. Reynolds, R. A.; Mirkin, C. A.; Letsinger, R. L. Homogeneous, Nanoparticle-Based Quantitative Colorimetric Detection of Oligonucleotides. *Journal of the American Chemical Society* **2000,** *122*, 3795-3796.

80. Kang, S. H.; Shortreed, M. R.; Yeung, E. S. Real-Time Dynamics of Single-DNA Molecules Undergoing Adsorption and Desorption at Liquid-Solid Interfaces. *Analytical Chemistry* **2001,** *73*, 1091-1099.

81. Holden, M. A.; Cremer, P. S. Microfluidic Tools for Studying the Specific Binding, Adsorption, and Displacement of Proteins at Interfaces. *Annual Review of Physical Chemistry* **2005,** *56*, 369-387.

82. Wong, E. L. S.; Chow, E.; Gooding, J. J. DNA Recognition Interfaces: The Influence of Interfacial Design on the Efficiency and Kinetics of Hybridization. *Langmuir* **2005,** *21*, 6957-6965.

83. Chen, D.; Wang, G.; Li, J. Interfacial Bioelectrochemistry: Fabrication, Properties and Applications of Functional Nanostructured Biointerfaces. *Journal of Physical Chemistry C* **2007,** *111*, 2351-2367.

84. Brown, G. E. Surface Science - How Minerals React with Water. *Science* **2001,** *294*, 67-69.

85. Yildirim, E. *Surface Chemistry of Solid and Liquid Interfaces*. Blackwell Publishing: Malden, MA, 2006; p 352.

86. Williams, C. T.; Beattie, D. A. Probing Buried Interfaces with Non-Linear Optical Spectroscopy. *Surface Science* **2002,** *500*, 545-576.

87. Hochella, M. F.; White, A. F. Mineral-Water Interface Geochemistry; An Overview. *Reviews in Mineralogy and Geochemistry* **1990,** *23*, 1-16.

88. Parks, G. A. Surface Energy and Adsorption at Mineral/Water Interfaces; An Introduction. *Reviews in Mineralogy and Geochemistry* **1990,** *23*, 133-175.

89. White, A. F.; Brantley, S. L. Chemical Weathering Rates of Silicate Minerals; An Overview. *Reviews in Mineralogy and Geochemistry* **1995,** *31*, 1-22.

90. Lasic, D. D.; Needham, D. The "Stealth" Liposome: A Prototypical Biomaterial. *Chemical Reviews* **1995,** *95*, 2601-2628.

91. Chrisey, D. B.; Pique, A.; McGill, R. A.; Horwitz, J. S.; Ringeisen, B. R.; Bubb, D. M.; Wu, P. K. Laser Deposition of Polymer and Biomaterial Films. *Chemical Reviews* **2003,** *103*, 553-576.

92. Ha, C. S.; Gardella, J. A. Surface Chemistry of Biodegradable Polymers for Drug Delivery Systems. *Chemical Reviews* **2005,** *105*, 4205-4232.

93. Rosi, N. L.; Mirkin, C. A. Nanostructures in Biodiagnostics. *Chemical Reviews* **2005,** *105*, 1547-1562.

94. Gates, B. D.; Xu, Q.; Stewart, M.; Ryan, D.; Willson, C. G.; Whitesides, G. M. New Approaches to Nanofabrication: Molding, Printing, and Other Techniques. *Chemical Reviews* **2005,** *105*, 1171-1196.

95. Firestone, M.; Schmidt, J.; Malmstadt, N. *Biosurfaces and Biointerfaces*. Materials Research Society: Warrendale, PA, 2006; p 240.

96. Dahl, J. A.; Maddux, B. L. S.; Hutchison, J. E. Toward Greener Nanosynthesis. *Chemical Reviews* **2007,** *107*, 2228-2269.

97. Boskey, A. L.; Roy, R. Cell Culture Systems for Studies of Bone and Tooth Mineralization. *Chemical Reviews* **2008,** *108*, 4716-4733.

98. Ramsden, J. *Biomedical Surfaces*. Artech House: Norwood, MA, 2008; p 270.

99. Little, L.; Healy, K. E.; Schaffer, D. Engineering Biomaterials for Synthetic Neural Stem Cell Microenvironments. *Chemical Reviews* **2008,** *108*, 1787-1796.

100. Arlinghaus, H. F.; Kwoka, M. N.; Jacobson, K. B. Analysis of Biosensor Chips for Identification of Nucleic Acids. *Analytical Chemistry* **1997,** *69*, 3747-3753.

101. Turner, A. P. F. Biosensors: Sense and Sensitivity. *Science* **2000,** *290*, 1315-1317.

102. McFadden, P. Tech.Sight: Broadband Biodetection: Holmes on a Chip. *Science* **2002,** *297*, 2075-2076.

103. Vercoutere, W.; Akeson, M. Biosensors for DNA Sequence Detection. *Current Opinion in Chemical Biology* **2002,** *6*, 816-822.

104. Castillo, J.; Gaspara, S.; Leth, S.; Niculescu, M.; Mortari, A.; Bontidean, I.; Soukharev, V.; Dorneanu, S. A.; Ryabov, A. D.; Csoregi, E. Biosensors for Life Quality: Design, Development and Applications. *Sensors and Actuators B: Chemical* **2004,** *102*, 179-194.

105. Levicky, R.; Horgan, A. Physicochemical Perspectives on DNA Microarray and Biosensor Technologies. *Trends in Biotechnology* **2005,** *23*, 143-149.

106. Rasooly, A.; Jacobson, J. Development of Biosensors for Cancer Clinical Testing. *Biosensors and Bioelectronics* **2006,** *21*, 1851-1858.

107. Rich, R. L.; Myszka, D. G. Survey of the Year 2006 Commercial Optical Biosensor Literature. *Journal of Molecular Recognition* **2007,** *20*, 300-366.

108. Borisov, S. M.; Wolfbeis, O. S. Optical Biosensors. *Chemical Reviews* **2008,** *108*, 423-461.

109. Sassolas, A.; Leca-Bouvier, B. D.; Blum, L. J. DNA Biosensors and Microarrays. *Chemical Reviews* **2008,** *108*, 109-139.

110. Wang, J. From DNA Biosensors to Gene Chips. *Nucleic Acids Research* **2000,** *28*, 3011-3016.

111. Manz, A.; Graber, N.; Widmer, H. M. Miniaturized Total Chemical Analysis Systems: A Novel Concept for Chemical Sensing. *Sensors and Actuators B: Chemical* **1990,** *1*, 244-248.

112. El-Ali, J.; Sorger, P. K.; Jensen, K. Cells on Chips. *Nature* **2006,** *442*, 403-411.

113. Dittrich, P. S.; Manz, A. Lab-on-a-Chip: Microfluidics in Drug Discovery. *Nature Reviews Drug Discovery* **2006,** *5*, 210-218.

114. Chiesl, T. N.; Shi, W.; Barron, A. E. Poly(acrylamide-co-alkylacrylamides) for Electrophoretic DNA Purification in Microchannels. *Analytical Chemistry* **2005,** *77*, 772-779.

115. Li, S.; Szegedi, S.; Goluch, E.; Liu, C. Dip Pen Nanolithography Functionalized Electrical Gaps for Multiplexed DNA Detection. *Analytical Chemistry* **2008,** *80*, 5899-5904.

116. Schaffar, B. P. H.; Kontschieder, H.; Ritter, C.; Berger, H. Highly Miniaturized and Integrated Biosensor for Analysis of Whole Blood Samples. *Clinical Chemistry* **1999,** *45*, 1678-1679.

117. Lyandres, O.; Yuen, J. M.; Shah, N. C.; Van Duyne, R. P.; Walsh, J. T., Jr.; Glucksberg, M. R. Progress Toward an In Vivo Surface-Enhanced Raman Spectroscopy Glucose Sensor. *Diabetes Technology and Therapeutics* **2008,** *10*, 257-265.

118. Brahim, S.; Narinesingh, D.; Guiseppi-Elie, A. Amperometric Determination of Cholesterol in Serum Using a Biosensor of Cholesterol Oxidase Contained within a Polypyrrole-Hydrogel Membrane. *Analytica Chimica Acta* **2001,** *448*, 27-36.

119. Madaras, M. B.; Buck, R. P. Miniaturized Biosensors Employing Electropolymerized Permselective Films and Their Use for Creatinine Assays in Human Serum. *Analytical Chemistry* **1996,** *68*, 3832-3839.

120. Rowe-Taitt, C. A.; Golden, J. P.; Feldstein, M. J.; Cras, J. J.; Hoffman, K. E.; Ligler, F. S. Array Biosensor for Detection of Biohazards. *Biosensors and Bioelectronics* **2000,** *14*, 785-794.

121. Hartley, H. A.; Baeumner, A. J. Biosensor for the Specific Detection of a Single Viable *B. Anthracis* Spore. *Analytical and Bioanalytical Chemistry* **2003,** *376*, 319-327.

122. Baeummer, A. J.; Leonard, B.; McElwee, J.; Montagna, R. A. A Rapid Biosensor for Viable *B. Anthracis Spores*. *Analytical & Bioanalytical Chemistry* **2004,** *380*, 15-23.

123. Tims, T. B.; Lim, D. V. Rapid Detection of *Bacillus Anthracis* Spores Directly from Powders with an Evanescent Wave Fiber-Optic Biosensor. *Journal of Microbiological Methods* **2004,** *59*, 127-130.

124. Pal, R.; Yang, M.; Lin, R.; Johnson, B. N.; Srivastava, N.; Razzacki, S. Z.; Chromistek, K. J.; Hledsinger, D. C.; Haque, R. M.; Ugaz, V. M.; Thwar, P. K.; Chen, Z.; Alfano, K.; Yim, M. B.; Krishnan, M.; Fuller, A. O.; Larson, R. G.; Burke, D. T.; Burns, M. A. An Integrated Microfluidic Device for Influenza and Other Genetic Analyses. *Lab on a Chip* **2005,** *5*, 1024-1032.

125. Oh, K. J.; Cash, K. J.; Hugenberg, V.; Plaxco, K. W. Peptide Beacons: A New Design for Polypeptide-Based Optical Biosensors. *Bioconjugate Chemistry* **2007,** *18*, 607-609.

126. Haes, A. J.; Chang, L.; Klein, W. L.; Van Duyne, R. P. Detection of a Biomarker for Alzheimer's Disease from Synthetic and Clinical Samples Using a Nanoscale Optical Biosensor. *Journal of the American Chemical Society* **2005,** *127*, 2264-2271.

127. Vestergaard, M. d.; Kerman, K.; Tamiya, E. The Study of Alzheimer's Disease Biomarkers. *NanoBioTechnology* **2006,** *2*, 5-16.

128. Gardberg, A. S.; Dice, L. T.; Ou, S.; Rich, R. L.; Helmbrecht, E.; Ko, J.; Wetzel, R.; Myszka, D. G.; Patterson, P. H.; Dealwis, C. Molecular Basis for Passive Immunotherapy of Alzheimer's Disease. *Proceedings of the National Academy of Sciences of the United States of America* **2007,** *104*, 15659-15664.

129. Chung, B. G.; Flanagan, L. A.; Rhee, S. W.; Schwart, P. H.; Lee, A. P.; Monuki, E. S.; Jeon, N. L. Human Neural Stem Cell Growth and Differentiation in a Gradient-Generating Microfluidic Device. *Lab on a Chip* **2005,** *5*, 401-406.

130. Kohn, J. E.; Plaxco, K. W. Engineering a Signal Transduction Mechanism for Protein-Based Biosensors. *Proceedings of the National Academy of Sciences of the United States of America* **2005,** *102*, 10841-10845.

131. Potyrailo, R. A.; Conrad, R. C.; Ellington, A. D.; Hieftje, G. M. Adapting Selected Nucleic Acid Ligands (Aptamers) to Biosensors. *Analytical Chemistry* **1998,** *70*, 3419-3425.

132. Hermann, T.; Patel, D. J. Adaptive Recognition by Nucleic Acid Aptamers. *Science* **2000,** *287*, 820-825.

133. Liss, M.; Petersen, B.; Wolf, H.; Prohaska, E. An Aptamer-Based Quartz Crystal Protein Biosensor. *Analytical Chemistry* **2002,** *74*, 4488-4495.

134. Miki, Y.; Swensen, J.; Shattuck-Eidens, D.; Futreal, P. A.; Harshman, K.; Tavtigian, S.; Liu, Q.; Cochran, C.; Bennett, L. M.; Ding, W.; Bell, R.; Rosenthal, J.; Hussey, C.; Tran, T.; McClure, M.; Frye, C.; Hattier, T.; Phelps, R.; Haugen-Strano, A.; Katcher, H.; Yakumo, K.; Gholami, Z.; Shaffer, D.; Stone, S.; Bayer, S.; Wray, C.; Bogden, R.; Dayananth, P.; Ward, J.; Tonin, P.; Narod, S.; Bristow, P. K.; Norris, F. H.; Helvering, L.; Morrison, P.; Rosteck, P.; Lai, M.; Barrett, J. C.; Lewis, C.; Neuhausen, S.; Cannon-Albright, L.; Goldgar, D.; Wiseman, R.; Kamb, A.; Skolnick, M. H. A Strong Candidate for the Breast and Ovarian Cancer Susceptibility Gene BRCA1. *Science* **1994,** *266*, 66-71.

135. Wooster, R.; Neuhausen, S. L.; Mangion, J.; Quirk, Y.; Ford, D.; Collins, N.; Nguyen, K.; Seal, S.; Tran, T.; Averill, D.; Fields, P.; Marshall, G.; Narod, S.; Lenoir, G. M.; Lynch, H.; Feunteun, J.; Devilee, P.; Cornelisse, C. J.; Menko, F. H.; Daly, P. A.; Ormiston, W.; McManus, R.; Pye, C.; Lewis, C. M.; Cannon-Albright, L. A.; Peto, J.; Ponder, B. A. J.; Skolnick, M. H.; Easton, D. F.; Goldgar, D. E.; Stratton, M. R. Localization of a Breast Cancer Susceptibility Gene, BRCA2, to Chromosome 13q12-13. *Science* **1994,** *265*, 2088-2090.

136. Skolnick, M. H.; Goldgar, D. E.; Yoshio, M.; Swenson, J.; Kamb, A.; Harshman, K. D.; Shattuck-Eidens, D. M.; Tavtigian, S. V.; Wiseman, R. W.; Futreal, P. A. 17q-Linked Breast and Ovarian Cancer Susceptibility Gene. 1998.

137. Malone, F. D.; Canick, J. A.; Ball, R. H.; Nyberg, D. A.; Comstock, C. H.; Bukowski, R.; Berkowitz, R. L.; Gross, S. J.; Dugoff, L.; Craigo, S. D.; Timor-Tritsch, I. E.; Carr, S. R.; Wolfe, H. M.; Dukes, K.; Bianchi, D. W.; Rudnicka, A. R.; Hackshaw, A. K.; Lambert-Messerlian, G.; Wald, N. J.; D'Alton, M. E. First-Trimester or Second-Trimester Screening, or Both, for Down's Syndrome. *New England Journal of Medicine* **2005,** *353*, 2001-2011.

138. Pereira, L.; Reddy, A. P.; Jacob, T.; Thomas, A.; Schneider, K. A.; Dasari, S.; Lapidus, J. A.; Lu, X.; Rodland, M.; Roberts, C. T.; Gravett, M. G.; Nagalla, S. R. Identification of Novel Protein Biomarkers of Preterm Birth in Human Cervical-Vaginal Fluid. *Journal of Proteome Research* **2007,** *6*, 1269-1276.

139. Schmutz, J.; Wheeler, J.; Grimwood, J.; Dickson, M.; Yang, J.; Caoile, C.; Bajorek, E.; Black, S.; Chan, Y. M.; Denys, M.; Escobar, J.; Flowers, D.; Fotopulos, D.; Garcia, C.; Gomez, M.; Gonzales, E.; Haydu, L.; Lopez, F.; Ramirez, L.; Retterer, J.; Rodriguez, A.; Rogers, S.; Salazar, A.; Tsai, M.; Myers, R. M. Quality Assessment of the Human Genome Sequence. *Nature* **2004,** *429*, 365-368.

140. International Human Genome Sequencing Consortium. Finishing the Euchromatic Sequence of the Human Genome. *Nature* **2004,** *431*, 931-945.

141. Wang, J.; Wang, W.; Li, R.; Li, Y.; Tian, G.; Goodman, L.; Fan, W.; Zhang, J.; Li, J.; Zhang, J.; Guo, Y.; Feng, B.; Li, H.; Lu, Y.; Fang, X.; Liang, H.; Du, Z.; Li, D.; Zhao, Y.; Hu, Y.; Yang, Z.; Zheng, H.; Hellmann, I.; Inouye, M.; Pool, J.; Yi, X.; Zhao, J.; Duan, J.; Zhou, Y.; Qin, J.; Ma, L.; Li, G.; Yang, Z.; Zhang, G.; Yang, B.; Yu, C.; Liang, F.; Li, W.; Li, S.; Li, D.; Ni, P.; Ruan, J.; Li, Q.; Zhu, H.; Liu, D.; Lu, Z.; Li, N.; Guo, G.; Zhang, J.; Ye, J.; Fang, L.; Hao, Q.; Chen, Q.; Liang, Y.; Su, Y.; San, A.; Ping, C.; Yang, S.; Chen, F.; Li, L.; Zhou, K.; Zheng, H.; Ren, Y.; Yang, L.; Gao, Y.; Yang, G.; Li, Z.; Feng, X.; Kristiansen, K.; Wong, G. K.-S.; Nielsen, R.; Durbin, R.; Bolund, L.; Zhang, X.; Li, S.; Yang, H.; Wang, J. The Diploid Genome Sequence of an Asian Individual. *Nature* **2008,** *456*, 60-65.

142. Accurate Whole Human Genome Sequencing Using Reversible Terminator Chemistry. *Nature* **2008,** *456*, 53-59.

143. Wheeler, D. A.; Srinivasan, M.; Egholm, M.; Shen, Y.; Chen, L.; McGuire, A.; He, W.; Chen, Y.-J.; Makhijani, V.; Roth, G. T.; Gomes, X.; Tartaro, K.; Niazi, F.; Turcotte, C. L.; Irzyk, G. P.; Lupski, J. R.; Chinault, C.; Song, X.-z.; Liu, Y.; Yuan, Y.; Nazareth, L.; Qin, X.; Muzny, D. M.; Margulies, M.; Weinstock, G. M.; Gibbs, R. A.; Rothberg, J. M. The Complete Genome of an Individual by Massively Parallel DNA Sequencing. *Nature* **2008,** *452*, 872-876.

144. Sims, M. R.; Cullen, D. C.; Bannister, N. P.; Grant, W. D.; Henry, O.; Jones, R.; McKnight, D.; Thompson, D. P.; Wilson, P. K. The Specific Molecular Identification of Life Experiment (SMILE). *Planetary and Space Science* **2005,** *53*, 781-791.

145. Parro, V.; Rodriguez-Manfredi, J. A.; Briones, C.; Compostizo, C.; Herrero, P. L.; Vez, E.; Sebastian, E.; Moreno-Paz, M.; Garcia-Villadangos, M.; Fernandez-Calvo, P.; Gonzalez-Toril, E.; Perez-Mercader, J.; Fernandez-Remolar, D.; Gomez-Elvira, J. Instrument Development to Search for Biomarkers on Mars: Terrestrial Acidophile, Iron-Powered Chemolithoautotrophic Communities as Model Systems. *Planetary and Space Science* **2005,** *53*, 729-737.

146. Watson, J. D.; Crick, F. H. C. A Structure for Deoxyribose Nucleic Acid. *Nature* **1953,** *421*, 397-398.

147. Voet, D.; Voet, J. G. *Biochemistry*. 2nd ed.; John Wiley & Sons, Inc.: New York, 1995; p 1361.

148. Bloomfield, V. A.; Crothers, D. M.; Tinoco, I., Jr. *Nucleic Acids: Structures, Properties, and Functions*. University Science Books: Sausalito, CA, 2000; p 794.

149. Cooper, G. M.; Hausman, R. E. *The Cell: A Molecular Approach*. 4th ed.; Sinauer Associates, Inc.: Washington D.C., 2007; p 820.

150. Alivisatos, A. P.; Johnsson, K. P.; Peng, X.; Wilson, T. E.; Loweth, C. J.; Bruchez, M. P.; Schultz, P. G. Organization of "Nanocrystal Molecules" Using DNA. *Nature* **1996,** *382*, 609-611.

151. Fodor, S. P. A. DNA Sequencing: Massively Parallel Genomics. *Science* **1997,** *277*, 393-395.

152. Winzeler, E. A.; Richards, D. R.; Conway, A. R.; Goldstein, A. L.; Kalman, S.; McCullough, M. J.; McCusker, J. H.; Stevens, D. A.; Wodicka, L.; Lockhart, D. J.; Davis, R. W. Direct Allelic Variation Scanning of the Yeast Genome. *Science* **1998,** *281*, 1194-1197.

153. Taton, T. A.; Mirkin, C. A.; Letsinger, R. L. Scanometric DNA Array Detection with Nanoparticle Probes. *Science* **2000,** *289*, 1757-1760.

154. Heaton, R. J.; Peterson, A. W.; Georgiadis, R. M. Electrostatic Surface Plasmon Resonance: Direct Electric Field-Induced Hybridization and Denaturation in Monolayer Nucleic Acid Films and Label-Free Discrimination of Base Mismatches. *Proceedings of the National Academy of Sciences of the United States of America* **2001,** *98*, 3701-3704.

155. Seeman, N. C. DNA in a Material World. *Nature* **2003,** *421*, 427-431.

156. Greiner, M.; Carter, P.; Korn, B.; Zink, D. New Approach to Complete Automation in Sizing and Quantitation of DNA and Proteins by the Automated Lab-on-a-Chip Platform from Agilent Technologies. *Nature Methods* **2004,** *1*, 87-89.

157. Wilson, W. D. Analyzing Biomolecular Interactions. *Science* **2002,** *295*, 2103-2105.

158. Kohli, P.; Harrell, C. C.; Cao, Z.; Gasparac, R.; Tan, W.; Martin, C. R. DNA-Functionalized Nanotube Membranes with Single-Base Mismatch Selectivity. *Science* **2004,** *305*, 984-986.

159. Walt, D. R. Miniature Analytical Methods for Medical Diagnostics. *Science* **2005,** *308*, 217-219.

160. Nakamura, F.; Ito, E.; Sakao, Y.; Ueno, N.; Gatuna, I. N.; Ohuchi, F. S.; Hara, M. Preparation of a Branched DNA Self-Assembled Monolayer toward Sensitive DNA Biosensors. *Nano Lett.* **2003,** *3*, 1083-1086.

161. Demers, L. M.; Mirkin, C. A.; Mucic, R. C.; Reynolds, R. A., III; Letsinger, R. L.; Elghanian, R.; Viswanadham, G. A Fluorescence-Based Method for Determining the Surface Coverage and Hybridization Efficiency of Thiol-Capped Oligonucleotides Bound to Gold Thin Films and Nanoparticles. *Analytical Chemistry* **2000,** *72*, 5535-5541.

162. Strother, T.; Cai, W.; Zhao, X.; Hamers, R. J.; Smith, L. M. Synthesis and Characterization of DNA-Modified Silicon (111) Surfaces. *Journal of the American Chemical Society* **2000,** *122*, 1205-1209.

163. Osborne, M. A.; Furey, W. S.; Klenerman, D.; Balasubramanian, S. Single-Molecule Analysis of DNA Immobilized on Microspheres. *Analytical Chemistry* **2000,** *72*, 3678-3681.

164. Hazani, M.; Naaman, R.; Hennrich, F.; Kappes, M. M. Confocal Fluorescence Imaging of DNA-Functionalized Carbon Nanotubes. *Nano Letters* **2003,** *3*, 153-155.

165. Rant, U.; Arinaga, K.; Fujita, S.; Yokoyama, N.; Abstreiter, G.; Tornow, M. Structural Properties of Oligonucleotide Monolayers on Gold Surfaces Probed by Fluorescence Investigations. *Langmuir* **2004,** *20*, 10086-10092.

166. Castelino, K.; Kannan, B.; Majumdar, A. Characterization of Grafting Density and Binding Efficiency of DNA and Proteins on Gold Surfaces. *Langmuir* **2005,** *21*, 1956-1961.

167. Clapp, A. R.; Medintz, I. L.; Mauro, J. M.; Fisher, B. R.; Bawendi, M. G.; Mattoussi, H. Fluorescence Resonance Energy Transfer Between Quantum Dot Donors and Dye-Labeled Protein Acceptors. *Journal of the American Chemical Society* **2004,** *126*, 301-310.

168. Medintz, I. L.; Konnert, J. H.; Clapp, A. R.; Stanish, I.; Twigg, M. E.; Mattoussi, H.; Mauro, J. M.; Deschamps, J. R. A Fluorescence Resonance Energy Transfer-Derived Structure of a Quantum Dot-Protein Bioconjugate Nanoassembly. *Proceedings of the National Academy of Sciences of the United States of America* **2004,** *101*, 9612-9617.

169. Fan, C.; Plaxco, K. W.; Heeger, A. J. Biosensors Based on Binding-Modulated Donor-Acceptor Distances. *Trends in Biotechnology* **2005,** *23*, 186-192.

170. Edel, J. B.; Eid, J. S.; Meller, A. Accurate Single Molecule FRET Efficiency Determination for Surface Immobilized DNA Using Maximum Likelihood Calculated Lifetimes. *Journal of Physical Chemistry B* **2007,** *111*, 2986-2990.

171. Elghanian, R.; Storhoff, J. J.; Mucic, R. C.; Letsinger, R. L.; Mirkin, C. A. Selective Colorimetric Detection of Polynucleotides Based on the Distance-Dependent Optical Properties of Gold Nanoparticles. *Science* **1997,** *277*, 1078-1080.

172. Storhoff, J. J.; Elghanian, R.; Mucic, R. C.; Mirkin, C. A.; Letsinger, R. L. One-Pot Colorimetric Differentiation of Polynucleotides with Single Base Imperfections Using Gold Nanoparticle Probes. *Journal of the American Chemical Society* **1998,** *120*, 1959-1964.

173. Storhoff, J. J.; Elghanian, R.; Mirkin, C. A.; Letsinger, R. L. Sequence-Dependent Stability of DNA-Modified Gold Nanoparticles. *Langmuir* **2002,** *18*, 6666-6670.

174. Hurst, S. J.; Han, M. S.; Lytton-Jean, A. K. R.; Mirkin, C. A. Screening the Sequence Selectivity of DNA-Binding Molecules Using a Gold Nanoparticle-Based Colorimetric Approach. *Analytical Chemistry* **2007,** *79*, 7201-7205.

175. Zhang, N.; Appella, D. H. Colorimetric Detection of Anthrax DNA with a Peptide Nucleic Acid Sandwich-Hybridization Assay. *Journal of the American Chemical Society* **2007,** *129*, 8424-8425.

176. Lee, J. S.; Ulmann, P. A.; Han, M. S.; Mirkin, C. A. A DNA-Gold Nanoparticle-Based Colorimetric Competition Assay for the Detection of Cysteine. *Nano Letters* **2008,** *8*, 529-533.

177. Kawaguchi, T.; Shiro, T.; Iwata, K. A Device for Visual Detection of Antigens and Antibodies by Means of Light Interference. *Thin Solid Films* **1990,** *191*, 369-381.

178. Gauglitz, G.; Brecht, A.; Kraus, G.; Mahm, W. Chemical and Biochemical Sensors Based on Interferometry at Thin (Multi-) Layers. *Sensors and Actuators B: Chemical* **1993,** *11*, 21-27.

179. Piehler, J.; Brecht, A.; Gauglitz, G. Affinity Detection of Low Molecular Weight Analytes. *Analytical Chemistry* **1996,** *68*, 139-143.

180. Cai, W.; Peck, J. R.; van der Weide, D. W.; Hammers, R. J. Direct Electrical Detection of Hybridization at DNA-Modified Silicon Surfaces. *Biosensors and Bioelectronics* **2004,** *19*, 1013-1019.

181. Pan, S.; Rothberg, L. Chemical Control of Electrode Functionalization for Detection of DNA Hybridization by Electrochemical Impedance Spectroscopy. *Langmuir* **2005,** *21*, 1022-1027.

182. Gibbs, J. M.; Park, S.-J.; Anderson, D. R.; Watson, K. J.; Mirkin, C. A.; Nguyen, S. T. Polymer-DNA Hybrids as Electrochemical Probes for the Detection of DNA. *Journal of the American Chemical Society* **2005,** *127*, 1170-1178.

183. Jin, R.; Wu, G.; Li, Z.; Mirkin, C. A.; Schatz, G. C. What Controls the Melting Properties of DNA-linked Gold Nanoparticle Assemblies? *Journal of the American Chemical Society* **2003,** *125*, 1643-1654.

184. Nam, J. M.; Stoeva, S. I.; Mirkin, C. A. Bio-Bar-Code-Based DNA Detection with PCR-like Sensitivity. *J. Am. Chem. Soc.* **2004,** *126*, 5932-5933.

185. Lytton-Jean, A. K. R.; Mirkin, C. A. A Thermodynamic Investigation into the Binding Properties of DNA Functionalized Gold Nanoparticle Probes and Molecular Fluorophore Probes. *Journal of the American Chemical Society* **2005,** *127*, 12754-12755.

186. Chrisey, L. A.; Lee, G. U.; O'Ferrall, C. E. Covalent Attachment of Synthetic DNA to Self-Assembled Monolayer Films. *Nucleic Acids Research* **1996,** *24*, 3031-3039.

187. Finot, E.; Bourillot, E.; Meunier-Prest, R.; Lacroute, Y.; Legay, G.; Cherkaoui-Malki, M.; Latruffe, N.; Siri, O.; Braunstein, P.; Dereux, A. Performance of Interdigitated

Nanoelectrodes for Electrochemical DNA Biosensor. *Ultramicroscopy* **2003,** *97*, 441-449.

188. Patsenker, L.; Tatarets, A.; Kolosova, O.; Obukhova, O.; Povrozin, Y.; Fedyunyayeva, I.; Yermolenko, I.; Terpetschnig, E. Fluorescent Probes and Labels for Biomedical Applications. *Annals of the New York Academy of Sciences* **2008,** *1130*, 179-187.

189. Georgiadis, R.; Peterlinz, K. P.; Peterson, A. W. Quantitative Measurements and Modeling of Kinetics in Nucleic Acid Monolayer Films Using SPR Spectroscopy. *Journal of the American Chemical Society* **2000,** *122*, 3166-3173.

190. Nelson, B. P.; Grimsrud, T. E.; Liles, M. R.; Goodman, R. M.; Corn, R. M. Surface Plasmon Resonance Imaging Measurements of DNA and RNA Hybridization Adsorption onto DNA Microarrays. *Analytical Chemistry* **2001,** *73*, 1-7.

191. Wang, J.; Bard, A. J. Monitoring DNA Immobilization and Hybridization on Surfaces by Atomic Force Microscopy Force Measurements. *Analytical Chemistry* **2001,** *73*, 2207-2212.

192. Boman, F. C.; Musorrafiti, M. J.; Gibbs, J. M.; Stepp, B. R.; Salazar, A. M.; Nguyen SonBinh, T.; Geiger Franz, M. DNA Single Stands Tethered to Fused Quartz/Water Interfaces Studied by Second Harmonic Generation. *Journal of the American Chemical Society* **2005,** *127*, 15368-15369.

193. Stokes, G. Y.; Gibbs-Davis, J. M.; Boman, F. C.; Stepp, B. R.; Condie, A. G.; Nguyen, S. T.; Geiger, F. M. Making "Sense" of DNA. *Journal of the American Chemical Society* **2007,** *129*, 7492-7493.

194. Boman, F. C.; Gibbs-Davis, J. M.; Heckman, L. M.; Stepp, B. R.; Nguyen, S. T.; Geiger, F. M. DNA at Aqueous/Solid Interfaces- Chirality-Based Detection via Second Harmonic Generation Activity. *Journal of the American Chemical Society* **2008,** *in press*.

195. Homola, J. Present and Future of Surface Plasmon Resonance Biosensors. *Analytical and Bioanalytical Chemistry* **2003,** *377*, 528-539.

196. Homola, J. Surface Plasmon Resonance Sensors for Detection of Chemical and Biological Species. *Chemical Reviews* **2008,** *108*, 462-493.

197. Willets, K. A.; Van Duyne, R. P. Localized Surface Plasmon Resonance Spectroscopy and Sensing. *Annual Review of Physical Chemistry* **2006,** *58*, 267-297.

198. Zhao, J.; Das, A.; Schatz, G. C.; Sligar, S. G.; Van Duyne, R. P. Resonance Localized Surface Plasmon Spectroscopy: Sensing Substrate and Inhibitor Binding to Cytochrome P450. *Journal of Physical Chemistry B* **2008,** *112*, 13084-13088.

199. Anker, J. N.; Hall, W. P.; Lyandres, O.; Shah, N. C.; Zhao, J.; Van Duyne, R. P. Biosensing with Plasmonic Nanosensors. *Nature Materials* **2008,** *7*, 442-454.

200. Cloarec, J. P.; Martin, J. R.; Polychronakos, C.; Lawrence, I.; Lawrence, M. F.; Souteyrand, E. Functionalization of Si/SiO_2 Substrates with Homooligonucleotides for a DNA Biosensor. *Sensors and Actuators B: Chemical* **1999,** *B58*, 394-398.

201. Fritz, J.; Cooper, E. B.; Gaudet, S.; Sorger, P. K.; Manalis, S. R. Electronic Detection of DNA by Its Intrinsic Molecular Charge. *Proceedings of the National Academy of Sciences of the United States of America* **2002,** *99*, 14142-14146.

202. Katz, E.; Willner, I. Probing Biomolecular Interactions at Conductive and Semiconductive Surfaces by Impedance Spectroscopy: Routes to Impedimetric Immunosensors, DNA-Sensors, and Enzyme Biosensors. *Electroanalysis* **2003,** *15*, 913-947.

203. Ebato, H.; Gentry, C. A.; Herron, J. N.; Mueller, W.; Okahata, Y.; Ringsdorf, H.; Suci, P. A. Investigation of Specific Binding of Antifluorescyl Antibody and Fab to Fluorescein Lipids in Langmuir-Blodgett Deposited Films Using Quartz Crystal Microbalance Methodology. *Analytical Chemistry* **1994,** *66*, 1683-1689.

204. Caruso, F.; Rodda, E.; Furlong, D. N.; Niikura, K.; Okahata, Y. Quartz Crystal Microbalance Study of DNA Immobilization and Hybridization for Nucleic Acid Sensor Development. *Analytical Chemistry* **1997,** *69*, 2043-2049.

205. Huang, E.; Zhou, F.; Deng, L. Studies of Surface Coverage and Orientation of DNA Molecules Immobilized onto Preformed Alkanethiol Self-Assembled Monolayers. *Langmuir* **2000,** *16*, 3272-3280.

206. Cooper, M. Label-Free Screening of Bio-Molecular Interactions. *Analytical and Bioanalytical Chemistry* **2003,** *377*, 834-842.

207. Su, X.; Wu, Y.-J.; Robelek, R.; Knoll, W. Surface Plasmon Resonance Spectroscopy and Quartz Crystal Microbalance Study of Streptavidin Film Structure Effects on Biotinylated DNA Assembly and Target DNA Hybridization. *Langmuir* **2005,** *21*, 348-353.

208. Lenigk, R.; Carles, M.; Ip, N. Y.; Sucher, N. J. Surface Characterization of a Silicon-Chip-Based DNA Microarray. *Langmuir* **2001,** *17*, 2497-2501.

209. Mourougou-Candoni, N.; Naud, C.; Thibaudau, F. Adsorption of Thiolated Oligonucleotides on Gold Surfaces: An Atomic Force Microscopy Study. *Langmuir* **2003,** *19*, 682-686.

210. Liu, M.; Liu, G.-Y. Hybridization with Nanostructures of Single-Stranded DNA. *Langmuir* **2005,** *21*, 1972-1978.

211. Lallemand, D.; Rouillat, M. H.; Dugas, V.; Chevolot, Y.; Souteyrand, E.; Phaner-Goutorbe, M. AFM characterization of ss-DNA probes immobilization: A sequence effect on surface organization. *Journal of Physics: Conference Series* **2007,** *61*, 658-662.

212. Charles, P. T.; Vora, G. J.; Andreadis, J. D.; Fortney, A. J.; Meador, C. E.; Dulcey, C. S.; Stenger, D. A. Fabrication and surface characterization of DNA microarrays using amine- and thiol-terminated oligonucleotide probes. *Langmuir* **2003,** *19*, 1586-1591.

213. Ray, S. G.; Cohen, H.; Naaman, R.; Rabin, Y. Where is the Sodium in Self-Assembled Monolayers of Single-Stranded DNA? *Journal of the American Chemical Society* **2005,** *127*, 17138-17139.

214. Lee, C. Y.; Gong, P.; Harbers, G. M.; Grainger, D. W.; Castner, D. G.; Gamble, L. J. Surface Coverage and Structure of Mixed DNA/Alkylthiol Monolayers on Gold: Characterization by XPS, NEXAFS, and Fluorescence Intensity Measurements. *Analytical Chemistry* **2006,** *78*, 3316-3325.

215. Petrovykh, D. Y.; Kimura-Suda, H.; Whitman, L. J.; Tarlov, M. J. Quantitative Analysis and Characterization of DNA Immobilized on Gold. *Journal of the American Chemical Society* **2003,** *125*, 5219-5226.

216. Kimura-Suda, H.; Petrovykh, D. Y.; Tarlov, M. J.; Whitman, L. J. Base-Dependent Competitive Adsorption of Single-Stranded DNA on Gold. *Journal of the American Chemical Society* **2003,** *125*, 9014-9015.

217. Peelen, D.; Smith, L. M. Immobilization of Amine-Modified Oligonucleotides on Aldehyde-Terminated Alkanethiol Monolayers on Gold. *Langmuir* **2005,** *21*, 266-271.

218. Wurpel, G. W. H.; Sovago, M.; Bonn, M. Sensitive Probing of DNA Binding to a Cationic Lipid Monolayer. *Journal of the American Chemical Society* **2007,** *129*, 8420-8421.

219. Sartenaer, Y.; Tourillon, G.; Dreesen, L.; Lis, D.; Mani, A. A.; Thiry, P. A.; Peremans, A. Sum-Frequency Generation Spectroscopy of DNA Monolayers. *Biosensors and Bioelectronics* **2007,** *22*, 2179-2183.

220. Asanuma, H.; Noguchi, H.; Uosaki, K.; Yu, H.-Z. Metal Cation-Induced Deformation of DNA Self-Assembled Monolayers on Silicon: Vibrational Sum Frequency Generation Spectroscopy. *Journal of the American Chemical Society* **2008,** *130*, 8016-8022.

221. Shen, Y. R. Surface Studies by Optical Second Harmonic Generation: An Overview. *Journal of Vacuum Science and Technology B* **1985,** *3*, 1464-1466.

222. Simpson, G. J. New Tools for Surface Second-harmonic Generation. *Applied Spectroscopy* **2001,** *55*, 16A-32A.

223. Geiger, F. M. Second Harmonic Generation, Sum Frequency Generation, and Chi(3): Dissecting Environmental Interfaces with a Nonlinear Optical Swiss Army Knife. *Annual Review of Physical Chemistry* **2009,** *60*, 61-83.

224. Mifflin, A. L.; Gerth, K. A.; Geiger, F. M. Kinetics of Chromate Adsorption and Desorption at Fused Quartz/Water Interfaces Studied by Second Harmonic Generation. *Journal of Physical Chemistry A* **2003,** *107*, 9620-9627.

CHAPTER 2

1. Shen, Y. R. *The Principles of Nonlinear Optics*. John Wiley & Sons, Inc.: New York, 1984.

2. Boyd, R. W. *Nonlinear Optics*. 2nd ed.; Academic Press: New York, 2003; p 578.

3. Franken, P. A.; Hill, A. E.; Peters, C. W.; Weinreich, G. Generation of Optical Harmonics. *Physical Review Letters* **1961,** *7*, 118-119.

4. Shen, Y. R. Surface Studies by Optical Second Harmonic Generation: An Overview. *Journal of Vacuum Science and Technology B* **1985,** *3*, 1464-1466.

5. Hicks, J. M.; Kemnitz, K.; Eisenthal, K. B.; Heinz, T. F. Studies of Liquid Surfaces by Second Harmonic Generation. *Journal of Physical Chemistry* **1986,** *90*, 560-562.

6. Eisenthal, K. B. Equilibrium and Dynamic Processes at Interfaces by Second Harmonic and Sum Frequency Generation. *Annual Review of Physical Chemistry* **1992,** *43*, 627-661.

7. Corn, R. M.; Higgins, D. A. Optical Second Harmonic Generation as a Probe of Surface Chemistry. *Chemical Reviews* **1994,** *94*, 107-125.

8. Eisenthal, K. B. Liquid Interfaces Probed by Second-Harmonic and Sum-Frequency Spectroscopy. *Chemical Reviews* **1996,** *96*, 1343-1360.

9. Eisenthal, K. B. Second Harmonic Spectroscopy of Aqueous Nano- and Microparticle Interfaces. *Chemical Reviews* **2006,** *106*, 1462-1477.

10. Zhu, X. D.; Suhr, H.; Shen, Y. R. In *Surface Vibrational Spectroscopy by Infrared-Visible Sum-Frequency Generation*, XIV International Conference on Quantum Electronics, Part 2, San Francisco, CA, June 9-13, 1986; B, J. O. S. A., IEEE: 1986; P252.

11. Zhu, X. D.; Suhr, H.; Shen, Y. R. Surface Vibrational Spectroscopy by Infrared-Visible Sum Frequency Generation. *Physical Review B: Condensed Matter and Materials Physics* **1987,** *35*, 3047-3050.

12. Shen, Y. R. Surface Properties Probed by Second-Harmonic and Sum-Frequency Generation. *Nature* **1989,** *337*, 519-525.

13. Shen, Y. R. Exploring New Opportunities with Sum-Frequency Nonlinear Optical Spectroscopy. *Pure and Applied Chemistry* **2001,** *73*, 1589-1598.

14. Richmond, G. L. Molecular Bonding and Interactions at Aqueous Surfaces as Probed by Vibrational Sum Frequency Spectroscopy. *Chemical Reviews* **2002,** *102*, 2693-2724.

15. He, G. S.; Liu, S. H. *Physics of Nonlinear Optics*. World Scientific Publishing Co.: River Edge, NJ, 2000; p 576.

16. Eisenthal, K. B. Liquid Interfaces. *Accounts of Chemical Research* **1993,** *26*, 636-643.

17. Simpson, G. J. New Tools for Surface Second-harmonic Generation. *Applied Spectroscopy* **2001,** *55*, 16A-32A.

18. Geiger, F. M. Second Harmonic Generation, Sum Frequency Generation, and Chi(3): Dissecting Environmental Interfaces with a Nonlinear Optical Swiss Army Knife. *Annual Review of Physical Chemistry* **2009,** *60*, 61-83.

19. Ong, S.; Zhao, X.; Eisenthal, K. B. Polarization of Water Molecules at a Charged Interface: Second-Harmonic Studies of the Silica/Water Interface. *Chemical Physics Letters* **1992,** *191*, 327-335.

20. Wang, H.; Borguet, E.; Eisenthal, K. B. Polarity of Liquid Interfaces by Second Harmonic Generation Spectroscopy. *Journal of Physical Chemistry A* **1997,** *101*, 713-718.

21. Guyot-Sionnest, P.; Chen, W.; Shen, Y. R. General Considerations on Optical Second-Harmonic Generation from Surfaces and Interfaces. *Physical Review B* **1986,** *33*, 8254-8263.

22. Byers, J. D.; Yee, H. I.; Petralli-Mallow, T.; Hicks, J. M. Second-Harmonic Generation Circular-Dichroism Spectroscopy from Chiral Monolayers. *Physical Review B: Condensed Matter and Materials Physics* **1994,** *49*, 14643-14647.

23. Mifflin, A. L.; Gerth, K. A.; Weiss, B. M.; Geiger, F. M. Surface Studies of Chromate Binding to Fused Quartz/Water Interfaces. *Journal of Physical Chemistry A* **2003,** *107*, 6212-6217.

24. Al-Abadleh, H. A.; Mifflin, A. L.; Bertin, P. A.; Nguyen, S. T.; Geiger, F. M. Control of Carboxylic Acid and Ester Groups on Chromium (VI) Binding to Functionalized Silica/Water Interfaces Studied by Second Harmonic Generation. *Journal of Physical Chemistry B* **2005,** *109*, 9691-9702.

25. Hayes, P. L.; Malin, J. N.; Konek, C. T.; Geiger, F. M. Interaction of Nitrate, Barium, Strontium and Cadmium Ions with Fused Quartz/Water Interfaces Studied by Second Harmonic Generation. *Journal of Physical Chemistry A* **2008,** *112*, 660-668.

26. Konek, C. T.; Musorrafiti, M. J.; Voges, A. B.; Bertin, P. A.; Nguyen, S. T.; Geiger, F. M. Tracking the Interaction of Transition Metal Ions with Environmental Interfaces Using Second Harmonic Generation. In *Adsorption of Metals by Geomedia II*, Barnett, M.; Kent, D., Eds. Elsevier: New York, 2008; Vol. 7, pp 95-124.

27. Malin, J. N.; Hayes, P. L.; Geiger, F. M. Interactions of Zinc, Calcium, and Cadmium Ions at Buried Solid/Water Interfaces Studied by Second Harmonic Generation. *Journal of Physical Chemistry C* **2008,** *ASAP*.

28. Malin, J. N.; Hayes, P. L.; Geiger, F. M. Interactions of Ca, Zn, and Cd Ions at Buried Solid/Water Interfaces Studied by Second Harmonic Generation. *Journal of Physical Chemistry C* **2008**.

29. Musorrafiti, M.; Konek, C. T.; Hayes, P. L.; Geiger, F. M. Interaction of Chromium(VI) with the _-Aluminum Oxide-Water Interface. *Journal of Physical Chemistry C* **2008,** *112*, 2032-2039.

30. Salafsky, J. S.; Eisenthal, K. B. Protein Adsorption at Interfaces Detected by Second Harmonic Generation. *Journal of Physical Chemistry B* **2000,** *104*, 7752-7755.

31. Eckenrode, H. M.; Dai, H.-L. Nonlinear Optical Probe of Biopolymer Adsorption on Colloidal Particle Surface: Poly-L-lysine on Polystyrene Sulfate Microspheres. *Langmuir* **2004,** *20*, 9202-9209.

32. Polizzi, M. A.; Plocinik, R. M.; Simpson, G. J. Ellipsometric Approach for the Real-Time Detection of Label-Free Protein Adsorption by Second Harmonic Generation. *Journal of the American Chemical Society* **2004,** *126*, 5001-5007.

33. Salafsky, J. S.; Eisenthal, K. B. Protein Adsorption at Interfaces Detected by Second Harmonic Generation. [Erratum to document cited in CA133:248560]. *Journal of Physical Chemistry B* **2004,** *108*, 3376.

34. Konek, C. T.; Illg, K. D.; Al-Abadleh, H. A.; Voges, A. B.; Yin, G.; Musorrafiti, M. J.; Schmidt, C. M.; Geiger, F. M. Nonlinear Optical Studies of the Agricultural Antibiotic Morantel Interacting with Silica/Water Interfaces. *Journal of the American Chemical Society* **2005,** *127*, 15771-15777.

35. Mifflin, A. L.; Konek, C. T.; Geiger, F. M. Tracking Oxytetracycline Mobility Across Environmental Interfaces by Second Harmonic Generation. *Journal of Physical Chemistry B* **2006,** *110*, 22577-22585.

36. Hayes, P. L.; Gibbs-Davis, J. M.; Musorrafiti, M. J.; Mifflin, A. L.; Scheidt, K. A.; Geiger, F. M. Environmental Biogeochemistry Studied by Second-Harmonic Generation:

A Look at the Agricultural Antibiotic Oxytetracycline. *Journal of Physical Chemistry C* **2007,** *111*, 8796-8804.

37. Geiger, F. M.; Tridico, A. C.; Hicks, J. M. Second Harmonic Generation Studies of Ozone Depletion Reactions on Ice Surfaces Under Stratospheric Conditions. *Journal of Physical Chemistry B* **1999,** *103*, 8205-8215.

38. Mifflin, A. L.; Gerth, K. A.; Geiger, F. M. Kinetics of Chromate Adsorption and Desorption at Fused Quartz/Water Interfaces Studied by Second Harmonic Generation. *Journal of Physical Chemistry A* **2003,** *107*, 9620-9627.

39. Al-Abadleh, H. A.; Mifflin, A. L.; Musorrafiti, M. J.; Geiger, F. M. Kinetic Studies of Chromium (VI) Binding to Carboxylic Acid- and Methyl Ester-Functionalized Silica/Water Interfaces Important in Geochemistry. *Journal of Physical Chemistry B* **2005,** *109*, 16852-16859.

40. Shi, X.; Borguet, E.; Tarnovsky, A. N.; Eisenthal, K. B. Ultrafast Dynamics and Structure at Aqueous Interfaces by Second Harmonic Generation. *Chemical Physics* **1996,** *205*, 167-178.

41. Yan, E. C. Y.; Eisenthal, K. B. Rotational Dynamics of Anisotropic Microscopic Particles Studied by Second Harmonic Generation. *Journal of Physical Chemistry B* **2000,** *104*, 6686-6689.

42. Shang, X.; Benderskii, A. V.; Eisenthal, K. B. Ultrafast Solvation Dynamics at Silica/Liquid Interfaces Probed by Time-Resolved Second Harmonic Generation. *Journal of Physical Chemistry B* **2001,** *105*, 11578-11585.

43. Benderskii, A. V.; Eisenthal, K. B. Dynamical Time Scales of Aqueous Solvation at Negatively Charged Lipid/Water Interfaces. *Journal of Physical Chemistry A* **2002,** *106*, 7482-7490.

44. Pozniak, B.; Scherson, D. A. In Situ Dual-Beam Coincidence Second Harmonic Generation as a Probe of Spatially Resolved Dynamics at Electrochemical Interfaces. *Journal of the American Chemical Society* **2004,** *126*, 14696-14697.

45. Ries, R. S.; Choi, H.; Blunck, R.; Bezanilla, F.; Heath, J. R. Black Lipid Membranes: Visualizing the Structure, Dynamics, and Substrate Dependence of Membranes. *Journal of Physical Chemistry B* **2004,** *108*, 16040-16049.

46. Hirose, Y.; Yui, H.; Sawada, T. Second Harmonic Generation-Based Coherent Vibrational Spectroscopy for a Liquid Interface under the Nonresonant Pump Condition. *Journal of Physical Chemistry B* **2005,** *109*, 13063-13066.

47. Srivastava, A.; Eisenthal, K. B. Kinetics of Molecular Transport Across a Liposome Bilayer. *Chemical Physics Letters* **1998,** *292*, 345-351.

48. Yan, E. C. Y.; Eisenthal, K. B. Effect of Cholesterol on Molecular Transport of Organic Cations Across Liposome Bilayers Probed by Second Harmonic Generation. *Biophysical Journal* **2000,** *79*, 898-903.

49. Shang, X.; Liu, Y.; Yan, E.; Eisenthal, K. B. Effects of Counterions on Molecular Transport Across Liposome Bilayer: Probed by Second Harmonic Generation. *Journal of Physical Chemistry B* **2001,** *105*, 12816-12822.

50. Simpson, G. J.; Rowlan, K. L. Orientation-Insensitive Methodology for Second Harmonic Generation. 2. Application to Adsorption Isotherm and Kinetics Measurements. *Analytical Chemistry* **2000,** *72*, 3407-3411.

51. Simpson, G. J.; Rowlan, K. L. Orientation-Insensitive Methodology for Second Harmonic Generation. 1. Theory. *Analytical Chemistry* **2000,** *72*, 3399-3406.

52. Salafsky, J. S.; Eisenthal, K. B. Second Harmonic Spectroscopy: Detection and Orientation of Molecules at a Biomembrane Interface. *Chemical Physics Letters* **2000,** *319*, 435-439.

53. Burke, B. J.; Moad, A. J.; Polizzi, M. A.; Simpson, G. J. Experimental Confirmation of the Importance of Orientation in the Anomalous Chiral Sensitivity of Second Harmonic Generation. *Journal of the American Chemical Society* **2003,** *125*, 9111-9115.

54. Lagugne-Labarthet, F.; Sourisseau, C.; Schaller, R. D.; Saykally, R. J.; Rochon, P. Chromophore Orientations in a Nonlinear Optical Azopolymer Diffraction Grating: Even and Odd Order Parameters from Far-Field Raman and Near-Field Second Harmonic Generation Microscopies. *Journal of Physical Chemistry B* **2004,** *108*, 17059-17068.

55. Plocinik, R. M.; Simpson, G. J. Polarization Characterization in Surface Second Harmonic Generation by Nonlinear Optical Null Ellipsometry. *Analytica Chimica Acta* **2003,** *496*, 133-142.

56. Leray, A.; Leroy, L.; Le Grand, Y.; Odin, C.; Renault, A.; Vie, V.; Rouede, D.; Mallego., T.; Mongin, O.; Werts, M. H. V.; Blanchard-Desce, M. Organization and Orientation of Amphiphilic Push-Pull Chromophores Deposited in Langmuir-Blodgett Monolayers Studied by Second Harmonic Generation and Atomic Force Microscopy. *Langmuir* **2004,** *20*, 8165-8171.

57. Simpson, G. J.; Dailey, C. A.; Plocinik, R. M.; Moad, A. J.; Polizzi, M. A.; Everly, R. M. Direct Determination of Effective Interfacial Optical Constants by Nonlinear Optical Null Ellipsometry of Chiral Films. *Analytical Chemistry* **2005,** *77*, 215-224.

58. Mitchell, S. A. Nonlinear Susceptibility of a Cyanobiphenyl Derivative at the Air/Water Interface: Improved Measurement of Molecular Orientation by Optical Second Harmonic Generation. *Journal of Physical Chemistry B* **2006,** *110*, 883-890.

59. Zhao, X.; Subrahmanyan, S.; Eisenthal, K. B. Determination of pK_a at the Air/Water Interface by Second Harmonic Generation. *Chemical Physics Letters* **1990,** *171*, 558-562.

60. Zhao, X.; Ong, S.; Eisenthal, K. B. Polarization of Water Molecules at a Charged Interface. Second Harmonic Studies of Charged Monolayers at the Air/Water Interface. *Chemical Physics Letters* **1993,** *202*, 513-520.

61. Yan, E. C. Y.; Liu, Y.; Eisenthal, K. B. New Method for Determination of Surface Potential of Microscopic Particles by Second Harmonic Generation. *Journal of Physical Chemistry B* **1998,** *102*, 6331-6336.

62. Liu, Y.; Yan, E. C. Y.; Zhao, X.; Eisenthal, K. B. Surface Potential of Charged Liposomes Determined by Second Harmonic Generation. *Langmuir* **2001,** *17*, 2063-2066.

63. Liu, Y.; Yan, E. C. Y.; Eisenthal, K. B. Effects of Bilayer Surface Charge Density on Molecular Adsorption and Transport across Liposome Bilayers. *Biophysical Journal* **2001,** *80*, 1004-1012.

64. Konek, C. T.; Musorrafiti, M. J.; Al-Abadleh, H. A.; Bertin, P. A.; Nguyen, S. T.; Geiger, F. M. Interfacial Acidities, Charge Densities, Potentials, and Energies of Carboxylic Acid-Functionalized Silica/Water Interfaces Determined by Second Harmonic Generation. *Journal of the American Chemical Society* **2004,** *126*, 11754-11755.

65. Fitts, J. P.; Shang, X.; Flynn, G. W.; Heinz, T. F.; Eisenthal, K. B. Electrostatic Surface Charge at Aqueous/a-Al_2O_3 Single-Crystal Interfaces as Probed by Optical Second-Harmonic Generation. *Journal of Physical Chemistry B* **2005,** *109*, 7981-7986.

66. Koelsch, P.; Motschmann, H. Varying the Counterions at a Charged Interface. *Langmuir* **2005,** *21*, 3436-3442.

67. Petralli-Mallow, T.; Wong, T. M.; Byers, J. D.; Yee, H. I.; Hicks, J. M. Circular Dichroism Spectroscopy at Interfaces: A Surface Second Harmonic Generation Study. *Journal of Physical Chemistry* **1993,** *97*, 1383-1388.

68. Byers, J. D.; Hicks, J. M. Electronic Spectral Effects on Chiral Surface Second Harmonic Generation. *Chemical Physics Letters* **1994,** *231*, 216-224.

69. Byers, J. D.; Yee, H. I.; Hicks, J. M. A Second Harmonic Generation Analog of Optical Rotatory Dispersion for the Study of Chiral Monolayers. *The Journal of Chemical Physics* **1994,** *101*, 6233-6241.

70. Kauranen, M.; Verbiest, T.; Maki, J. J.; Persoons, A. Second-Harmonic Generation from Chiral Surfaces. *The Journal of Chemical Physics* **1994,** *101*, 8193-8199.

71. Petralli-Mallow, T. P.; Hicks, J. M. In *Laser Probes of Chirality at Interfaces*, Book of Abstracts, 212th ACS National Meeting, Orlando, FL, August 25-29, 1996; 1996; CATL-009.

72. Maki, J. J.; Verbiest, T.; Kauranen, M.; Van Elshocht, S.; Persoons, A. Comparison of Linearly and Circularly Polarized Probes of Second-Order Optical Activity of Chiral Surfaces. *The Journal of Chemical Physics* **1996,** *105*, 767-772.

73. Hicks, J. M.; Petralli-Mallow, T. Nonlinear Optics of Chiral Surface Systems. *Applied Physics B: Lasers and Optics* **1999,** *B68*, 589-593.

74. Simpson, G. J. Structural Origins of Circular Dichroism in Surface Second Harmonic Generation. *The Journal of Chemical Physics* **2002,** *117*, 3398-3410.

75. Kriech, M. A.; Conboy, J. C. Counterpropagating Second-Harmonic Generation: A New Technique for the Investigation of Molecular Chirality at Surfaces. *Journal of the Optical Society of America B: Optical Physics* **2004,** *21*, 1013-1022.

76. Boyd, G. T.; Shen, Y. R.; Hansch, T. W. Continuous-Wave Second-Harmonic Generation as a Surface Microprobe. *Optics Letters* **1986,** *11*, 97-99.

77. Florsheimer, M.; Sulmen, H.; Bosch, M.; Brillert, C.; Wierschem, M.; Fuchs, H. Molecular Surface Orientation Field of a Langmuir Monolayer Determined by Second-Harmonic Microscopy. *Advanced Materials* **1997,** *9*, 1056-1060.

78. Moreaux, L.; Sandre, O.; Blanchard-Desce, M.; Mertz, J. Membrane Imaging by Simultaneous Second-Harmonic Generation and Two-Photon Microscopy. *Optics Letters* **2000,** *25*, 320-322.

79. Bouevitch, O.; Lewis, A.; Pinevsky, I.; Wuskell, J. P.; Loew, L. M. Probing Membrane Potential with Nonlinear Optics. *Biophysical Journal* **1993,** *65*, 672-679.

80. Campagnola, P. J.; Wei, M.-d.; Lewis, A.; Loew, L. M. High-Resolution Nonlinear Optical Imaging of Live Cells by Second Harmonic Generation. *Biophysical Journal* **1999,** *77*, 3341-3349.

81. Schaller, R. D.; Roth, C.; Raulet, D. H.; Saykally, R. J. Near-Field Second Harmonic Imaging of Granular Membrane Structures in Natural Killer Cells. *Journal of Physical Chemistry B* **2000,** *104*, 5217-5220.

82. Kriech, M. A.; Conboy, J. C. Imaging Chirality with Surface Second Harmonic Generation Microscopy. *Journal of the American Chemical Society* **2005,** *127*, 2834-2835.

83. Boman, F. C.; Musorrafiti, M. J.; Gibbs, J. M.; Stepp, B. R.; Salazar, A. M.; Nguyen SonBinh, T.; Geiger Franz, M. DNA Single Stands Tethered to Fused Quartz/Water Interfaces Studied by Second Harmonic Generation. *Journal of the American Chemical Society* **2005,** *127*, 15368-15369.

84. Stokes, G. Y.; Gibbs-Davis, J. M.; Boman, F. C.; Stepp, B. R.; Condie, A. G.; Nguyen, S. T.; Geiger, F. M. Making "Sense" of DNA. *Journal of the American Chemical Society* **2007,** *129*, 7492-7493.

85. Boman, F. C.; Gibbs-Davis, J. M.; Heckman, L. M.; Stepp, B. R.; Nguyen, S. T.; Geiger, F. M. DNA at Aqueous/Solid Interfaces- Chirality-Based Detection via Second Harmonic Generation Activity. *Journal of the American Chemical Society* **2008,** *in press*.

86. Heinz, T. F. Second-Order Nonlinear Optical Effects at Surfaces and Interfaces. In *Nonlinear Surface Electromagnetic Phenomena*, Ponath, H.; Stegeman, G., Eds. Elsevier Publishers: Amsterdam, NY, 1991; pp 353-416.

87. *All Diode-Pumped Kilohertz Ti:Sapphire Regenerative Amplifier Syster User's Manual: Hurricane*. Spectra-Physics: Mountain View, CA, 2000.

88. *Multi-Kilohertz, Intra-Cavity Doubled, Diode-Pumped Nd:YLF Laser User's Manual: Evolution*. Positive Light, Inc.: Los Gatos, CA, 2001.

89. *Diode-Pumped, Mode-Locked Ti:Sapphire Laser User's Manual: Mai Tai*. Spectra-Physics: Mountain View, CA, 2002.

90. *Ultrafast Optical Parametric Amplifier User's Manual: OPA-800C*. Spectra-Physics: Mountain View, CA, 2001.

CHAPTER 3

1. Pirrung, M. C. How to Make a DNA Chip. *Angewandte Chemie International Edition* **2002,** *41*, 1276-1289.

2. Onclin, S.; Ravoo, B. J.; Reinhoudt, D. N. Engineering Silicon Oxide Surfaces Using Self-Assembled Monolayers. *Angewandte Chemie International Edition* **2005,** *44*, 6282-6304.

3. Szunerits, S.; Boukherroub, R. Preparation and Characterization of Thin Films of SiO_x on Gold Substrates for Surface Plasmon Resonance Studies. *Langmuir* **2006,** *22*, 1660-1663.

4. Zisman, W. A. Surface Chemistry of Plastics Reinforced by Strong Fibers. *Industrial & Engineering Chemistry Product Research Development* **1969,** *8*, 98-111.

5. Lee, L.-H. Wettability and Conformation of Reactive Polysiloxanes. *Journal of Colloid and Interface Science* **1968,** *27*, 751-760.

6. Kahn, F. J.; Taylor, G. N.; Schonhorn, H. Surface-Produced Alignment of LIquid Crystals. *Proceedings of the IEEE* **1973,** *61*, 823-828.

7. Sagiv, J. Organized Monolayers by Adsorption. 1. Formation and Structure of Oleophobic Mixed Monolayers on Solid Surfaces. *Journal of the American Chemical Society* **1980,** *102*, 92-98.

8. Zhuravlev, L. T. Concentration of Hydroxyl Groups on the Surface of Amorphous Silicas. *Langmuir* **1987,** *3*, 316-318.

9. Tripp, C. P.; Kazmaier, P.; Hair, M. L. A Low Frequency Infrared and ab Initio Study of the Reaction of Trichlorosilane with Silica. *Langmuir* **1996,** *12*, 6404-6406.

10. Thirtle, P. N.; Li, Z. X.; Thomas, R. K.; Rennie, A. R.; Satija, S. K.; Sung, L. P. Structure of Nonionic Surfactant Layers Adsorbed at the Solid/Liquid Interface on Self-Assembled Monolayers with Different Surface Functionality: A Neutron Reflection Study. *Langmuir* **1997,** *13*, 5451-5458.

11. Stevens, M. J. Thoughts on the Structure of Alkylsilane Monolayers. *Langmuir* **1999,** *15*, 2773-2778.

12. Nuzzo, R. G.; Allara, D. L. Adsorption of Bifunctional Organic Disulfides on Gold Surfaces. *Journal of the American Chemical Society* **1983,** *105*, 4481-4483.

13. Finklea, H. O.; Robinson, L. R.; Blackburn, A.; Richter, B.; Allara, D.; Bright, T. Formation of an Organized Monolayer by Solution Adsorption of

Octadecyltrichlorosilane on Gold: Electrochemical Properties and Structural Characterization. *Langmuir* **1986,** *2*, 239-244.

14. Ulman, A. Formation and Structure of Self-Assembled Monolayers. *Chemical Reviews* **1996,** *96*, 1533-1554.

15. Sullivan, T. P.; Huck, W. T. S. Reactions on Monolayers: Organic Synthesis in Two Dimensions. *European Journal of Organic Chemistry* **2003,** *2003*, 17-29.

16. Patrick, T. Synthesis of Well-Defined Polymeric Activated Esters. *Journal of Polymer Science Part A: Polymer Chemistry* **2008,** *46*, 6677-6687.

17. Wojtyk, J. T. C.; Morin, K. A.; Boukherroub, R.; Wayner, D. D. M. Modification of Porous Silicon Surfaces with Activated Ester Monolayers. *Langmuir* **2002,** *18*, 6081-6087.

18. Jin, L.; Horgan, A.; Levicky, R. Preparation of End-Tethered DNA Monolayers on Siliceous Surfaces Using Heterobifunctional Cross-Linkers. *Langmuir* **2003,** *19*, 6968-6975.

19. Voicu, R.; Boukherroub, R.; Bartzoka, V.; Ward, T.; Wojtyk, J. T. C.; Wayner, D. D. M. Formation, Characterization, and Chemistry of Undecanoic Acid-Terminated Silicon Surfaces: Patterning and Immobilization of DNA. *Langmuir* **2004,** *20*, 11713-11720.

20. Lockett, M. R.; Phillips, M. F.; Jarecki, J. L.; Peelen, D.; Smith, L. M. A Tetrafluorophenyl Activated Ester Self-Assembled Monolayer for the Immobilization of Amine-Modified Oligonucleotides. *Langmuir* **2008,** *24*, 69-75.

21. Silberzan, P.; Leger, L.; Ausserre, D.; Benattar, J. J. Silanation of Silica Surfaces. A nNew Method of Constructing Pure or Mixed Monolayers. *Langmuir* **1991,** *7*, 1647-1651.

22. Plueddemann, E. P. *Silane Coupling Agents*. Plenum Press: New York, 1991; p 253.

23. Pangborn, A. B.; Giardello, M. A.; Grubbs, R. H.; Rosen, R. K.; Timmers, F. J. Safe and Convenient Procedure for Solvent Purification. *Organometallics* **1996,** *15*, 1518-1520.

24. Untereker, D. F.; Lennox, J. C.; Wier, L. M.; Moses, P. R.; Murray, R. W. Chemically Modified Electrodes: Part IV. Evidence for Formation of Monolayers of Bonded Organosilane Reagents. *Journal of Electroanalytical Chemistry* **1977,** *81*, 309-318.

25. Voet, D.; Voet, J. G. *Biochemistry*. 2nd ed.; John Wiley & Sons, Inc.: New York, 1995; p 1361.

26. Bloomfield, V. A.; Crothers, D. M.; Tinoco, I., Jr. *Nucleic Acids: Structures, Properties, and Functions*. University Science Books: Sausalito, CA, 2000; p 794.

27. Cooper, G. M.; Hausman, R. E. *The Cell: A Molecular Approach*. 4th ed.; Sinauer Associates, Inc.: Washington D.C., 2007; p 820.

28. Ulman, A. *An Introduction to Ultrathin Organic Films: From Langmuir-Blodgett to Self-Assembly*. Academic Press: Boston, 1991; p 442.

29. Mittal, K. L. *Contact Angle, Wettability, and Adhesion*. V.S.P. Intl Science: Utrecht, 2003; Vol. 3, p 519.

30. Gentle, I. *Interfacial Science: An Introduction.* Oxford University Press: New York, 2005; p 247.

31. Van Oss, C. J. *Interfacial Forces in Aqueous Media*. Taylor and Francis: Boca Raton, FL, 2006; p 438.

32. Yildirim, E. *Surface Chemistry of Solid and Liquid Interfaces*. Blackwell Publishing: Malden, MA, 2006; p 352.

CHAPTER 4

1. Franken, P. A.; Hill, A. E.; Peters, C. W.; Weinreich, G. Generation of Optical Harmonics. *Physical Review Letters* **1961,** *7*, 118-119.

2. Shen, Y. R. *The Principles of Nonlinear Optics*. John Wiley & Sons, Inc.: New York, 1984.

3. Shen, Y. R. Surface Studies by Optical Second Harmonic Generation: An Overview. *Journal of Vacuum Science and Technology B* **1985,** *3*, 1464-1466.

4. Hicks, J. M.; Kemnitz, K.; Eisenthal, K. B.; Heinz, T. F. Studies of Liquid Surfaces by Second Harmonic Generation. *Journal of Physical Chemistry* **1986,** *90*, 560-562.

5. Eisenthal, K. B. Equilibrium and Dynamic Processes at Interfaces by Second Harmonic and Sum Frequency Generation. *Annual Review of Physical Chemistry* **1992,** *43*, 627-661.

6. Corn, R. M.; Higgins, D. A. Optical Second Harmonic Generation as a Probe of Surface Chemistry. *Chemical Reviews* **1994,** *94*, 107-125.

7. Eisenthal, K. B. Liquid Interfaces Probed by Second-Harmonic and Sum-Frequency Spectroscopy. *Chemical Reviews* **1996,** *96*, 1343-1360.

8. Boyd, R. W. *Nonlinear Optics*. 2nd ed.; Academic Press: New York, 2003; p 578.

9. Eisenthal, K. B. Second Harmonic Spectroscopy of Aqueous Nano- and Microparticle Interfaces. *Chemical Reviews* **2006,** *106*, 1462-1477.

10. Zhao, X.; Subrahmanyan, S.; Eisenthal, K. B. Determination of pK_a at the Air/Water Interface by Second Harmonic Generation. *Chemical Physics Letters* **1990,** *171*, 558-562.

11. Zhao, X.; Ong, S.; Eisenthal, K. B. Polarization of Water Molecules at a Charged Interface. Second Harmonic Studies of Charged Monolayers at the Air/Water Interface. *Chemical Physics Letters* **1993,** *202*, 513-520.

12. Yan, E. C. Y.; Liu, Y.; Eisenthal, K. B. New Method for Determination of Surface Potential of Microscopic Particles by Second Harmonic Generation. *Journal of Physical Chemistry B* **1998,** *102*, 6331-6336.

13. Liu, Y.; Yan, E. C. Y.; Zhao, X.; Eisenthal, K. B. Surface Potential of Charged Liposomes Determined by Second Harmonic Generation. *Langmuir* **2001,** *17*, 2063-2066.

14. Xiao, X. D.; Vogel, V.; Shen, Y. R. Probing the Proton Excess at Interfaces by Second Harmonic Generation. *Chemical Physics Letters* **1989,** *163*, 555-559.

15. Watson, J. D.; Crick, F. H. C. A Structure for Deoxyribose Nucleic Acid. *Nature* **1953,** *421*, 397-398.

16. Voet, D.; Voet, J. G. *Biochemistry*. 2nd ed.; John Wiley & Sons, Inc.: New York, 1995; p 1361.

17. Bloomfield, V. A.; Crothers, D. M.; Tinoco, I., Jr. *Nucleic Acids: Structures, Properties, and Functions*. University Science Books: Sausalito, CA, 2000; p 794.

18. Zhao, X.; Ong, S.; Wang, H.; Eisenthal, K. B. New Method for Determination of Surface pK_a Using Second Harmonic Generation. *Chemical Physics Letters* **1993,** *214*, 203-207.

19. Konek, C. T.; Musorrafiti, M. J.; Al-Abadleh, H. A.; Bertin, P. A.; Nguyen, S. T.; Geiger, F. M. Interfacial Acidities, Charge Densities, Potentials, and Energies of Carboxylic Acid-Functionalized Silica/Water Interfaces Determined by Second Harmonic Generation. *Journal of the American Chemical Society* **2004,** *126*, 11754-11755.

20. Boman, F. C.; Musorrafiti, M. J.; Gibbs, J. M.; Stepp, B. R.; Salazar, A. M.; Nguyen SonBinh, T.; Geiger Franz, M. DNA Single Stands Tethered to Fused Quartz/Water Interfaces Studied by Second Harmonic Generation. *Journal of the American Chemical Society* **2005,** *127*, 15368-15369.

21. Stokes, G. Y.; Gibbs-Davis, J. M.; Boman, F. C.; Stepp, B. R.; Condie, A. G.; Nguyen, S. T.; Geiger, F. M. Making "Sense" of DNA. *Journal of the American Chemical Society* **2007,** *129*, 7492-7493.

22. Hayes, P. L.; Malin, J. N.; Konek, C. T.; Geiger, F. M. Interaction of Nitrate, Barium, Strontium and Cadmium Ions with Fused Quartz/Water Interfaces Studied by Second Harmonic Generation. *Journal of Physical Chemistry A* **2008,** *112*, 660-668.

23. Malin, J. N.; Hayes, P. L.; Geiger, F. M. Interactions of Zinc, Calcium, and Cadmium Ions at Buried Solid/Water Interfaces Studied by Second Harmonic Generation. *Journal of Physical Chemistry C* **2008,** *ASAP*.

24. Terhune, R. W.; Maker, P. D.; Savage, C. M. Optical Harmonic Generation in Calcite. *Physical Review Letters* **1962,** *8*, 404-406.

25. Bloembergen, N.; Pershan, P. S. Light Waves at the Boundary of Nonlinear Media. *Physical Review* **1962,** *128*, 606-622.

26. Lee, C. H.; Chang, R. K.; Bloembergen, N. Nonlinear Electroreflectance in Silicon and Silver. *Physical Review Letters* **1967,** *18*, 167-170.

27. Adamson, A. W. *Physical Chemistry of Surfaces*. 5th ed.; John Wiley & Sons, Inc.: New York, 1990; p 777.

28. Ong, S.; Zhao, X.; Eisenthal, K. B. Polarization of Water Molecules at a Charged Interface: Second-Harmonic Studies of the Silica/Water Interface. *Chemical Physics Letters* **1992,** *191*, 327-335.

29. Salafsky, J. S.; Eisenthal, K. B. Protein Adsorption at Interfaces Detected by Second Harmonic Generation. *Journal of Physical Chemistry B* **2000,** *104*, 7752-7755.

30. Kielich, S. Optical Second-Harmonic Generation by Electrically Polarized Isotropic Media. *IEEE Journal of Quantum Electronics* **1969,** *5*, 562-568.

31. Levine, B. F.; Bethea, C. G. Molecular Hyperpolarizabilities Determined from Conjugated and Nonconjugated Organic Liquids. *Applied Physics Letters* **1974,** *24*, 445-447.

32. Levine, B. F.; Bethea, C. G. Absolute Signs of Hyperpolarizabilities in the Liquid State. *The Journal of Chemical Physics* **1974,** *60*, 3856-3858.

33. Levine, B. F.; Bethea, C. G. Second and Third Order Hyperpolarizabilities of Organic Molecules. *The Journal of Chemical Physics* **1975,** *63*, 2666-2682.

34. Levine, B. F.; Bethea, C. G. Effects on Hyperpolarizabilities of Molecular Interactions in Associating Liquid Mixtures. *The Journal of Chemical Physics* **1976,** *65*, 2429-2438.

35. Boman, F. C.; Gibbs-Davis, J. M.; Heckman, L. M.; Stepp, B. R.; Nguyen, S. T.; Geiger, F. M. DNA at Aqueous/Solid Interfaces- Chirality-Based Detection via Second Harmonic Generation Activity. *Journal of the American Chemical Society* **2008,** *in press*.

36. Eisenthal, K. B. Liquid Interfaces. *Accounts of Chemical Research* **1993,** *26*, 636-643.

37. Gibbs-Davis, J. M.; Kruk, J. J.; Konek, C. T.; Sheidt, K. A.; Geiger, F. M. Jammed Acid-Base Chemistry at Interfaces. *Journal of the American Chemical Society* **2008,** *130*, 15444-15447.

38. Geiger, F. M. Second Harmonic Generation, Sum Frequency Generation, and Chi(3): Dissecting Environmental Interfaces with a Nonlinear Optical Swiss Army Knife. *Annual Review of Physical Chemistry* **2009,** *60*, 61-83.

39. Stiopkin, I. V.; Jayathilake, H. D.; Bordenyuk, A. N.; Benderskii, A. V. Heterodyne-Detected Vibrational Sum Frequency Generation Spectroscopy. *Journal of the American Chemical Society* **2008,** *130*, 2271-2275.

40. Zanni, M. T.; Gnanakaran, S.; Stenger, J.; Hochstrasser, R. M. Heterodyned Two-Dimensional Infrared Spectroscopy of Solvent-Dependent Conformations of Acetylproline-NH_2. *Journal of Physical Chemistry B* **2001,** *105*, 6520-6535.

41. Krummel, A. T.; Mukherjee, P.; Zanni, M. T. Inter and Intrastrand Vibrational Coupling in DNA Studied with Heterodyned 2D-IR Spectroscopy *Journal of Physical Chemistry B* **2003,** *107*, 9165-9169.

42. Brixner, T.; Stiopkin, I. V.; Fleming, G. R. Tunable Two-dimensional Femtosecond Spectroscopy. *Optics Letters* **2004,** *29*, 884-886.

43. Lepetit, L.; Cheriaux, G.; Joffre, M. Linear Techniques of Phase Measurement by Femtosecond Spectral Interferometry for Applications in Spectroscopy. *Journal of the Optical Society of America B: Optical Physics* **1995,** *12*, 2467-2474.

44. Vaughan, J. C.; Hornung, T.; Stone, K. W.; Nelson, K. A. Coherently Controlled Ultrafast Four-Wave Mixing Spectroscopy. *Journal of Physical Chemistry A* **2007,** *111*, 4873-4883.

45. Kaufman, L. J.; Heo, J.; Ziegler, L. D.; Fleming, G. R. Heterodyne-Detected Fifth-Order Nonresonant Raman Scattering from Room Temperature CS_2. *Physical Review Letters* **2002,** *88*, 207402.

46. Xu, Q. H.; Ma, Y. Z.; Fleming, G. R. Different Real and Imaginary Components of the Resonant Third-Order Polarization Revealed by Optical Heterodyne Detected Transient Grating Spectroscopic Studies of Crystal Violet: Model and Experiment. *Journal of Physical Chemistry A* **2002,** *106*, 10755-10763.

47. Demirdoven, N.; Cheatum, C. M.; Chung, H. S.; Khalil, M.; Knoester, J.; Tokmakoff, A. Two-Dimensional Infrared Spectroscopy of Antiparallel _-Sheet Secondary Structure. *Journal of the American Chemical Society* **2004,** *126*, 7981-7990.

48. Lyklema, J. *Fundamentals of Interface and Colloid Science*. Academic Press: New York, 1995; Vol. 2, p 768.

49. Stumm, W.; Morgan, J. J. *Aquatic Chemistry: Chemical Equilibria and Rates in Natural Waters*. 3rd ed.; John Wiley & Sons, Inc.: New York, 1996; p 1022.

50. Gouy, L. G. Constitution of the Electric Charge at the Surface of an Electrolyte. *Journal de Physique* **1910,** *9*, 457-467.

51. Chapman, D. L. A Contribution to the Theory of Electrocapillarity. *Philosophical Magazine* **1913,** *25*, 475-481.

52. Morel, F. M. M.; Hering, J. G. *Principles and Applications of Aquatic Chemistry*. John Wiley & Sons, Inc.: New York, 1993; p 588.

53. Langmuir, D. *Aqueous Environmental Geochemistry*. Prentice Hall: Upper Saddle River, NJ, 1997; p 600.

54. Hayes, K. F.; Redden, G.; Ela, W.; Leckie, J. O. Surface Complexation Models: An Evaluation of Model Parameter Estimation Using FITEQL and Oxide Mineral Titration Data. *Journal of Colloid and Interface Science* **1991,** *142*, 448-469.

55. Koopal, L. K. Mineral Hydroxides: From Homogeneous to Heterogeneous Modeling. *Electrochimica Acta* **1996,** *41*, 2293-2305.

56. Brown, G. E.; Henrich, V. E.; Casey, W. H.; Clark, D. L.; Eggleston, C.; Felmy, A.; Goodman, D. W.; Gratzel, M.; Maciel, G.; McCarthy, M. I.; Nealson, K. H.; Sverjensky, D. A.; Toney, M. F.; Zachara, J. M. Metal Oxide Surfaces and Their Interactions with Aqueous Solutions and Microbial Organisms. *Chemical Reviews* **1999,** *99*, 77-174.

57. Schellman, J. A.; Stigter, D. Electrical Double Layer, Zeta Potential, and Electrophoretic Charge of Double-Stranded DNA. *Biopolymers* **1977,** *16*, 1415-1434.

58. Stigter, D. Interactions of Highly Charged Colloidal Cylinders with Applications to Double-Stranded DNA. *Biopolymers* **1977,** *16*, 1435-1448.

59. Piunno, P. A. E.; Watterson, J.; Wust, C. C.; Krull, U. J. Considerations for the Quantitative Transduction of Hybridization of Immobilized DNA. *Analytica Chimica Acta* **1999,** *400*, 73-89.

60. Brown, G. E. Surface Science - How Minerals React with Water. *Science* **2001,** *294*, 67-69.

61. Stillinger Jr., F., H. Intefacial Solutions of the Poisson-Boltmann Equation. *The Journal of Chemical Physics* **1961,** *35*, 1584-1589.

62. Atkins, P. *Physical Chemistry*. 6th ed.; W. H. Freeman and Company: New York, 1998; p 999.

63. Hasted, J. B. *Aqueous Dielectrics*. Chapman and Hall: London, 1973; p 302.

64. Strother, T.; Cai, W.; Zhao, X.; Hamers, R. J.; Smith, L. M. Synthesis and Characterization of DNA-Modified Silicon (111) Surfaces. *Journal of the American Chemical Society* **2000,** *122*, 1205-1209.

65. Nelson, B. P.; Grimsrud, T. E.; Liles, M. R.; Goodman, R. M.; Corn, R. M. Surface Plasmon Resonance Imaging Measurements of DNA and RNA Hybridization Adsorption onto DNA Microarrays. *Analytical Chemistry* **2001,** *73*, 1-7.

66. Pirrung, M. C. How to Make a DNA Chip. *Angewandte Chemie International Edition* **2002,** *41*, 1276-1289.

67. Petrovykh, D. Y.; Kimura-Suda, H.; Whitman, L. J.; Tarlov, M. J. Quantitative Analysis and Characterization of DNA Immobilized on Gold. *Journal of the American Chemical Society* **2003,** *125*, 5219-5226.

68. Mourougou-Candoni, N.; Naud, C.; Thibaudau, F. Adsorption of Thiolated Oligonucleotides on Gold Surfaces: An Atomic Force Microscopy Study. *Langmuir* **2003,** *19*, 682-686.

69. Moses, S.; Brewer, S. H.; Lowe, L. B.; Lappi, S. E.; Gilvey, L. B. G.; Sauthier, M.; Tenent, R. C.; Feldheim, D. L.; Franzen, S. Characterization of Single- and Double-Stranded DNA on Gold Surfaces. *Langmuir* **2004,** *20*, 11134-11140.

70. Ladd, J.; Boozer, C.; Yu, Q.; Chen, S.; Homola, J.; Jiang, S. DNA-Directed Protein Immobilization on Mixed Self-Assembled Monolayers via a Streptavidin Bridge. *Langmuir* **2004,** *20*, 8090-8095.

71. Swami, N. S.; Chou, C.-F.; Terberueggen, R. Two-Potential Electrochemical Probe for Study of DNA Immobilization. *Langmuir* **2005,** *21*, 1937-1941.

72. Castelino, K.; Kannan, B.; Majumdar, A. Characterization of Grafting Density and Binding Efficiency of DNA and Proteins on Gold Surfaces. *Langmuir* **2005,** *21*, 1956-1961.

73. Lyklema, J. *Fundamentals of Interface and Colloid Science*. Academic Press: New York, 1991; Vol. 1, p 736.

74. Kosmulski, M. Adsorption of Cadmium on Alumina and Silica: Analysis of the Values of Stability Constants of Surface Complexes Calculated for Different Parameters of Triple Layer Model. *Colloids and Surfaces A: Physicochemical and Engineering Aspects* **1996,** *117*, 201-214.

75. Robertson, A. P.; Leckie, J. O. Cation Binding Predictions of Surface Complexation Models: Effects of pH, Ionic Strength, Cation Loading, Surface Complex, and Model Fit. *Journal of Colloid and Interface Science* **1997,** *188*, 444-472.

76. Sahai, N.; Sverjensky, D. A. Evaluation of Internally Consistent Parameters for the Triple-Layer Model by the Systematic Analysis of Oxide Surface Titration Data. *Geochimica et Cosmochimica Acta* **1997,** *61*, 2801-2826.

77. Delgado, A. V.; Gonzalez-Caballero, R.; Hunter, R. J.; Koopal, L. K.; Lyklema, J. Measurement and Interpretation of Electrokinetic Phenomena (IUPAC Technical Report). *Pure and Applied Chemistry* **2005,** *77*, 1753-1805.

78. Davis, J. A.; Kent, D. B. Surface Complexation Modeling in Aqueous Geochemistry. *Reviews in Mineralogy and Geochemistry* **1990,** *23*, 177-260.

79. Shapovalov, V. L.; Brezesinski, G. Breakdown of the Gouy-Chapman Model for Highly Charged Langmuir Monolayers: Counterion Size Effect. *Journal of Physical Chemistry B* **2006,** *110*, 10032-10040.

80. Yates, D. E.; Samuel, L.; Healy, T. W. Site-Binding Model of the Electrical Double Layer at the Oxide/Water Interface. *Journal of the Chemical Society, Faraday Transactions 1* **1974,** *70*, 1807-1818.

81. Huang, E.; Satjapipat, M.; Han, S.; Zhou, F. Surface Structure and Coverage of an Oligonucleotide Probe Tethered onto a Gold Substrate and Its Hybridization Efficiency for a Polynucleotide Target. *Langmuir* **2001,** *17*, 1215-1224.

82. Peterson, A. W.; Heaton, R. J.; Georgiadis, R. M. The Effect of Surface Probe Density on DNA Hybridization. *Nucleic Acids Research* **2001,** *29*, 5163-5168.

83. Nakamura, F.; Ito, E.; Sakao, Y.; Ueno, N.; Gatuna, I. N.; Ohuchi, F. S.; Hara, M. Preparation of a Branched DNA Self-Assembled Monolayer toward Sensitive DNA Biosensors. *Nano Lett.* **2003,** *3*, 1083-1086.

84. Vainrub, A.; Pettitt, B. M. Sensitive Quantitative Nucleic Acid Detection Using Oligonucleotide Microarrays. *J. Am. Chem. Soc.* **2003,** *125*, 7798-7799.

85. Levicky, R.; Horgan, A. Physicochemical Perspectives on DNA Microarray and Biosensor Technologies. *Trends in Biotechnology* **2005,** *23*, 143-149.

86. Mirmomtaz, E.; Castronovo, M.; Grunwald, C.; Bano, F.; Scaini, D.; Ensafi, A. A.; Scoles, G.; Casalis, L. Quantitative Study of the Effect of Coverage on the Hybridization Efficiency of Surface-Bound DNA Nanostructures. *Nano Letters* **2008,** *ASAP*.

87. Vainrub, A.; Pettitt, B. M. Thermodynamics of Association to a Molecule Immobilized in an Electric Double Layer. *Chemical Physics Letters* **2000,** *323*, 160-166.

88. Parks, G. A. Surface Energy and Adsorption at Mineral/Water Interfaces; An Introduction. *Reviews in Mineralogy and Geochemistry* **1990,** *23*, 133-175.

CHAPTER 5

1. Franken, P. A.; Hill, A. E.; Peters, C. W.; Weinreich, G. Generation of Optical Harmonics. *Physical Review Letters* **1961,** *7*, 118-119.

2. Shen, Y. R. *The Principles of Nonlinear Optics*. John Wiley & Sons, Inc.: New York, 1984.

3. Shen, Y. R. Surface Studies by Optical Second Harmonic Generation: An Overview. *Journal of Vacuum Science and Technology B* **1985,** *3*, 1464-1466.

4. Hicks, J. M.; Kemnitz, K.; Eisenthal, K. B.; Heinz, T. F. Studies of Liquid Surfaces by Second Harmonic Generation. *Journal of Physical Chemistry* **1986,** *90*, 560-562.

5. Eisenthal, K. B. Equilibrium and Dynamic Processes at Interfaces by Second Harmonic and Sum Frequency Generation. *Annual Review of Physical Chemistry* **1992,** *43*, 627-661.

6. Corn, R. M.; Higgins, D. A. Optical Second Harmonic Generation as a Probe of Surface Chemistry. *Chemical Reviews* **1994,** *94*, 107-125.

7. Eisenthal, K. B. Liquid Interfaces Probed by Second-Harmonic and Sum-Frequency Spectroscopy. *Chemical Reviews* **1996,** *96*, 1343-1360.

8. Eisenthal, K. B. Second Harmonic Spectroscopy of Aqueous Nano- and Microparticle Interfaces. *Chemical Reviews* **2006,** *106*, 1462-1477.

9. Burton, K. *Biochemistry of Nucleic Acids*. University Park Press: Baltimore, 1974; p 364.

10. Voet, D.; Voet, J. G. *Biochemistry*. 2nd ed.; John Wiley & Sons, Inc.: New York, 1995; p 1361.

11. Bloomfield, V. A.; Crothers, D. M.; Tinoco, I., Jr. *Nucleic Acids: Structures, Properties, and Functions*. University Science Books: Sausalito, CA, 2000; p 794.

12. Neidle, S. *Principles of Nucleic Acid Structure*. 1st ed.; Academic Press: Boston, 2007; p 289.

13. Tinoco, I., Jr. Hypochromism in Polynucleotides. *Journal of the American Chemical Society* **1960,** *82*, 4785-90.

14. Lorentzon, J.; Fuelscher, M. P.; Roos, B. O. Theoretical Study of the Electronic Spectra of Uracil and Thymine. *Journal of the American Chemical Society* **1995,** *117*, 9265-9273.

15. Fulscher, M. P.; Serrano-Andres, L.; Roos, B. O. A Theoretical Study of the Electronic Spectra of Adenine and Guanine. *J. Am. Chem. Soc*. **1997,** *119*, 6168-6176.

16. Tonzani, S.; Schatz, G. C. Electronic Excitations and Spectra in Single-Stranded DNA. *J. Am. Chem. Soc*. **2008,** *130*, 7607-7612.

17. Xiao, X. D.; Vogel, V.; Shen, Y. R. Probing the Proton Excess at Interfaces by Second Harmonic Generation. *Chemical Physics Letters* **1989,** *163*, 555-559.

18. Zhao, X.; Subrahmanyan, S.; Eisenthal, K. B. Determination of pK_a at the Air/Water Interface by Second Harmonic Generation. *Chemical Physics Letters* **1990,** *171*, 558-562.

19. Watson, J. D.; Crick, F. H. C. A Structure for Deoxyribose Nucleic Acid. *Nature* **1953,** *421*, 397-398.

20. Tinoco, I. Nucleic Acid Structures, Energetics, and Dynamics. *Journal of Physical Chemistry* **1996,** *100*, 13311-13322.

21. SantaLucia, J., Jr. A Unified View of Polymer, Dumbbell, and Oligonucleotide DNA Nearest-Neighbor Thermodynamics. *Proceedings of the National Academy of Sciences of the United States of America* **1998,** *95*, 1460-1465.

22. Spink, C. H.; Chaires, J. B. Effects of Hydration, Ion Release, and Excluded Volume on the Melting of Triplex and Duplex DNA. *Biochemistry* **1999,** *38*, 496-508.

23. Dabkowska, I.; Gonzalez, H. V.; Jurecka, P.; Hobza, P. Stabilization Energies of the Hydrogen-Bonded and Stacked Structures of Nucleic Acid Base Pairs in the Crystal Geometries of CG, AT, and AC DNA Steps and in the NMR Geometry of the 5'-d(GCGAAGC)-3' Hairpin: Complete Basis Set Calculations at the MP2 and CCSD(T) Levels. *Journal of Physical Chemistry A* **2005,** *109*, 1131-1136.

24. Buyukdagli, S.; Sanrey, M.; Joyeux, M. Towards More Realistic Dynamical Models for DNA Secondary Structure. *Chemical Physics Letters* **2006,** *419*, 434-438.

25. Jaffe, H. H.; Orchin, M. *Theory and Applications of Ultraviolet Spectroscopy*. John Wiley & Sons, Inc.: New York, 1962; p 624.

26. Skoog, D. A.; Holler, F. J.; Neiman, T. A. *Principles of Instrumental Analysis*. Harcourt Brace College Publishers: Philadelphia, 1998; p 960.

27. Hollas, J. M. *Modern Spectroscopy*. John Wiley & Sons, Inc.: New York, 1998; p 391.

28. Rao, C. N. R. *Ultra-Violet and Visible Spectroscopy: Chemical Applications*. Plenum Press: New York, 1967; p 210.

29. Voet, D.; Gratzer, W. B.; Cox, R. A.; Doty, P. Absorption Spectra of Nucleotides, Polynucleotides, and Nucleic Acids in the Far Ultraviolet. *Biopolymers* **1963,** *1*, 193-208.

30. Fuelscher, M. P.; Roos, B. O. Theoretical Study of the Electronic Spectrum of Cytosine. *Journal of the American Chemical Society* **1995,** *117*, 2089-2095.

31. Fuelscher, M. P.; Serrano-Andres, L.; Roos, B. O. A Theoretical Study of the Electronic Spectra of Adenine and Guanine. *J. Am. Chem. Soc.* **1997,** *119*, 6168-6176.

32. Nir, E.; Pluetzer, C.; Kleinermanns, K.; de Vries, M. Properties of Isolated DNA Bases, Base Pairs and Nucleosides Examined by Laser Spectroscopy. *European Physical Journal D: Atomic, Molecular and Optical Physics* **2002,** *20*, 317-329.

33. Murphy, J. H.; Trapane, T. L. Concentration and Extinction Coefficient Determination for Oligonucleotides and Analogs Using a General Phosphate Analysis. *Analytical Biochemistry* **1996,** *240*, 273-282.

34. Rhodes, W. Hypochromism and Other Spectral Properties of Helical Polynucleotides. *Journal of the American Chemical Society* **1961,** *83*, 3609-3617.

35. Tinoco, I. Hypochromism in Polynucleotides. *J. Am. Chem. Soc.* **1960,** *82*, 4785-4790.

36. Mergny, J.-L.; Lacroix, L. Analysis of Thermal Melting Curves. *Oligonucleotides* **2003,** *13*, 515-537.

37. Townes, C. H.; Schawlow, A. L. *Microwave Spectroscopy*. Dover Publications: New York, 1955; p 698.

38. Steel, W. H.; Walker, R. A. Measuring dipolar width across liquid-liquid interfaces with molecular rulers'. *Nature* **2003,** *424*, 296.

39. Boyd, R. W. *Nonlinear Optics*. 2nd ed.; Academic Press: New York, 2003; p 578.

40. Lorentzon, J.; Fuelscher, M. P.; Roos, B. O. Theoretical Study of the Electronic Spectra of Uracil and Thymine. *J. Am. Chem. Soc.* **1995,** *117*, 9265-9273.

41. Fuelscher, M. P.; Serrano-Andres, L.; Roos, B. O. A Theoretical Study of the Electronic Spectra of Adenine and Guanine. *J. Am. Chem. Soc.* **1997,** *119*, 6168-6176.

42. Bach, H.; Krause, D. *Thin Films on Glass*. Academic Press: New York, 2003; p 436.

CHAPTER 6

1. Franken, P. A.; Hill, A. E.; Peters, C. W.; Weinreich, G. Generation of Optical Harmonics. *Physical Review Letters* **1961,** *7*, 118-119.

2. Shen, Y. R. *The Principles of Nonlinear Optics*. John Wiley & Sons, Inc.: New York, 1984.

3. Shen, Y. R. Surface Studies by Optical Second Harmonic Generation: An Overview. *Journal of Vacuum Science and Technology B* **1985,** *3*, 1464-1466.

4. Hicks, J. M.; Kemnitz, K.; Eisenthal, K. B.; Heinz, T. F. Studies of Liquid Surfaces by Second Harmonic Generation. *Journal of Physical Chemistry* **1986,** *90*, 560-562.

5. Eisenthal, K. B. Equilibrium and Dynamic Processes at Interfaces by Second Harmonic and Sum Frequency Generation. *Annual Review of Physical Chemistry* **1992,** *43*, 627-661.

6. Corn, R. M.; Higgins, D. A. Optical Second Harmonic Generation as a Probe of Surface Chemistry. *Chemical Reviews* **1994,** *94*, 107-125.

7. Eisenthal, K. B. Liquid Interfaces Probed by Second-Harmonic and Sum-Frequency Spectroscopy. *Chemical Reviews* **1996,** *96*, 1343-1360.

8. Eisenthal, K. B. Second Harmonic Spectroscopy of Aqueous Nano- and Microparticle Interfaces. *Chemical Reviews* **2006,** *106*, 1462-1477.

9. Boman, F. C.; Musorrafiti, M. J.; Gibbs, J. M.; Stepp, B. R.; Salazar, A. M.; Nguyen SonBinh, T.; Geiger Franz, M. DNA Single Stands Tethered to Fused Quartz/Water Interfaces Studied by Second Harmonic Generation. *Journal of the American Chemical Society* **2005,** *127*, 15368-15369.

10. Boman, F. C.; Gibbs-Davis, J. M.; Heckman, L. M.; Stepp, B. R.; Nguyen, S. T.; Geiger, F. M. DNA at Aqueous/Solid Interfaces- Chirality-Based Detection via Second Harmonic Generation Activity. *Journal of the American Chemical Society* **2008,** *in press*.

11. Tinoco, I., Jr. Hypochromism in Polynucleotides. *Journal of the American Chemical Society* **1960,** *82*, 4785-90.

12. Lorentzon, J.; Fuelscher, M. P.; Roos, B. O. Theoretical Study of the Electronic Spectra of Uracil and Thymine. *Journal of the American Chemical Society* **1995,** *117*, 9265-9273.

13. Fulscher, M. P.; Serrano-Andres, L.; Roos, B. O. A Theoretical Study of the Electronic Spectra of Adenine and Guanine. *J. Am. Chem. Soc*. **1997,** *119*, 6168-6176.

14. Tonzani, S.; Schatz, G. C. Electronic Excitations and Spectra in Single-Stranded DNA. *J. Am. Chem. Soc.* **2008,** *130*, 7607-7612.

15. Kauranen, M.; Verbiest, T.; Maki, J. J.; Persoons, A. Second-Harmonic Generation from Chiral Surfaces. *The Journal of Chemical Physics* **1994,** *101*, 8193-8199.

16. Kauranen, M.; Verbiest, T.; Persoons, A. Second-Order Nonlinear Optical Signatures of Surface Chirality. *Journal of Modern Optics* **1998,** *45*, 403-424.

17. Burton, K. *Biochemistry of Nucleic Acids*. University Park Press: Baltimore, 1974; p 364.

18. Voet, D.; Voet, J. G. *Biochemistry*. 2nd ed.; John Wiley & Sons, Inc.: New York, 1995; p 1361.

19. Bloomfield, V. A.; Crothers, D. M.; Tinoco, I., Jr. *Nucleic Acids: Structures, Properties, and Functions*. University Science Books: Sausalito, CA, 2000; p 794.

20. Neidle, S. *Principles of Nucleic Acid Structure*. 1st ed.; Academic Press: Boston, 2007; p 289.

21. Chrisey, L. A.; Lee, G. U.; O'Ferrall, C. E. Covalent Attachment of Synthetic DNA to Self-Assembled Monolayer Films. *Nucleic Acids Research* **1996,** *24*, 3031-3039.

22. Strother, T.; Cai, W.; Zhao, X.; Hamers, R. J.; Smith, L. M. Synthesis and Characterization of DNA-Modified Silicon (111) Surfaces. *Journal of the American Chemical Society* **2000,** *122*, 1205-1209.

23. Finot, E.; Bourillot, E.; Meunier-Prest, R.; Lacroute, Y.; Legay, G.; Cherkaoui-Malki, M.; Latruffe, N.; Siri, O.; Braunstein, P.; Dereux, A. Performance of Interdigitated Nanoelectrodes for Electrochemical DNA Biosensor. *Ultramicroscopy* **2003,** *97*, 441-449.

24. Jin, R.; Wu, G.; Li, Z.; Mirkin, C. A.; Schatz, G. C. What Controls the Melting Properties of DNA-linked Gold Nanoparticle Assemblies? *Journal of the American Chemical Society* **2003,** *125*, 1643-1654.

25. Patsenker, L.; Tatarets, A.; Kolosova, O.; Obukhova, O.; Povrozin, Y.; Fedyunyayeva, I.; Yermolenko, I.; Terpetschnig, E. Fluorescent Probes and Labels for Biomedical Applications. *Annals of the New York Academy of Sciences* **2008,** *1130*, 179-187.

26. Boncheva, M.; Scheibler, L.; Lincoln, P.; Vogel, H.; Aakerman, B. Design of Oligonucleotide Arrays at Interfaces. *Langmuir* **1999,** *15*, 4317-4320.

27. Georgiadis, R.; Peterlinz, K. P.; Peterson, A. W. Quantitative Measurements and Modeling of Kinetics in Nucleic Acid Monolayer Films Using SPR Spectroscopy. *Journal of the American Chemical Society* **2000,** *122*, 3166-3173.

28. Nelson, B. P.; Grimsrud, T. E.; Liles, M. R.; Goodman, R. M.; Corn, R. M. Surface Plasmon Resonance Imaging Measurements of DNA and RNA Hybridization Adsorption onto DNA Microarrays. *Analytical Chemistry* **2001,** *73*, 1-7.

29. Wang, J.; Bard, A. J. Monitoring DNA Immobilization and Hybridization on Surfaces by Atomic Force Microscopy Force Measurements. *Analytical Chemistry* **2001,** *73*, 2207-2212.

30. Stokes, G. Y.; Gibbs-Davis, J. M.; Boman, F. C.; Stepp, B. R.; Condie, A. G.; Nguyen, S. T.; Geiger, F. M. Making "Sense" of DNA. *Journal of the American Chemical Society* **2007,** *129*, 7492-7493.

31. Rodger, A.; Norden, B. *Circular Dichroism and Linear Dichroism*. Oxford University Press: New York, 1997; Vol. 1, p 150.

32. Baase, W. A.; Johnson, W. C., Jr. Circular Dichroism and DNA Secondary Structure. *Nucleic Acids Research* **1979,** *6*, 797-814.

33. Self, B. D.; Moore, D. S. Nucleic Acid Vibrational Circular Dichroism, Absorption, and Linear Dichroism Spectra. I. A DeVoe Theory Approach. *Biophysical Journal* **1997,** *73*, 339-347.

34. Self, B. D.; Moore, D. S. Nucleic Acid Vibrational Circular Dichroism, Absorption, and Linear Dichroism Spectra. II. A DeVoe Theory Approach. *Biophysical Journal* **1998,** *74*, 2249-2258.

35. Kejnovska, I.; Kypr, J.; Vorlickova, M. Circular Dichroism Spectroscopy of Conformers of (Guanine + Adenine) Repeat Strands of DNA. *Chirality* **2003,** *15*, 584-592.

36. Rajendra, J.; Rodger, A. The Binding of Single-Stranded DNA and PNA to Single-Walled Carbon Nanotubes Probed by Flow Linear Dichroism. *Chemistry - A European Journal* **2005,** *11*, 4841-4847.

37. Moffitt, W. Optical Rotatory Dispersion of Helical Polymers. *The Journal of Chemical Physics* **1956,** *25*, 467-478.

38. Power, E. A.; Thirunamachandran, T. Circular Dichroism: A General Theory Based on Quantum Electrodynamics. *The Journal of Chemical Physics* **1974,** *60*, 3695-3701.

39. Riehl, J. P.; Richardson, F. S. General Theory of Circularly Polarized Emission and Magnetic Circularly Polarized Emission from Molecular Systems. *The Journal of Chemical Physics* **1976,** *65*, 1011-1021.

40. Charney, E. *The Molecular Basis of Optical Activity: Optical Rotatory Dispersion and Circular Dichroism*. John Wiley & Sons, Inc.: New York, 1979; p 364.

41. Collett, E. *Polarized Light: Fundamentals and Applications*. Marcel Dekker, Inc.: New York, 1993; p 581.

42. Brosseau, C. *Fundamentals of Polarized Light: A Statistical Optics Approach*. John Wiley & Sons, Inc.: New York, 1998; p 405.

43. Atkins, P. *Physical Chemistry*. 6th ed.; W. H. Freeman and Company: New York, 1998; p 999.

44. Petralli-Mallow, T. Second Harmonic Generation Circular Dichroism of Adsorbed Cytochrome C. Georgetown University, Washington D.C., 1997.

45. Petralli-Mallow, T.; Wong, T. M.; Byers, J. D.; Yee, H. I.; Hicks, J. M. Circular Dichroism Spectroscopy at Interfaces: A Surface Second Harmonic Generation Study. *Journal of Physical Chemistry* **1993,** *97*, 1383-1388.

46. Rosenfeld, L. Quantenmechanische Theorie der Naturlichen Optischen Aktivitat von Flussigkeiten und Gasen. *Zeitschrift fur Physik* **1928,** *52*, 161-174.

47. Hicks, J. M.; Petralli-Mallow, T.; Byers, J. D. Consequences of Chirality in Second-Order Non-Linear Spectroscopy at Surfaces. *Faraday Discussions* **1994**, 341-357.

48. Hicks, J. M.; Petralli-Mallow, T. Nonlinear Optics of Chiral Surface Systems. *Applied Physics B: Lasers and Optics* **1999,** *B68*, 589-593.

49. Byers, J. D.; Yee, H. I.; Hicks, J. M. A Second Harmonic Generation Analog of Optical Rotatory Dispersion for the Study of Chiral Monolayers. *The Journal of Chemical Physics* **1994,** *101*, 6233-6241.

50. Petralli-Mallow, T. P.; Hicks, J. M. In *Laser Probes of Chirality at Interfaces*, Book of Abstracts, 212th ACS National Meeting, Orlando, FL, August 25-29, 1996; 1996; CATL-009.

51. Maki, J. J.; Verbiest, T.; Kauranen, M.; Van Elshocht, S.; Persoons, A. Comparison of Linearly and Circularly Polarized Probes of Second-Order Optical Activity of Chiral Surfaces. *The Journal of Chemical Physics* **1996,** *105*, 767-772.

52. Simpson, G. J. Structural Origins of Circular Dichroism in Surface Second Harmonic Generation. *The Journal of Chemical Physics* **2002,** *117*, 3398-3410.

53. Burke, B. J.; Moad, A. J.; Polizzi, M. A.; Simpson, G. J. Experimental Confirmation of the Importance of Orientation in the Anomalous Chiral Sensitivity of Second Harmonic Generation. *Journal of the American Chemical Society* **2003,** *125*, 9111-9115.

54. Plocinik, R. M.; Everly, R. M.; Moad, A. J.; Simpson, G. J. Modular Ellipsometric Approach for Mining Structural Information from Nonlinear Optical Polarization Analysis. *Physical Review B: Condensed Matter and Materials Physics* **2005,** *72*, 125409-125414.

55. Maki, J. J.; Kauranen, M.; Persoons, A. Surface Second-Harmonic Generation from Chiral Materials. *Physical Review B: Condensed Matter and Materials Physics* **1995,** *51*, 1425-1434.

56. Oh-e, M.; Yokoyama, H.; Yorozuya, S.; Akagi, K.; Belkin, M. A.; Shen, Y. R. Sum-Frequency Vibrational Spectroscopy of a Helically Structured Conjugated Polymer. *Physical Review Letters* **2004,** *93*, 267402.

57. Plocinik, R. M.; Simpson, G. J. Polarization Characterization in Surface Second Harmonic Generation by Nonlinear Optical Null Ellipsometry. *Analytica Chimica Acta* **2003,** *496*, 133-142.

58. Simpson, G. J. Molecular Origins of the Remarkable Chiral Sensitivity of Second-Order Nonlinear Optics. *ChemPhysChem* **2004,** *5*, 1301-1310.

59. Wampler, R. D.; Zhou, M.; Thompson, D. H.; Simpson, G. J. Mechanism of the Chiral SHG Activity of Bacteriorhodopsin Films. *Journal of the American Chemical Society* **2006,** *128*, 10994-10995.

60. Verbiest, T.; Kauranen, M.; Persoons, A.; Ikonen, M.; Kurkela, J.; Lemmetyinen, H. Nonlinear Optical Activity and Biomolecular Chirality. *Journal of the American Chemical Society* **1994,** *116*, 9203-9205.

61. Hache, F.; Mesnil, H.; Schanne-Klein, M. C. Application of Classical Models of Chirality to Surface Second Harmonic Generation. *The Journal of Chemical Physics* **2001,** *115*, 6707-6715.

62. Pershan, P. S. Nonlinear Optical Properties of Solids: Energy Considerations. *Physical Review* **1963,** *130*, 919-929.

63. Adler, E. Nonlinear Optical Frequency Polarization in a Dielectric. *Physical Review* **1964,** *134*, A728-A733.

64. Kauranen, M.; Maki, J. J.; Verbiest, T.; Van Elshocht, S.; Persoons, A. Quantitative Determination of Electric and Magnetic Second-Order Susceptibility Tensors of Chiral Surfaces. *Physical Review B: Condensed Matter and Materials Physics* **1997,** *55*, R1985-R1988.

65. Boyd, R. W. *Nonlinear Optics*. 2nd ed.; Academic Press: New York, 2003; p 578.

66. Moad, A. J.; Simpson, G. J. A Unified Treatment of Selection Rules and Symmetry Relations for Sum-Frequency and Second Harmonic Spectroscopies. *Journal of Physical Chemistry B* **2004,** *108*, 3548-3562.

67. Brooks, B. R.; Bruccoleri, R. E.; Olafson, D. J.; States, D. J.; Swaminathan, S.; Karplus, M. CHARMM: A Program for Macromolecular Energy, Minimization, and Dynamics Calculations. *Journal of Computational Chemistry* **1983,** *4*, 187-217.

68. MacKerell Jr., A. D.; Brooks III, C. L.; Nilsson, L.; Roux, B.; Won, Y.; Karplus, M. CHARMM: The Energy Function and Its Parameterization with an Overview of the Program. In *The Encyclopedia of Computational Chemistry*, Schleyer, Ed. John Wiley & Sons: Chinchester, 1998; Vol. 1, pp 271-277.

69. MacKerell Jr., A. D.; Banavali, N.; Foloppe, N. Development and Current Status of the CHARMM Force Field for Nucleic Acids. *Biopolymers* **2000,** *56*, 257-265.

70. Feig, M.; Pettitt, B. M. Sodium and Chlorine Ions as Part of the DNA Solvation Shell. *Biophysical Journal* **1999,** *77*, 1769-1781.

71. Wong, K.-Y.; Pettitt, B. M. Orientation of DNA on a Surface From Simulation. *Biopolymers* **2004,** *73*, 570-578.

72. Kriech, M. A.; Conboy, J. C. Label-Free Chiral Detection of Melittin Binding to a Membrane. *Journal of the American Chemical Society* **2003,** *125*, 1148-1149.

73. MacKerell, A. D., Jr.; Bashford, D.; Bellott, M.; Dunbrack, R. L.; Evanseck, J. D.; Field, M. J.; Fischer, S.; Gao, J.; Guo, H.; Ha, S.; Joseph-McCarthy, D.; Kuchnir, L.; Kuczera, K.; Lau, F. T. K.; Mattos, C.; Michnick, S.; Ngo, T.; Nguyen, D. T.; Prodhom, B.; Reiher, W. E.; Roux, B.; Schlenkrich, M.; Smith, J. C.; Stote, R.; Straub, J.; Watanabe, M.; Wiorkiewicz-Kuczera, J.; Yin, D.; Karplus, M. All-Atom Empirical Potential for Molecular Modeling and Dynamics Studies of Proteins. *Journal of Physical Chemistry B* **1998,** *102*, 3586-3616.

74. Cruz-Chu, E. R.; Aksimentiev, A.; Schulten, K. Water-Silica Force Field for Simulating Nanodevices. *Journal of Physical Chemistry B* **2006,** *110*, 21497-21508.

75. Osborne, M. A.; Furey, W. S.; Klenerman, D.; Balasubramanian, S. Single-Molecule Analysis of DNA Immobilized on Microspheres. *Analytical Chemistry* **2000,** *72*, 3678-3681.

76. Hazani, M.; Naaman, R.; Hennrich, F.; Kappes, M. M. Confocal Fluorescence Imaging of DNA-Functionalized Carbon Nanotubes. *Nano Letters* **2003,** *3*, 153-155.

77. Vaidya, A. A.; Norton, M. L. DNA Attachment Chemistry at the Flexible Silicone Elastomer Surface: Toward Disposable Microarrays. *Langmuir* **2004,** *20*, 11100-11107.

78. Pawley, J. B. *Handbook of Biological Confocal Microscopy*. Springer: New York, 2006; p 656.

79. Edel, J. B.; Eid, J. S.; Meller, A. Accurate Single Molecule FRET Efficiency Determination for Surface Immobilized DNA Using Maximum Likelihood Calculated Lifetimes. *Journal of Physical Chemistry B* **2007,** *111*, 2986-2990.

80. Zhang, J.; Fu, Y.; Lakowicz, J. R. Fluorescence Images of DNA-Bound YOYO between Coupled Silver Particles. *Langmuir* **2007,** *23*, 11734-11739.

81. de Silva, A. P.; Gunaratne, H. Q. N.; Gunnlaugsson, T.; Huxley, A. J. M.; McCoy, C. P.; Rademacher, J. T.; Rice, T. E. Signaling Recognition Events with Fluorescent Sensors and Switches. *Chemical Reviews* **1997,** *97*, 1515-1566.

82. Weber, G.; Teale, F. W. J. Fluorescence Excitation Spectrum of Organic Compounds in Solution. Part 1.—Systems with Quantum Yield Independent of the Exciting Wavelength. *Transactions of the Faraday Society* **1958,** *54*, 640-648.

83. Parker, C. A.; Rees, W. T. Correction of Fluorescence Spectra and Measurement of Fluorescence Quantum Efficiency. *The Analyst* **1960,** *85*, 587-600.

84. Lavis, L. D.; Rutkoski, T. J.; Raines, R. T. Tuning the pK_a of Fluorescein to Optimize Binding Assays. *Analytical Chemistry* **2007,** *79*, 6775-6782.

CHAPTER 7

1. Boman, F. C.; Musorrafiti, M. J.; Gibbs, J. M.; Stepp, B. R.; Salazar, A. M.; Nguyen SonBinh, T.; Geiger Franz, M. DNA Single Stands Tethered to Fused Quartz/Water Interfaces Studied by Second Harmonic Generation. *Journal of the American Chemical Society* **2005,** *127*, 15368-15369.

2. Stokes, G. Y.; Gibbs-Davis, J. M.; Boman, F. C.; Stepp, B. R.; Condie, A. G.; Nguyen, S. T.; Geiger, F. M. Making "Sense" of DNA. *Journal of the American Chemical Society* **2007,** *129*, 7492-7493.

3. Boman, F. C.; Gibbs-Davis, J. M.; Heckman, L. M.; Stepp, B. R.; Nguyen, S. T.; Geiger, F. M. DNA at Aqueous/Solid Interfaces- Chirality-Based Detection via Second Harmonic Generation Activity. *Journal of the American Chemical Society* **2008,** *in press*.

4. Lorentzon, J.; Fuelscher, M. P.; Roos, B. O. Theoretical Study of the Electronic Spectra of Uracil and Thymine. *Journal of the American Chemical Society* **1995,** *117*, 9265-9273.

5. Tinoco, I., Jr. Hypochromism in Polynucleotides. *Journal of the American Chemical Society* **1960,** *82*, 4785-90.

6. Tonzani, S.; Schatz, G. C. Electronic Excitations and Spectra in Single-Stranded DNA. *J. Am. Chem. Soc*. **2008,** *130*, 7607-7612.

7. Fulscher, M. P.; Serrano-Andres, L.; Roos, B. O. A Theoretical Study of the Electronic Spectra of Adenine and Guanine. *J. Am. Chem. Soc*. **1997,** *119*, 6168-6176.

8. Plocinik, R. M.; Everly, R. M.; Moad, A. J.; Simpson, G. J. Modular Ellipsometric Approach for Mining Structural Information from Nonlinear Optical Polarization Analysis. *Physical Review B: Condensed Matter and Materials Physics* **2005,** *72*, 125409-125414.

9. Simpson, G. J. Structural Origins of Circular Dichroism in Surface Second Harmonic Generation. *The Journal of Chemical Physics* **2002,** *117*, 3398-3410.

10. Burke, B. J.; Moad, A. J.; Polizzi, M. A.; Simpson, G. J. Experimental Confirmation of the Importance of Orientation in the Anomalous Chiral Sensitivity of Second Harmonic Generation. *Journal of the American Chemical Society* **2003,** *125*, 9111-9115.

11. Maki, J. J.; Verbiest, T.; Kauranen, M.; Van Elshocht, S.; Persoons, A. Comparison of Linearly and Circularly Polarized Probes of Second-Order Optical Activity of Chiral Surfaces. *The Journal of Chemical Physics* **1996,** *105*, 767-772.

12. Bloomfield, V. A.; Crothers, D. M.; Tinoco, I., Jr. *Nucleic Acids: Structures, Properties, and Functions*. University Science Books: Sausalito, CA, 2000; p 794.

13. Burton, K. *Biochemistry of Nucleic Acids*. University Park Press: Baltimore, 1974; p 364.

14. Neidle, S. *Principles of Nucleic Acid Structure*. 1st ed.; Academic Press: Boston, 2007; p 289.

15. Voet, D.; Voet, J. G. *Biochemistry*. 2nd ed.; John Wiley & Sons, Inc.: New York, 1995; p 1361.

16. Sassolas, A.; Leca-Bouvier, B. D.; Blum, L. J. DNA Biosensors and Microarrays. *Chemical Reviews* **2008,** *108*, 109-139.

17. Hurst, S. J.; Han, M. S.; Lytton-Jean, A. K. R.; Mirkin, C. A. Screening the Sequence Selectivity of DNA-Binding Molecules Using a Gold Nanoparticle-Based Colorimetric Approach. *Analytical Chemistry* **2007,** *79*, 7201-7205.

18. Kohli, P.; Harrell, C. C.; Cao, Z.; Gasparac, R.; Tan, W.; Martin, C. R. DNA-Functionalized Nanotube Membranes with Single-Base Mismatch Selectivity. *Science* **2004,** *305*, 984-986.

19. Lewis, F. D.; Zhang, L.; Liu, X.; Zuo, X.; Tiede, D. M.; Long, H.; Schatz, G. C. DNA as Helical Ruler: Exciton-Coupled Circular Dichroism in DNA Conjugates. *Journal of the American Chemical Society* **2005,** *127*, 14445-14453.

20. Senthilkumar, K.; Grozema, F. C.; Guerra, C. F.; Bickelhaupt, F. M.; Lewis, F. D.; Berlin, Y. A.; Ratner, M. A.; Siebbeles, L. D. A. Absolute Rates of Hole Transfer in DNA. *Journal of the American Chemical Society* **2005,** *127*, 14894-14903.

21. Shkel, I. A.; Record, M. T., Jr. Effect of the Number of Nucleic Acid Oligomer Charges on the Salt Dependence of Stability (ΔG°_{37}) and Melting Temperature (T_m): NLPB Analysis of Experimental Data. *Biochemistry* **2004,** *43*, 7090-7101.

22. Smith, E. A.; Kyo, M.; Kumasawa, H.; Nakatani, K.; Saito, I.; Corn, R. M. Chemically Induced Hairpin Formation in DNA Monolayers. *Journal of the American Chemical Society* **2002,** *124*, 6810-6811.

23. Xu, D.; Xu, D.; Yu, X.; Liu, Z.; He, W.; Ma, Z. Label-Free Electrochemical Detection for Aptamer-Based Array Electrodes. *Analytical Chemistry* **2005,** *77*, 5107-5113.

24. Silverman, A. P.; Kool, E. T. Detecting RNA and DNA with Templated Chemical Reactions. *Chemical Reviews* **2006,** *106*, 3775-3789.

25. Strother, T.; Cai, W.; Zhao, X.; Hamers, R. J.; Smith, L. M. Synthesis and Characterization of DNA-Modified Silicon (111) Surfaces. *Journal of the American Chemical Society* **2000,** *122*, 1205-1209.

26. Potyrailo, R. A.; Conrad, R. C.; Ellington, A. D.; Hieftje, G. M. Adapting Selected Nucleic Acid Ligands (Aptamers) to Biosensors. *Analytical Chemistry* **1998,** *70*, 3419-3425.

27. Famulok, M.; Hartig, J. S.; Mayer, G. Functional Aptamers and Aptazymes in Biotechnology, Diagnostics, and Therapy. *Chemical Reviews* **2007,** *107*, 3715-3743.

28. LaFratta, C. N.; Walt, D. R. Very High Density Sensing Arrays. *Chemical Reviews* **2008,** *108*, 614-637.

29. Seeman, N. C. DNA in a Material World. *Nature* **2003,** *421*, 427-431.

30. Bugaut, A.; Jantos, K.; Wietor, J.-L.; Rodriguez, R.; Sanders, J. K. M.; Balasubramanian, S. Exploring the Differential Recognition of DNA G-Quadruplex Targets by Small Molecules Using Dynamic Combinatorial Chemistry13. *Angewandte Chemie International Edition* **2008,** *47*, 2677-2680.

31. Burge, S.; Parkinson, G. N.; Hazel, P.; Todd, A. K.; Neidle, S. Quadruplex DNA: Sequence, Topology and Structure. *Nucleic Acids Research* **2006,** *34*, 5402-5415.

32. Tang, Z.; Mallikaratchy, P.; Yang, R.; Kim, Y.; Zhu, Z.; Wang, H.; Tan, W. Aptamer Switch Probe Based on Intramolecular Displacement. *Journal of the American Chemical Society* **2008,** *130*, 11268-11269.

33. Higuchi, A.; Siao, Y.-D.; Yang, S.-T.; Hsieh, P.-V.; Fukushima, H.; Chang, Y.; Ruaan, R.-C.; Chen, W.-Y. Preparation of a DNA Aptamer-Pt Complex and Its Use in the Colorimetric Sensing of Thrombin and Anti-Thrombin Antibodies. *Analytical Chemistry* **2008,** *80*, 6580-6586.

34. Zhao, X.; Subrahmanyan, S.; Eisenthal, K. B. Determination of pK_a at the Air/Water Interface by Second Harmonic Generation. *Chemical Physics Letters* **1990,** *171*, 558-562.

35. Zhao, X.; Ong, S.; Eisenthal, K. B. Polarization of Water Molecules at a Charged Interface. Second Harmonic Studies of Charged Monolayers at the Air/Water Interface. *Chemical Physics Letters* **1993,** *202*, 513-520.

36. Yan, E. C. Y.; Liu, Y.; Eisenthal, K. B. New Method for Determination of Surface Potential of Microscopic Particles by Second Harmonic Generation. *Journal of Physical Chemistry B* **1998,** *102*, 6331-6336.

37. Liu, Y.; Yan, E. C. Y.; Zhao, X.; Eisenthal, K. B. Surface Potential of Charged Liposomes Determined by Second Harmonic Generation. *Langmuir* **2001,** *17*, 2063-2066.

38. Xiao, X. D.; Vogel, V.; Shen, Y. R. Probing the Proton Excess at Interfaces by Second Harmonic Generation. *Chemical Physics Letters* **1989,** *163*, 555-559.

39. Lyklema, J. *Fundamentals of Interface and Colloid Science*. Academic Press: New York, 1991; Vol. 1, p 736.

40. Hayes, K. F.; Redden, G.; Ela, W.; Leckie, J. O. Surface Complexation Models: An Evaluation of Model Parameter Estimation Using FITEQL and Oxide Mineral Titration Data. *Journal of Colloid and Interface Science* **1991,** *142*, 448-469.

41. Morel, F. M. M.; Hering, J. G. *Principles and Applications of Aquatic Chemistry*. John Wiley & Sons, Inc.: New York, 1993; p 588.

42. Stumm, W.; Morgan, J. J. *Aquatic Chemistry: Chemical Equilibria and Rates in Natural Waters*. 3rd ed.; John Wiley & Sons, Inc.: New York, 1996; p 1022.

43. Koopal, L. K. Mineral Hydroxides: From Homogeneous to Heterogeneous Modeling. *Electrochimica Acta* **1996,** *41*, 2293-2305.

44. Kosmulski, M. Adsorption of Cadmium on Alumina and Silica: Analysis of the Values of Stability Constants of Surface Complexes Calculated for Different Parameters of Triple Layer Model. *Colloids and Surfaces A: Physicochemical and Engineering Aspects* **1996,** *117*, 201-214.

45. Langmuir, D. *Aqueous Environmental Geochemistry*. Prentice Hall: Upper Saddle River, NJ, 1997; p 600.

46. Robertson, A. P.; Leckie, J. O. Cation Binding Predictions of Surface Complexation Models: Effects of pH, Ionic Strength, Cation Loading, Surface Complex, and Model Fit. *Journal of Colloid and Interface Science* **1997,** *188*, 444-472.

47. Sahai, N.; Sverjensky, D. A. Evaluation of Internally Consistent Parameters for the Triple-Layer Model by the Systematic Analysis of Oxide Surface Titration Data. *Geochimica et Cosmochimica Acta* **1997,** *61*, 2801-2826.

48. Brown, G. E.; Henrich, V. E.; Casey, W. H.; Clark, D. L.; Eggleston, C.; Felmy, A.; Goodman, D. W.; Gratzel, M.; Maciel, G.; McCarthy, M. I.; Nealson, K. H.; Sverjensky, D. A.; Toney, M. F.; Zachara, J. M. Metal Oxide Surfaces and Their Interactions with Aqueous Solutions and Microbial Organisms. *Chemical Reviews* **1999,** *99*, 77-174.

49. Delgado, A. V.; Gonzalez-Caballero, R.; Hunter, R. J.; Koopal, L. K.; Lyklema, J. Measurement and Interpretation of Electrokinetic Phenomena (IUPAC Technical Report). *Pure and Applied Chemistry* **2005,** *77*, 1753-1805.

50. Mergny, J.-L.; Lacroix, L. Analysis of Thermal Melting Curves. *Oligonucleotides* **2003,** *13*, 515-537.

51. Tinoco, I. Nucleic Acid Structures, Energetics, and Dynamics. *Journal of Physical Chemistry* **1996,** *100*, 13311-13322.

52. Rosi, N. L.; Mirkin, C. A. Nanostructures in Biodiagnostics. *Chemical Reviews* **2005,** *105*, 1547-1562.

53. Kriech, M. A.; Conboy, J. C. Imaging Chirality with Surface Second Harmonic Generation Microscopy. *Journal of the American Chemical Society* **2005,** *127*, 2834-2835.

54. Ji, N.; Zhang, K.; Yang, H.; Shen, Y.-R. Three-Dimensional Chiral Imaging by Sum-Frequency Generation *Journal of the American Chemical Society* **2006,** *128*, 3482-3483.

55. Nuriya, M.; Jiang, J.; Nemet, B.; Eisenthal, K. B.; Yuste, R. Imaging Membrane Potential in Dendritic Spines. *Proceedings of the National Academy of Sciences of the United States of America* **2006,** *103*, 786-790.

56. Schaller, R. D.; Johnson, J. C.; Wilson, K. R.; Lee, L. F.; Haber, L. H.; Saykally, R. J. Nonlinear Chemical Imaging Nanomicroscopy: From Second and Third Harmonic Generation to Multiplex (Broad-Bandwidth) Sum Frequency Generation Near-Field Scanning Optical Microscopy. *Journal of Physical Chemistry B* **2002,** *106*, 5143-5154.

57. Cimatu, K.; Baldelli, S. Chemical Imaging of Corrosion: Sum Frequency Generation Imaging Microscopy of Cyanide on Gold at the Solid-Liquid Interface. *Journal of the American Chemical Society* **2008,** *130*, 8030-8037.

58. Rechsteiner, P.; Hulliger, J.; Floersheimer, M. Phase-Sensitive Second Harmonic Microscopy Reveals Bipolar Twinning Of Markov-Type Molecular Crystals. *Chemistry of Materials* **2000,** *12*, 3296-3300.

59. Millard, A. C.; Jin, L.; Wuskell, J. P.; Boudreau, D. M.; Lewis, A.; Loew, L. M. Wavelength- and Time-Dependence of Potentiometric Non-linear Optical Signals from Styryl Dyes. *Journal of Membrane Biology* **2005,** *208*, 103-111.

60. Jin, R.; Jureller, J.; Kim, H. Y.; Scherer, N. F. Correlating Second Harmonic Optical Responses of Single Ag Nanoparticles with Morphology *Journal of the American Chemical Society* **2005,** *127*, 12482-12483.

61. Long, J. P.; Simpkins, B. S.; Rowenhorst, D. J.; Pehrsson, P. E. Far-field Imaging of Optical Second-Harmonic Generation in Single GaN Nanowires *Nano Letters* **2007,** *7*, 831-836.

62. Salaita, K.; Wang, Y.; Mirkin, C. A. Applications of Dip-Pen Nanolithography. *Nature Nanotechnology* **2007,** *2*, 145-155.

63. Zanni, M. T.; Gnanakaran, S.; Stenger, J.; Hochstrasser, R. M. Heterodyned Two-Dimensional Infrared Spectroscopy of Solvent-Dependent Conformations of Acetylproline-NH_2. *Journal of Physical Chemistry B* **2001,** *105*, 6520-6535.

64. Krummel, A. T.; Mukherjee, P.; Zanni, M. T. Inter and Intrastrand Vibrational Coupling in DNA Studied with Heterodyned 2D-IR Spectroscopy *Journal of Physical Chemistry B* **2003,** *107*, 9165-9169.

65. Brixner, T.; Stiopkin, I. V.; Fleming, G. R. Tunable Two-dimensional Femtosecond Spectroscopy. *Optics Letters* **2004,** *29*, 884-886.

66. Demirdoven, N.; Cheatum, C. M.; Chung, H. S.; Khalil, M.; Knoester, J.; Tokmakoff, A. Two-Dimensional Infrared Spectroscopy of Antiparallel _-Sheet Secondary Structure. *Journal of the American Chemical Society* **2004,** *126*, 7981-7990.

67. Xu, Q. H.; Ma, Y. Z.; Fleming, G. R. Different Real and Imaginary Components of the Resonant Third-Order Polarization Revealed by Optical Heterodyne Detected Transient Grating Spectroscopic Studies of Crystal Violet: Model and Experiment. *Journal of Physical Chemistry A* **2002,** *106*, 10755-10763.

68. Lepetit, L.; Cheriaux, G.; Joffre, M. Linear Techniques of Phase Measurement by Femtosecond Spectral Interferometry for Applications in Spectroscopy. *Journal of the Optical Society of America B: Optical Physics* **1995,** *12*, 2467-2474.

69. Kaufman, L. J.; Heo, J.; Ziegler, L. D.; Fleming, G. R. Heterodyne-Detected Fifth-Order Nonresonant Raman Scattering from Room Temperature CS_2. *Physical Review Letters* **2002,** *88*, 207402.

70. Vaughan, J. C.; Hornung, T.; Stone, K. W.; Nelson, K. A. Coherently Controlled Ultrafast Four-Wave Mixing Spectroscopy. *Journal of Physical Chemistry A* **2007,** *111*, 4873-4883.

71. Stiopkin, I. V.; Jayathilake, H. D.; Bordenyuk, A. N.; Benderskii, A. V. Heterodyne-Detected Vibrational Sum Frequency Generation Spectroscopy. *Journal of the American Chemical Society* **2008,** *130*, 2271-2275.

72. Chang, R. K.; Ducuing, J.; Bloembergen, N. Relatice Phase Measurement Between Fundamental and Second-Harmonic Light. *Physical Review Letters* **1965,** *15*, 6-8.

73. Kemnitz, K.; Bhattacharyya, K.; Hicks, J. M.; Pinto, G. R.; Eisenthal, K. B.; Heinz, T. F. The Phase of Second-harmonic Light Generated at an Interface and its Relation to Absolute Molecular Orientation. *Chemical Physics Letters* **1986,** *131*, 285-290.

74. Mifflin, A. L.; Musorrafiti, M. J.; Konek, C. T.; Geiger, F. M. Second Harmonic Generation Phase Measurements of Cr(VI) at a Buried Interface. *Journal of Physical Chemistry B* **2005,** *109*, 24386-24390.

75. Na, C.; Kendall, T. A.; Martin, S. T. Surface-Potential Heterogeneity of Reacted Calcite and Rhodochrosite. *Environmental Science & Technology* **2007,** *41*, 6491-6497.

76. Schrock, D. S.; Baur, J. E. Chemical Imaging with Combined Fast-Scan Cyclic Voltammetry-Scanning Electrochemical Microscopy. *Analytical Chemistry* **2007,** *79*, 7053-7061.

77. Evans, R.; Timmel, C. R.; Hore, P. J.; Britton, M. M. Magnetic Resonance Imaging of the Manipulation of a Chemical Wave Using an Inhomogeneous Magnetic Field. *Journal of the American Chemical Society* **2006,** *128*, 7309-7314.

78. Kendall, T. A.; Martin, S. T. Water-Induced Reconstruction that Affects Mobile Ions on the Surface of Calcite. *Journal of Physical Chemistry A* **2007,** *111*, 505-514.

APPENDIX 1

1. Shriver, D. F. *The Manipulation of Air-Sensitive Compounds*. 2nd ed.; Wiley: New York, 1986; p 326.

2. Pangborn, A. B.; Giardello, M. A.; Grubbs, R. H.; Rosen, R. K.; Timmers, F. J. Safe and Convenient Procedure for Solvent Purification. *Organometallics* **1996,** *15*, 1518-1520.

3. Perrin, D. D.; Armarego, W. L. F. *Purification of Laboratory Chemicals*. 3rd ed.; Pergamon Press: New York, 1988.

4. Shelkov, R.; Nahmany, M.; Melman, A. Selective Esterifications of Alcohols and Phenols Through Carbodiimide Couplings. *Organic and Biomolecular Chemistry* **2004,** *2*, 397-401.

APPENDIX 2

1. Hicks, J. M.; Urbach, L. E.; Plummer, E. W.; Dai, H.-L. Can Pulsed Laser Excitation of Surfaces Be Described by a Thermal Model? *Physical Review Letters* **1988,** *61*, 2588-2591.

2. Shen, Y. R. *The Principles of Nonlinear Optics*. John Wiley & Sons, Inc.: New York, 1984.

3. Boyd, R. W. *Nonlinear Optics*. 2nd ed.; Academic Press: New York, 2003; p 578.

4. *Diode-Pumped, Mode-Locked Ti:Sapphire Laser User's Manual: Mai Tai*. Spectra-Physics: Mountain View, CA, 2002.

5. Milonni, P. W.; Eberly, J. H. *Lasers*. John Wiles & Sons, Inc.: New York, 1988; p 731.

6. Voges, A., B.; Al-Abadleh Hind, A.; Geiger, F., M. Applications of Nonlinear Optical Techniques for Studying Heterogeneous Systems Relevant in the Natural Environment. In *Environmental Catalysis*, Grassain, V. H., Ed. CRC Press: New York, 2005; pp 83-128.

7. Foskett, J. K.; Grinstein, S. *Noninvasive Techniques in Cell Biology*. Wiley-Liss: New York, 1990; Vol. 9, p 423.

8. Mason, W. T. *Fluorescent and Luminescent Probes for Biological Activity*. 2nd ed.; Academic Press: San Diego, CA, 1999; p 647.

APPENDIX 3

1. Jones, R. C. A New Calculus for the Treatment of Optical Systems. *Journal of the Optical Society of America* **1941,** *31*, 488-493.

2. Collett, E. *Polarized Light: Fundamentals and Applications*. Marcel Dekker, Inc.: New York, 1993; p 581.

3. Brosseau, C. *Fundamentals of Polarized Light: A Statistical Optics Approach*. John Wiley & Sons, Inc.: New York, 1998; p 405.

4. Plocinik, R. M.; Everly, R. M.; Moad, A. J.; Simpson, G. J. Modular Ellipsometric Approach for Mining Structural Information from Nonlinear Optical Polarization Analysis. *Physical Review B: Condensed Matter and Materials Physics* **2005,** *72*, 125409-125414.

APPENDIX 4

1. Liebermann, T.; Knoll, W.; Sluka, P.; Herrmann, R. Complement Hybridization from Solution to Surface-Attached Probe-Oligonucleotides Observed by Surface-Plasmon-Field-Enhanced Fluorescence Spectroscopy. *Colloids and Surfaces A: Physicochemical and Engineering Aspects* **2000,** *169*, 337-350.

2. Moses, S.; Brewer, S. H.; Lowe, L. B.; Lappi, S. E.; Gilvey, L. B. G.; Sauthier, M.; Tenent, R. C.; Feldheim, D. L.; Franzen, S. Characterization of Single- and Double-Stranded DNA on Gold Surfaces. *Langmuir* **2004,** *20*, 11134-11140.

3. Castelino, K.; Kannan, B.; Majumdar, A. Characterization of Grafting Density and Binding Efficiency of DNA and Proteins on Gold Surfaces. *Langmuir* **2005,** *21*, 1956-1961.

4. Lee, C. Y.; Gong, P.; Harbers, G. M.; Grainger, D. W.; Castner, D. G.; Gamble, L. J. Surface Coverage and Structure of Mixed DNA/Alkylthiol Monolayers on Gold: Characterization by XPS, NEXAFS, and Fluorescence Intensity Measurements. *Analytical Chemistry* **2006,** *78*, 3316-3325.

5. Demers, L. M.; Mirkin, C. A.; Mucic, R. C.; Reynolds, R. A., III; Letsinger, R. L.; Elghanian, R.; Viswanadham, G. A Fluorescence-Based Method for Determining the Surface Coverage and Hybridization Efficiency of Thiol-Capped Oligonucleotides Bound to Gold Thin Films and Nanoparticles. *Analytical Chemistry* **2000,** *72*, 5535-5541.

6. Lenigk, R.; Carles, M.; Ip, N. Y.; Sucher, N. J. Surface Characterization of a Silicon-Chip-Based DNA Microarray. *Langmuir* **2001,** *17*, 2497-2501.

7. Voicu, R.; Boukherroub, R.; Bartzoka, V.; Ward, T.; Wojtyk, J. T. C.; Wayner, D. D. M. Formation, Characterization, and Chemistry of Undecanoic Acid-Terminated Silicon Surfaces: Patterning and Immobilization of DNA. *Langmuir* **2004,** *20*, 11713-11720.

8. Watterson, J. H.; Piunno, P. A. E.; Krull, U. J. Towards the Optimization of an Optical DNA Sensor: Control of Selectivity Coefficients and Relative Surface Affinities. *Analytica Chimica Acta* **2002,** *457*, 29-38.

9. Pawley, J. B. *Handbook of Biological Confocal Microscopy*. Springer: New York, 2006; p 656.

10. Osborne, M. A.; Furey, W. S.; Klenerman, D.; Balasubramanian, S. Single-Molecule Analysis of DNA Immobilized on Microspheres. *Analytical Chemistry* **2000,** *72*, 3678-3681.

11. Hazani, M.; Naaman, R.; Hennrich, F.; Kappes, M. M. Confocal Fluorescence Imaging of DNA-Functionalized Carbon Nanotubes. *Nano Letters* **2003,** *3*, 153-155.

12. Vaidya, A. A.; Norton, M. L. DNA Attachment Chemistry at the Flexible Silicone Elastomer Surface: Toward Disposable Microarrays. *Langmuir* **2004,** *20*, 11100-11107.

13. Edel, J. B.; Eid, J. S.; Meller, A. Accurate Single Molecule FRET Efficiency Determination for Surface Immobilized DNA Using Maximum Likelihood Calculated Lifetimes. *Journal of Physical Chemistry B* **2007,** *111*, 2986-2990.

14. Zhang, J.; Fu, Y.; Lakowicz, J. R. Fluorescence Images of DNA-Bound YOYO between Coupled Silver Particles. *Langmuir* **2007,** *23*, 11734-11739.

15. Manning, G. S. On the Application of Polyelectrolyte "Limiting Laws" to the Helix-Coil Transition of DNA. I. Excess Univalent Cations. *Biopolymers* **1972,** *11*, 937-949.

16. Burton, K. *Biochemistry of Nucleic Acids*. University Park Press: Baltimore, 1974; p 364.

17. Record, M. T., Jr.; Anderson, C. F.; Lohman, T. M. Thermodynamic Analysis of Ion Effects on the Binding and Conformational Equilibriums of Proteins and Nucleic Acids: The Roles of Ion Association or Release, Screening, and Ion Effects on Water Activity. *Quarterly Reviews of Biophysics* **1978,** *11*, 103-178.

18. Spink, C. H.; Chaires, J. B. Effects of Hydration, Ion Release, and Excluded Volume on the Melting of Triplex and Duplex DNA. *Biochemistry* **1999,** *38*, 496-508.

19. Neidle, S. *Principles of Nucleic Acid Structure*. 1st ed.; Academic Press: Boston, 2007; p 289.

APPENDIX 5

1. Shen, Y. R. *The Principles of Nonlinear Optics*. John Wiley & Sons, Inc.: New York, 1984.

2. Zhu, X. D.; Suhr, H.; Shen, Y. R. In *Surface Vibrational Spectroscopy by Infrared-Visible Sum-Frequency Generation*, XIV International Conference on Quantum Electronics, Part 2, San Francisco, CA, June 9-13, 1986; B, J. O. S. A., IEEE: 1986; P252.

3. Zhu, X. D.; Suhr, H.; Shen, Y. R. Surface Vibrational Spectroscopy by Infrared-Visible Sum Frequency Generation. *Physical Review B: Condensed Matter and Materials Physics* **1987,** *35*, 3047-3050.

4. Shen, Y. R. Surface Properties Probed by Second-Harmonic and Sum-Frequency Generation. *Nature* **1989,** *337*, 519-525.

5. Eisenthal, K. B. Equilibrium and Dynamic Processes at Interfaces by Second Harmonic and Sum Frequency Generation. *Annual Review of Physical Chemistry* **1992,** *43*, 627-661.

6. Shen, Y. R. Exploring New Opportunities with Sum-Frequency Nonlinear Optical Spectroscopy. *Pure and Applied Chemistry* **2001,** *73*, 1589-1598.

7. Richmond, G. L. Molecular Bonding and Interactions at Aqueous Surfaces as Probed by Vibrational Sum Frequency Spectroscopy. *Chemical Reviews* **2002,** *102*, 2693-2724.

8. Belkin, M. A.; Kulakov, T. A.; Ernst, K. H.; Yan, L.; Shen, Y. R. Sum-Frequency Vibrational Spectroscopy on Chiral Liquids: A Novel Technique to Probe Molecular Chirality. *Physical Review Letters* **2000,** *85*, 4474-4477.

9. Nafie, L. A.; Keiderling, T. A.; Stephens, P. J. Vibrational Circular Dichroism. *Journal of the American Chemical Society* **1976,** *98*, 2715-2723.

10. Keiderling, T. A. Vibrational CD of Biopolymers. *Nature* **1986,** *322*, 851-852.

11. Keiderling, T. A. Vibrational Circular Dichroism: Comparison of Techniques and Practical Considerations. In *Practical Fourier Transform Infrared Spectroscopy*, Ferraro, J. R.; Krishnan, K., Eds. Academic Press, Inc.: New York, 1990; pp 203-284.

12. Petralli-Mallow, T.; Wong, T. M.; Byers, J. D.; Yee, H. I.; Hicks, J. M. Circular Dichroism Spectroscopy at Interfaces: A Surface Second Harmonic Generation Study. *Journal of Physical Chemistry* **1993,** *97*, 1383-1388.

13. Burke, B. J.; Moad, A. J.; Polizzi, M. A.; Simpson, G. J. Experimental Confirmation of the Importance of Orientation in the Anomalous Chiral Sensitivity of Second Harmonic Generation. *Journal of the American Chemical Society* **2003,** *125*, 9111-9115.

14. Ji, N.; Shen, Y.-R. Optically Active Sum Frequency Generation from Molecules with a Chiral Center: Amino Acids as Model Systems. *Journal of the American Chemical Society* **2004,** *126*, 15008-15009.

15. Boyd, R. W. *Nonlinear Optics*. 2nd ed.; Academic Press: New York, 2003; p 578.

16. Heinz, T. F. Second-Order Nonlinear Optical Effects at Surfaces and Interfaces. In *Nonlinear Surface Electromagnetic Phenomena*, Ponath, H.; Stegeman, G., Eds. Elsevier Publishers: Amsterdam, NY, 1991; pp 353-416.

17. Eisenthal, K. B. Liquid Interfaces Probed by Second-Harmonic and Sum-Frequency Spectroscopy. *Chemical Reviews* **1996,** *96*, 1343-1360.

18. Shen, Y. R.; Ostroverkhov, V. Sum-Frequency Vibrational Spectroscopy on Water Interfaces: Polar Orientation of Water Molecules at Interfaces. *Chemical Reviews* **2006,** *106*, 1140-1154.

19. Voges, A. B.; Al-Abadleh, H. A.; Musorrafiti, M. J.; Bertin, P. A.; Nguyen, S. T.; Geiger, F. M. Carboxylic Acid- and Ester-Functionalized Siloxane Scaffolds on Glass Studied by Broadband Sum Frequency Generation. *Journal of Physical Chemistry B* **2004,** *108*, 18675-18682.

20. Voges, A., B.; Al-Abadleh Hind, A.; Geiger, F., M. Applications of Nonlinear Optical Techniques for Studying Heterogeneous Systems Relevant in the Natural Environment. In *Environmental Catalysis*, Grassain, V. H., Ed. CRC Press: New York, 2005; pp 83-128.

21. Voges, A. B.; Stokes, G. Y.; Gibbs-Davis, J. M.; Lettan, R. B.; Bertin, P. A.; Pike, R. C.; Nguyen, S. T.; Scheidt, K. A.; Geiger, F. M. Insights into Heterogeneous Atmospheric Oxidation Chemistry: Development of a Tailor-Made Synthetic Model for Studying Tropospheric Surface Chemistry. *Journal of Physical Chemistry C* **2007,** *111*, 1567-1578.

22. *All Diode-Pumped Kilohertz Ti:Sapphire Regenerative Amplifier Syster User's Manual: Hurricane*. Spectra-Physics: Mountain View, CA, 2000.

23. *Ultrafast Optical Parametric Amplifier User's Manual: OPA-800C*. Spectra-Physics: Mountain View, CA, 2001.

24. Esenturk, O.; Walker, R. A. Surface Structure at Hexadecane and Halo-hexadecane Liquid/Vapor Interfaces. *Journal of Physical Chemistry B* **2004,** *108*, 10631-10635.

25. Richter, L. J.; Petralli-Mallow, T. P.; Stephenson, J. C. Vibrationally Resolved Sum-Frequency Generation with Broad-bandwidth/Infrared Pulses. *Optics Letters* **1998,** *23*, 1594-1596.

26. Jin, L.; Horgan, A.; Levicky, R. Preparation of End-Tethered DNA Monolayers on Siliceous Surfaces Using Heterobifunctional Cross-Linkers. *Langmuir* **2003,** *19*, 6968-6975.

27. Voicu, R.; Boukherroub, R.; Bartzoka, V.; Ward, T.; Wojtyk, J. T. C.; Wayner, D. D. M. Formation, Characterization, and Chemistry of Undecanoic Acid-Terminated Silicon Surfaces: Patterning and Immobilization of DNA. *Langmuir* **2004,** *20*, 11713-11720.

28. Lockett, M. R.; Phillips, M. F.; Jarecki, J. L.; Peelen, D.; Smith, L. M. A Tetrafluorophenyl Activated Ester Self-Assembled Monolayer for the Immobilization of Amine-Modified Oligonucleotides. *Langmuir* **2008,** *24*, 69-75.

29. Burton, K. *Biochemistry of Nucleic Acids*. University Park Press: Baltimore, 1974; p 364.

30. Voet, D.; Voet, J. G. *Biochemistry*. 2nd ed.; John Wiley & Sons, Inc.: New York, 1995; p 1361.

31. Bloomfield, V. A.; Crothers, D. M.; Tinoco, I., Jr. *Nucleic Acids: Structures, Properties, and Functions*. University Science Books: Sausalito, CA, 2000; p 794.

32. Neidle, S. *Principles of Nucleic Acid Structure*. 1st ed.; Academic Press: Boston, 2007; p 289.

33. Dickerson, R. E.; Drew, H. R.; Conner, B. N.; Wing, R. M.; Fratini, A. V.; Kopka, M. L. The anatomy of A-, B-, and Z-DNA. *Science* **1982,** *216*, 475-485.

APPENDIX 1

Synthesis of NHS Linker and DNA Oligonucleotides

Portions of this chapter are reproduced in part
with permission from the American Chemical Society:

Boman, F.C.; Musorrafiti, M.J.; Gibbs, J.M.; Stepp B.R.; Salazar, A.M.; Nguyen, S.T.; Geiger, F.M. "DNA Single Strands Tethered to Fused Quartz/Water Interfaces Studied by Second Harmonic Generation." *Journal of the American Chemical Society*, **2005**, *127*, 15368-15369.

Stokes, G.Y.; Gibbs-Davis, J.M.; Boman, F.C.; Stepp, B.R.; Condie, A.G.; Nguyen, S.T.; Geiger, F.M. "Making 'Sense' of DNA." *Journal of the American Chemical Society*, **2007**, *129*, 7492-7493.

Boman, F.C.; Gibbs-Davis, J.M.; Heckman, L.M.; Stepp, B.R.; Nguyen, S.T.; Geiger, F.M. "DNA at Aqueous/Solid Interfaces- Chirality-Based Detection via Second Harmonic Generation Activity." *Journal of the American Chemical Society*, **2008**, *in press.*

A1.1 General Considerations and Materials

All synthetic manipulations and initial surface functionalization reactions were performed under a dry nitrogen atmosphere using either standard Schlenk techniques[1] or in a controlled nitrogen atmosphere system (Nexus, VAC) unless otherwise noted. Solvents were dried on the Dow-Grubbs solvent system[2] installed by Glass Contours. Solvents were collected under argon, degassed under vacuum, stored under nitrogen in a Strauss flask, and saturated with argon prior to use. Ultrapure water (18.2 MΩ·cm resistivity) was obtained from a Millipore Milli-Q Biocel system. 10-Undecylenic acid chloride was purchased from Acros Organics. All other reagents were purchased from Aldrich and used without further purification, unless otherwise noted. Trichlorosilane was distilled over quinoline[3] and vacuum transferred into an airtight solvent bulb followed by transfer to a nitrogen glove box. All flash column chromatography was carried out using a 56-mm inner-diameter column containing a 200-mm plug of silica gel under a positive pressure of nitrogen. Dr. Julianne Gibbs-Davis, Dr. Brian Stepp, and Ehow Chen synthesized the NHS linker in bulk as needed. Dr. Brian Stepp synthesized the DNA.

A1.2 Synthesis of 11-(Trichlorosilyl)-Undecanoic Acid NHS Ester

The reaction of undecanoic acid and NHS to form the undecylenic and 11-(trichlorosilyl)-undecanoic acid NHS esters is shown in Figure A1.1. *N*-hydroxysuccinimide (NHS, 0.96 g, 8.38 mmol) and triethylamine (2.7 mL, 18 mmol) were added into a 50-mL Schlenk flask, placed under nitrogen, dry dichloromethane (10 mL) was added via cannula, and the mixture was cooled to 0 °C in an ice bath. 10-Undecylenic acid chloride (1.5 mL, 7.0 mmol) was added slowly via syringe to the stirring mixture and stirred overnight as it was allowed to reach room temperature.

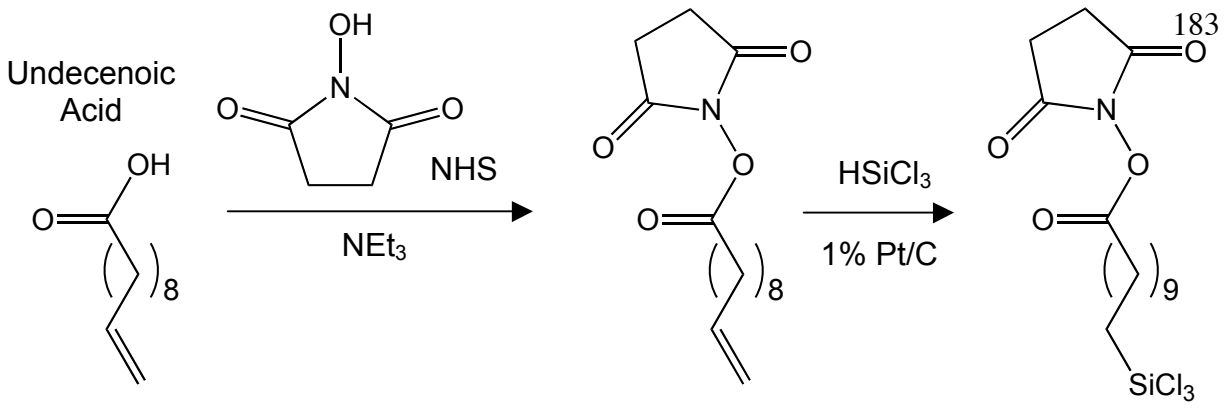

Figure A1.1. Synthesis of 11-(Trichlorosilyl)-Undecanoic Acid NHS Ester
10-Undecylenic acid chloride was added to *N*-hydroxysuccinimide (NHS) and NEt_3 to form the undecylenic acid NHS ester. Trichlorosilane and Pt/C catalyst were then combined with the product to form the 11-(trichlorosilyl)-undecanoic acid NHS ester.

The reaction mixture was then extracted with dichloromethane (25 mL) and washed with water (2 x 25 mL). The organic layer was dried over sodium sulfate and filtered, and the solvent was removed under reduced pressure. The crude product was purified by silica gel chromatography using 50% ethyl acetate in hexanes as eluent to yield the product as a white powder (1.76 g, 6.24 mmol, 89%). NMR characterization data for the product matched those reported in the literature.[4]

Undecylenic acid NHS ester (0.488 g, 1.73 mmol), trichlorosilane (175 μL, 1.73 mmol), and Pt/C catalyst (0.04 g, 3% Pt) were combined under nitrogen in a 40-mL pressure tube (Ace Glass #8648-09) with dry toluene (20 mL). The mixture was stirred at 100 °C for 2 days. The progress of the reaction was monitored by the disappearance of olefinic protons by ^{1}H-NMR spectroscopy. The starting material was still present by NMR analysis, therefore, additional trichlorosilane (160 μL, 1.60 mmol) and of Pt/C (30 mg) were added to the reaction mixture, which was recapped and stirred overnight at 100 °C at which time the NMR data indicated that there was less than 5% starting material.

The reaction was cooled down and filtered over Celite in the dry box, and the solid was rinsed with dry toluene (10 mL). Excess trichlorosilane and toluene were removed under reduced pressure under an inert atmosphere. The crude product was dissolved in dry dichloromethane and filtered, and the solvent was removed from the filtrate under reduced pressure to give a colorless gel (520 mg, 1.25 mmol, 72%, >95% purity). The main impurity was the olefinic starting material, which does not affect the surface functionalization, therefore, the product was used without further purification. ^{1}H and ^{13}C NMR spectra were recorded on an INOVA 500 FT-NMR spectrometer (Varian) (499.6 MHz for ^{1}H NMR, 125.6 MHz for ^{13}C NMR). ^{1}H NMR ($CDCl_3$): δ 1.20-1.39 (m, 14H, (CH_2-(CH_2)$_7$-CH_2-C(O)), 1.52 (m, 2H, CH_2-CH_2SiCl_3), 1.71 (t, 2H,

CH_2SiCl_3), 2.60 (t, 2H, CH_2-C(O)-N), 2.84 (b, 4H, succinimidyl). ^{13}C NMR ($CDCl_3$): ^{13}C NMR ($CDCl_3$) σ: 22.72, 24.78, 25.03, 26.08, 29.22-30.92, 31.42, 32.26, 169.16, 169.66.

A1.3 Synthesis of DNA Oligonucleotides

Synthesis of single strand DNA was performed on an Expedite 8909 Nucleic Acid system using standard reagents and 3'-amino-, 3'-dT-, and 3'-dA-modified controlled porosity glass (CPG) solid supports (Glen Research, 3'-amino-modifier C_7 CPG, 20-2958-41). DNA was purified on an Agilent 1100 HPLC equipped with a Varian Dynamax column (250 × 10.0 mm^2 (L x ID) Microsorb 300-10 C_{18}) using a gradient method of 100% 0.03 M triethylammonium acetate (TEAA) buffer in H_2O at time 0 going to 50% acetonitrile (containing 5% of the 0.03 M TEAA buffer) over 50 minutes with a flow rate of 3 mL/min. DNA was desalted with an Illustra NAP-5 desalting column (GE Healthcare) and lyophilized with a FreeZone benchtop freeze dry system (Labconco) in the final steps to remove any remaining buffer salts. DNA concentrations were measured at 260 nm with a Cary 100 Bio UV-Vis spectrophotometer (Varian).

DNA strands were synthesized with T_n and A_n sequences (10-50 nmol), where n = 15, 25, 30, 35, or 40. The T_n sequences were attached to the NHS-functionalized surfaces via a 3'-amine-terminated C_7 hydrocarbon chain linker (Figure A1.2). Additional 3'-amino-T_{25} and A_{25} DNA, including all fluorescently-tagged DNA, was purchased from Integrated DNA Technologies, Inc. and used without further modification. The 3'-amino-T_{25} strand was labeled with a 5'-6-FAM tag, and the A_{25} strand was labeled with a 3'-6-FAM tag (Figure A1.3a-b).

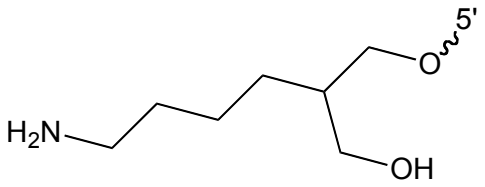

Figure A1.2. DNA 3'-Amino Modifier
The DNA strands were terminated with an H_2N-C_7H_{13}(OH)-tether on their 3' end.

A

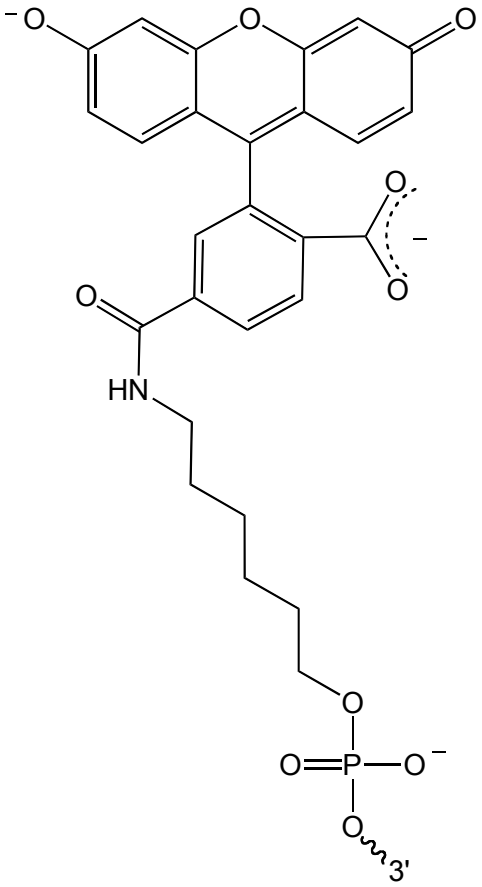

B

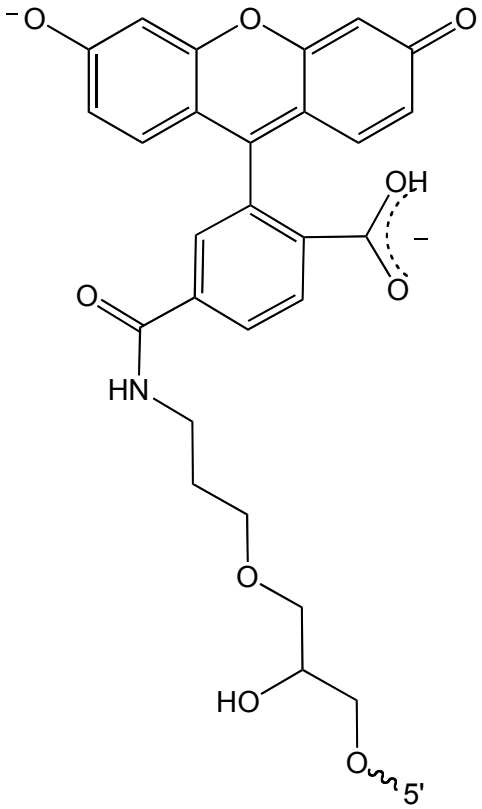

Figure A1.3. DNA Fluorescent Tags
The fluorescent DNA strands were tagged with **A**) 5'-6-FAM on the T_{25} sequences and **B**) 3'-6-FAM on the complementary A_{25} sequences.

APPENDIX 2

Verification of Second Harmonic Signal

Portions of this chapter are reproduced in part
with permission from the American Chemical Society:

Boman, F.C.; Musorrafiti, M.J.; Gibbs, J.M.; Stepp B.R.; Salazar, A.M.; Nguyen, S.T.; Geiger, F.M. "DNA Single Strands Tethered to Fused Quartz/Water Interfaces Studied by Second Harmonic Generation." *Journal of the American Chemical Society*, **2005**, *127*, 15368-15369.

Boman, F.C.; Gibbs-Davis, J.M.; Heckman, L.M.; Stepp, B.R.; Nguyen, S.T.; Geiger, F.M. "DNA at Aqueous/Solid Interfaces- Chirality-Based Detection via Second Harmonic Generation Activity." *Journal of the American Chemical Society*, **2008**, *in press*.

A2.1 Input Energy Studies

The detected signal was determined to be due to SHG by measuring its input energy dependence. To avoid thermal damage,[1] all experiments were performed between 0.50 and 0.75 μJ with a 120-fsec pulse duration and a 1-kHz rep rate (see Chapter 2.3.3). Energy studies on the interfaces functionalized with the NHS linker and the single and double strand DNA (ssDNA and dsDNA) verify that this range is below the damage threshold. The SH signal intensity, I_{SHG}, is equal to the square modulus of the second-order susceptibility tensor, $\vec{\vec{\chi}}^{(2)}$, multiplied by the applied field intensities, I_ω (i.e. I_{SHG} has a quadratic dependence on $I_{\omega.}$).[2,3]

$$I_{2\omega} \propto \left|\vec{\vec{\chi}}^{(2)}\right|^2 I_\omega I_\omega \tag{A2.1}$$

Consequently, the square root of the SH signal, $\sqrt{I_{SHG}}$, is equal to the magnitude of the SH E-field, $E_{2\omega}$, assuming constructive interference, which is linearly proportional to I_ω.[2,3]

$$\sqrt{I_{SHG}} = E_{2\omega} \propto \vec{\vec{\chi}}^{(2)} I_\omega \tag{A2.2}$$

I_ω is proportional to the energy of the applied electric field.

The SH E-fields from the interfaces were found to display the expected linear dependence on input energy for non-resonant (Figure A2.1) and resonant wavelengths (Figure A2.2), confirming that the signal is due to SHG. A nonlinear relationship was observed for higher energies, which indicates thermal breakdown. Therefore, the DNA-functionalized surfaces remained stable throughout the SHG measurements and were not thermally damaged within the range of input energy levels used.

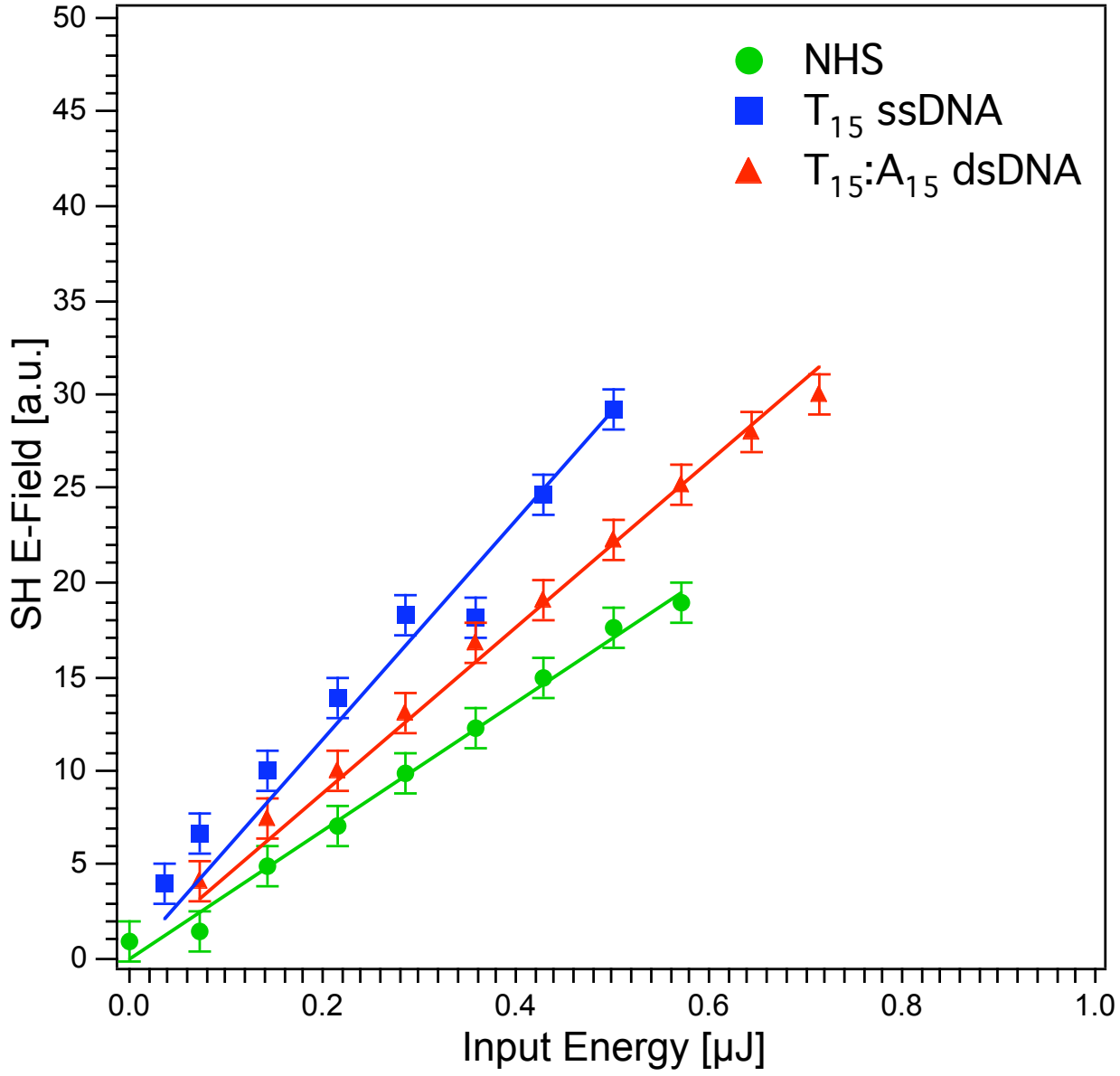

Figure A2.1. Energy Study Off DNA Electronic Resonance
The SH E-field vs. the input energy is shown for the NHS linker (green circles), T_{25} ssDNA (blue squares), and T_{25}:A_{25} dsDNA (red triangles) interfaces under 0.15 M NaCl at pH 7. The interface was probed with 630-660 nm, and the SH signal was collected at 315-330 nm (see Table A2.1b). The energy ranged up to 0.75 μJ. A linear fit was applied to each interface (green, blue, and red lines).

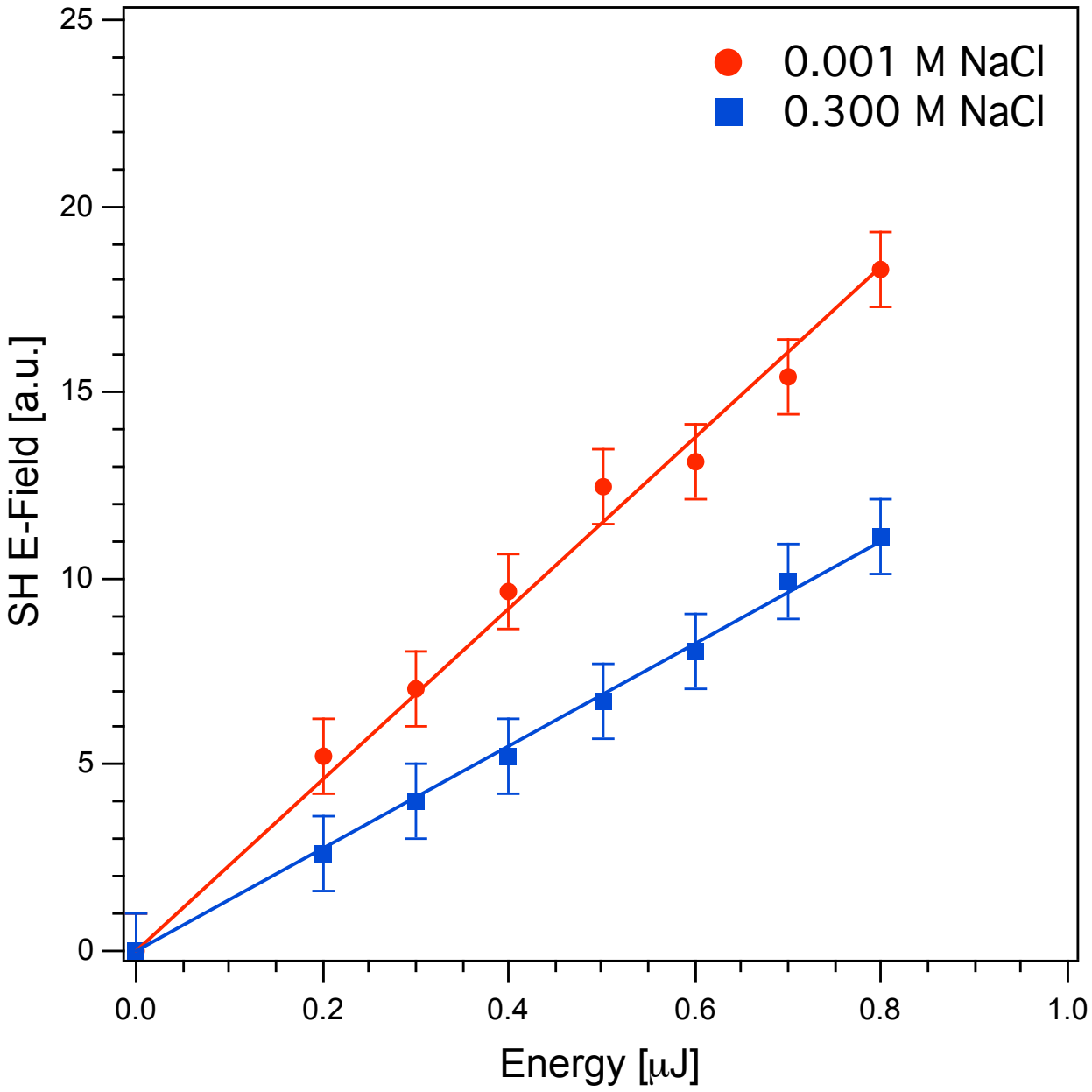

Figure A2.2. Energy Study On DNA Electronic Resonance
The SH E-field vs. the input energy is shown for the T_{25} ssDNA interface under 0.001 M (red circles) and 0.300 M (blue squares) NaCl at pH 7. The interface was probed with 520 nm, and the SH signal was collected at 260 nm. The energy ranged up to 0.8 μJ. A linear fit was applied to each interface (red and blue lines).

A2.2 Output Second Harmonic Signal

The SH signal was also determined to be due to SHG by measuring its spectral bandwidth at full width-half maximum (FWHM). For a transform-limited Gaussian pulse shape, the expression for the time-bandwidth product is shown below:[4]

$$\Delta t \cdot \Delta \nu = 0.441 \tag{A2.3}$$

where Δt is the FWHM of the intensity envelope of the pulse ($\Delta t = 1.20 \times 10^{13}$ sec for our laser system), and $\Delta \nu$ is the FWHM of the spectrum of the pulse, or the bandwidth. The theoretical FWHM of the pulse, $\Delta \lambda$, can be calculated by the following:

$$\Delta \lambda = \frac{\Delta \nu \cdot \lambda}{\nu} \tag{A2.4}$$

where ν and λ are the frequency and wavelength of the pulse, respectively. For example, when $\lambda = 520$ nm, $\Delta \lambda = 3.3$ nm. However this theoretical bandwidth does not account for frequency broadening and assumes a perfect Gaussian pulse.[2,3,5] The fundamental beam passes through the several optics and nonlinear crystals in the OPA before it is incident on the sample, and the SH beam passes through a series of optics before it enters the monochromator. This causes dispersion in the beams and increases $\Delta \lambda$.

The spectra of the input beams of the functionalized interfaces were collected by reflecting into a UV-Vis spectrometer (Figure A2.3a-c), and the spectra of the output SH beams were collected by scanning the monochromator (Figure A2.3d-f). The corresponding FWHM were calculated by fitting a Gaussian function to the spectra (Table A2.1). The SH FWHM values are on the order of $1/\sqrt{2}$ times the fundamental FWHM values.[2,3,6] This verifies that the measured signal does not originate from white light, due to high laser power, or from

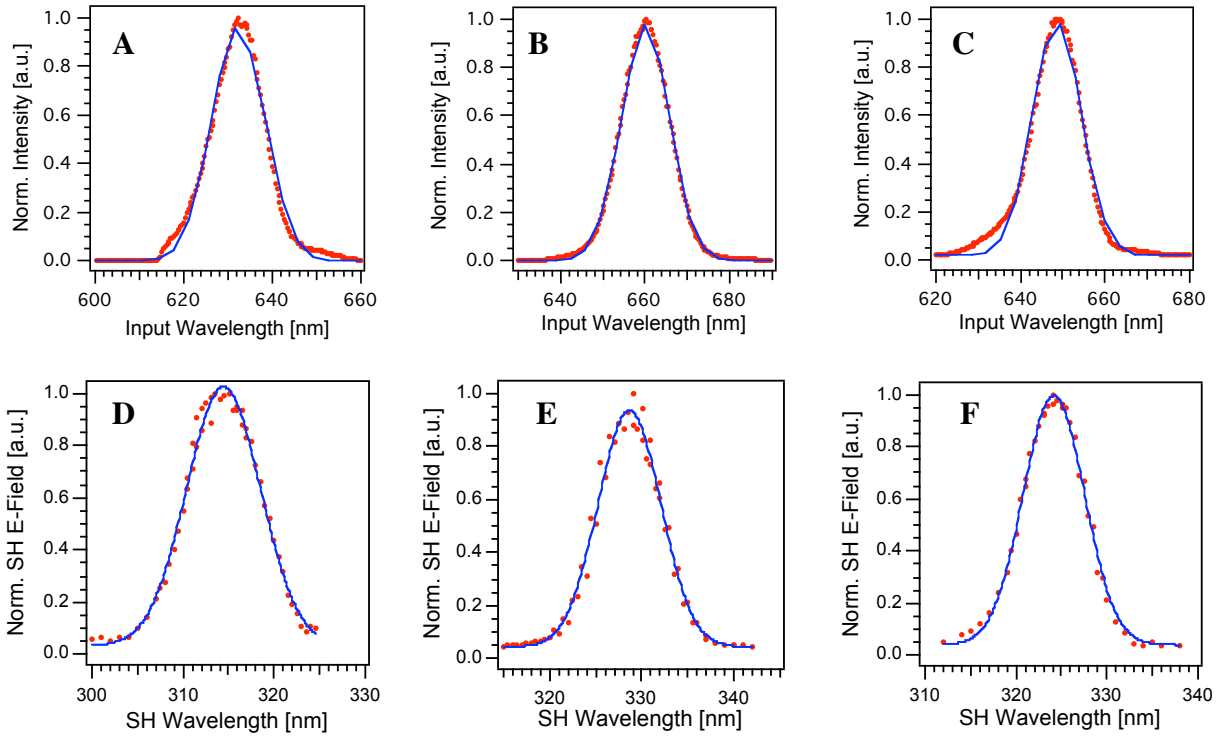

Figure A2.3. Spectral Input and Output of SH Signal
The input spectra of the fundamental beam were measured with a UV-Vis spectrometer for the **A**) NHS linker (ω= 630 nm), **B**) T_{15} ssDNA (ω= 660 nm), and **C**) T_{15}:A_{15} dsDNA (ω= 650 nm) functionalized interfaces. All spectra were normalized to 1, and a Gaussian function was fit to the data (blue lines). The output spectra of the SH beam were measured by scanning the monochromator for the **D**) NHS linker (2ω= 315 nm), **E**) T_{15} ssDNA (2ω= 330 nm), and **F**) T_{15}:A_{15} dsDNA (2ω= 325 nm) functionalized interfaces. The monochromator in front of the photomultiplier tube has a 3-nm resolution. The fitting parameters are listed in Table A2.1.

Interface	Input λ (nm)	Input FWHM (nm)	Output λ (nm)	Output FWHM (nm)
NHS	632.2(1)	17.0(1)	314.4(1)	11.5(3)
T_{15}	660.0(1)	16.2(1)	328.7(1)	9.6(2)
T_{15}:A_{15}	648.6(1)	16.3(1)	324.2(1)	9.5(2)

Table A2.1. Spectral Bandwidths for Fundamental and SH Beams
The input fundamental beam was measured with a UV-Vis spectrometer, and the output SH beam was measured by scanning the SH signal with a monochromator over 300-345 nm. A Gaussian function was used to fit the spectra from the NHS linker, T_{15} ssDNA, and T_{15}:A_{15} dsDNA functionalized interfaces. The measured input and output wavelengths along with their bandwidths are included in the table. The resolution of the monochromator in front of the photomultiplier tube is 3 nm.

fluorescence, where typical FWHM are approximately 30-100 nm.[7,8] Spectral broadening around this bandwidth range is indicative of optical breakdown, but since our measured values for $\Delta\lambda$ are well below this limit, this does not occur and the measured signal is due to SHG.

APPENDIX 3

Theoretical Framework for Polarized Light

A3.1 Waveplates and Polarizers

In order to probe a surface with a chiral spectroscopy, the polarization of the light must be controlled with a waveplate or selected with a linear polarizer. When light passes through an optical element, it can be linearly polarized (lp) or circularly polarized (cp). A Jones vector, $\vec{E}$, represents the normalized electric field polarization for light propagating in the z direction, oscillating in time, t, at frequency ω, and a Jones matrix, M, describes the optical elements.[1-3]

$$\vec{E} = \begin{bmatrix} E_x \\ E_y \end{bmatrix} = \begin{bmatrix} E_o e^{i\delta_x} \\ E_o e^{i\delta_y} \end{bmatrix} \text{ and } M = \begin{bmatrix} M_{xx} & M_{xy} \\ M_{yx} & M_{yy} \end{bmatrix} \tag{A3.1}$$

The electric field components along the x- and y-axes are E_x and E_y, the matrix elements are M_{xx}, M_{xy}, M_{yx}, and M_{yy}, and δ is a phase shift.

A3.2 Jones Vectors and Jones Matrices

A polarized electric field passing through an optical element and then emerging with a new polarization state can be mathematically described by the operation of a Jones matrix on a Jones vector to produce a new Jones vector.[1-3]

$$\begin{bmatrix} E'_x \\ E'_y \end{bmatrix} = \begin{bmatrix} M_{xx} & M_{xy} \\ M_{yx} & M_{yy} \end{bmatrix} \begin{bmatrix} E_x \\ E_y \end{bmatrix} \tag{A3.2}$$

The normalized Jones vectors, for linearly and circularly polarized light and, are shown below:

$$\vec{E}_p = \begin{bmatrix} 0 \\ 1 \end{bmatrix}, \vec{E}_s = \begin{bmatrix} 1 \\ 0 \end{bmatrix}, \vec{E}_{-45^\circ} = \frac{1}{\sqrt{2}} \begin{bmatrix} 1 \\ -1 \end{bmatrix}, \text{ and } \vec{E}_{+45^\circ} = \frac{1}{\sqrt{2}} \begin{bmatrix} 1 \\ 1 \end{bmatrix} \tag{A3.3}$$

$$\vec{E}_{R_{cp}} = \frac{1}{\sqrt{2}} \begin{bmatrix} 1 \\ -i \end{bmatrix} \text{ and } \vec{E}_{L_{cp}} = \frac{1}{\sqrt{2}} \begin{bmatrix} 1 \\ i \end{bmatrix} \tag{A3.4}$$

where p (vertical), s (horizontal), -45°, and +45° refer to plane-polarization state of light.

The matrices for the optical elements used in our experiments, a polarizer, half-waveplate, and quarter-waveplate, rotated at a particular angle, θ, for electric fields that are in-phase with each other (i.e. $e^{i\delta}=1$ for t=0) have been derived.[1-3] A polarizer selects for the polarization of an electric field, and generates linear, plane-polarized light. The Jones matrices for a polarizer and for p-, s-, -45°-, and +45°-polarized light are described by:[1-4]

$$M_{pol,\theta} = \begin{bmatrix} \cos^2\theta & \sin\theta\cos\theta \\ \sin\theta\cos\theta & \sin^2\theta \end{bmatrix} \tag{A3.5}$$

$$M_p = \begin{bmatrix} 0 & 0 \\ 0 & 1 \end{bmatrix},\ M_s = \begin{bmatrix} 1 & 0 \\ 0 & 0 \end{bmatrix},\ M_{-45^\circ} = \begin{bmatrix} 1 & -1 \\ -1 & 1 \end{bmatrix},\ \text{and}\ M_{+45^\circ} = \begin{bmatrix} 1 & 1 \\ 1 & 1 \end{bmatrix} \tag{A3.6}$$

A half waveplate (λ/2) changes the polarization of an electric field and generates linear, plane-polarized light. The Jones matrices for a λ/2 and for p, s, -45°, and +45° are described by:[1-4]

$$M_{\frac{\lambda}{2},\theta} = \begin{bmatrix} \cos 2\theta & \sin 2\theta \\ \sin 2\theta & -\cos 2\theta \end{bmatrix} \tag{A3.7}$$

$$M_p = \begin{bmatrix} 1 & 0 \\ 0 & -1 \end{bmatrix},\ M_s = \begin{bmatrix} 0 & -1 \\ -1 & 0 \end{bmatrix},\ M_{-45} = \begin{bmatrix} 1 & 1 \\ -1 & 1 \end{bmatrix},\ \text{and}\ M_{+45} = \begin{bmatrix} 1 & -1 \\ 1 & 1 \end{bmatrix} \tag{A3.8}$$

A quarter waveplate (λ/4) changes the polarization of the electric field, and generates circular polarized light. The Jones matrices for a λ/4 and for L_{cp} and R_{cp} are also described by:[1-4]

$$M_{\frac{\lambda}{4},\theta} = \frac{1}{\sqrt{2}} \begin{bmatrix} 1 + i\cos 2\theta & i\sin 2\theta \\ i\sin 2\theta & 1 - i\cos 2\theta \end{bmatrix} \tag{A3.9}$$

$$M_{L_{cp}} = \frac{1}{\sqrt{2}} \begin{bmatrix} 1 & -i \\ i & 1 \end{bmatrix}\ M_{R_{cp}} = \frac{1}{\sqrt{2}} \begin{bmatrix} 1 & i \\ -i & 1 \end{bmatrix} \tag{A3.10}$$

APPENDIX 4

Fluorescence Confocal Microscopy

Portions of this chapter are reproduced in part
with permission from the American Chemical Society:

Boman, F.C.; Gibbs-Davis, J.M.; Heckman, L.M.; Stepp, B.R.; Nguyen, S.T.; Geiger, F.M. “DNA at Aqueous/Solid Interfaces- Chirality-Based Detection via Second Harmonic Generation Activity." *Journal of the American Chemical Society*, **2008**, *in press*.

A4.1 Introduction

Fluorescence-based techniques have been used to study surface coverage and hybridization efficiency of DNA on gold,[1-4] nanoparticles,[5] silicon,[6,7] and fused silica[8] surfaces. Here we used fluorescence confocal microscopy[9-14] to image our single strand and double strand (ssDNA and dsDNA) surfaces, test for specific binding, and optimize the surface preparation method. Fluorescence experiments were performed as described in Chapter 6.4.1 with an LSM 510 Meta Laser Scanning Microscope (Zeiss), a 20x objective, and 55-nm xy resolution.

A4.2 Specific and Non-Specific-Binding

Controls were conducted on T_{25}:A_{25} dsDNA surfaces to verify that only specific binding of the tagged complementary DNA strand to the surface-bound (sb) DNA was observed. The tagged A_{25} strand was hybridized to the T_{25} sb-DNA and rinsed with 0.25 M NaCl to remove any non-specific binding. In order to verify that the complementary strand was reversibly bound and could be removed by melting, the surfaces were rinsed with water. Water causes the negatively charged strands to become unstable and repel each other, separating them.[15-19] NHS samples were also exposed to the tagged DNA salt solution for one hour and rinsed with either salt or water.

The fluorescence emission intensities for the DNA and NHS linker surfaces after salt and water rinsing are shown in Figure A4.1a-d. The bright intensity of the samples after salt rinsing shows the dsDNA remains stable on the surface. The sharp decrease in intensity after water rinsing confirms this is an effective way of melting the DNA, removing all specifically bound strands. The fluorescence of the NHS linker surfaces sharply decreased for both types of rinsing. These results show that rinsing with NaCl effectively removes all non-specifically bound DNA.

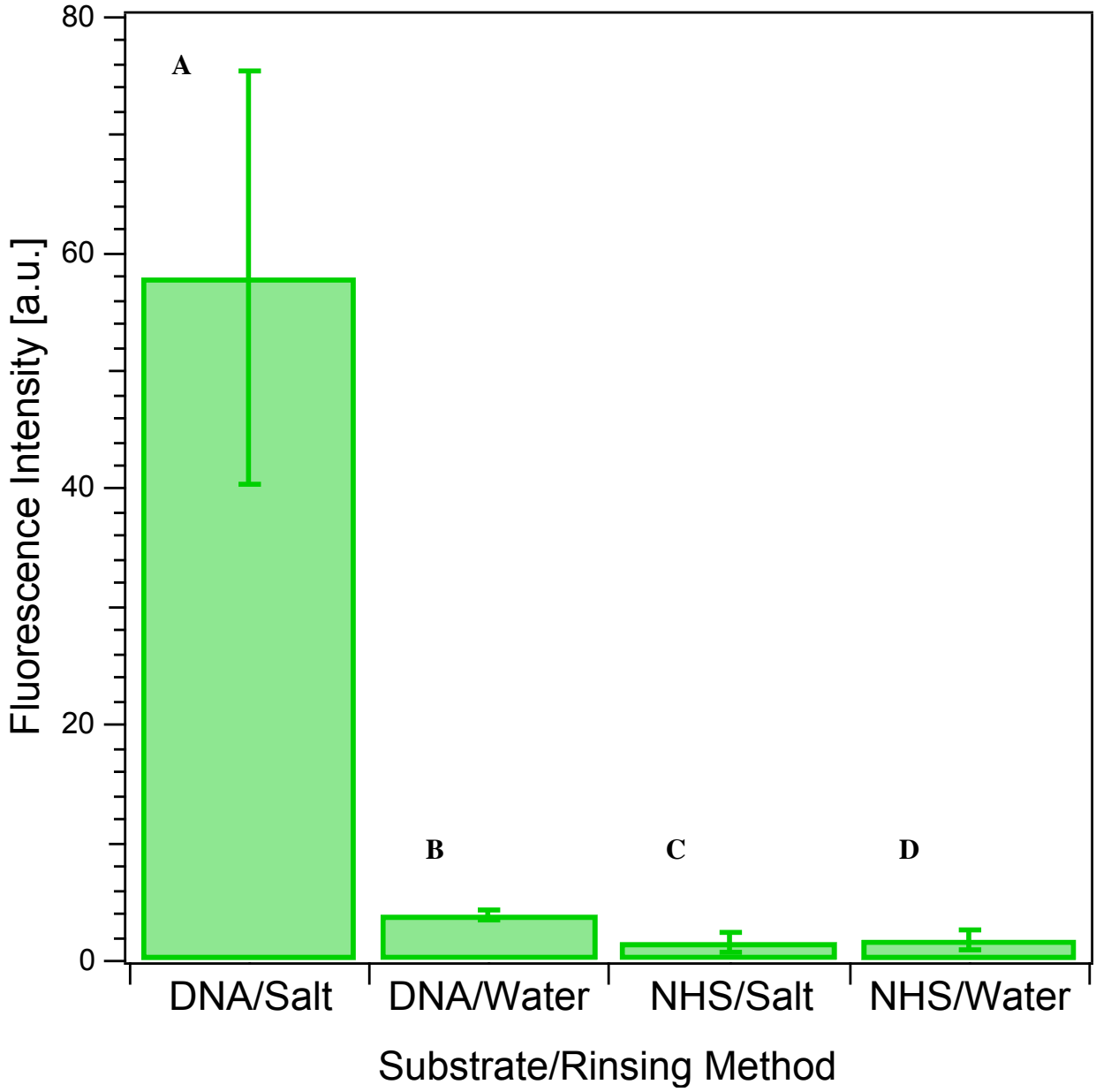

Figure A4.1. Test for Specific Binding of DNA
A-B. Fluorescence intensities recorded from T_{25} ssDNA-functionalized glass slides after exposure to the complementary fluorescently tagged A_{25} DNA strand in **A**) 0.25 M NaCl solution at pH 7 and in **B**) Millipore water. **C-D**. Fluorescence intensities recorded from NHS-functionalized glass slide after exposure to the fluorescently tagged A_{25} DNA strand in **C**) 0.25 M NaCl solution at pH 7 and in **D**) Millipore water.

A4.3 Optimization of Surface Functionalization

Similarly to Chapter 3.1.3, the rinsing and sonicating steps of the surface functionalization were also evaluated using fluorescence microscopy to determine which rinsing procedure resulted in a more even distribution of DNA, as well as a more even distribution of NHS linker. Two different methods have been used for NHS-functionalization (See Chapter 3.2.2). In our current method, following the linker glove box reaction, the samples were 1) rinsed with toluene 2) washing in toluene for 5 minutes in an ultrasonic bath, 3) rinsed with toluene, 4) rinsed with methanol and water, and 5) annealed in an oven at 100 °C. Previously, steps 2-4 were not included. Figure A4.2a-b shows dsDNA samples prepared by both methods. The non-sonicated sample clearly shows clusters of NHS linker, due dense spots of fluorescently tagged DNA. Sonicating the samples allowed for a more even distribution of DNA on the surface, removing any large clusters of NHS due to polymerization.

A4.4 Summary

We have verified with fluorescence confocal microscopy that rinsing with a 0.25 M NaCl salt solution removes non-specifically bound DNA from our functionalized interfaces. Water rinsing melts the hybridized dsDNA strands and removes all DNA that is not covalently bound to the NHS linker. These fluorescent images have increased our understanding of the DNA-functionalization process and have allowed us to optimize our surface preparation. In order to prepare an interface with an even distribution of NHS linker and, therefore, DNA, the samples must be sonicated in toluene following the reaction in the glove box. This sonication step is necessary for removing the polymerized clusters that remain on the surface after a toluene rinse.

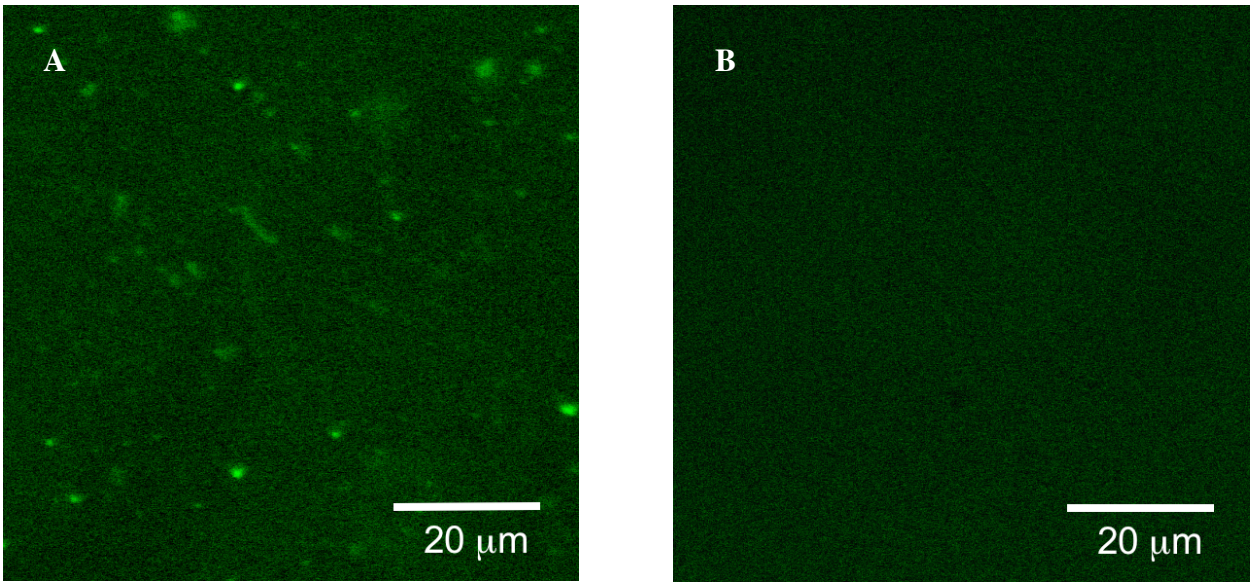

Figure A4.2. Removal of NHS Linker Clusters by Sonication
Fluorescence images of T_{25}:A_{25} dsDNA slides prepared **A**) with and **B**) without sonication.

APPENDIX 5

Additional Nonlinear Optical Applications

Portions of this chapter are reproduced in part
with permission from the American Chemical Society:

Stokes, G.Y.; Gibbs-Davis, J.M.; Boman, F.C.; Stepp, B.R.; Condie, A.G.; Nguyen, S.T.; Geiger, F.M. "Making 'Sense' of DNA." *Journal of the American Chemical Society*, **2007**, *129*, 7492-7493.

A5.1 Introduction

We have deciphered the molecular structure of surface-bound (sb) oligonucleotides in both single-strand and duplex forms by using polarization-resolved vibrational sum frequency generation (SFG) spectroscopy.[1-7] Taking advantage of the mixed polarizations of light (p±45p) experiment pioneered by Shen and coworkers,[8] we have obtained detailed structural information on sb-DNA, including the chirality of individual stereogenic centers in the strands and the secondary structure of the strands upon duplex formation. We have driven the chiral nonlinear optical response of the oscillators by probing the CH stretching region with p±45p. The difference of the p-polarized SFG spectra may be viewed as a second-order analog of a vibrational circular dichroism (VCD) spectrum.[9-11] The key advantage of the SFG approach is that the second order CD effect can be greatly enhanced over the linear response.[12-14]

A5.2 Sum Frequency Generation

A5.2.1 Theoretical Description

Sum frequency generation (SFG)[1-7] is a nonlinear optical process where visible and IR light fields are directed at a surface and overlapped in space and time to produce a light field which is at the sum of their frequencies (Figure A5.1a-b). This effect is due to the noncentrosymmetry of the interface. The resulting photons contain vibrational information about the identity and orientation of the molecules at the surface. SFG has been described elsewhere,[1-7] and a brief overview is presented here.

The SFG signal, I_{SFG},[1,6,7,15] is directly proportional to the square modulus of the second-order nonlinear polarization, $\vec{P}^{(2)}_{SFG}$, which is equal to the square modulus of the second-order

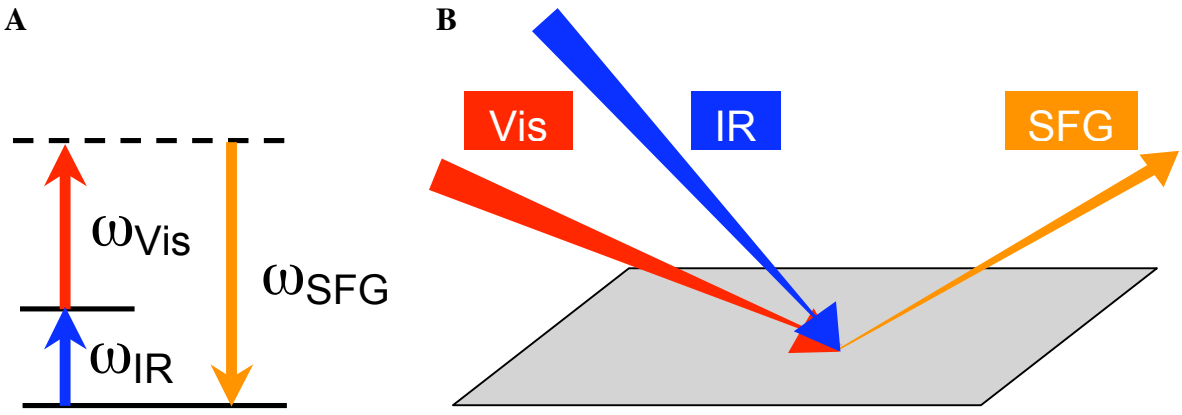

Figure A5.1. Schematic of Sum Frequency Generation
A) Energy level diagram of SFG. The frequencies of the visible and IR light fields, ω_{Vis} and ω_{IR}, are equal to the frequency of the SF light field, ω_{SFG}. The ω_{IR} probes vibrational transitions in molecules adsorbed at the interface. **B**) A schematic representation of the overlapping visible and IR light fields at the interface that produce the SF light field.

susceptibility tensor, $\vec{\vec{\chi}}^{(2)}$, multiplied by the visible and IR light field intensities, I_{Vis} and I_{IR}.

$$I_{SFG} \propto \left|\vec{P}^{(2)}_{SFG}\right|^2 = \left|\vec{\vec{\chi}}^{(2)}\right|^2 I_{Vis} I_{IR} \tag{A5.1}$$

The $\vec{\vec{\chi}}^{(2)}$ tensor is composed of a non-resonant, $\vec{\vec{\chi}}^{(2)}_{NR}$, and resonant, $\vec{\vec{\chi}}^{(2)}_{R\nu}$, term, where:[1,15]

$$\left|\vec{\vec{\chi}}^{(2)}\right|^2 = \left|\vec{\vec{\chi}}^{(2)}_{NR} + \sum_{\nu=1}^{n} \vec{\vec{\chi}}^{(2)}_{R\nu} e^{i\gamma_\nu}\right|^2 \tag{A5.2}$$

The resonant term in Equation A5.2 includes the contributions from the resonant modes, ν, and their relative phases, γ_ν. It is proportional to the number of adsorbed molecules, N_{ads}, and the molecular hyperpolarizability tensor, $\vec{\beta}_\nu$, averaged over molecular orientations, shown below:[1,15]

$$\vec{\vec{\chi}}^{(2)}_{R\nu} \propto N_{ads} \left\langle \vec{\beta}_\nu \right\rangle \tag{A5.3}$$

Under conditions where the incoming IR beam, ω_{IR}, probes the surface at a frequency that matches a vibrational transition frequency, ω_ν, in a surface-bound molecule, $\vec{\beta}_\nu$ becomes resonantly enhanced. The expression for this enhancement is given by:[1,15]

$$\vec{\beta}_\nu \propto \frac{A_{\nu,ij} M_{\nu,k}}{(\omega_{IR} - \omega_\nu + i\Gamma_\nu)} \tag{A5.4}$$

where $A_{\nu,ij}$ is the Raman transition probability and $M_{\nu,k}$ is the IR transition dipole moment for a given mode, ν. The subscripts i, j, and k represent the surface coordinate system, and Γ_ν is a damping coefficient. When $\vec{\beta}_\nu$ is enhanced, $\vec{\vec{\chi}}^{(2)}_{R\nu}$ and, therefore, I_{SFG} are enhanced as well.

A5.2.2 Experimental Description

Detailed descriptions of the experimental aspects of sum frequency generation (SFG) are available elsewhere[1,3,7,16-18] and our specific optical setup has been described previously.[19-21] Grace Stokes collected all SFG spectra. Briefly, the current studies were carried out using an

800-nm, 120-fs regeneratively amplified Ti:sapphire system (Hurricane, Spectra-Physics).[22] The Hurricane system pumps an optical parametric amplifier (OPA-800CF, Spectra Physics)[23] to produce IR light around 3.3 μm with a bandwidth (full width-half maximum) about 140 cm^{-1}. The energy of the incident IR and visible light fields was measured using an energy meter (EPM1000-0110L99, Molectron) and ranged between 1.4 and 2.9 μJ for the IR and 3.6 and 5.0 μJ for the visible light fields. The IR beam passed through an IR half waveplate ($CdGaS_4$, 10-mm diameter, Altechna Co. Ltd.), before being overlapped with the visible beam and focused onto the surface under investigation. The reflected SFG signal was collected with a 0.5-m spectrograph (SP-2556, Acton Research) and detected with a digital CCD spectroscopy system (Spec-10:400B/LN, Roper Scientific). Following the work of Esenturk and Walker,[24] we recorded broadband SFG spectra with several different input IR center frequencies to ensure that all vibrational modes in the C-H frequency region were probed. The broadband[25] spectra presented here are averaged from 7 spectra collected within 1-10 minutes each. The signal normalization and summing procedures are described in our previous work.[21] All spectra are referenced to the 2955 cm^{-1} C-H symmetric stretch of the methoxy groups in poly(methyl) methacrylate (PMMA).[19]

A5.3 Vibrational Spectra of DNA Interfaces

A5.3.1 Substrate Preparation

We chemically attached T_{15} single strand DNA (ssDNA) to glass microscope slides using established protocols[26-28] that result in a range of surface coverage from 10^{11} to 10^{12} strands/cm^2 (see Chapters 3 and 4). Each T_{15} strand contains 15 methyl groups from the thymine bases,

providing a handle for subsequent interrogation with vibrational spectroscopy. To form the sb-duplex with the complementary A_{15} sequence, the T_{15}-functionalized substrate was placed in a 10-μM solution of A_{15} in 10-mM phosphate buffered saline (PBS, pH 7, 0.25 M NaCl) overnight, followed by copious rinsing with 0.25 M NaCl. Since adenine does not contain methyl groups, the sb-T_{15}:A_{15} duplex still contains only 15 methyl groups, however, the number of bases doubles to 30. The vibrational properties of these DNA-functionalized substrates in both single-strand and duplex forms were then probed using the broadband SFG setup.[19,21] The DNA base methyl, ribose methylene, and ribose methine functional group locations are shown in Figure A5.2.

A5.3.2 Differentiation Between Single and Double Strand DNA

Figure A5.3 shows ssp-polarized SFG spectra of the sb-T_{15} single strand (blue trace) and the sb-T_{15}:A_{15} duplex (red trace) which probe transitions with a component perpendicular to the interface. While the symmetric and asymmetric methylene stretch modes at 2850 and 2930 cm^{-1}, respectively, are clearly observable in both spectra, the T_{15} strand does not exhibit methyl asymmetric stretch contributions (2950 cm^{-1}). The methyl symmetric stretch intensity (2875 cm^{-1}) is very small, even though there are 15 methyl groups on the T_{15} strand. These results suggest a lack of order on the surface, especially with respect to the methyl groups in the thymine strand. Interestingly, methine CH vibrations are only visible at ~2900 cm^{-1} in the sps-polarized SFG spectra, which probe transitions with a component parallel to the interface (Figure A5.4).

After hybridizing the sb-T_{15} single strand with its complementary A_{15} strand, the methyl asymmetric and symmetric stretch signatures of the 15 thymine moieties are clearly apparent (red trace, Figure A5.3). This stark change indicates a more ordered methyl group arrangement in the sb-T_{15}:A_{15} duplex, which we attribute to the formation of a double helix.[29-32] The induced

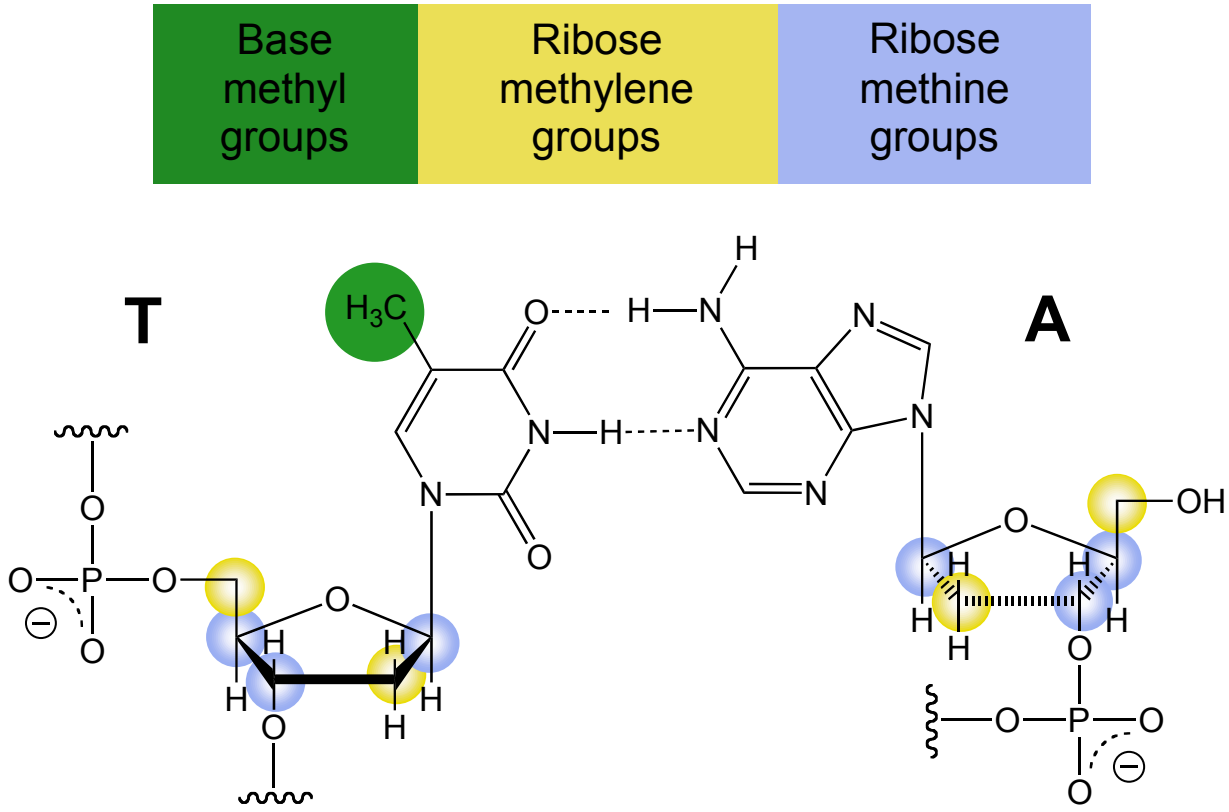

Figure A5.2. CH Vibrational Modes of an A:T DNA Base Pair
A DNA base pair between thymine and adenine is shown. The methyl group (CH_3) in the thymine base is shown in green and does not appear in the adenine base. The ribose methylene (CH_2) and methine (CH) groups in the sugar rings are shown in yellow and blue, respectively, and are present in both bases.

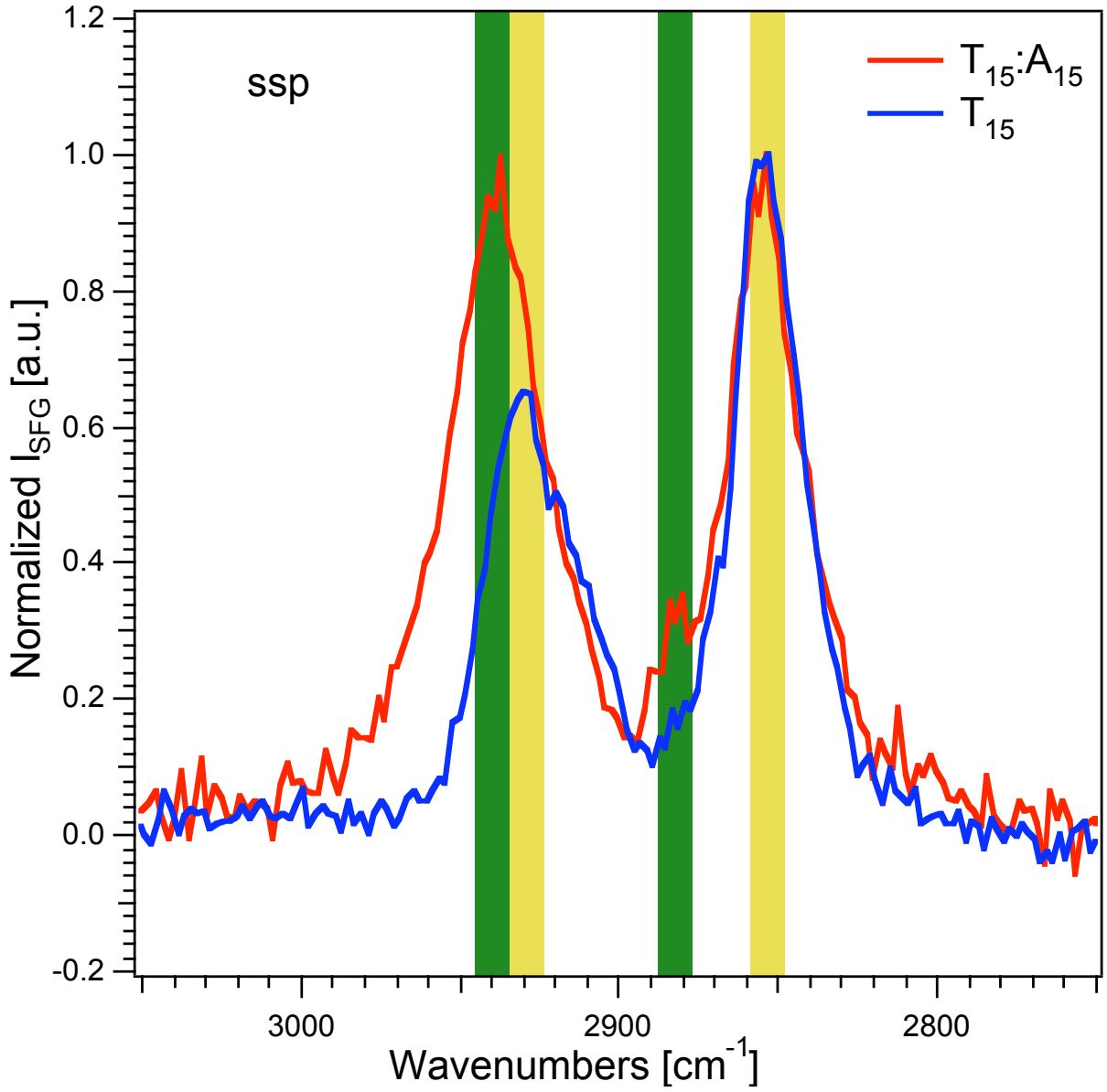

Figure A5.3. ssp-Polarized SFG Spectra of DNA Surfaces
ssp-Polarized SFG spectra of glass substrates functionalized with T_{15} ssDNA (blue trace) and T_{15}:A_{15} dsDNA (red trace). Spectra were collected over a 2-minute acquisition time. The methyl (-CH_3) stretching region is shaded in green, and the methylene (-CH_2) stretching region is shaded in yellow. The -CH_3 modes only appear in the duplex spectrum, even though the methyl groups in the thymine base are present in both surfaces.

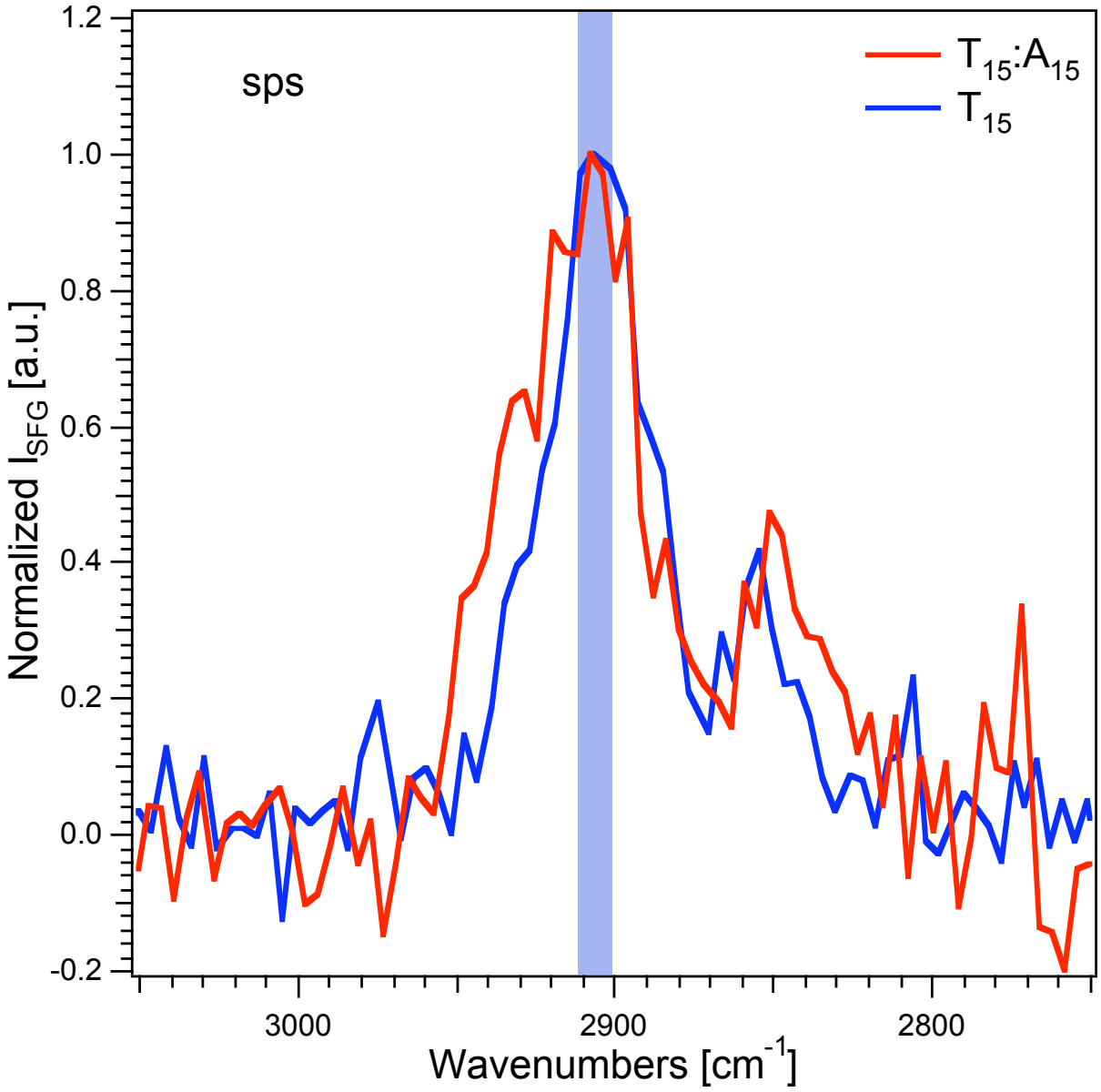

Figure A5.4. sps-Polarized SFG Spectra of DNA Surfaces
sps-Polarized SFG spectra of glass substrates functionalized with T_{15} ssDNA (blue trace) and T_{15}:A_{15} dsDNA (red trace). Spectra were collected over a 10-minute acquisition time. The methine (-CH) stretching region, shaded in blue, appears in both spectra but is very weak.

ordering of the oligonucleotides in the helix has already been simulated with a CHARMM macromolecular model calculation (see Chapter 6.3.1) If this is indeed the case, the handedness of the helix and the directionality imparted by the surface should control the rotation direction of the methyl groups in the double helix.

A5.4 Detection of Chirality

A5.4.1 Local Stereogenic Centers in Ribose Sugar Rings

In order to detect the chirality of the individual stereogenic centers from the ribose sugar rings, as well as the secondary structure of the DNA strands upon duplex formation, we have probed our surfaces with mixed polarizations of light. Probing the CH stretching region using IR light polarized parallel to the plane of incidence (p), we have driven the chiral NLO response of the oscillators with 800-nm upconverting light fields that are plane-polarized at $m = \pm 45^{o}$ away from the plane of incidence. Achiral molecules are expected to exhibit identical responses from both polarization combinations, whereas chiral molecules should exhibit a difference between the p±45p spectra.[8] Therefore, mixed polarization SFG experiments are a good probe for detecting surface chirality.

As a proof of concept, p±45p polarized SFG spectra of an octadecyltrichlorosilane (OTS)-modified glass slide are shown in Figure A5.5. The two peaks at 2967 and 2881 cm^{-1} are consistent with methyl asymmetric and symmetric stretch modes, respectively. It can be seen that the spectra are identical within error, which is expected given the fact that OTS is achiral.

The chirality of a DNA duplex was probed using the p±45p polarization combination. Spectra were collected of two different DNA surfaces, T_{15}:A_{15} dsDNA and $A_{12}T_3$:A_3T_{12} dsDNA,

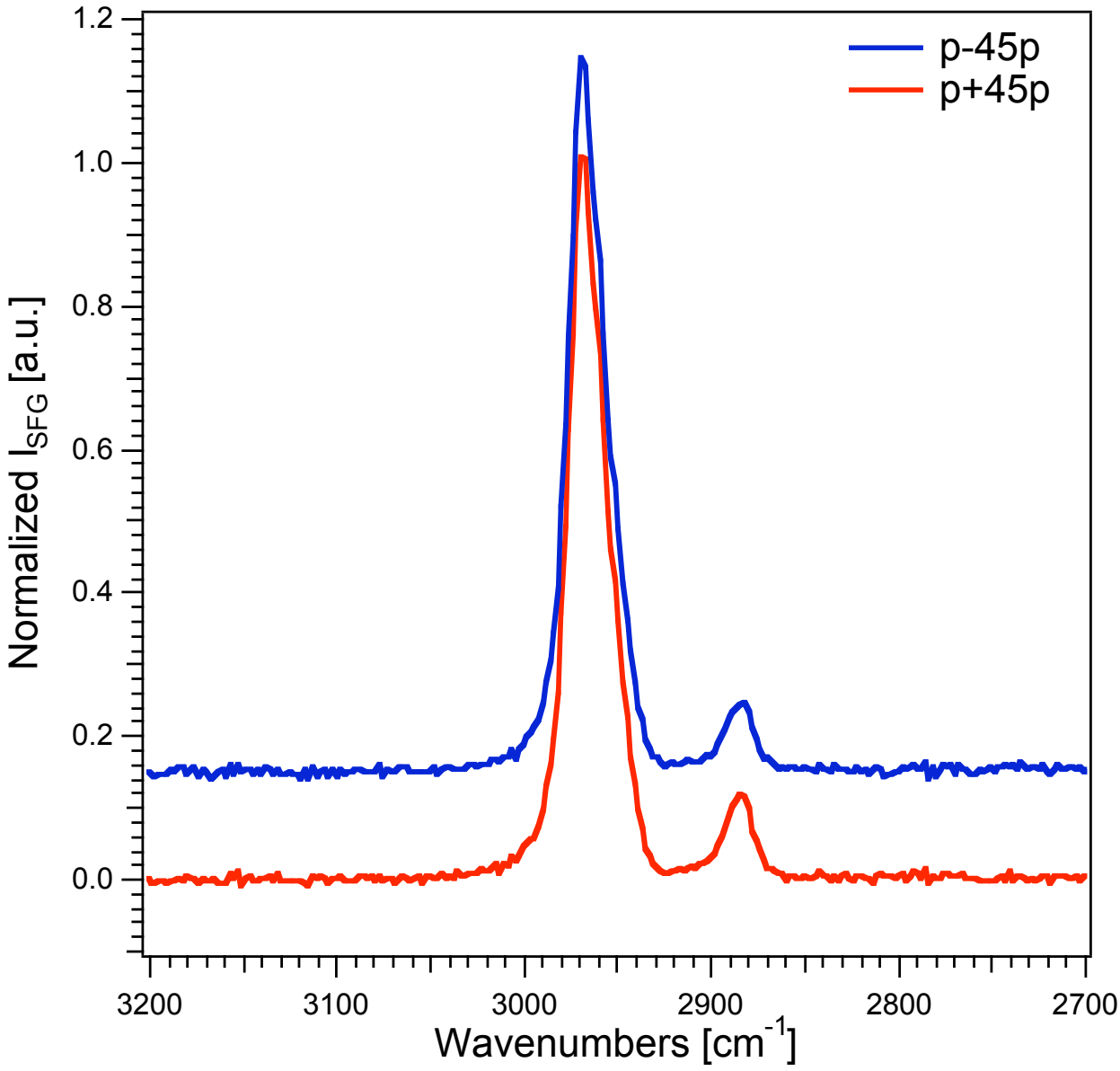

Figure A5.5. SFG Spectra of Achiral OTS with Mixed Polarizations
SFG spectra of an achiral octadecyltrichlorosilane (OTS)-modified glass slide collected with the p+45p (red line) and the p-45p (blue line) polarization combination. Spectra are offset for clarity.

and the p+45p spectra were subtracted from the p-45p spectra to produce the difference spectra. A DNA strand composed entirely of adenine presents a steric hindrance due to the purine bases, therefore, the $A_{12}T_3$ sequence was chosen instead of A_{15}. The pyrimidine bases of the thymine are easier to couple to the NHS ester and are useful as a primer on the 3' end of the sb-strand. The sb-T_{15}:A_{15} duplex shows two distinct p±45p spectra (Figure A5.6), whose spectral difference results in a negative methyl asymmetric stretch (2960 cm^{-1}) contribution (Figure A5.7). The deoxyribose methine stretch (2900 cm^{-1}) also exhibits negative intensity differences.

In contrast, when the surface is functionalized with $A_{12}T_3$ ssDNA before hybridizing with complementary strand, A_3T_{12}, the methyl asymmetric stretch contribution from the resulting duplex displays a positive intensity difference. The methine stretches (2900 cm^{-1}) from the 30 ribose groups of the sb-$A_{12}T_3$:A_3T_{12} duplex still exhibit negative intensity differences, which is not surprising as both duplexes have the same number of sugars, whose arrangement within the helix should not depend on the hybridization history. The striking difference in the two spectra shown in Figure A5.7 arises from the clear intensity differences in the methyl asymmetric stretch contributions. The T_{15}:A_{15} duplex has a positive difference peak for the methyl asymmetric stretch, whereas the $A_{12}T_3$:A_3T_{12} duplex has a negative difference peak.

A5.4.2 Supramolecular Chirality in the DNA Double Helix

The DNA surface undergoes a chiral transition upon the hybridization process when a right-handed, anti-parallel double helix forms between the sb-DNA and its complementary strand.[29-33] In theory, if our surfaces were first functionalized with T_{15} oligonucleotides, the arrangement of the methyl symmetric stretch modes from the thymine bases should follow a counter-clockwise rotation (Figure A5.8a-b). Due to the anti-parallel duplex DNA configuration,

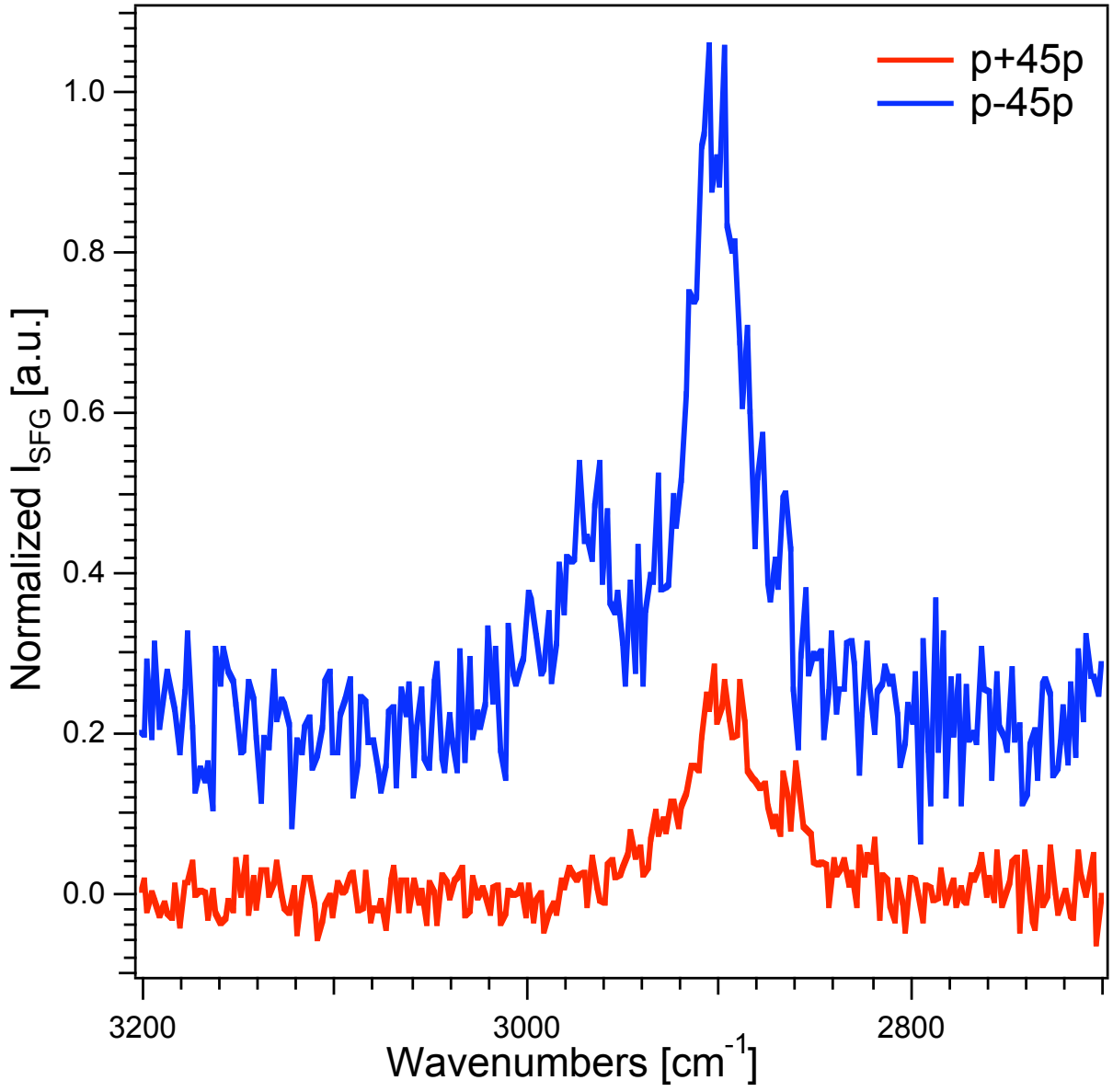

Figure A5.6. SFG Spectra of a Chiral DNA Duplex with Mixed Polarizations
p±45p-Polarized SFG spectra of glass substrates functionalized with a sb-T_{15}:A_{15} duplex. Spectra were collected over a 4-minute acquisition time. The spectra utilize the p+45p (red line) and p-45p (blue line) polarization combinations to probe the -CH_3 (2960 cm^{-1}) and -CH (2900 cm^{-1}) vibrational modes. Spectra are offset for clarity.

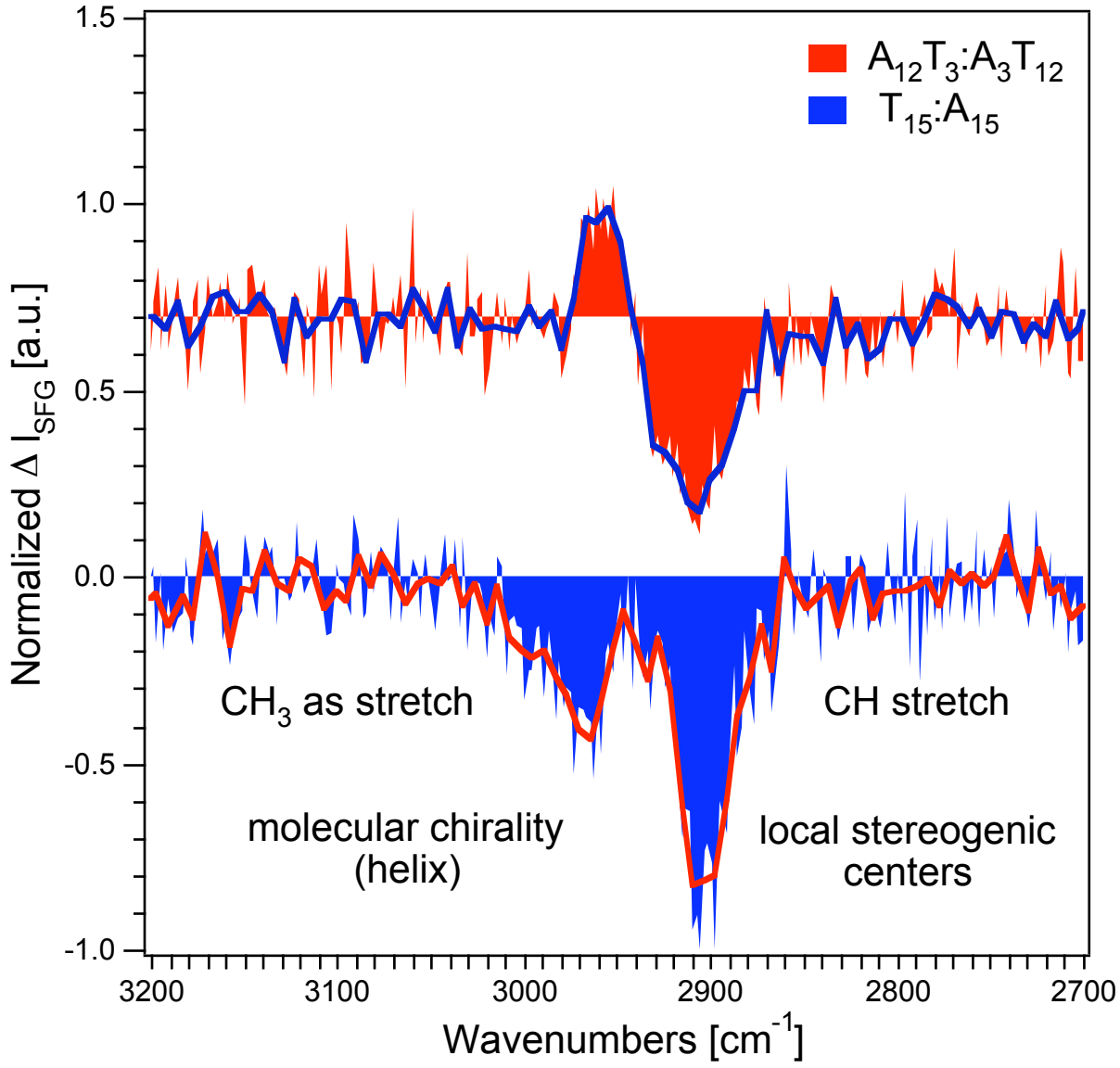

Figure A5.7. SFG Difference Spectra of Chiral DNA Duplexes
The SFG difference spectra of glass substrates functionalized with T_{15}:A_{15} dsDNA (bottom) and $A_{12}T_3$:$T_{12}A_3$ dsDNA (top). The thick solid lines represent a 3-point boxcar average of the difference spectra. The -CH_3 asymmetric stretch (2960 cm^{-1}) probes the molecular chirality of the helix, whereas the -CH stretch (2900 cm^{-1}) probes the local stereogenic centers of the ribose rings. Spectra are offset for clarity.

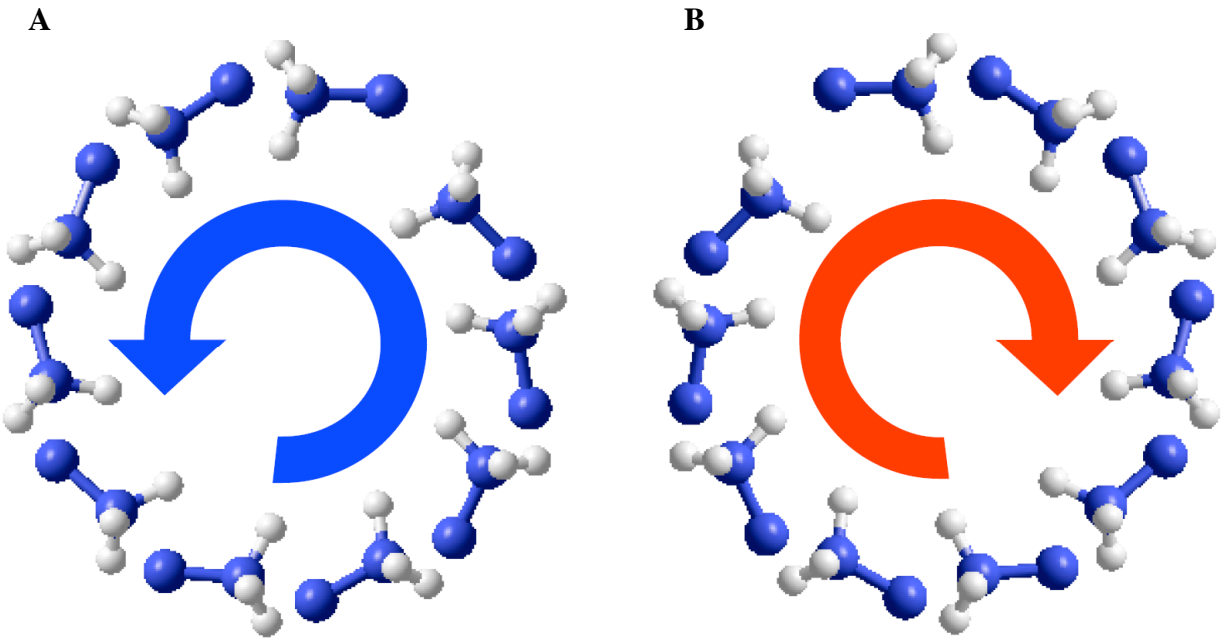

Figure A5.8. Top Down View of DNA Duplex Methyl Groups
Top view of **A**) sb-T_{15}:A_{15} (left, blue arrow) and **B**) sb-A_{15}:T_{15} (right, red arrow) duplexes with only thymine methyl groups (R-CH_3) visible in the molecular packing diagram, including their sense of rotational arrangement.

this rotational direction would be reversed if the surface was first functionalized with A_{15} oligonucleotides and then hybridized with T_{15} oligonucleotides. While these geometrical considerations are irrelevant in isotropic environments such as an aqueous phase, they become very important in the analysis of sb-DNA duplexes.

The spectra are consistent with the formation of a double helix upon hybridization that contains methyl groups from the thymine bases whose arrangement depends on an external reference point, which is the surface. The p±45p polarization combination, thus, provides information on oscillators associated with stereogenic carbon atoms (methine CH groups, 2900 cm^{-1}), as well as molecular chirality (helically arranged methyl groups, 2960 cm^{-1}). Therefore, the change in DNA secondary structure upon hybridization can be used as a probe of the order of assembly of DNA strands. We stress that it would be impossible to observe these stereoscopic differences in isotropic media such as bulk aqueous solutions.

A5.5 Summary

In summary, we have successfully obtained surface vibrational spectra of surface-bound ssDNA and dsDNA and have verified the highly ordered arrangement of the thymine bases within the double helix formed by Watson-Crick base pairing. These are the first measurements of vibrational signatures from stereogenic carbon atoms in sb-DNA duplexes, as well as the macroscopic chirality generated in these double helices upon hybridization. The high sensitivity and the label-free, molecularly specific nature of our approach should pave the way for a plethora of fundamental investigations into the nature of surface-bound biopolymers.

ABOUT THE AUTHOR

Faith Boman was born and raised in Ann Arbor, MI by her parents Larry and Barbara Boman along with her brother Joshua. During high school, she attended Saline Christian School and Plymouth Christian Academy, where she enjoyed playing volleyball and participating in science fairs. She graduated *summa cum laude* from Washtenaw Technical Middle College in 1999. She then went on to attend the University of Michigan where she received the Seyhan N. Ege Women in Science and Engineering Award and the William J. Branstrom Freshman Prize in Chemistry. In 2003, Ms. Boman received double Bachelors of Science degrees in Chemistry and Biochemistry *magna cum laude*. During her time at Michigan, she was a member of the American Chemical Society (ACS) and the Alpha Beta chapter of the Alpha Chi Sigma, a professional chemistry fraternity. As an undergraduate, she performed physical chemistry research under the direction of Prof. Robert Kuczkowski, studying the rotational spectra of fluorobenzene and HCl isotopomers by pulsed molecular beam techniques in a microwave spectrometer, which was later published in *The Journal of Chemical Physics*. She also did biophysical chemistry research under the direction of Prof. James Penner-Hahn, carrying out bioinformatics structural calculations on biological macromolecules with metal centers. In her senior year, she had the opportunity to help teach a studio-based general chemistry lab that focused on analyzing the water downstream of the Pfizer R&D facilities.

In the fall of 2003, Ms. Boman moved to Evanston, IL to pursue her doctoral degree in chemistry at Northwestern University. She joined the environmental chemistry lab of Prof. Franz Geiger and began to research DNA-functionalized fused quartz/water interfaces with second harmonic generation spectroscopy using a Ti:sapphire regenerative laser system, which had

never been done before. She received support from the National Science Foundation- Nanoscale Science and Engineering Center (NSEC) and recently received their Outstanding Researcher Award. She participated as a mentor in the NSEC summer research program for undergraduates, as well as a reviewer for NSEC undergraduate journal *Nanoscape*. Along with her friend Ami Patel, she co-founded the Chicago Cultural Club, funded by The Graduate School, in which she organized cultural and scientific trips for graduate students and won the Best Community-Building Group Award from the Graduate Student Association. She worked as a teaching assistant in the general chemistry and physical/analytical chemistry labs and developed a training workshop for new graduate students as part of the Searle Center of NU. She was a member of the Alpha Gamma chapter of Phi Lambda Upsilon, a chemistry honors society, and volunteered in a science outreach program in the Chicago Public School system for elementary students.

As a graduate student, Ms. Boman had the opportunity to present her research throughout the United States and in Europe to thanks to numerous travel awards, including three Gordon Research Conferences, three ACS National Meetings, two Nonlinear Optics Chautauquas at Purdue University, an ACS/PRF summer course in Telluride, CO, and an International CD Conference in the Netherlands, where she won the Best Poster Award. She has published her research in two first-author and one third-author papers in the *Journal of the American Chemical Society*, of which the latter was featured as the "News of the Week" in *C&E News*. Ms. Boman currently lives in Chicago, IL with her roommates, Paige Hall and Jen Carbon. She expects to earn her Ph.D. in December 2008, after which she plans to work as a consultant.